UNIVERSITÀ DEGLI STUDI DI PARMA

Dottorato di ricerca in Progettazione e Sintesi di Composti Biologicamente Attivi

Ciclo XXVII

Mass spectrometry in structure-property relationships studies: allosteric inhibitors of monoacylglycerol lipase and prodrugs of palmitoylethanolamide

Coordinatore:

Chiar.mo Prof. Marco Mor

Tutor:

Chiar.ma Prof.ssa Federica Vacondio

Dottorando:

Michele Bassi

Abstract

Mass spectrometry is a highly versatile and multi faceted analytical technique, which can be successfully applied to the study of structure-property relationships of small molecules, as new drug candidates, and to better characterize macromolecular targets. During the three years of Ph.D. project, mass spectrometry was employed as analytical tool to solve different tasks related to two main research themes: prodrugs of palmitoylethanolamide (PEA) and allosteric inhibitors of the serine hydrolase monoacylglycerol lipase (MGL). Palmitoylethanolamide (PEA), belonging to the family of fatty acid amide lipid mediators, has antinflammatory and antinociceptive properties widely exploited in veterinary and human medicine, despite its poor pharmacokinetics. Looking for prodrugs that could progressively release PEA to maintain effective plasma concentrations, carbonates, esters and carbamates at the hydroxyl group of PEA were tested for their chemical stability (pH=7.4) and stability in rat plasma and liver homogenate by *in vitro* assays and high performance liquid chromatography/tandem mass spectrometry (HPLC/MS/MS). Carbonates and carbamates resulted too labile and too resistant in plasma, respectively. With ester derivatives, prepared by conjugating PEA with various amino acids, it was possible to modulate the kinetics of PEA release in plasma and their stability in liver homogenate. L-Val-PEA, with suitable PEA release in plasma, and D-Val-PEA, with high resistance to hepatic degradation, were orally administered to rats and plasma levels of prodrugs and PEA were measured at different time points. Both prodrugs showed significant release of PEA, but lower than that obtained with equimolar doses of PEA. Amino-acid esters of PEA are a promising class to develop prodrugs, even if they need further chemical optimization.

The second research project involved the characterization of the chemical reactivity for a series of benzisothiazolone-based compounds, designed to allosterically inhibit the serine hydrolase MGL, a chief enzyme in the metabolism of the main endocannabinoid, 2-arachidonoylglycerol, by targeting selected cysteine residues known to regulate MGL enzymatic activity. Starting from a lead compound, a series of chemical modifications were made by introducing at position 5 and 6 of the benzisothiazolone ring a set of substituents endowed with opposite electronic properties. The reactivity of the newly synthesized compounds was tested *in vitro* versus glutathione setting up HPLC-MS/MS analytical methods to detect all reaction species in order to have a crucial information about the oxidative potential of each benzisothiazolinone.

The role of these regulatory cysteine residues in the fine tuning of MGL activity, their sensitivity towards the redox state of the surrounding environment and their capacity to respond to changes in the redox potential were further explored in a series of pharmacological assays on purified human MGL.

In these experiments, hMGL was pre-incubated for a certain period of time in buffer with different oxidizing or reducing agents, subsequently with a probe (dimedone) for identifying an hypothesized oxidized species of cysteine, sulfenic acid. Employing MALDI-TOF/TOF mass spectrometry on oxidized hMGL after trypsin digestion, it was possible to identify which cysteine residue was oxidized to sulfenic acid and which cysteine-containing peptide had been covalently modified by dimedone.

Finally, during a three months period spent in the laboratory of Prof. Kasper Rand, at the university of Copenhagen, the conformational changes in hMGL following the interaction with a benzisothiazolone inhibitor were investigated, employing the hydrogen/deuterium exchange mass spectrometry technique (H/DX-MS).

Table of Contents

1. Mass spectrometry: an introduction

The origins of mass spectrometry go back to the characterization of "positive rays" by J. J. Thomson in the early 1900s.[1] The technique was in the domain of physicists and physical chemists for the next 60 years, during which there were significant advances in both instrumentation configurations and applications. Mass spectrometry has grown immeasurably over the last 20 years. This progress has led to the advent of entirely new instruments. New atmospheric pressure sources were developed,[2,3] existing analysers were perfected and new hybrid instruments were realized by new combinations of analysers.

Mass spectrometers are important instruments that deserve a brief history. The first revolution in mass spectrometry consisted in the commercialization of the interfacing with gas chromatography in the late 1960s. The coupling of the two techniques enabled the separation of complex mixtures so that individual components could be admitted sequentially into the mass spectrometer. However, the main problem with this technique was that samples needed to be in the vapor phase, so polar compounds, that included the vast majority of molecules of biological interest, decomposed when heated, prior to vaporization. Chemical derivatization enabled the analysis of some polar compounds, also with the development of fast atom bombardment (FAB) in the late 1970s. The latter technique was discarded in the 1990s when mass spectrometry was revolutionized again, this time by the commercialization of electrospray ionization (ESI) and matrix-assisted laser desorption/ionization (MALDI) ion sources. In fact, ESI facilitated the coupling of liquid chromatography (LC) with mass spectrometry, allowing the on-line analysis of polar, bioactive compounds. In addition, and more importantly, ESI and MALDI enabled mass spectrometry to move into the field of protein and other biopolymer analysis.

It is important also to define what is a mass spectrometer: it is an analytical instrument that produces a beam of gas phase ions from samples (*analytes*), that sorts the resulting mixture of ions according to their *mass-to-charge* (*m/z*) ratios using electrical or magnetic fields (or combinations thereof), and provides analog or digital output signals (*peaks*) from which the mass-to-charge ratio and the *intensity* (abundance) of each detected ionic species may be determined. In general, three basic steps are involved in mass spectrometry analysis: 1) ionization that converts analyte molecules or atoms into gas-phase ionic species. This step requires the removal or addition of an electron or proton(s); 2) separation and mass analysis of the molecular ions and their charged fragments on the basis of their *m/z* ratios; 3) finally, the ion current due to these mass-separated ions is measured, amplified, and displayed in the form of a mass spectrum.

In Figure 1 the major components that compose a mass spectrometer are shown. There are six major components: 1) a sample introduction system (inlet system), 2) an ion source where the analytes are vaporized and ions are produced, 3) a mass analyser, in which the ions are separated according to their *m/z* ratios, 4) an ion detector where the signal intensities of each separated *m/z* value are determined, 5) a vacuum system, needed to prevent the loss of ions through collisions with neutral gas molecules as well as with the walls of the mass analyser, the detector, and sometimes the ion source, and 6) computers to control the operation of the instrument, record, and process the generated data.

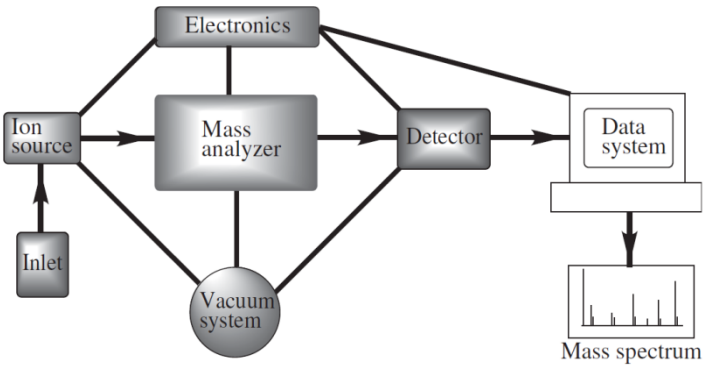

Figure 1: *Basic components of a mass spectrometer.*

1.1 Ion sources

As previously said, there is a need to ionize a molecule before to analyze it. This is needed because molecules are electrically neutral, so they cannot be manipulated by electrical or magnetic fields, that are the most common processes to focus, separate and detect the molecules. The ionization process involves the addition of energy to the molecules of analyte. There are a wide variety of ways to form ions both inside and outside the mass spectrometer. The method of ionization determines the amount of energy added to the analyte. Until the 1990s, the ionization step (primarily electron and chemical ionization) occurred in ion sources located within the vacuum chamber of the mass spectrometer and the ionizing "agents", used to produce ions, included electrons, ions, electric fields, photons, and lasers. In recent years, methods have been developed in which the ionization step occurs outside the vacuum chamber, at atmospheric pressure. Examples of *in vacuo* ionization techniques are: electron ionization (EI), chemical ionization (CI), and matrix-assisted laser desorption/ionization (MALDI). Ionization techniques carried out outside the vacuum system are collectively termed atmospheric pressure ionization (API) methods. The most important API methods are: electrospray ionization (ESI), atmospheric pressure chemical ionization (APCI), atmospheric pressure photo-ionization (APPI), desorption electrospray ionization (DESI), and direct analysis in real time (DART).

It is not the aim of the present Ph.D. dissertation to explain all the over mentioned ionization techniques, but attention will be mainly focused on those which have been employed experimentally during this three year Ph.D. program.

1.1.1 Atmospheric pressure chemical ionization (APCI)

The atmospheric-pressure chemical ionization (APCI) technique is efficiently employed to analyze LC effluents by mass spectrometry. It is generally applicable to compounds which are of relatively low polarity and thermally stable with an upper m/z ratio of around 1500 Da. These characteristics allow the analytes to be readily protonated and not disintegrated when exposed to the heat necessary to remove the solvent.

As it can be seen in the Fig. 2, an APCI ion source consists of three main parts: a removable heated nebulizer probe (350 to 500°C), an ionization region, and an intermediate-pressure ion-transfer region.

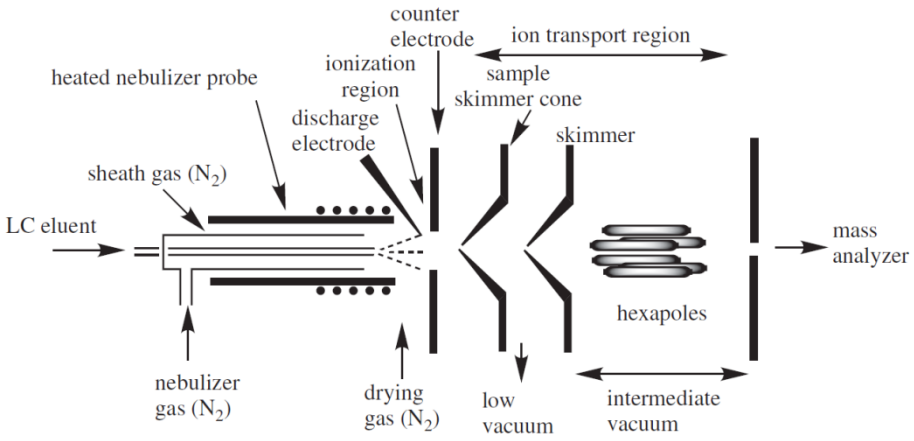

Figure 2: *Block diagram of atmospheric pressure chemical ionization source (APCI).*

The LC effluent flows through a fused-silica capillary tube, and is evaporated by heating and adding a gas, usually nitrogen, to sweep the resulting vapor into the ionization region. The ionization region contains a discharge electrode (corona pin), which is held at 2 to 3 kV potential with respect to the exit aperture of the counter-electrode.

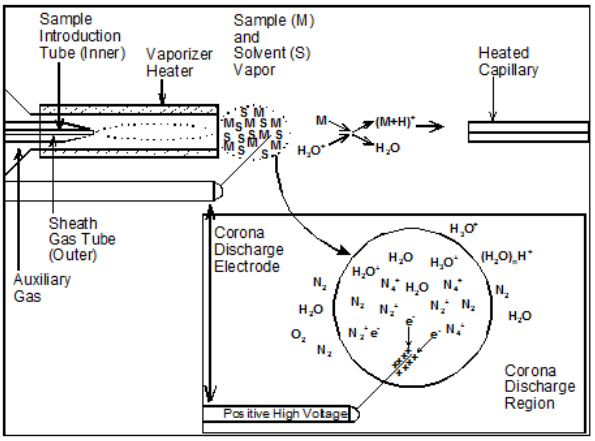

Figure 3: *Ionization process occurring in the APCI source, in positive-ion mode.*[4]

A discharge occurs as the plume of solvent is swept past the corona pin, creating a plasma in which both positive (protonated) solvent ions and electrons are generated (Fig. 3). It is believed that primary ions of the type N^{2+}, N^{4+}, and H_2O^+ are first formed by interaction of the corona-created electrons with the atmospheric gas. Charge-transfer reactions of these primary ions with H_2O, methanol, and acetonitrile, present in the aerosol, produce a set of solvated charged species $H_3O^+(H_2O)_n$, $CH_3OH_2^+(CH_3OH)_n$, and $CH_4CN^+(CH_3CN)_n$, respectively. Finally, the transfer of a proton from these solvated ions ionizes the sample molecules to produce monoprotonated $[M + H]^+$ ions. In the negative-ion mode, $[M - H]^-$ ions are produced via the ion–molecule reactions of the solvated oxygen anions. It is known that other ions can also be formed, such as $[M]^+$ and $[M]^-$, because there is a set of ion-molecule reactions involving proton transfer, electron capture, charge transfer and exchange, clustering and substitutions. The ions formed are sampled through a small orifice skimmer, called the nozzle or sample skimmer cone, and are transported through additional skimmer and ion-focusing lenses into the mass analyzer for subsequent mass analysis. Typical applications of the APCI technology include the analysis of steroids, pesticides, and pharmaceutical drugs.

1.1.2 Electrospray ionization (ESI)

ElectroSpray Ionization (ESI) is the most common API application. It has undergone remarkable growth in recent years and is frequently used for LC/MS of thermally labile and high molecular weight compounds. ESI is the softest ionization technique; the energies involved are barely above those necessary to generate ions, and it is for this reason why it has become so popular: it was finally possible to volatilize polar compounds without causing their decomposition. It appeared, moreover, that ESI allowed a very high sensitivity to be reached and it was easy to couple to high-performance liquid chromatography HPLC, μHPLC or capillary electrophoresis. ESI principles and biological applications have been extensively reviewed.[5,6,7] In ESI ionization mode, analytes are dissolved in an electrically conductive liquid medium, usually acetonitrile:water and methanol:water mixture, the addition of a little acid, 0.1% v/v acetic or formic acid, to the solvent increases chromatographic separation and supplies protons for the ionization process. It is important to underline that not all the acids commonly used in reverse-phase HPLC-UV methods are suitable for ESI-MS, for example trifluoroacetic acid (TFA) can compromise ion formation because of the strong ion pair formation between the analytes and TFA. ESI is produced by applying a strong electric field, under atmospheric pressure, to the liquid passing through a steel capillary tube where ions are subjected to a high voltage, 2–5 kV (positive or negative), with respect to the vacuum chamber.

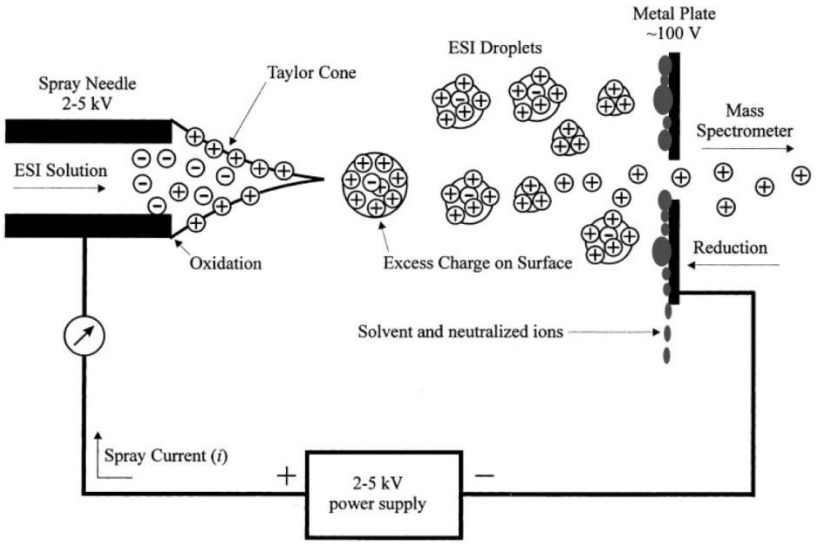

Figure 4: *Schematic of the electrospray ionization process.*[8]

The mechanism for the ionization process is not well understood and there are different theories trying to explain this ionization process. However, it is generally believed that ionization in electrospray involves three different processes: droplet formation, droplet shrinkage, and desorption of gaseous ions. At the onset of the electrospray process, the electrostatic force on the liquid leads to a partial separation of charges. For example in the positive-ion mode, cations concentrate at the tip of the metal capillary and tend to migrate toward the counter-electrode, whereas anions migrate inside the capillary away from the tip. The migration of the accumulated positive ions towards the counter-electrode is counter-balanced by the surface tension of the liquid, giving rise to a Taylor cone at the tip of the capillary. The continuous production of charged species is assisted by electrochemical redox processes. Formation of the Taylor cone at the tip of the ESI

probe is important because it results in a stable stream of droplets from which the ions are eventually released. When there is a sufficient electric force, the solution reaches the Rayleigh limit,[9] the point at which Coulombic repulsion of the surface charge is equal to the surface tension of the solution; droplets that contain an excess of positive (or negative) charge detach from the tip, forming a mist of fine droplets, yielding a solution where there is only one charge type. There is also one, or two, outer tubes, coaxial with the tube carrying the liquid, through which there is a nitrogen flow acting as a sheath gas, and the second flow as auxiliary gas, that nebulizes the eluate into a spray of charged droplets. Evaporation of the solvent from these droplets leads to droplet shrinkage. The desolvation causes the density of the electric field of the droplets to increase to the point where disintegration occurs. When the repulsive Coulombic forces between the charges on the surface of the droplets exceed the forces attributable to surface tension (the Rayleigh instability limit), the droplets disintegrate into smaller units which still remain charged. When the droplets are reduced to a radius of ~10 nm, and under the influence of the strong electric field, deformation of the droplet occurs. The droplet elongates under the force resulting from the accumulation of charge, similarly to what occurred at the probe tip, and finally produces a new Taylor cone. From this Taylor cone, smaller droplets are released. A drawing of a decomposing droplet is displayed in Fig. 5. These small, highly charged droplets will continue to lose solvent, and when the electric field on their surface becomes large enough, desorption of ions from the surface occurs. Under the combined influence of a voltage gradient, and the vacuum behind the entrance, the ions deviate from the angle at which they originated (from the ESI probe) and enter the analyser.

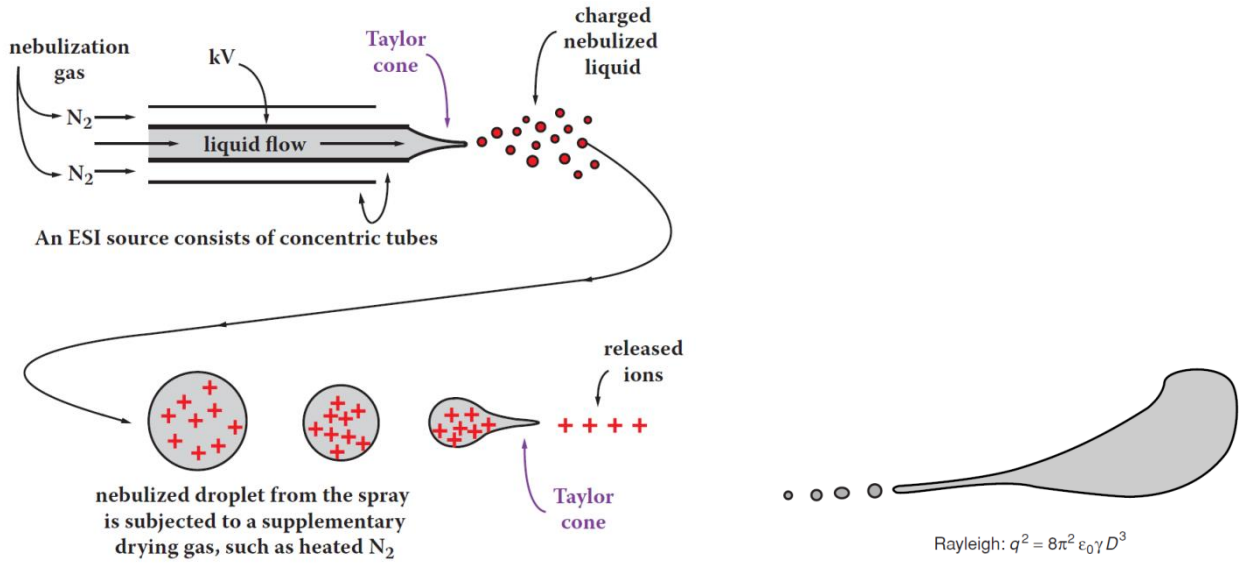

Figure 5: *Left: Taylor cone formation occurs both at the end of the ESI tube and as the droplets disintegrate to release ions. Right: A decomposing droplet in an electrospray source; q, charge; ε_0, permittivity of the environment; γ, surface tension and D, diameter of a supposed spherical droplet.*[10]

The desorption of charged molecules occurs from the surface of droplets. This means that sensitivity is higher for compounds whose concentration at the surface is higher. Moreover when mixtures of compounds are analyzed, those present at the surface of droplets can mask, even completely, the presence of compounds which are more soluble in the bulk. In positive ESI, ions are formed from neutral analytes by protonation or

other cation attachment. The charge is usually provided by addition of a proton to yield $[M + H]^+$ ions. However, alkali metal cations (particularly sodium and potassium), and also the ammonium cation, can be added to analytes to form $[M + Na]^+$, $[M + K]^+$, and $[M + NH_4]^+$ ions, respectively. Otherwise in the negative ion mode, deprotonation or anion attachment occurs, with ions forming through the loss of a proton, $[M–H]^–$, often by a carboxylic acid. It is also possible an addition of a negatively charged species, such as from an acetate anion or an halogen, to form $[M + CH_3COO]^–$ and $[M + Cl]^–$. But the most important characteristic of ESI is that it is able to produce multiply charged ions from large molecules, allowing to analyze them with instruments whose mass range is limited to as low as 2000 Th (Thomson = 1 Da/*e*, Da represents the unit dalton, and *e* represents the elementary charge which is the electric charge unit in the atomic unit system). With this technique it is possible to analyze, for example, a protein, and to measure the raw data (*m/z*) of multiply charged ion envelopes, then, with commercial software packages it is possible to deconvolute the spectrum into the average (zero charge) mass of the analyte by solving a set of simultaneous equations.

1.1.3 Matrix-assisted laser desorption/ionization (MALDI)

For many years lasers have been used to ionize molecules directly with varying degrees of success. Nd:YAG (neodymium-doped yttrium aluminium garnet) lasers (frequency multiplied to provide a 355 nm output) predominate in modern instruments because of the high repetition rates available and their long lifetimes. Nitrogen (337 nm) lasers are also used in older instruments. The energy added to the analytes was usually excessive and resulted in their destruction or extensive fragmentation. The significant conceptual difference between direct laser ionization and MALDI is that in the latter there is a matrix present, usually an aromatic acid, in vast molar excess over the analyte, whose function is to absorb most of the energy supplied by the laser. As the analyte itself does not absorb the laser energy directly, the method is considered a "soft" ionization technique, allowing the analysis of complex biomolecules up to several hundred KDa.[11] The use of the most suitable MALDI matrix, which provides for both desorption and ionization of the analyte, is the crucial factor for the success of this ionization method. The method is characterized by easy sample preparation and has a large tolerance to contamination by salts, buffers and detergents.[12,13]

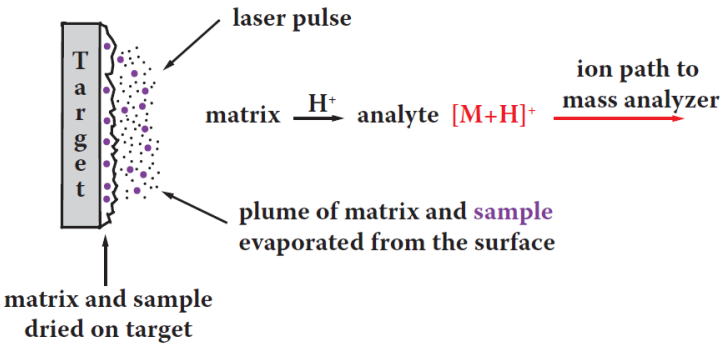

Figure 6: *Diagram of the principle of MALDI.*

MALDI ionization normally consists in two steps: in the first step, the compound in solution is mixed with a large molar excess, usually 10000:1, of a small organic molecules, usually an aromatic acid, called the

matrix. These molecules have a strong absorption at the laser wavelength so absorbs most of the energy supplied by the laser. The matrix and analyte solutions are co-deposited onto special plates, usually steel, where hundreds of sample "spots" can be placed. The mixture is dried before analysis and any liquid solvent used is removed. The result is a "solid solution" deposit of analyte-doped matrix crystal. The analyte molecules are embedded throughout the matrix so that they are completely isolated from one another.

The second step occurs when the sample plate is placed into the vacuum chamber, the components of these crystals are transferred into the vapor phase by the energy absorbed on exposure to a pulsed (UV) laser. The excess, as well as the aromaticity, of the matrix provides the absorption of most of the energy from the laser. As previously said the laser adds excess energy very rapidly (nanoseconds) to the sample, raising the temperature to about 1000 °C, when explosive evaporation occurs. The speed of the process reduces the probability of degrading the analyte. The exact mechanism of the MALDI process is not completely elucidated. The most widely accepted ion formation mechanism involves a two-step process: a primary ionization event, followed by in-plume secondary ion–molecule reactions. Generation of the first ions in MALDI remains the most controversial aspect of the method. Of the two main modern approaches for UV-MALDI, one argues that excited matrix is intimately and crucially involved, another views the matrix as mainly the desorption/ablation vehicle.

In the first model, or photoexcitation/pooling model, primary matrix ions are generated by laser excitation of individual matrix molecules or an "exciton-pooling process", in which two nearby excited matrix molecules redistribute their energy and concentrate it on one molecule. Then analyte ions are produced in the expanding gas plume, that it is an area just above the matrix surface, via extensive secondary ion-molecule charge-transfer reactions between the primary matrix ions previously formed and neutral analyte molecules. The matrix-related active species can be protonated, sodiated, or deprotonated matrix molecule or a radical cation. These species might participate in proton transfer, cation transfer, electron transfer, or electron-capture reactions.

In the second model, or cluster model, the ions were taken to be largely preformed in the solid matrix, and undergo extensive neutralization in the plume, often by electrons in the case of positive ions. There are two pathways that have been proposed to explain this model. First pathway assumes that the analyte exists as multiply charged ions and that the clusters are formed by trapping those ions along with their counter-ions in a large chunk of matrix. The clusters are released in the desorption plume by laser irradiation. The analyte ions are then formed by evaporation from these matrix-rich clusters of the excess matrix molecules or of other neutrals formed from trapped ionic species by proton transfer reactions. The second pathway of charging the matrix-analyte cluster is photoionization.

The ions in the gas phase are then accelerated by an electrostatic field towards the analyser. Analyte ions may also be generated by adduct formation, for example $[M + Na]^+$, $[M + K]^+$, depending on the availability of alkali metals from the sample or from the original solution.

Matrix selection and optimization of the sample preparation protocol are the most important steps in the analysis because the quality of the results depends on good sample preparation. However, the preparation

procedures are still empirical. The selection of the matrix is of major importance in MALDI because the amount of energy transferred to the analyte is matrix-specific, moreover there are some requirements that the matrix should have simultaneously. These are strong absorbance at the laser wavelength, low enough mass to be sublimable, vacuum stability, ability to promote analyte ionization, solubility in solvents compatible with analyte and lack of chemical reactivity. There are multiple ways to "spot" samples. For instance, the sample and matrix may be mixed before spotting, or either solution may be spotted first with or without drying in-between. Often it is worth trying multiple approaches to sample loading to see which provides the best signal-to-noise ratio.

1.2 Mass analysers

Once ions have been formed, either outside the mass spectrometer using API methods or within the vacuum system by EI, CI, or MALDI, the ions must be separated according to their *m/z* ratios. Indeed a moving charged particle can be distinguished from another ion on the basis of differences in their momentum, kinetic energy, and velocity. Current mass analyzers include quadrupole, quadrupole ion trap (QIT), quadrupole linear ion trap (LIT), orbitrap, time-of-flight (TOF), ion cyclotron resonance (ICR) and much lesser extent magnetic sector. Each mass analyser has its advantages and limitations and they can be grouped on the basis of different properties, for example ion beam versus ion trapping types, continuous versus pulsed analysis, low versus high kinetic energies.

	Quadrupole	Ion trap	TOF	TOF reflectron	Magnetic	FTICR	Orbitrap
Mass limit	4000 Th	6000 Th	>1000 000 Th	10 000 Th	20 000 Th	30 000 Th	50 000 Th
Resolution FWHM (*m/z* 1000)	2000	4000	5000	20 000	100 000	500 000	100 000
Accuracy	100 ppm	100 ppm	200 ppm	10 ppm	<10 ppm	<5 ppm	<5 ppm
Ion sampling	Continuous	Pulsed	Pulsed	Pulsed	Continuous	Pulsed	Pulsed
Pressure	10^{-5} Torr	10^{-3} Torr	10^{-6} Torr	10^{-6} Torr	10^{-6} Torr	10^{-10} Torr	10^{-10} Torr
Tandem mass spectrometry	Triple quadrupoles MS/MS fragments precursors neutral loss	— MS^n fragments	— —	PSD or TOF/TOF MS/MS fragments	Consecutive sectors MS/MS fragments precursors neutral loss	— MS^n fragments	— —
	Low-energy collision	Low-energy collision	—	Low- or high-energy collision	High-energy collision	Low-energy collision	—

Table 1: *List of mass analysers.*

The five main characteristics for measuring the performance of a mass analyser are the mass range limit, the analysis speed, the transmission, the mass accuracy and the resolution.

The mass range is the maximum allowable *m/z* ratio amenable to analysis.

The analysis speed, also called the scan speed, is the rate at which the analyser measures over a particular mass range.

The transmission is express as the ratio of the number of ions reaching the detector and the number of ions entering the mass analyser. The transmission generally includes ion losses through other sections of the mass analyser such as electric lenses before and after the analyser.

The mass accuracy is the measured error in *m/z* divided by the accurate *m/z*. The precision obtained on the mass of the analyzed sample depends also on the determination of the centroid of the peak.
The resolution, or resolving power, is the ability of a mass analyser to yield distinct signals for two ions with a small *m/z* difference.

1.2.1 Quadrupole

As the name implies, quadrupole analysers consist of a set of four rods. These rods, which are metal (molybdenum) or metal-coated ceramic with lengths of 10–20 cm and diameters up to 1 cm, are placed parallel to each other in a square with the opposite pairs connected electrically. The mass separation is accomplished by the stable vibratory motion of ions in a oscillating electric field that is created by applying direct-current (dc) and radio-frequency (RF) potentials to these electrodes. During their trajectory, only ions with one specific *m/z* value have a stable oscillatory trajectory along the axis of the quadrupole to the detector. All other ions with different *m/z* values develop unstable oscillation patterns perpendicular to the flight path and are lost. Quadrupole analysers have unit resolution, so they are classified as low-resolution instruments which are poorly suited to obtain accurate mass data, indeed the peaks are broad (~1 *m/z* wide), and thus it is difficult to obtain precise measurements of the centroids.

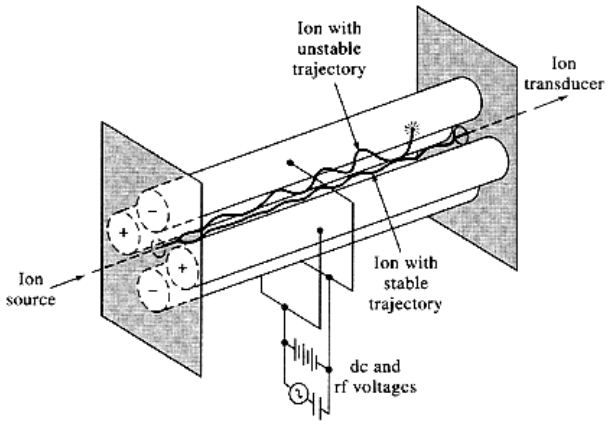

Figure 7: *Quadrupole mass analyser.*

Ions travelling along the z axis are subjected to the influence of a total electric field made up of a quadrupolar alternative field superposed on a constant field resulting from the application of the potentials upon the rods:

$$\Phi_0 = +(U - V \cos \omega t) \text{ and } -\Phi_0 = -(U - V \cos \omega t)$$

In this equation, Φ_0 represents the potential applied to the rods, ω the angular frequency (in radians per second=$2\pi\nu$, where ν is the frequency of the RF field), U is the direct potential and V is the 'zero-to-peak' amplitude of the RF voltage. When discussing quadrupole theory, it is customary to mention the Mathieu Equation that can be deduce like this:

$$U=a_u \frac{m}{z}\frac{\omega^2 {r_0}^2}{8e} \text{ and } V=q_u \frac{m}{z}\frac{\omega^2 {r_0}^2}{4e}$$

The last terms of both the U and V equations is a constant for a given quadrupole instrument, as they operate at constant ω. As it can be seen that switching from one *m/z* to another results in a proportional multiplication of a_u and q_u, which means changing the scale of the drawing in U, V coordinates; thus the triangular area it will change from one mass to another, like proportional triangles.

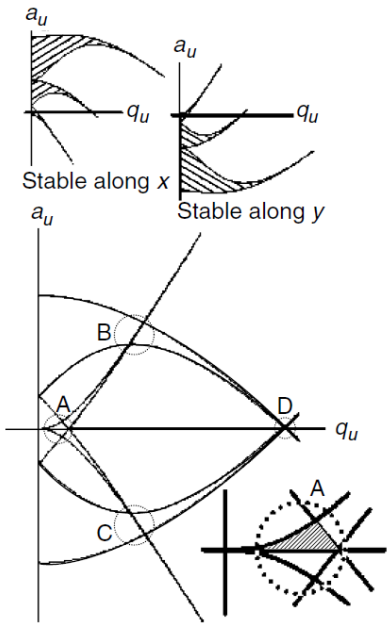

Figure 8: *Stability areas for an ion along x or y (above) and along x and y (below) the 4 regions of simultaneous stability are at A, B, C, and D. Of these, region A is the most used.*

Figure 9 represents in a U, V diagram the areas A obtained with different masses. As it can be seen in the diagram that scanning along a line maintaining the U/V ratio constant allows the successive detection of the different masses. So long as the line keeps going through stability areas, then the higher the slope, the better the resolution.

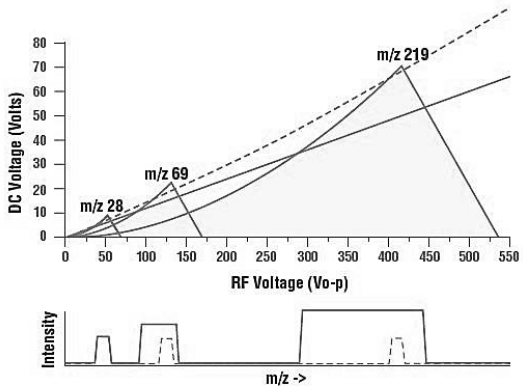

Figure 9: *Stability diagrams for m/z 28, 69 and 219 plotted in RF-DC space.*

All ions that fit with points on this line will travel the entire length of the quadrupole assembly without interruption. The mass resolution is an inverse function of the width of the stable region. The optimum mass separation is obtained when the mass-scan line is made to intersect the tip of the stability diagram.

When U is equal to zero (quadrupole operating in the RF only mode) all of the ions with a mass higher than a given limit selected by adjusting the value of the RF voltage V have a stable trajectory. Under these conditions all ions, those emerging from the ion source that enter the quadrupole are transmitted, regardless

of their *m/z* values, this is known as ion guide. In this mode it is common that are used different combinations of rods, for example hexapoles or octapoles because ion transmission is more efficient with these formats. In conclusion, quadrupoles, hexapoles, octapoles and other multipoles operating in RF only mode are able to focus efficiently ions from a mass range towards their axis without significantly affecting the axial kinetic energy of the transmitted ions. As these devices work at atmospheric pressure as well as under high vacuum, they can serve to connect high- and low-pressure regions of the mass spectrometer or also as collision cells.

1.2.2 Ion trap

An ion trap is a device that uses an oscillating electric field to store ions. The ion trap works by using an RF quadrupolar field that traps ions in two or three dimensions. In the quadrupole analyser only ions stable in a specific field are passed to the detector, while the unstable ions are lost. In the ion trap analyser all of stable ions are trapped in a stable sinusoidal trajectory within the cell. This task is accomplished with an oscillating electric field that is created within the boundaries of a three-electrode structure.

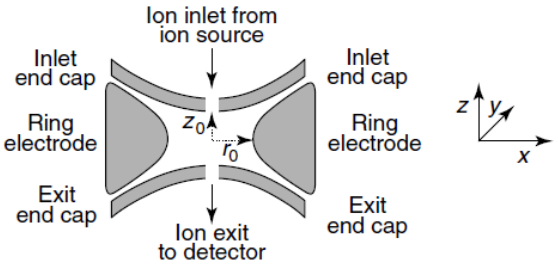

Figure 10: *Schematic view of an ion trap.*

Ions are produced in an external ion source and only a controlled number is allowed to enter the trap through one of the end caps. Then ions of different masses are present together inside the trap, and the ions of different masses are stored together in the trap. The three-dimensional quadrupole field is created by applying a potential of a certain amplitude of the dc and RF potentials to the ring electrode and maintaining the end-cap electrodes at ground potential. The trapped ions process in the trapping field with a frequency that is dependent upon their *m/z* ratio. When the ion trap is operated with helium in the trap (pressure ~1 mTorr) the gas causes the ions to cluster and remain close to the center of the cell where the electrical field is most symmetrical, resulting in the ions staying in their most stable orbits also to cool the ions collisionally. Then the combination of an amplified RF voltage on the ring electrode with an RF voltage on the end caps ejects ions from the cell through the end cap beyond which the detector is located. Indeed the other end-cap electrode has several perforations for the ejection of ions toward an externally located detector. Then the "resonance ejection" is used to obtain mass spectra by ejecting ions from the trap sequentially, according to their *m/z* values. It is also possible to retain a specific band of *m/z* values by ejecting all ions above and below the selected range. With this latter technique is possible to fragment the retained ions with collision-induced dissociation (CID) by introducing an additional pulse of gas into the trap. This technique is known as MS/MS. The characteristic of the MS/MS into an ion trap is that is possible to create an isolation and

fragmentation cycle of ions, in order to provide a MS^n spectra. The method is usually pursued only as far as MS^3, but is possible also up to MS^6 and higher, the only problem is that there is a significant reduction in the signal as the number of iterations increases.

It is also develop the linear ion trap (LIT) where ions can oscillate in a linear fashion along the length of a quadrupole. This because in a 3D ion trap have the limit on the number of ions that can be placed in it before space-charge effects distort the spectra and reduce sensitivity. The LIT is similar of the 3D ion trap with the same limitations in resolution, mass accuracy, but have the advantage to use a much larger number of ions, thus providing significant improvement of detection limit.

1.2.3 Time-of-flight (TOF)

A time-of-flight (TOF) mass spectrometer is one of the simplest mass-analyzing devices. The TOF analyser separates ions, after their initial acceleration by an electric field, according to their velocities when they drift in a free-field region that is called a flight tube.

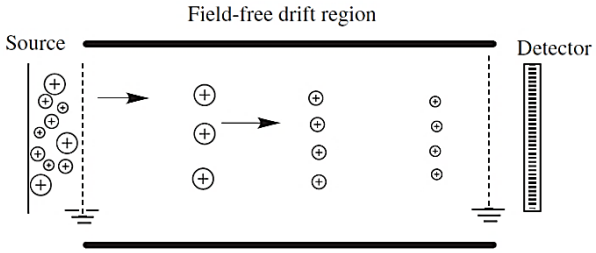

Figure 11: *Schematic diagram of a linear TOF.*

Ions are expelled from the source in bundles which are either produced by an intermittent process such as plasma or laser desorption, or expelled by a transient application of the required potentials on the source focusing lenses. The time-of-flight for the passage of an ion in a TOF analyser is a function of its momentum, and therefore its *m/z*. The acceleration voltage and, consequently the kinetic energy (momentum), is the same for all ions. Indeed the velocities, *v*, of ions are an inverse function of the square root of their (*m/q* or *m/z*) values:

$$v = \sqrt{\frac{2qV}{m}}$$

Thus those ions with the lowest *m/z* will travel fastest, dispersed into packets of isomass ions, and arrive at the detector first, followed by the sequential arrival of ions with successively higher *m/z*. The time of arrival of an ion, in a flight tube of length L (ca. 100 cm in length) is given by

$$t = \frac{L}{v} = L\sqrt{\frac{m}{2qV}}$$

In conclusion, the measured arrival times of all ions provides a time spectrum that is converted into a mass spectrum by calibrating the instrument.

A pulsed sources such as MALDI is to be well suited to the TOF analyser, however the quality of its pulsed ion beam is insufficient to obtain the high resolution and high mass accuracy. In order to improve the

resolution and accuracy of TOF-MS two techniques are developed: delayed pulsed extraction and the reflectron.

Delayed pulsed extraction in MALDI-TOF instruments addresses the spatial distribution problem by aligning and concentrating ions at an electronic gate prior to their release into the analyser. After the formation of ions in a MALDI-TOF, the ions are then "lined up" at the delayed extraction grid prior to their release into the analyser tube, with a time of the delay in the 50-750 ns range. Then all ions together are subjected to the same acceleration voltage and have the same distance to travel to the detector. So the use of the delayed extraction grid improves resolution by reducing the spatial differences among the ions and, to some extent, the inhomogeneity of their energy content. However the resolution of the linear TOF instrument is limited by the spreading out of ions that have the same empirical formula and *m/z* value, because ions with the same *m/z* but slightly different energies will travel at different speeds, causing differences in their arrival times at the detector.

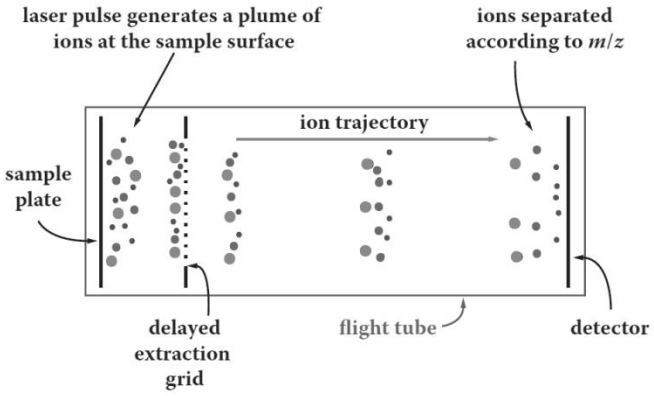

Figure 12: *Schematic description of a delayed pulsed extraction mode in a linear TOF-MS.*

If delayed extraction increases the mass resolution without degradation of sensitivity compared with continuous extraction, it also has limitations. Indeed, delayed extraction complicates the mass calibration procedure.

Another way to improve mass resolution is to use an electrostatic reflector. A reflectron is an energy-correcting device that can minimize the effects of initial spatial and energy spreads. It creates a retarding field that acts as an ion mirror by deflecting the ions and sending them back through the flight tube. A reflectron is a cylinder composed of concentric rings and grids onto which a voltage gradient is applied, thereby creating an electrical field of increasing strength into which the ions enter. The field is set to the same polarity as that of the ions analyzed. Ions entering the electrical field are slowed and their direction is reversed out of the reflectron. The reflectron corrects the kinetic energy dispersion of the ions leaving the source with the same *m/z* ratio.

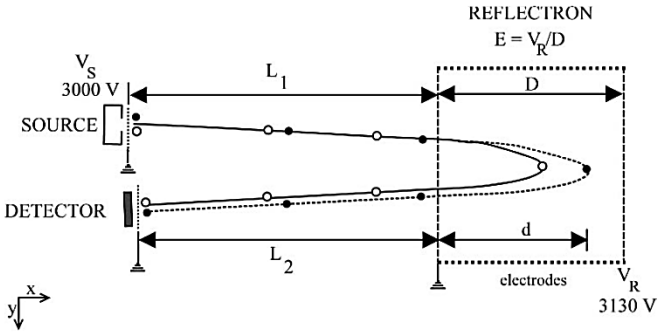

Figure 13: *Schematic description of a TOF instrument equipped with a reflectron.*

Delayed extraction and a reflectron each provide about 10-fold increases in the resolution of MALDI-TOF instruments.

Another technique is developed in order to permits to transform a continuous ion beam from an ion sources, like ESI, into a pulsed process for TOF analyser, this technique is called orthogonal acceleration. The analyser is set at a right angle (orthogonal) to the ion beam emerging from the source. Ion packets are created in a pusher region using a pulsed voltage. The trajectories of the ions entering the analyser have both horizontal and vertical components. The former arise from the direction that ions are traveling from the source, and the latter from the pusher voltage acting at 90°.

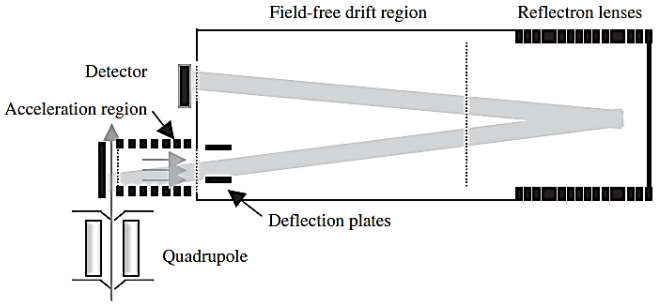

Figure 14: *Schematic description of orthogonal acceleration with linear mass analyser.*

1.2.4 Orbitrap

At the top end of the resolution scale are the Fourier transform (FT) instruments, including the orbitrap and the ion cyclotron resonance (ICR) analysers. Both these analysers are ion traps; however, unlike the quadrupole-based traps, and indeed any other class of analyser, the analytical cell in FT instruments is also the detector, with the ions being recorded as an image current (also called a transient).

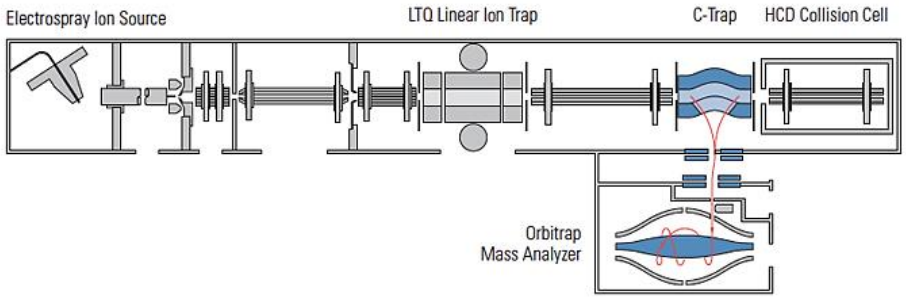

Figure 15: *Scheme of the orbitrap instrument.*

In the most common commercially available orbitrap instrument (Fig. 15), ions generated in the atmospheric pressure ionization (API) ion source are trapped in the LIT mass analyser, where they are analyzed using the instrument's MS and MS^n scan modes. Following this, ions are axially ejected from the LIT, stored in the C-trap, and then pulsed toward the central point of the C-trap arc that coincides with the Orbitrap entrance aperture. It is present also an additional octopole at the rear of the C-trap, used to dissociate precursor ions injected from the C-trap. Ions are then captured in the Orbitrap by rapidly increasing the voltage on the inner electrode.

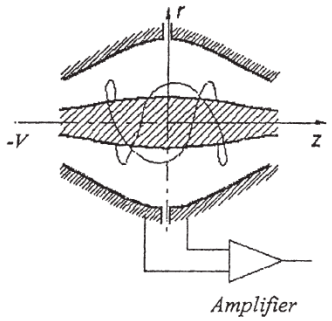

Figure 16: *The electrostatic trap or "orbitrap".*

Indeed, the orbitrap (Fig. 16) consists of an external part that is an electrode having the shape of a barrel cut into two equal parts with a small interval. The central electrode has a spindle shape and his maximum diameter is 8mm and of the outer one 20 mm. The trapped ions undergo rotation around the central electrode and harmonic oscillations along its length. The *m/z* values of the trapped ions are related to the frequencies of their harmonic oscillations. So only the axial frequency is used for mass analysis because it is completely independent of the energy and spatial distribution of the ions, given by the following equation, where ω is the oscillation frequency and k is an instrumental constant:

$$\omega = \sqrt{\frac{q}{mk}}$$

This equation shows that the frequency is directly linked to the *m/q* ratio and is independent of the kinetic energy of the injected ions. After voltages are stabilized, the oscillating ions produce a signal on the outer electrodes, which is detected as an image current by a differential amplifier and converted into a frequency spectrum using a Fourier transform algorithm, yielding the mass spectrum.

The resolution of orbitraps can exceed 200,000. This is less than that of FT-ICR systems, but is still much higher than any other analyser. Other advantages include mass measurement with high accuracy and a dynamic range of $>10^3$. A disadvantage is that the number of ions that can be held in the trap is limited, and this may affect the detection of minor sample components, particularly when there are multiply charged analytes, as all the isotope ions within each of the charge states contribute to the total number of ions.

1.2.5 Ion mobility

Ion mobility (IM) mass spectrometers are hybrid instruments that combine an IM separation system with conventional MS systems. The mobility of ions is measured under the influence of an electrical field gradient and cross-flow of a buffer gas, and depends on ion's collision cross section and net charge. The IMS cell is

placed inside the vacuum chamber between the two mass analyzers of an MS/MS system, operates at mTorr pressures, and consists of a series of plates along which voltage waves travel. Alternating phases of RF voltage are applied to a stacked ring ion guide on which a travelling wave is superimposed (Fig. 17). The cell is filled with nitrogen, flowing in the direction opposite to that of the voltage waves. Entering ions are pushed along in front of the potential wave. Due to the reverse gas flow, those ions with low mobilities experience the most friction. The speeds at which ions with the same *m/z* (e.g., isomers) travel through the nitrogen gas is a function of their three-dimensional shapes. The resistance created by the nitrogen flow results in a reduced ability of the voltage wave to carry ions with larger cross-sectional areas; those ions fall off the back of the wave, only to be pushed on by the next wave.

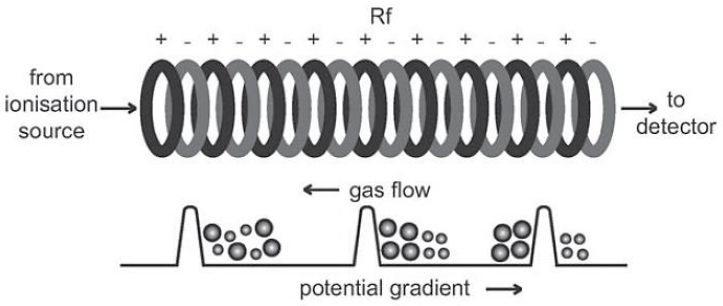

Figure 17: *Schematic representation of a travelling wave IM combined with MS (TWIMS).*[14]

Structures with different cross sections become separated as the retardation mechanism happens successively through the cell. The time scale for mobility separations is in milliseconds; thus, IMS can be combined conveniently with LC-TOF instruments where the LC peaks are seconds wide and the TOF analysers operate on a microsecond scale.

A schematic representation of a commercial travelling wave IMS is show in Figure 18. After the Z-electrospray ionization source, it is present a travelling wave ion guide (TWIG) that is used instead of a classical hexapole or octapole lens. A quadrupole mass analyser for *m/z* selection of ions is followed by three consecutive TWIGs, which function as trapping or collision cell, ion mobility cell and transfer or additional collision cell. A different gas may be introduced in the trap and transfer region as the ion mobility device is in a separate chamber. Finally, ions are mass analysed in the TOF.[15]

With this type of instrument different analysis approaches are possible. For example it is possible to change only the TOF part of the instrument: in the "resolution" mode it is turn off the ion mirror so the ions, pulsed by the pusher, are reflected one time by the reflectron, with a V trajectory; in order to increase the resolution it is possible to turn on the ion mirror so the ions have a W trajectory, called "high resolution" mode, which is represented in the Fig. 18. Even though they will be discussed in the next section, also a large number of interesting possibility in the MS/MS analysis are possible using Electron transfer dissociation (ETD). Considering the "tri-wave" section in the Figure 18 it is possible: 1) to fragment a specific parent in the trap, then to separate the isobaric fragment in the ion mobility and analyze them in the transfer; 2) to select precursor ions in the trap, then separated by ion mobility and finally show fragment ions time aligned to the

respective parent; 3) combine the previously mode together, so to fragment precursor ions in the trap, to separate them by ion mobility and then to fragment them again in the transfer.

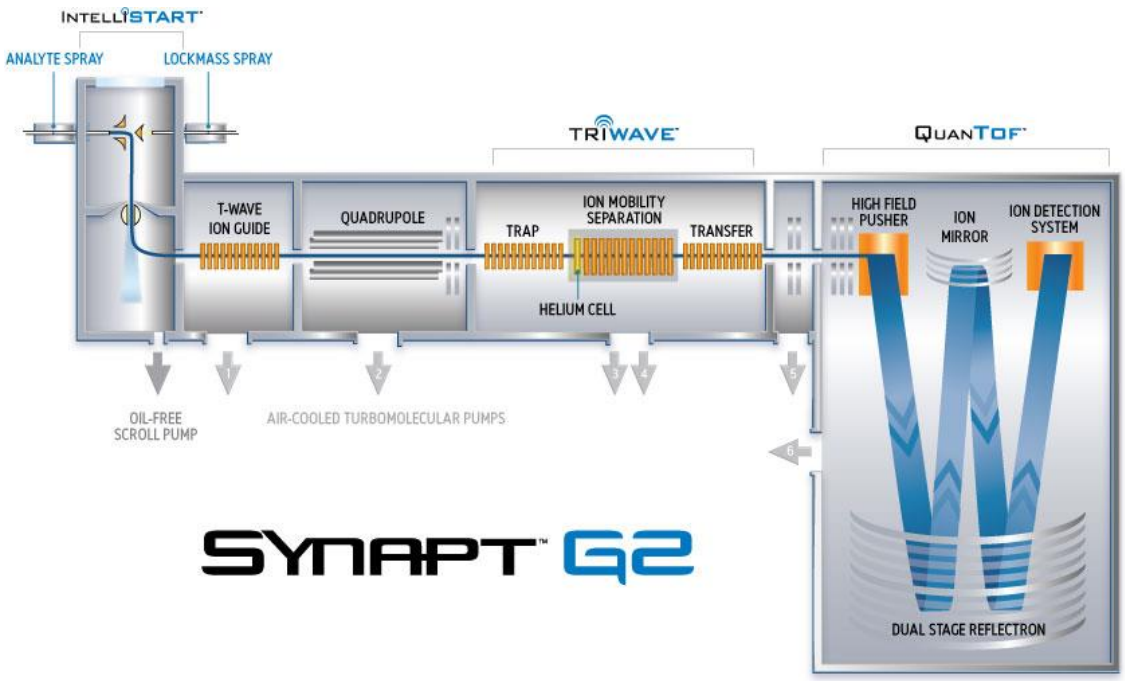

Figure 18: *Schematic representation of a commercially available Q-IMS-TOF.*

1.2.6 Tandem mass analysers

The need to investigate not only the mass but also the structure of ions was an important factor in the development of multianalyser mass spectrometers. There are several formats of MS/MS systems based on combinations of quadrupole, ion trap (Q and FT), and TOF analysers. Combinations that use the same type of analysers are tandem instruments, whereas different separation methods are used in sequence in hybrid systems. The fundamental process of MS/MS (in a tandem mass spectrometer) is that a particular precursor ion is fragmented (decomposed) into a smaller product ion accompanied by the loss of a neutral fragment. By far the most common means of ion activation and dissociation of ions of organic and bioorganic molecules is collision-induced dissociation (CID). The CID process consists of two steps: the first is very fast (10^{-14} to 10^{-16} s), the fast-moving mass-selected precursor ions are excited to higher-energy states by collisions with atoms of an inert gas such as helium or argon, during this excitation process a fraction of the ion translational energy is converted into internal energy, bringing the ion into an excited state. The second step is the unimolecular decomposition of the activated ion.

- First step of CID (collision activation): $m_p^+ + N \rightarrow [m_p+]^* + N'$
- Second step of CID (unimolecular dissociation): $[m_p^+]^* + m_n$

In the first reaction m_p^+ is the mass-selected precursor ion and N and N' are pre- and post-collision forms of the neutral target, in the second reaction m_1^+ and m_n are fragments.

CID can be performed in either a high- or a low-energy regime. In high-energy collisions, implemented primarily in magnetic sector and TOF tandem instruments, ions have translational energies in the keV range

(3 to 10 keV). In low-energy collisions, implemented in quadrupole and ion trap based tandem instrument, ions have energies above 200eV.

The CID process (in positive ion mode) is effective only for protonated molecules. For example, if the *m/z* selected in the first analyser corresponds to a sodiated species, $[M + Na]^+$, then the stability of these ions results in either no fragmentation, regardless of how much energy is added, or that a point is reached where the acquired energy leads to the complete disintegration of the ion.

Two among the others alternative techniques to obtain fragmentation from selected ions, are called Electron transfer dissociation (ETD) and electron capture dissociation (ECD). These techniques are important because they provide structural information that is difficult to obtain, especially with peptides or polymers. ETD is used with QqQ, QTOF, and orbitrap instruments. Reagent species, such as fluoranthene, anthracene and nitrosobenzene, are activated by conversion to their respective radical anions in a corona discharge. The radicals are then mixed with the analyte (that has been ionized using ESI), resulting in the transfer of an electron from the reagent to the analyte. The transfer of an electron induces fragmentation in the peptide backbone to produce sequence-specific c- and $z^{\bullet}$-type ions. ECD, used with FT-ICRMS instruments, is an alternative way to produce fragmentations similar to those obtained by ETD. The mechanism of ECD involves an excitation of the mass-selected protonated ion by the capture of a low-energy (<0.2 eV) electron and subsequent fragmentation of the resulting odd-electron ion $[M + nH]^{(n-1)+\bullet}$.

The four main scan modes available using tandem mass spectrometry are represented in Figure 19, but many other MS/MS scan modes are possible.

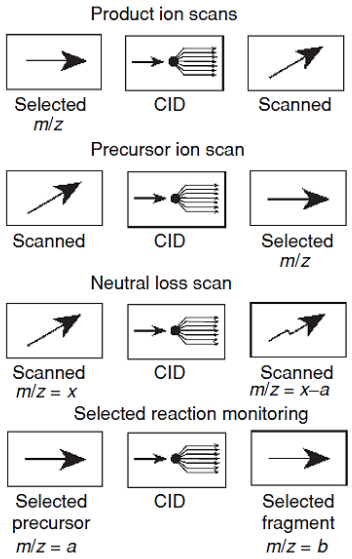

Figure 19: *Representation of four scan modes of tandem mass spectrometry.*

1. The product ion scan: provide structural information on ions with a specified *m/z*, selected in Q1. It consists of selecting a precursor ion of a chosen mass-to-charge ratio and determining all of the product ions resulting from collision-induced-dissociation CID. To acquire this spectrum, the first mass analyser is set to transmit only the precursor on chosen, and the second mass spectrometer is scanned over a required *m/z* range.

2. The precursor ion scan: determine the precursor ions that yield the product ion (*m/z*) selected in Q3. The spectrum is obtained by adjusting the second mass spectrometer to transmit a chosen product ion and scanning the first mass analyser over a certain *m/z* range to transmit only those precursor ions that fragment to yield the chosen product ion.

3. Neutral loss scan: consists of selecting a neutral fragment and detecting all the fragmentations leading to the loss of that neutral. To obtain this information, both mass analysers are scanned simultaneously, but with a mass offset that correlates with the mass of the specified neutral.

4. Selected reaction monitoring (SRM): is used for quantification. Improved signal:noise ratios at the selected *m/z* are observed in Q3. Conceptually, this scan mode is similar to the product-ion scan, but in the Q3 there is no scan. To obtain this spectrum the ions are selected by the first mass analyser and they are only detected if they produce a given fragment, by a selected reaction.

1.3 The role of mass spectrometry in the bioanalysis of lipid mediators

Historically considered as key structural components of cell membranes, lipids have been recognized recently as protagonists in the mediation of different signals that can regulate many physiological processes. These bioactive lipids belong mainly to two classes of compounds: N-acylethanolamines (NAEs) and acylesters.[16] Within the first group, the most studied representatives are arachidonoylethanolamide (AEA), also called anandamide, palmitoylethanolamide (PEA), oleoylethanolamide (OEA), together with a number of other less characterized NAEs.[17] In the second group, mainly composed of intermediates in triacylglycerol and phospholipid metabolism, among 2-monoacylglycerols (MAGs), the most important are 2-arachidonoylglycerol (2-AG), its isomer 1-AG and 2-oleoylglycerol (2-OG).[18,19]

2-AG and AEA both act on cannabinoid receptor type 1 (CB_1) and type 2 (CB_2) and for this reason are known as endocannabinoids (eCBs), meanwhile neither PEA nor OEA activate the cannabinoid receptors, but they share catabolic, and some metabolic, pathways with AEA.[20,21] PEA and OEA have been found to be agonists at peroxisome proliferator-activated-receptor alpha (PPAR-α)[22,23,24], and they influence AEA metabolism. For their structural resemblance with the true endocannabinoids AEA and 2-AG, combined with their lack of effects on the two cannabinoid receptors, some of NAEs, such as the over mentioned PEA and OEA and MAGs, such as 2-OG, are also known as non-endocannabinoid, or endocannabinoid related compounds (ERC). Strong pharmacological and biochemical evidences have demonstrated that eCBs and related molecules are also able to interact with non-CBR targets, increasing the complexity of the endocannabonoid system (ECS) and of the molecular pathways trigged thereof. In particular, the best known non-CBR target of eCBs is the transient receptor potential vanilloid type 1 (TRPV1) channel, which is activated by both AEA[25] and 2-AG.[26] Other potential receptors activated by eCBs are peroxisome proliferator-activated receptor (PPAR)α and γ,[27] and the orphan G protein-coupled receptor GPR55.[28]

Structurally, AEA and 2-AG possess an arachidonic acid chain in their structure which is conjugated to an ethanolamine molecule through an amide bond and to a glycerol molecule through an ester bond, respectively. In the structural analogs of AEA and 2-AG that cannot activate the CBRs, the arachidonic acid

(20:4*n*-6) is substituted with shorter-chain unsaturated fatty acids such as oleic acid (18:1*n*-9) and saturated fatty acids such as palmitic acid (16:0), as it can be seen in Fig. 20.

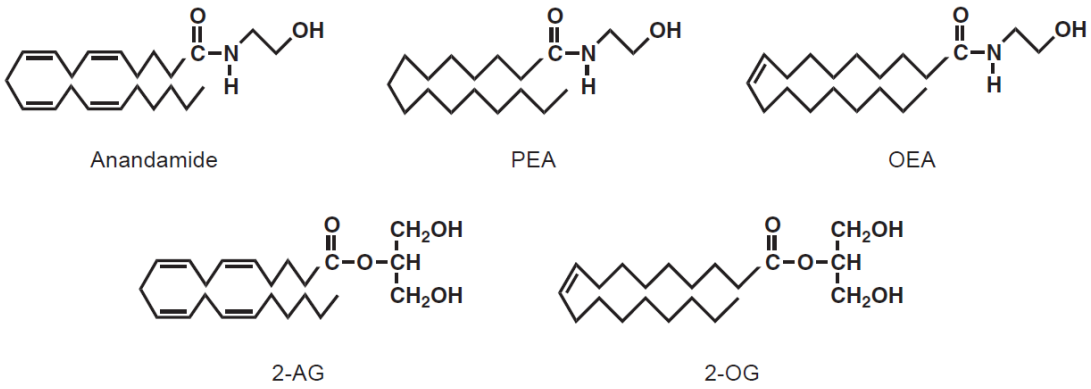

Figure 20: *Chemical structure of endocannabinoids and related compounds.*

The two groups of lipids (MAGs and NAEs) are apparently found in all eukaryotic organisms, but while 2-MAGs are abundantly and ubiquitously present as intermediates in triacylglycerol (TAG) and phospholipid turnover,[29,30] NAEs are less well-known, although they are also present in very small amounts in most eukaryotes such as yeast, slime molds, plants, insects and mammals. Although both the NAEs and the 2-MAGs have been known for more than 50 years as lipids in biological systems, their biology is still not fully understood and new physiological as well as pharmacological roles are currently revealing themselves at a high frequency.[31]

Endocannabinoids (2-AG, AEA) and related N-acylethanolamides (PEA, OEA) are known to play an essential role in many physiological processes, including energy metabolism, immune function and both central and peripheral nervous system function.[32] They are also implicated in a considerable number of pathophysiological conditions such as cardiovascular disorders,[33] systemic inflammation and neuroinflammation,[34,35] obesity and the metabolic syndrome,[36] cancer[37] and mental disorders such as depression[38] and schizophrenia.[17]

The biological actions of eCBs and congeners are controlled through not yet fully characterized cellular mechanisms, that include key agents responsible for: 1) AEA and 2-AG synthesis, like the *N*-acyl-phosphatidylethanolamine-hydrolyzing phospholipase D (NAPE-PLD) and the *sn*-1-specific diacylglycerol lipase (DAGL), respectively; 2) their degradation, like the enzymes fatty acid amide hydrolase (FAAH) and monoacylglycerol lipase (MGL), respectively.

Remarkably, during the last few years multiple pathways have been described for eCBs metabolism, especially for NAEs.[16] PEA and some other NAEs including OEA, as already said, as primary biological effects are assumed to be mediated via other receptors including the PPAR-α, TRPV1 and GPR55; there may be other yet unidentified targets, as well.

Bioactive Lipids	Molecular Targets	Biosynthetic Enzymes	Catabolic Enzymes
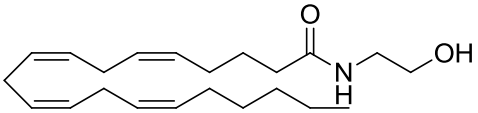 AEA	CB1 [39] CB2 [39] TRPV1 [25] PPAR-α [27] PPAR-γ [27] GPR55 [28]	NAT [21] iNAT [40,74,75] NAPE-PLD [41] ABHD4 [42,43,44] Lyso-PLD [42,43,44] GDE1 [42,43,44] PTPN22 [42,43,44]	FAAH-1 [79] FAAH-2 [45] NAAH [80] LOXx [46] COX-2 [47,48] CytP450 [49]
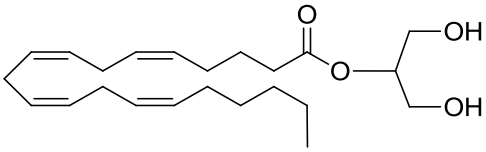 2AG	CB1 [39] CB2 [39] TRPV1 [26]	PLCβ [50,51] DAGLα [52] DAGLβ [52]	MGL [53] FAAH-1 [79] ABHD6 [70,71] ABHD12 [70,71] COX-2 [47,48]
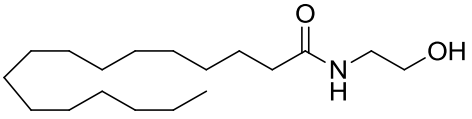 PEA	PPAR-α [54] GPR55 [55] GPR119 [56]	NAT [21] iNAT [40,74,75] NAPE-PLD [41] Lyso-PLD [42,43,44] GDE1 [42,43,44] PTPN22 [42,43,44]	FAAH-1 [57] FAAH-2 [80] NAAA [58]
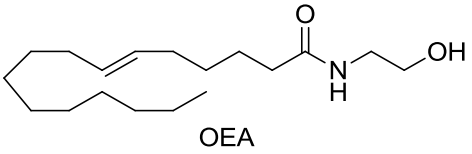 OEA	PPAR-α [54] GPR55 [55] GPR119 [56]	NAT [21] iNAT [40,74,75] NAPE-PLD [41] ABHD4 [42,43,44] Lyso-PLD [42,43,44] GDE1 [42,43,44] PTPN22 [42,43,44]	FAAH-1 [57] FAAH-2 [80] NAAA [58]
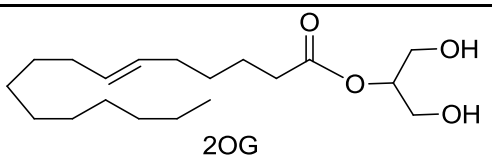 2OG	GPR119 [56]	PLCβ [50,51] DACLα [52] DACLβ [52]	MGL [53] FAAH-1 [57]

Table 2: *eCBs and eCBs-like compounds, their molecular targets, biosynthetic and catabolic enzymes.*

Due to the complexity related to the high number of these lipid mediators and of their mutual interactions, understanding eCBs and eCB- related compounds pharmacology, physiology and pathophysiology requires a deep investigation of these classes of lipids with analytical tools possessing a high degree of sensitivity, specificity and accuracy. It is critical to develop analytical techniques that can simultaneously measure several eCBs and entourage compounds derived from biological tissues under normal and pathological conditions. Furthermore, the development of easily accessible, accurate, and reproducible analytical techniques to monitor eCBs and related lipids will aid preclinical and clinical testing of new chemical entities (NCEs) able to modulate the eCB system, such as FAAH or MGL inhibitors.

Mass spectrometry has proven to be an essential technique for the analysis of anandamide and endocannabinoid-like compounds. More in general, quantitation of pharmaceutical compounds, their metabolites and endogenous metabolites in biological matrices, such as plasma and urine, is nowadays

mostly accomplished by liquid chromatography coupled with atmospheric pressure tandem mass spectrometry (HPLC-MS/MS).[59] Similarly, liquid chromatography coupled to high resolution mass spectrometry detection has proven to be an essential analytical technique to evaluate the interactions of NCEs with biological targets, such as proteins, and to study the conformational effects produced on macromolecular targets by inhibitor binding. Some of these mass spectrometry applications will be presented and discussed in the following sections of the present Ph.D. thesis. An endocannabinoid-related substance, palmitoylethanolamide, together with a set of its prodrug derivatives and the main enzyme responsible of the metabolism of the endocannabinoid 2-arachidonoylglycerol, monoacylglycerol lipase (MGL), and its allosteric inhibitors have been deeply characterized by means of low and high resolution mass spectrometry techniques and will be described in details in the following chapters.

2. Endocannabinoids and endocannabinoid-related compounds

2.1 The endocannabinoid system (ECS)

Endocannabinoids are signaling lipids involved in a wide variety of biological processes, named after the plant that led to their discovery, *cannabis sativa*. Together with their receptors and enzymes involved in their synthesis and breakdown, they all together constitute the 'endocannabinoid system' (ECS). According to the current classification by the International Union of Basic and Clinical Pharmacology (IUPHAR), the term endocannabinoid is officially restricted to those compounds with significant affinity at the cannabinoid receptors CB_1 and CB_2.[60] Endocannabinoids and their receptors are found throughout the body: in the brain, organs, connective tissues, glands, and immune cells. The ECS is perhaps the most important physiological system involved in establishing and maintaining human health.

In the central nervous system (CNS) the ECS regulates many physiological processes including neurogenesis, axon guidance, neuronal migration and synaptic plasticity. The mechanisms of endocannabinoid signaling in the nervous system differ considerably from those of the classic neurotransmission systems (e.g., cholinergic, aminoacidergic, and monoaminergic). In the classic model of neurotransmission, depolarization of the presynaptic neuron by an action potential results in the release of neurotransmitters, which then traverse the synaptic cleft to bind and activate their cognate receptors on the postsynaptic neuron.[61] In contrast, the signaling mechanism of the ECS requires a retrograde operation. Indeed, the stimulation of the postsynaptic neuron induces the biosynthesis of eCBs, that are then carried to activate their receptors by a mechanism not yet completely known: it is then possible to inhibit the release of both excitatory and inhibitory neurotransmitters. As already said, two subtypes of cannabinoid receptors, termed cannabinoid-1 (CB_1) and cannabinoid-2 (CB_2) receptors, have been cloned.[62] Both CB_1 and CB_2 receptors belong to the superfamily of G protein–coupled receptors (GPCRs), they are receptors with seven transmembrane helices G-protein coupled with a glycosylated extracellular N-terminal domain and an intracellular C-terminal domain. They are expressed in the developing and adult brain including neural progenitors and their progeny. The two cannabinoid receptors exhibit 48% amino acid sequence identity. Both receptor types are coupled through G-proteins to adenylyl cyclase and mitogen-activated protein kinase (MAPK).[63] Aberrant eCB signalling is associated with a large number of neuropsychiatric disorders and neurodegenerative diseases. Components of eCB signalling system are considered potential therapeutic targets for many conditions such as anxiety, depression, schizophrenia, Alzheimer's and Parkinson's diseases.[64]

Although CB_1 receptors are expressed by certain non-neuronal cells and tissues, for example the pituitary gland, immune cells and reproductive tissues, they are most abundantly expressed in the central nervous system (CNS), most densely in motor and limbic regions, and in areas that are involved in pain transmission and modulation, such as periaqueductal grey (PAG), rostral ventromedial medulla (RVM), spinal cord dorsal horn, and in the periphery. Inhibition of neurotransmitter release is their major function, the activation of CB_1 receptors leads to a decrease in cyclic adenosine monophosphate (cAMP) accumulation and hence to

inhibition of cAMP-dependent protein kinase (PKA). CB_1 activation leads to stimulation of mitogen-activated protein (MAP) kinase activity, which is a mechanism by which cannabinoids affect synaptic plasticity, cell migration, and possibly neuronal growth. CB_1 receptors are also coupled, through $G_{i/o}$ proteins, to several types of calcium and potassium channels. As CB_1 activation acts to inhibit neurotransmission, the ultimate outcome of endocannabinoid signaling depends on the nature of the participating cells. If CB_1 is activated on glutamatergic neurons, for instance, endocannabinoid signaling will be overall inhibitory, whereas if CB_1 activation takes place on GABAergic neurons, the net result will be "disinhibitory" (or excitatory).

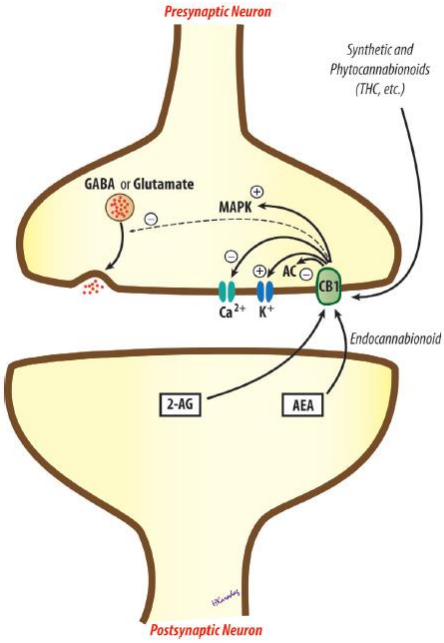

Figure 21: *Transduction mechanisms for cannabinoid CB1 receptors. AC, adenylate cyclase GABA, gamma-aminobutyric acid; MAPK, mitogen-activated protein kinase; THC, tetrahydrocannabinol*.

CB_2 receptors, on the other hand, are found mainly, but not exclusively, outside the CNS, predominantly in peripheral tissues with immune functions, and most densely in the spleen.[65] It seems that the CB_2 receptor is part of a general protective system: indeed CB_2 receptors are expressed in almost all human peripheral blood immune cells with the following rank order of mRNA levels: B cells > NK cells > monocytes > PMNs > T cells.[66] This may explain the inhibitory effects of *cannabis* on the functions of this system, moreover it is interesting to notice that lipid endocannabinoid signaling through CB_2 receptors may represent an example and/or part of such a protective system.

Both AEA and 2-AG are able to stimulate both cannabinoid receptor subtypes, however 2-AG possesses equal selectivity for the CB_1 and CB_2 receptors, while AEA is characterized by a greater selectivity for the CB_1 receptor. In addition, similar to the THC, AEA is a partial agonist to the CB_1 receptor in vitro, whereas 2-AG is a total agonist.[67] Basal levels of 2-AG in the brain are approximately 2 orders of magnitude higher than the levels of anandamide.[68]

These two principal ligands of ECR are not stored within cells, but they are synthesized on demand and when their action is ended, they are hydrolyzed by enzymatic action by two hydrolases in particular: the fatty acid amide hydrolase (FAAH) and the monoacylglycerol lipase (MGL).

2.1.1 2-arachidonoylglycerol (2-AG): biosynthesis and metabolism

It is generally accepted that 2-AG is formed in postsynaptic neurons in response to depolarization and stimulation of $G_{q/11}$-coupled receptors. The resultant 2-AG is released, and mediates retrograde synaptic suppression through CB_1 receptors at presynaptic terminals. There are several pathways for 2-AG generation. The main pathway is the combination of phospholipase C (PLC) and diacylglycerol lipase (DAGL). As the first step, PLC hydrolyzes 2-arachidonoyl-phosphatidylinositol (PtdIns) and produces arachidonic acid-containing diacylglycerol. Then, 2-AG is produced from diacylglycerol by the action of DAGL. The most abundant PtdIns molecule in mammalian tissues is 1-stearoyl-2-arachidonoyl-PtdIns, enabling the effective generation of 2-AG over other MAGs. Others possible pathways for 2-AG generation so far proposed include the sequential reactions by phospholipase A_1 (PLA_1) and lysoPI-specific PLC, the conversion from 2-arachidonoyl lysophosphatidic acid to 2-AG by phosphatase, and the formation from 2-arachidonoyl phosphatidic acid through 1-acyl-2-arachidonoylglycerol. The biosynthetic pathways for 2-AG might be different in different tissues and cells.[69]

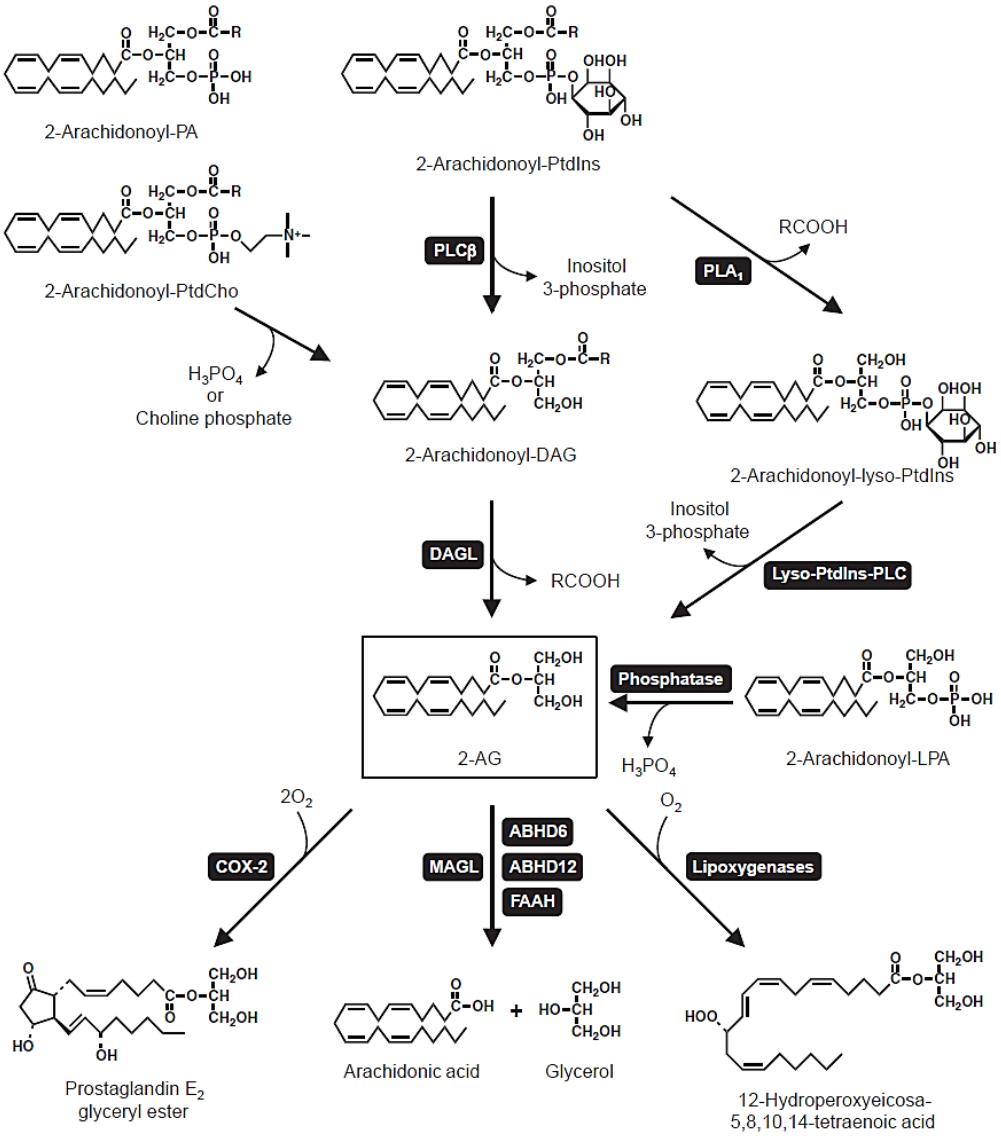

Figure 22: *Metabolic pathways of 2-AG.*

The catabolic pathway of 2-AG is performed mainly by a monoacylglycerol lipase (MGL). This enzyme, which is a serine hydrolase with the classic catalytic triad Ser-Asp-His, catalyzes the hydrolysis of this glycerol ester and release free arachidonic acid. It is known that MGL mRNA is present in various organs including brain. MGL is considered the main catabolic enzyme of 2-AG, which is responsible for the ~85% of its degradation, and the remaining 15% is mostly catalyzed by two additional serine hydrolases, α/β-hydrolase domain 6 (ABHD6) and 12 (ABHD12).[70] MGL, ABHD6 and ABHD12 show a distinct distribution within the CNS, that is suggestive of a different physiological function of these three enzymes in regulating 2-AG signaling.[71] A second pathway of degradation involves the enzymes cyclooxygenase (COX-2) and lipoxygenase (LOX), which induce oxidation of the arachidonic acid moiety of the endocannabinoid.

2.2 Endocannabinoid-related compounds

AEA belongs to a class of naturally occurring molecules, NAEs, known and studied for a long time. One of its members, palmitoylethanolamide (PEA), was first reported almost 50 years ago in humans, yet its physiological relevance remained under debate as its mechanism of action was different from the activation of cannabinoid receptor subtypes. Indeed, PEA, together with OEA and other endocannabinoid-like compounds sharing a structural resemblance to the endocannabinoids are active players in the endocannabinoid system, where they can potentiate the effect of eCBs at their receptor targets by competitively inhibiting their hydrolysis, or by allosterically modulating their receptor binding: the so-called "entourage effect". The anti-inflammatory agent PEA and the appetite-suppressor OEA are some of the most studied endocannabinoid-like compounds.

Their biological activity involves the activation of PPAR-α and TRPV1, although some of their actions are prevented by CB_1 antagonists. OEA is the endocannabinoid-like compound with the highest affinity for PPAR-α, but the antinociceptive properties of OEA are exercised also through a PPARα-independent mechanism. OEA, PEA and 2-OG can activate GPR119, which is expressed in human and rat pancreas, suggesting that the effects of OEA on food intake may be mediated via this receptor. GPR55, as previously said, is engaged as well by OEA and PEA. It was reported that the endogenous levels of these endocannabinoid-like compounds (PEA, OEA) are affected by different dietary regimens, with different hits in the brain compared to peripheral tissues.[72] Since PEA, OEA and other saturated NAEs more or less stimulate the same receptors their pharmacological functions are often also closely related and include regulation of food intake as well as anti-inflammatory effects.

It is important to note that PEA, due to the lack of adverse side-effects at central CB_1 receptors holds potential for the development of innovative medicines, and it is currently marketed as a dietary supplement to cure neuropathic and pelvic pain.

2.2.1 N-acylethanolamides: biosynthesis and metabolism

As already said, NAEs constitute a diverse set of endogenous mediators, acting at different receptors and exerting a variety of effects. AEA is an endocannabinoid, classically exerting its actions by activation of two

G protein-coupled receptors (GPCR), the CB_1 and CB_2 cannabinoid receptors. It is also a known ligand for the ion channel transient receptor potential vanilloid receptor (TRPV1) and the PPAR nuclear receptors. OEA is an anorexigenic compound, known to exert its actions through activation of PPAR-α, GPR119 and TRPV1. PEA is a known anti-inflammatory compound with analgesic, neuroprotective and antiallergic properties. NAEs are synthesized and released in cells on demand, according to specific physiological and pathological stimuli, such as neuronal depolarization, and their endogenous levels are regulated primarily by the enzymes responsible for their synthesis and for their degradation. However, the mechanisms governing the formation of PEA and OEA differ from those involved in the production of anandamide in two important aspects. First, many cell types in the body, including dorsal root ganglia (DRG) neurons and skin cells, generate substantial amounts of OEA and PEA even in the absence of external stimuli, which are required instead to trigger on-demand anandamide release. Second, many pro-inflammatory stimuli dampen the production of OEA and PEA even as they trigger anandamide formation in the same cell.

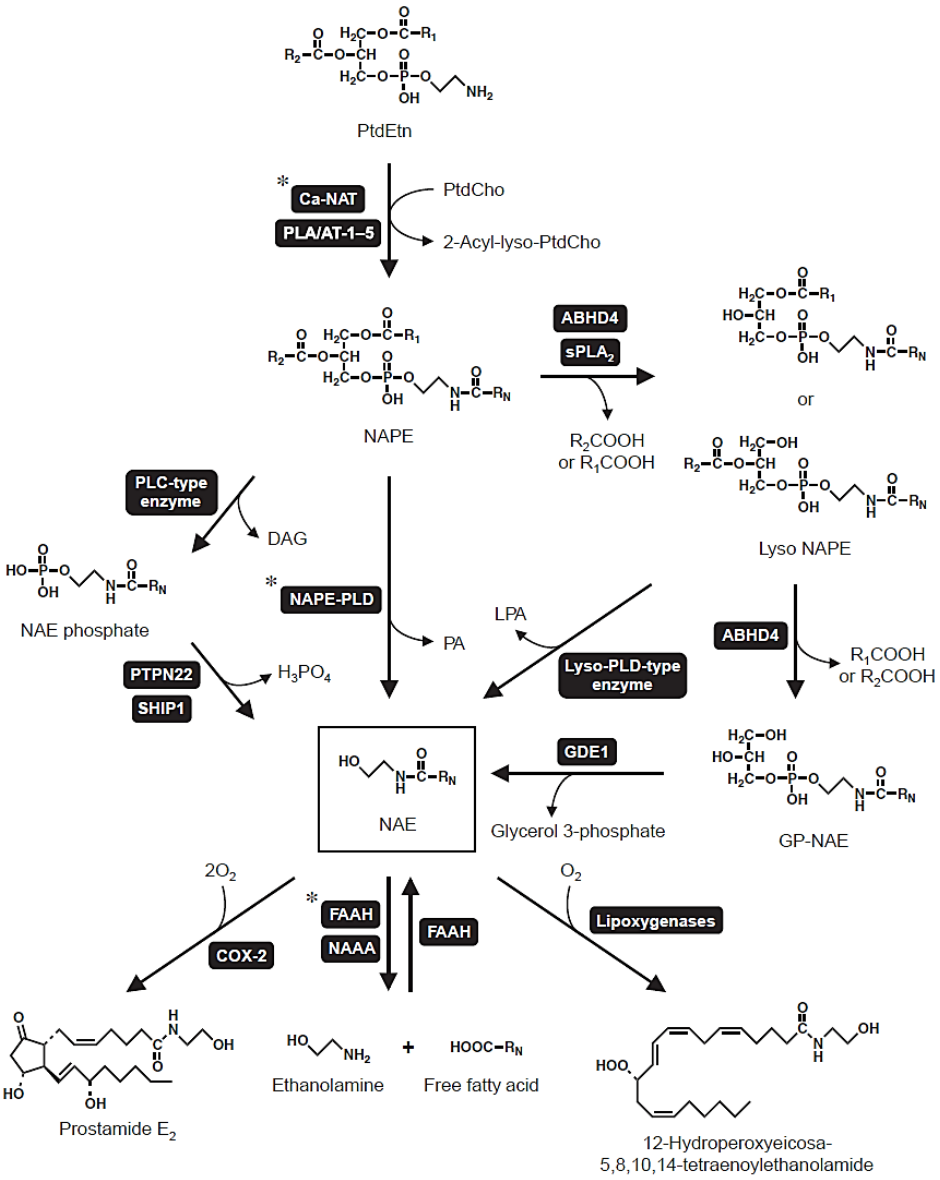

Figure 23: *Metabolic pathways of NAEs. Asterisks indicate the enzymes included in the "classic" pathway.*

There are five known enzymatic pathways described to synthesize NAE, three of them with NAPE as a precursor, and the most important of these involving the enzyme NAPE-phospholipase D (NAPE-PLD). The remaining two pathways include a reaction between ethanolamide and fatty acyl-S-CoA and a reaction between a fatty acid and ethanolamine, but they are believed to have no relevance *in vivo*[73] (Fig. 23).

The so called "classic biosynthetic route" consists of two enzymatic reaction, involving a Ca^{2+}-dependent *N*-acyltransferase (Ca-NAT) and a *N*-acyl-phosphatidylethanolamine-hydrolyzing phospholipase D (NAPE-PLD). The first reaction is a fatty acyl chain transfer from membrane phospholipids to a phosphatidylethanolamine, resulting in the formation of *N*-acylphosphatidyletanolamine (NAPE), by the first enzyme, a yet-unidentified Ca-NAT or a Ca^{2+}-independent counterpart (iNAT).[74] The NAT activity is potently stimulated by Ca^{2+}, and generally thought to be the rate-limiting step in NAEs production. Being the palmitoyl and oleoyl acids preferentially incorporated in *sn*-1 position, NAT preferably produces PEA and OEA rather than AEA. Instead, iNAT removes a fatty acyl group from both the *sn*-1 position and the *sn*-2 position (where arachidonic acid is most abundant) of phosphatidylcholine (PC), that is the acyl donor.[75] The second reaction is catalyzed by the membrane protein NAPE-LPD, which is an enzyme that belongs to the metallo-β-lactamase family. Indeed, this PLD is an isoform different from others phospholipases D: it is the only enzyme that can produce NAEs starting from NAPE.[76] Accumulated evidence indicates, however, the existence of additional pathways for NAEs formation. Indeed, through the use of knock-out mice several enzymes and metabolites involved in the NAPE-PLD-independent biosynthesis of NAEs have been identified and characterized, as it can be seen in Fig. 23. Apart from all of these pathways, AEA may be formed also by the condensation of free arachidonic acid with ethanolamine in the reverse reaction of FAAH[77] and could be spontaneously formed from arachidonoyl-CoA and ethanolamine.[78] Newly formed AEA acts near its sites of production, as an autocrine or paracrine messenger, and is rapidly eliminated through a process consisting of carrier-mediated transport into cells followed by intracellular breakdown to arachidonic acid and ethanolamine.

The catabolic pathway of NAEs is performed mainly by fatty acid amide hydrolase (FAAH).[79] FAAH-1 is an intracellular membrane-bound serine hydrolase with Ser-Ser-Lys as catalytic triad that is active at neutral and alkaline pH. This enzyme is present mostly in the brain, with a subcellular distribution that overlaps on that of CB_1 receptors. Some years after the characterization of FAAH-1, two other hydrolases able to hydrolyze NAEs were reported: an isoform of FAAH (FAAH-2) and a lysosomal cysteine hydrolase termed N-acylethanolamine-hydrolyzing acid amidase (NAAA), [80] that is active at acidic pH (4.5–5) and inactive at alkaline pH. FAAH-2 is permanently-associated with adiposomes, where AEA can be stored, and was localized also on lipid droplets. FAAH-1 and -2 share limited sequence identity (~20%), while no homology exists between them and NAAA, an enzyme that shows a substrate preference towards other saturated or monounsaturated NAEs, especially PEA. NAAA is not upregulated when FAAH is out of function. There is also evidence of oxidative endocannabinoid metabolism by cyclooxygenases (COX), lipoxygenases (LOX), and P450 cytochromes.[81] COX-2 is responsible for the oxidation of AEA to oxygenated derivatives of prostaglandins, namely prostaglandin ethanolamides (prostamides). 12-LOX and 15-LOX generate structural

derivatives known as 12-hydroperoxyanandamide and 15-hydroperoxyanandamide. The metabolism of endocannabinoids by P450 cytochromes has been rarely studied, but non-oxygenated AEA derivatives may be generated through this pathway. At least 20 different AEA products may be generated in reactions mediated by cytochromes P450, including epoxidation, o-hydroxylation, lipoxigenation, and oxidation.[82,83]

3. Palmitoylethanolamide: a prodrug strategy for PK optimization

3.1 Introduction

Palmitoylethanolamide (PEA) appears to exist in every mammalian cell at low levels, i.e. a few hundred pmol per gram tissue. As already detailed in the previous chapter, the tissue levels of PEA are finely regulated by the balance between the enzymatic formation from different anabolic pathways and its degradation by the enzymes fatty acid amide hydrolases (FAAH-1 and FAAH-2) and N-acylethanolamine acid amidase (NAAA). The receptors mediating the effects of PEA had been elusive until recently, with increasing evidence that the anti-inflammatory and nociceptive effects of PEA are mediated, at least in part, by PPAR-α activation. It was initially hypothesized that PEA could bind to the CB_2 receptor. However subsequent studies demonstrated a different phenomenon, called "entourage effect". It was demonstrated that PEA could alter AEA metabolism, competing with AEA for FAAH-mediated hydrolysis, thus causing an increase in AEA levels, which would then activate the CB2 receptors. Moreover PEA can allosterically interact with transient receptor potential vanilloid type 1 (TRPV1), increasing AEA affinity for this receptor.[84]

PEA possesses a large spectrum of pharmacological properties: anti-inflammatory activity, analgesia, anti-epilepsy and neuroprotection, inhibition of food intake, reduction of gastrointestinal motility, inhibition of cancer cell proliferation, and protection of the vascular endothelium in the ischemic heart.[22]

PEA is currently marketed as a dietary supplement to cure neuropathic (Normast®) and pelvic (Pelvilen®) pain, and is one of the main components of a cream (Physiogel®) used for inflamed or irritated skin of subjects with atopic dermatitis.

The main role of PEA in inflammation and nociception has been largely documented. PEA has been shown to reduce inflammatory pain *in vivo* in a variety of animal models.[85,86,87] The anti-inflammatory actions of PEA, leading to a reduction of peripheral and central sensitization, are mediated by neuronal and non-neuronal cells. The latter comprise glia (in particular, astrocytes and microglia) as well as peripheral and central mast cells. In this context, PEA can function in maintaining cellular homeostasis, not only by inhibiting mast cell activation[88] in the CNS and regulating microglial cell activity, but also by blocking peripheral mast cell activation and hence signaling pathways from the periphery to the brain.[89]

One of the first preclinical studies which supported the view of PEA as an endogenous anti-inflammatory agent, showed that PEA, if orally given, was able to reduce dose-dependently (0.1–10 mg/kg) the carrageenan-induced hyperalgesia, as well as carrageenan-, formalin- and dextran-induced edema in rodent models.[88] In different studies it was clear that the anti-inflammatory effect of PEA was not accompanied by tolerance following repeated administration of high doses; the lack of any side effect has also been reported in several published clinical studies.[90] A veterinary dermatological trial in 2001 reported that one month-treatment with PEA resulted in decreased pruritus, erythema and alopecia in cats affected with hypersensitivity skin disorders.[91]

3.2 Analytical challenges for detecting PEA in biological samples

Considering the potential involvement of N-acylethanolamines in the regulation of diverse patho-physiological processes, it is important to develop a method for the accurate identification and precise quantification of these molecules. The concentrations of NAEs in animal tissues can vary a lot depending on the species, sex, age and physiological status; furthermore, it is important to maintain the treatment protocol of the sample constant, as the tissutal levels of NAEs may also change as a consequence of a different tissue manipulation.

The developments in bio-analysis, in particular in the field of liquid chromatography coupled to tandem mass spectrometry, have resulted in an increasing number of methods to analyze N-acylethanolamines in biological matrices. Indeed, due to their low tissue concentrations, proper quantification of NAEs is challenging and requires carefully optimized sample extraction procedures. PEA is present in cells, but can also be detected in plasma where it is likely bound to albumin, with reported concentrations in the 1-10 ng/mL range for plasma, and 10-100 ng/g for tissues. Despite the relatively high amount of papers reporting PEA tissutal and plasma concentrations, there are not adequate validation data or performance indicators on sample clean-up procedures and also the protocols of quantification have not always been described in details. In general, however, liquid chromatography coupled to tandem mass spectrometry is the analytical technique of choice, at least in more recent papers, whereas solvent-based sample extraction is the most employed method of sample preparation.

A brief summary of the methods used for the quantification of PEA is reported in Table 3.

	Amount of Material	**Solvent Extraction**	**SPE**	**Species**	**Concentration**
Plasma	50 µL-1 mL	toluene	/	human	
	1 mL	acetonitrile	C8	human	1.4 ng/ml
	1 mL	acetone, chloroform-methanol	/	human	8.4 ng/mL blood (from serum)
	50 µL	acetonitrile	/	human	1.1-3.5 ng/mL
	400 µL	acetone	/	human	1.8-2.1 ng/mL
	0.5 mL	/	HLB	human	5.1 ng/mL
	0.5 mL	toluene	/	human	2.2-8.4 ng/mL
Adipose tissue	100 mg	acetonitrile	/	mouse	38-60 ng/g
	ND	chloroform/methanol	silica	human	30-120 ng/g
Liver	100 mg (freeze-dryed)	acetonitrile	C8	mouse	141-284 ng/g
	ND	9:1 ethylacetate-hexane, chloroform	silica	rat	~15 ng/g
Intestinal tissue	100 mg (freeze-dryed)	acetonitrile	C8	mouse	38-270 ng/g
	ND	9:1 ethylacetate-hexane, chloroform	silica	rat	30-60 ng/g
Brain	ND	3:1 acetone-phosphate buffered saline, methanol, chloroform	/	rat	456 ng/g (frontal cortex)
	ND	9:1 ethylacetate-hexane	silica	rat	209-1524 ng/g depending on brain area
Reproductive fluids	ND	acetone, chloroform-methanol	/	human	9.3 ng/mL (seminal plasma) 9 ng/mL (oviductal fluid) 3.4 ng/mL (follicular fluid)
	0.5 mL	/	HLB	human	4.6 ng/mL (seminal plasma)

Table 3: *Analytical methods for quantification of PEA in biological matrices. ND: not disclosed.*[92]

Some critical points in the analytical procedure could be found in: (1) the sampling phase, (2) sample storage and (3) sample clean-up.

3.2.1 Sampling and storage

As a general standard protocol, the biological sample should be processed and analyzed as soon as possible, in order to prevent artefacts or degradation of the analytes. When analyzing blood samples, it is recommended to separate plasma from blood cells. Indeed, it was demonstrated that blood cells can release NAEs, particularly AEA *ex vivo*,[93] which could create artefacts in the analytical results; for PEA this phenomenon is not yet reported. However, it is known that in brain tissues, PEA concentrations can increase rapidly *post mortem*. Regarding the storage conditions of plasma, it is recommended to maintain the sample at -80°C until the day of analysis. In these condition, the FAAH activity should be blocked and, as a consequence, the degradation of PEA should be prevented. Some papers suggests to store plasma or tissues in the presence of FAAH inhibitors, such as phenylmethylsulphonyl fluoride (PMSF). Another aspect related to sample manipulation is the absorption of molecules on laboratory materials which could decrease the concentration of the analytes during regular sample preparation and treatment. It was observed that the endocannabinoids AEA and 2-AG absorb to commonly used plastic and glass ware, with greater absorption to plastic surfaces compared to glass surfaces.[94]

3.2.2 Extraction from biological matrices

As previously said, PEA is present in tissues in low concentrations and the complexity of the background matrix requires adequate sample clean-up and concentration procedures. This is particularly important when HPLC–MS/MS is employed as method of detection. In general, HPLC–MS/MS-based methods are associated with problems originating from the biological matrix.[95] Phospholipids present in plasma and in other biological samples have been recognized as a major contributor to matrix-effects in HPLC–MS/MS methods employed for numerous endogenous substances. In fact, if these compounds co-elute with analytes, such as PEA, they should decrease ionization, so analytes are more difficult to detect, especially at their lowest concentrations. For those reasons, sample extraction is a critical step of sample clean-up; an optimized extraction protocol can minimize co-extraction of compounds that interfere with ionization, while ensuring maximum recovery of the analytes of interest. The published procedures include the use of a single or a mixtures of organic solvent extraction and solid-phase extraction (SPE), often in combination. Given their lipophilic character and lack of electrical charge across a wide pH-range, NAEs are usually well extracted from matrices using water-immiscible solvents. One of the most widely used are chloroform/methanol mixtures of varying compositions. The relative strong lipophilic character of the chloroform can extract highly lipophilic molecules, including NAEs, however it is important to recognize that chloroform/methanol extracts contain the class of phospholipids which cause considerable matrix-effects using HPLC-MS/MS methods. The presence of these contaminants in the extracts could be excluded with a subsequent SPE step, and also in this case the large abundance of lipophilic molecules could overload the

column itself. A more specific solvent extraction of NAEs from plasma and other biological samples has been described by the aromatic solvent toluene. The major advantage over other solvent extraction procedures is that toluene extracts are almost free of phospholipids causing matrix-effects. Particularly in HPLC-based methods, protein precipitation by acetone or by other water-miscible organic solvents such as acetonitrile, methanol or methanol-acetonitrile mixtures are commonly used for NAEs extraction. With these methods, precipitated proteins are eliminated by centrifugation and highly lipophilic compounds are excluded giving cleaner extracts, whereas NAEs are present in the supernatant, which can be also be further purified by SPE. Protein precipitation by organic solvents, in particular acetonitrile which is the most efficient in protein precipitation, is simple, practicable, rapid and compatible with automatic processing in LC-MS/MS analysis. The use of SPE, both reverse- (C18) and normal-phase (silica) materials could be particularly convenient and it is a frequently applied for analytes enrichment. However, using these protocols could lead to a dramatic problem in terms of recovery, it is noted that yield may vary between 20% and 100% depending on the brand and type of the phase of SPE material. In general, however, it is recommended to optimize the sample extraction protocol testing different mixtures and volumes of solvents, and to test its compatibility in combination with further sample preparation steps.

3.2.3 HPLC-MS/MS analysis of PEA

Recent advances in the field of HPLC-MS technology have led to ultra performance liquid chromatography (UPLC) systems coupled to highly sensitive MS equipment. As the name implies, UPLC systems can work at higher pressures, if compared to conventional HPLC systems, so analytical columns with small internal diameters and small particle sizes can now tolerate higher flow rates, which is translated into a faster and improved chromatographic separation and a higher sensitivity due to narrower peaks. However, shorter times gradients can reduce the sensibility resulting in co-elution of analytes and different compounds from the extraction solution that can cause ion-suppression; a less steep gradient could easily solve this problem. Most of the chromatographic systems involve a C18 reverse phase column and a mobile phase constituted by water and a second mobile phase constituted by acetonitrile, which gives narrower peaks, or methanol or a mixtures of them. PEA on that specific stationary phase is well retained and gives a relative long retention time, often elutes some minutes after the gradient reached the 100% of organic phase. For those reasons numerous methods use a thermostatic column, maintaining the temperature around 40°C, while the samples in the autosampler is constantly maintained to 5°C.

Regarding ionization methods, most published methods use electrospray ionization (ESI), although atmospheric pressure chemical ionization (APCI) is also employed. Positive ESI (ESI+) of PEA yields three cations, i.e. the protonated molecule $[M+H]^+$ at *m/z* 300, and two cations from the PEA molecule adducted with Na^+ at *m/z* 322 $[M+Na]^+$ and with K^+ at *m/z* 338 $[M+K]^+$. The yield of $[M+H]^+$ can be increased by adding formic acid to the mobile phase, ranging from 0.05 vol.% to 0.25 vol.%, usually 0.1 vol.%. Subjection of $[M+H]^+$ at *m/z* 300 to CID yields the highly characteristic product ion at *m/z* 62, because this ion represents the protonated ethanolamine moiety ($[HOCH_2CH_2NH_3]^+$) of PEA. Another characteristic

product ion is represented by the loss of the hydroxyl group, given the *m/z* 282, but it is lesser intense than the *m/z* 62, which is chosen as the standard transition. Remarkably, the $[M+Na]^+$ ion is very resistant to CID with argon as the collision gas, so that the precursor ion at *m/z* 322 is not suitable for LC–MS/MS analysis of PEA. However, the ion $[M+Na]^+$ at *m/z* 322 can be monitored in LC-MS analysis.

Several internal standards can be used for quantification purposes, in particular the use of PEA-d4 as internal standard is preferred because it has the same retention time as PEA, thus ensuring proper correction for ion suppression and loss of analyte during sample preparation. Moreover it is also useful for the CID transitions, not only for its difference for the *m/z* of the parent ion $[PEA\text{-}d4+H]^+$ which is 304, but also for the main transition that is increased, indeed the protonated ethanolamine moiety ($[HOCD_2CD_2NH_3]^+$) of PEA-d4 is now *m/z* 66. This allows less interference in the mass spectra.

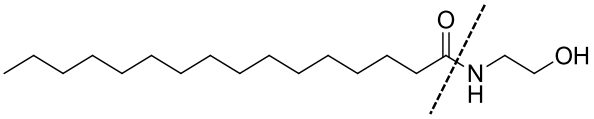

PEA
m/z 300.2 → 62.3

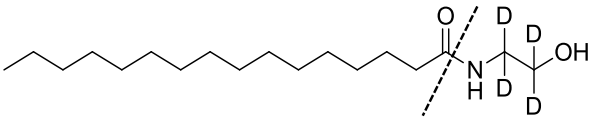

PEA-d_4
m/z 304.2 → 66.3

3.3 Premises to experimental work

3.3.1 Pharmacokinetic data on PEA

A recently published paper showed that a single oral dose of PEA (10 mg/kg) significantly reduced the wheal and flare reaction in dogs with skin hypersensitivity.[96] The latter work was also one of the few examples of a pharmacokinetic (PK) evaluation of exogenously administered PEA, in Beagle dogs. It was observed that after the oral administration of a 30 mg/kg dose, PEA reached the maximal plasma concentration (C_{max}) after 1-2 hours, with an increase of five-fold of its basal plasma levels (Fig. 24). A similar pharmacokinetic profile of PEA (given as a ultra-micronized preparation) was reported in a US patent,[97] where PEA was orally administered to Beagle dogs in a 15 mg/kg dose. In this specific case, PEA reached the C_{max} 1 hour after administration, with an increase of two-fold of its basal plasma level and returning to basal levels after 2 hours. PEA was orally administered also to humans, with an average increase between 2-9-fold in plasma basal levels, depending on the dose.[92]

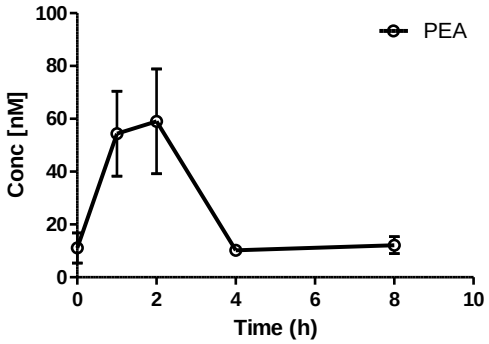

Figure 24: *PEA plasma levels after oral administration (30 mg/kg) to Beagle dogs.*[96]

Considering these data, it is possible to state that PEA, when orally administered at medium-high doses, can produce only limited systemic exposure levels, with plasma concentrations in nM range and with significant increases of PEA plasma concentrations for a short period of time. Different physico-chemical and metabolic issues could be evoked as responsible for the limited systemic exposure to oral PEA. PEA is a fatty acid amide presenting a high lipophilicity accompanied by a low aqueous solubility, physico-chemical factors which could limit its gastro-intestinal absorption, especially at medium-high doses. Indeed, the formulation strategy of administering orally to humans an ultra-micronized powder of PEA goes into the direction of maximizing absorption through an increase of water-exposed area of the powder.

Moreover, in many tissues PEA is hydrolyzed to its components palmitic acid and ethanolamine by the already cited specific enzymes NAAA and FAAH.

3.3.2 Medicinal chemistry strategies to increase PEA levels *in vivo*

From a medicinal chemistry point of view, two different strategies could be followed to increase PEA levels within the body in order to get the desired pharmacological outcome: one strategy, which has also been developed in the past years by our group, is to increase PEA levels by inhibiting the enzymes responsible for its metabolism, thus targeting the enzymes FAAH and NAAA. It is beyond the scope of this Ph. D. thesis to provide a detailed description within the complex field of FAAH and NAAA inhibitors, which has grown a lot during the past 10-15 years. However, in the table below some examples of the most relevant discovered chemotypes are presented.

Name	Structure	FAAH	NAAA
FAAH Inhibitors			
URB597	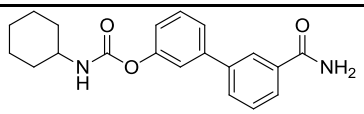	IC_{50}=5nM; K_{inact}/K_i = 1590 M^{-1} s^{-1}	No inhibition
PF-3845	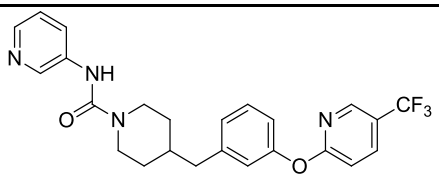	K_{inact}/K_i = 12600 M^{-1} s^{-1}	ND

PF-04457845	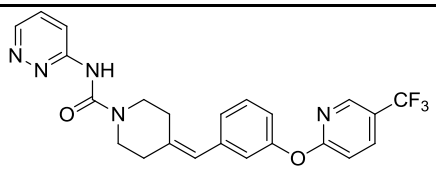	IC_{50} = 7–50 nM; K_{inact}/K_i = 40,300 M^{-1} s^{-1}	ND
NAAA Inhibitors			
(S)-OOPP	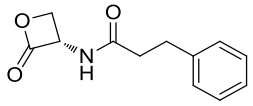	No inhibition	IC_{50} = 420 nM
ARN077 / URB913	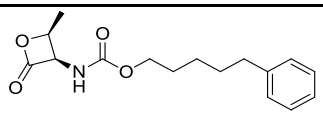	No inhibition	IC_{50} = 50–130 nM
14q	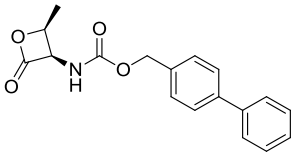	No inhibition	IC_{50} = 7 nM
AM9023	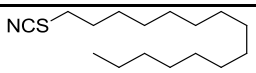	No inhibition	IC_{50} = 600 nM

Table 4: *Selected FAAH and NAAA inhibitors.*[98]

FAAH is a serine hydrolase with an atypical catalytic triad constituted of Lys142–Ser217–Ser241, rather than the typical catalytic triad, Ser–His–Asp, of serine hydrolase, with Ser241 acting as the catalytic nucleophile. X-ray crystal structures of FAAH in complex with various inhibitors permitted to deeply understand the interactions between inhibitors and the enzyme, and different studies conducted with the use of activity-based protein profiling technologies, favored the development of highly selective inhibitors. Among the different classes of FAAH inhibitors that have recently been described, the most promising ones included α-ketoheterocycles, β-lactames, carbamates (URB597) and arylureas (PF-3845 and PF-04457845). URB597 is the most widely used FAAH irreversible inhibitor, its activity is based on a carbamate moiety that carbamilates the catalytic serine of the enzyme.[99,100] It is a potent and rather selective inhibitor, indeed it has no affinity for MGL and NAAA, although it inhibits several carboxylesterases in the liver.[101] In *in vivo* studies, URB597 can induce a strong increase in AEA levels in the brain, liver and several other tissues.[102] A recent evolution of URB597 is the peripherally restricted URB937, which will enable researchers to distinguish between centrally and peripherally mediated effects of FAAH inhibition.[103] Also several urea derivatives were developed as FAAH inhibitors, increasing the reactivity of the urea moiety towards the catalytic triad. PF-3845 is one of the most widely used urea inhibitors in animal models, for its high potency and selectivity towards FAAH, which is inhibited in a covalent and irreversible way. PF-04457845 is the evolution of the PF-3845, which combines the high potency and selectivity with oral bioavailability.[104] Both these inhibitors increase AEA levels up to 24h *in vivo*.[105]

NAAA is a lysosomal cysteine hydrolase belonging to the N-terminal nucleophile hydrolase superfamily. The active form of the enzyme results from an autocatalytic cleavage taking place at an acidic pH and involving the catalytic nucleophile Cys126. The catalytic triad comprises the Cys126-Arg142-Asp145

residues. These differences in structures and catalytic mechanisms between FAAH and NAAA allowed the development of selective inhibitors. The first selective inhibitor described for NAAA was a β-lactone, (S)-OOPP, which demonstrated a submicromolar range of inhibition of NAAA without inhibiting FAAH. Another inhibitor, derived from (S)-OOPP, was a 2-methyl-β-lactone, known as ARN077/URB913, showing an improved potency towards NAAA.[106] These new compounds could inhibit NAAA with a covalent interaction to the Cys126 residue in the catalytic site and it was demonstrated *in vivo* that could lead to an increase in PEA levels. However, the major drawback was the poor *in vivo* stability of this class of compounds. The last example of NAAA inhibitor was represented by AM9023, which is a lipophilic isothiocyanate, that could inhibit the enzyme in a reversible way.[107]

There are some challenges for the use of FAAH and NAAA inhibitors to increase endogenous PEA levels. First of all, it must be considered that FAAH does not hydrolyze PEA with the same efficiency as AEA, so pharmacological inhibition of this enzyme, or even its genetic deletion, does not always lead to increased PEA levels. The NAAA inhibitor ARN077/URB913 increased PEA levels without affecting AEA levels. Moreover, it has to be remembered that the administration of a FAAH or NAAA inhibitor can resulted in the increase of NAEs levels not only locally, but throughout the body. FAAH inhibition doesn't seem to be correlated to significant toxicity, as confirmed by toxicity studies conducted on the carbamate URB597, although a large number of bioactive lipids, besides NAEs, are hydrolyzed by the enzyme. Its inhibition can increase NAEs levels, but also, for instance, increase levels of the bioactive N-acyltarines.[108] It has not been described so far if NAAA inhibition *in vivo* might affect other mediators levels besides NAEs.

3.3.3 Prodrug approach

The second medicinal chemistry strategy that could lead to an increase in PEA plasma levels after oral administration of PEA is the strategy of prodrugs. As already said, administration of PEA has shown efficacy in many different preclinical animal models for chronic and neuropathic pain, but its unfavorable physico-chemical or pharmacokinetic properties have minimized its systemic exposure after oral administration. Prodrug approach is one of the most popular strategies used to overcome problems caused by undesirable physico-chemical and pharmacokinetics properties of a variety of drugs. Many prodrugs are already available to target the gastro-intestinal active transport systems to increase absorption and bioavailability of the drug itself. A significant example is valaciclovir, the valine ester of aciclovir, here the conjugation with the amino acid causes the recognition of the molecule by the active transport system of the di- and tri-peptides PepT1, and results in an oral bioavailability five-fold higher than aciclovir. The same strategy has been employed in the design of prodrugs of the anticancer drugs floxuridine and gemcitabine designing amino acid ester conjugates, as well as the inhibitor of the kinases VEGFR-2/FGFR-1 brivanib alinate.[109] This prodrug was finally discovered after a screening of different ester prodrugs of brivanib conjugated with various amino acids, in order to improve the aqueous solubility of the drug and consequently its oral bioavailability. A prodrug-based strategy could also be useful to increase the half-life of the drug. An example is the bronchodilator bambuterol, which is a terbutaline prodrug, where the phenolic groups are

masked as carbamates and are then slowly hydrolyzed by aspecific plasma cholinesterase: the result is that bambuterol can be administered once a day, while terbutaline needs to be given three times daily.
Focusing back on PEA, in a recent work it was described a new PEA prodrug, having a galactosyl moiety connected by an ester bond, through a succinyl spacer, to the hydroxyl group of PEA.[110] This compound was tested *in vitro* on cell cultures, showing improved cytoprotection in 6-hydroxydopamine-mediated cell death and prolonged intra-cellular levels of PEA, if compared to direct administration of PEA itself.

3.4 Experimental design and aim of the project

Given these premises, the aim of the present work is to apply the prodrug strategy to palmitoylethanolamide (PEA) in order to search for a prodrug alternative to oral PEA with improved physico-chemical and pharmacokinetic properties. PEA is a molecule with a large potential in terms of its pharmacological properties, but its therapeutic efficacy is affected by a poor oral bioavailability, probably due to a rapid metabolism by aspecific and specific (FAAH, NAAA) enzymes and to a rapid distribution to lipophilic compartments. To resolve these drawbacks, the pro-moiety attached to the PEA hydroxyl group should be cleaved by plasma esterases at a convenient rate to allow gradual and prolonged release of PEA in tissue.
At the same time, the prodrug should be stable enough toward amidases to avoid degradation of the PEA moiety itself.
There are several challenges associated with the design and identification of a palmitoylethanolamide prodrug suitable for oral administration, such as:

1. conjugation with a non-toxic molecule
2. use of a cleavable moiety
3. resistance to first-pass effect
4. resistance to the endogenous amidases.

Prodrugs synthesized by the laboratories of the Drug Design and Discovery group at the Dipartimento di Farmacia are conjugated with amino acids, appropriately chosen to avoid any *in vivo* toxicity after hydrolysis. Moreover, conjugation with amino acids is a successful technique that had led to significant improvements in oral bioavailability when applied to a variety of drugs, such as the previously described nucleoside analogs aciclovir and ganciclovir,[111,112] and the anticancer drugs floxuridine[113] and gemcitabine.[114]
To evaluate the other needed characteristics of prodrugs, two *in vitro* models were employed for a systematic analysis of the capacity of the prodrug to release PEA in different biological tissues, before testing the prodrugs *in vivo*: rat plasma and rat liver homogenate. Both these substrates are important to analyze the time-course of prodrug cleavage and the subsequent increase in PEA concentration over time. Rat plasma can be useful because it contains a lot of different esterases (carboxylesterases, cholinesterases, etc)[115] so it is a first-choice biological matrix for stability assays of new prodrug candidates having hydrolysable promoieties. Nevertheless, rat plasma does not contain specific catabolic enzymes for NAEs, such as FAAH and NAAA. In order to study the stability against these two specific enzymes, and also to simulate in vitro the hydrolytic first-pass metabolism, the prodrug stability was tested in rat liver homogenates. Indeed liver

homogenate is both a reliable, recognized model for hydrolytic first-pass metabolism and it contains a high concentration of FAAH, which is responsible for the specific amidase activity on PEA.

In the prodrug design phase, three functional groups were initially selected to conjugate PEA at its hydroxyl group with the pro-moieties: carbonates, carbamates and esters. As carbonate prodrugs, acyloxymethylcarbonate derivatives (**1**-**3**, Table 5) were prepared, which are expected to be substrates of plasma esterases at their terminal acyloxy group. The size of the terminal group was varied to test the possibility to modulate its plasmatic half-life. In the case of ester and carbamate prodrugs, a first exploratory set of amino acid derivatives was prepared, with the aminoacids L-glycine (L-Gly), L-alanine (L-Ala) and L-valine (L-Val) conjugated to PEA at their α-carboxyl (**7**-**8**) or α-amino functions (**4**-**6**), respectively.

Then after preliminary results, it was decided to deeply analyze the structure-stability relationships within the set of ester-based prodrugs, given their superior performance in terms of prodrug stability and PEA release.

Several amino-acids were conjugated to PEA by an ester linkage to its hydroxyl group trying to modulate the bi- and tri-dimensional steric hindrance, the hydro-lipophilic balance[116] and the chirality of the amino-acid side chain and searching for the optimal ratio between in vitro prodrug stability and PEA release.

Ester prodrugs of PEA with L-isoleucine (L-Ile, **9**) and L-tryptophan (L-Trp, **10**) were therefore synthetized and tested for their hydrolytic stability in rat plasma and rat liver homogenate. **10** has an indolic group in which all carbons are hybridized *sp2*, so it has a large planar steric hindrance, whereas **9** is a representative of hydrophobic amino-acids with branched alkyl side-chains.

Another subset of compounds consisted in ester prodrugs of PEA with hydrophilic amino acids with polar amide, L-asparagine (**11**) and L-glutamine (**12**), or acidic, L-aspartate, side chains. The latter amino acid was conjugated with the hydroxyl group of PEA with both the α-carboxyl (**13**) or the ω-carboxyl (**14**) of the amino acid. Another aspect that was evaluated was the amino-acid chirality. In general, prodrug conjugates of D-amino acids are usually characterized *in vitro* by a slower transformation to the parent compound, if compared to the corresponding L-amino acids.[117,118] This could have important implications for in vivo tissue distribution. For this purpose D-valine (**15**) and D-asparagine (**16**) ester prodrugs were synthesized and analyzed by the same experimental protocol. Table below shows the carbonate, carbamate and ester prodrugs tested for this first in vitro exploration of structure-stability relationships.

Table 5: *Chemical structures of PEA prodrugs.*

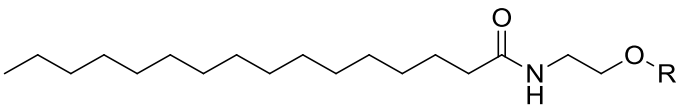

Compound	R	Amino acid
PEA	H	
1	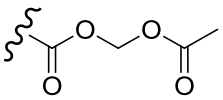	/
2	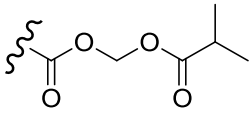	/

3	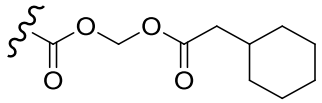	/
4	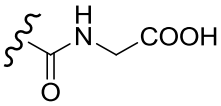	L-Gly
5	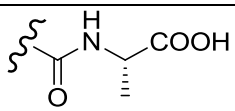	L-Ala
6	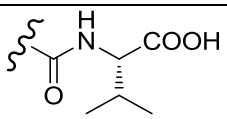	L-Val
7	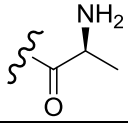	L-Ala
8	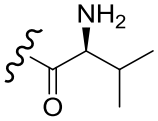	L-Val
9	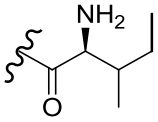	L-Ile
10	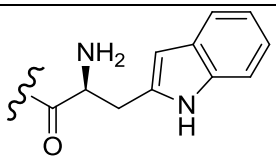	L-Trp
11	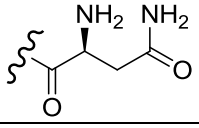	L-Asn
12	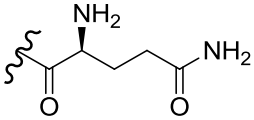	L-Gln
13	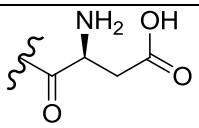	L-Asp
14	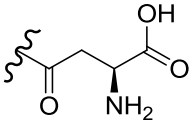	ω-L-Asp
15	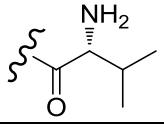	D-Val
16	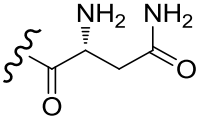	D-Asn

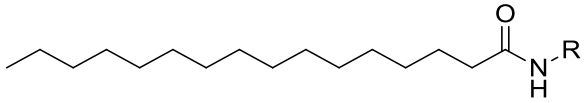

17	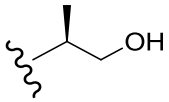	/
18	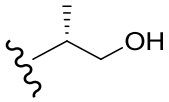	/
19	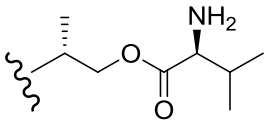	L-Val

3.5 Results and Discussion

A high performance liquid chromatography/tandem mass spectrometry method (HPLC-ESI-MS/MS) was set up for the simultaneous quantification of prodrug derivatives and PEA in the chosen biological matrices (rat plasma, rat liver homogenate). As previously described, it is well known that the extraction from blood/plasma of these fatty acid ethanolamides implies the resolution of some problems. Matrix-effects caused primarily by co-extracted phospholipids may further compromise analysis.

3.5.1 Optimization of analyte extraction conditions

In order to optimize the analyte extraction phase from the biological matrices, the efficiencies of different organic solvents, among those already employed in literature,[119,92] and/or of their mixtures and corresponding matrix-effects in the HPLC–MS/MS analysis of PEA and of a sample prodrug (i.e. the L-valine ester of PEA) were compared. The use of different solvents for liquid/liquid extraction was assayed in order to obtain the highest recovery of the analyte and the lowest matrix effect, mainly due to co-extracted phospholipids. Briefly, rat plasma samples containing a 50 nM final concentration of deuterated PEA and sample prodrug **8**, the L-valine ester prodrug was processed with a two-fold volume of acetonitrile, toluene, ethyl acetate and a solution of ethyl acetate/heptane 1:9 v/v.

Solvent	**% Recovery PEA-d_4**	**% Recovery 8**
Acetonitrile	96.2	92.0
Toluene	27.9	13.4
Ethyl acetate – Heptane	34.3	5.9
Ethyl acetate	83.3	35.4

Table 6: *Percentage of recovery with different sample processing.*

As it can be seen in Table 6, the most efficient method of extraction for PEA-d4 and prodrug resulted in adding a double volume of acetonitrile to the plasma sample.

3.5.2 Evaluation of matrix effect and sample stability

Matrix effect was instead evaluated comparing the peak area ratios of PEA/PEA-d_4 and prodrug **8**/PEA-d_4 in acetonitrile and in the biological matrix pre-extracted with acetonitrile. The difference between the samples was below 5%. The stability of processed samples was evaluated by maintaining them at room temperature for up to three hours. For both PEA and **8** the percentages recovered were superior to 95%.

In conclusion, the extraction of PEA and prodrug from rat plasma by means of acetonitrile addition (2:1) allows a rapid and simple processing of biological samples, with high percentages of recovery for both analytes, with low matrix effects and good stability of the processed samples.

3.5.3 Precision and accuracy of the analytical method

The precision of an analytical method is defined as the closeness of agreement (degree of scatter) between a series of measurements obtained from multiple sampling of the same homogeneous sample under the prescribed conditions. The accuracy of an analytical method is the closeness of agreement between the conventional true value or an accepted reference value and the value found.

For the evaluation of precision and accuracy of the HPLC-ESI-MS/MS analytical method for the quantification of PEA, three replicates a-day of calibration standards (intra-day variability) were measured, for four consecutive days (inter-day variability). Calibration curves were generated using the ratio between the peak areas of the analyte and of the internal standard, represented by deuterated PEA (PEA-d4), applying the equation of the linear regression with a weighting factor of 1/x. For all calibration curves of PEA and its prodrugs the correlation coefficient r^2 was always above 0.99 with a limit of quantification of 1 nM for each compound.

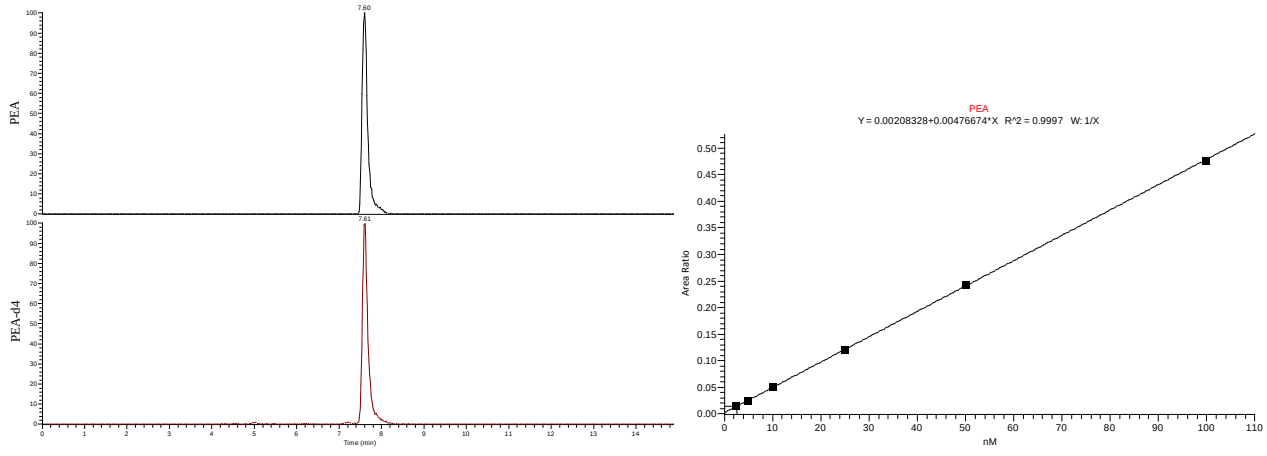

In Tables 7 and 8 average values of specified concentrations calculated on the basis of the calibration curve are reported, standard deviations (SD), relative standard deviations (% RSD = SD/average x 100), which is a good gauge of precision. In accordance to the guidelines for the validation of bioanalytical procedures, the calculated value for RSD cannot exceed 15% for all the concentrations, with the exception of the lower limit of quantification (LLOQ) for which a 20% can be tolerable. Accuracy, indicated as %bias and expressed as percentage of ratio between the difference of observed average concentration and specified concentration and

the specified concentration itself (%bias=100x[$Conc_{obs}$-$Conc_{spec}$]/$Conc_{spec}$). In accordance to the above cited guidelines, %bias cannot be more than 15% with respect to the nominal concentration, with the exception of the lower limit of quantification (LLOQ) for which a 20% can be accepted.

Specified amount (nM)	Calculated conc. (nM, average ± SD)	%Bias	%RSD
1	0.88 ± 0.08	-12.20	9.20
2.5	2.60 ± 0.35	4.18	13.32
5	5.03 ± 0.45	0.66	8.93
10	10.52 ± 0.66	5.22	6.31
25	25.09 ± 1.11	0.37	4.41
50	48.58 ± 1.86	-2.84	3.83
75	75.40 ± 4.64	0.54	6.16

Table 7: *Intra-day variability*

Specified amount (nM)	Calculated conc. (nM, average ± SD)	%Bias	%RSD
1	1.10 ± 0.18	9.66	16.28
2.5	2.59 ± 0.25	3.66	9.68
5	5.02 ± 0.52	0.32	10.32
10	10.62 ± 0.53	6.15	4.96
25	25.08 ± 0.47	0.30	1.88
50	48.30 ± 0.96	-3.39	2.00
75	75.40 ± 1.79	0.54	2.38

Table 8: *Inter-day variability between 4 days.*

As it can be seen in the tables above, the HPLC-ESI-MS/MS method reveals to be accurate and reproducible over the whole analyzed concentration range.

3.5.4 Chemical stability of PEA and related prodrugs

Chemical stability of PEA and related prodrugs was evaluated by measuring, in buffer PBS 0.1 M at physiological pH (pH 7.4) and at 37°C, both the residual concentration of the starting compound and the corresponding appearance of PEA by mass spectrometry (HPLC-ESI-MS/MS). In these conditions, PEA is very stable, with 95% of compound still present after 6 h (Table 9). Most of the analyzed prodrugs showed a very good recovery after 6h of incubation at pH 7.4, 37°C. In particular, carbamate-based prodrugs (**4-6**) remained completely intact and acyloxymethylcarbonates (**1-3**) were recovered with average percentages of about 85% after 6h of incubation. The stability of ester-based prodrugs varied depending on the structural characteristics of the conjugated amino acids. In fact, the branched L-isoleucine derivative **9** was more stable than the planar L-tryptophan **10** and the smaller L-valine **8** and L-alanine **7** conjugates. L- and D-asparagine derivatives (**11** and **16,** respectively) showed an high instability in buffer, with residual percentages of 3% after 6h. With these latter prodrugs, a slow deamidation reaction could occur at the amino acid side chain of asparagine and to a lesser extent also glutamine, with the final formation of aspartic acid or isoaspartic acid.

Compound	% Remaining Compound pH 7.4, 37°C, 6h
PEA	95 ± 1
1	86 ± 1
2	84 ± 1
3	84 ± 1
4	101 ± 1
5	103 ± 3
6	99 ± 1
7	64 ± 5
8	91 ± 2
9	103 ± 6
10	96 ± 1
11	3.3 ± 0.3
12	61 ± 3
13	85 ± 4
14	83 ± 3
15	3.5 ± 0.3
16	87 ± 2
17	96 ± 3
18	95 ± 2
19	93 ± 4

Table 9: *Chemical stability data for PEA and prodrugs (pH 7.4, 37 °C, 6h).*

3.5.5 Hydrolytic stability in rat plasma and rat liver homogenate

In vitro PEA stability in rat plasma and liver homogenate was first evaluated in order to compare its metabolic stability with that of the different prodrugs. Following the procedure described in the Materials and Methods chapter, PEA was added to a solution composed by pooled rat plasma (80% v/v) and phosphate buffer pH 7.4 and it was rather stable. PEA had basal levels of 20.1±5.6 nM in the starting solution of rat plasma 80%. After addition of 25 pmol of PEA in 500 µl, PEA levels showed a biphasic trend. From PEA concentrations of 71.9±2.1 nM at starting point, we an initial decay to 56.2±4.3 nM after 1 h was observed, followed by a much slower decrease, with a value of 44.0±3.2 nM after 6 h.

On the other hand, FAAH is highly expressed in rat liver, where a number of other hydrolases are also present. In fact, PEA was quickly metabolized in rat liver homogenate, with a half-life of about 25 min, a PEA concentration of 4.0±1.2 nM after 120 min and no detectable basal PEA levels.

Plasma stability

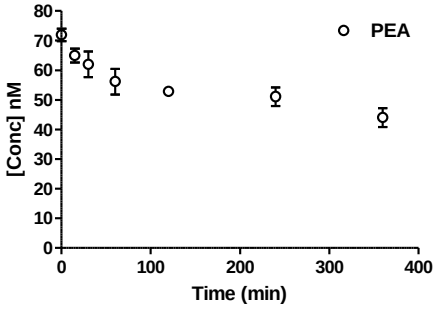

Liver stability

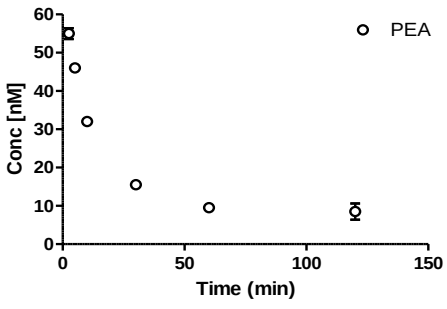

The results of enzymatic stability assays on PEA and all the tested prodrugs are reported in Table 10, where $t_{1/2}$ values were calculated from pseudo first-order rate constants; mean ± SD, n = 3, and in average PEA basal level in 80% rat plasma = 20.1±5.6 nM

Compound	Rat Plasma			Rat Liver
	Compd $t_{1/2}$ [min]	PEA C_{max} [nM]	PEA t_{max} [min]	Compd $t_{1/2}$ [min]
PEA	70 ± 2%[a]	72 ± 2	5	25 ± 5
1	<1	53 ± 5	5	<1
2	1.1 ± 0.2	52 ± 2	5	<1
3	5.1 ± 0.5	52 ± 3	15	1.2 ± 0.2
4	96 ± 4%[a]	-	-	23 ± 1
5	96 ± 2%[a]	-	-	29 ± 3
6	98 ± 1%[a]	-	-	92 ± 5%[b]
7	1.0 ± 0.1	65 ± 3	5	1.4 ± 0.5
8	46 ± 3	44 ± 4	300	26 ± 1
9	205 ± 16	18 ± 1	360	65 ± 5%[b]
10	4.5 ± 0.5	53 ± 1	30	36 ± 2
11	9.0 ± 0.5	43 ± 4	60	24 ± 1
12	18 ± 1	22 ± 1	30	80 ± 10
13	172 ± 2	26 ± 5	240	66 ± 5%[b]
14	262 ± 35	34 ± 5	360	21 ± 1
15	14 ± 1	36 ± 3	60	55 ± 4
16	173 ± 4	20 ± 1	360	67 ± 9%[b]
17	80 ± 4%[a]	-	-	79 ± 6%[b]
18	82 ± 4%[a]	-	-	87 ± 1%[b]
19	190 ± 3	26 ± 1[c]	360[c]	38 ± 2

Table 10: *Stability data for PEA and related prodrugs. [a] Percent remaining after a 6 h incubation at 37 °C in rat plasma. [b] Percent remaining after 2 h incubation at 37 °C in rat liver homogenate. [c] Referred to (R)-α-methyl-PEA.*

Prodrugs **1**-**3**, carrying the acyloxymethylcarbonate pro-moiety, showed a complete hydrolysis with the corresponding release of PEA within 5 minutes from the start of the incubation in both *in vitro* hydrolysis models. The introduction of a bigger substituent, such as the cyclohexyl group (**3)**, led to a greater hydrolytic stability compared to the other two prodrugs, characterized by the presence of a methyl or isopropyl group. These compounds were less stable in rat liver homogenate, with half-lives lower or equal to 1 min. The excessive liability of the carbonate function as a conjugating linker in both *in vitro* models of hydrolytic metabolism was the factor which prompted their exclusion from further characterizations or structural modulations.

The subset of carbamate-based prodrugs **4**-**6**, carrying the L-amino acids glycine, alanine and valine, were tested in order to evaluate the role of the steric hindrance of the amino acidic side chain on the enzymatic stability.

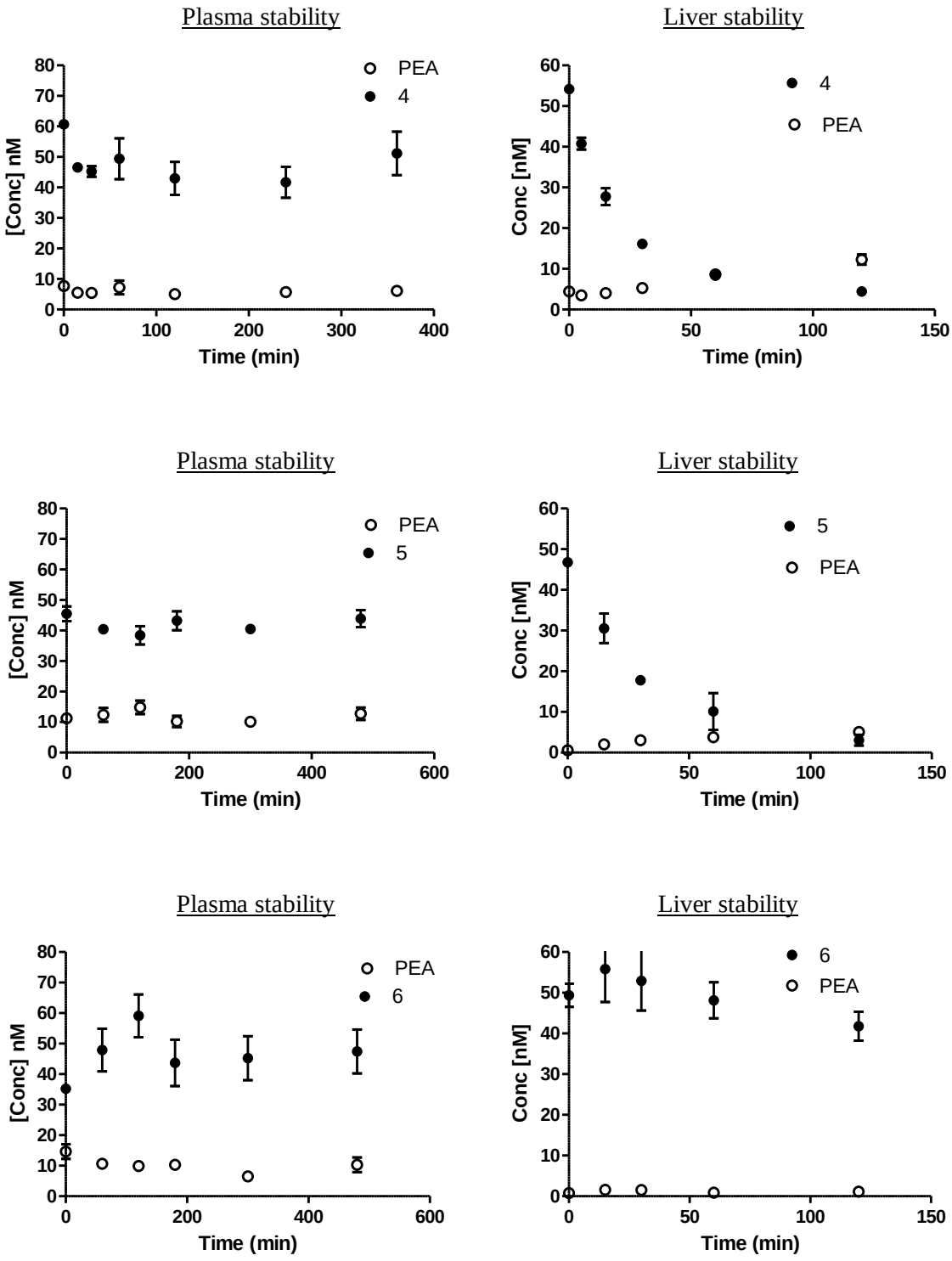

As it can be seen from the above graphs, the carbamate-based prodrugs were very stable in rat plasma (graphs on the left) with only < 4% of prodrug hydrolyzed after 6 hours of incubation. In rat liver homogenate, instead, the profiles of concentration vs. time seem to be influenced by the structural characteristics of the conjugated amino acid.

Compounds **4** and **5 (**L-glycine and L-alanine carbamate prodrugs) were characterized by a rapid hydrolysis (half-life of 23 and 25 minutes) not associated with a corresponding release of PEA, which remained at a rather constant concentration of less than 10 nM. The conjugate with the branched L-valine (**6**) was stable in the liver preparation, with 92±5% of the initial prodrug still remaining after 2h of incubation. Thus, for these

derivatives, the rate of hydrolysis of the carbamic bond is inversely proportional to the steric hindrance and the branching of the conjugate amino acid side chain. Opposite to what it had been observed for carbonates, the excessive plasma stability of carbamates and the lack of PEA release were the main reasons why also the carbamate linker was abandoned and not further developed.

The first group of ester derivatives that were analyzed were PEA conjugates with amino acids endowed with hydrophobic side chains of increasing steric hindrance, such as L-alanine (**7**), L-valine (**8**), L-isoleucine (**9**) and L-triptophan (**10**).

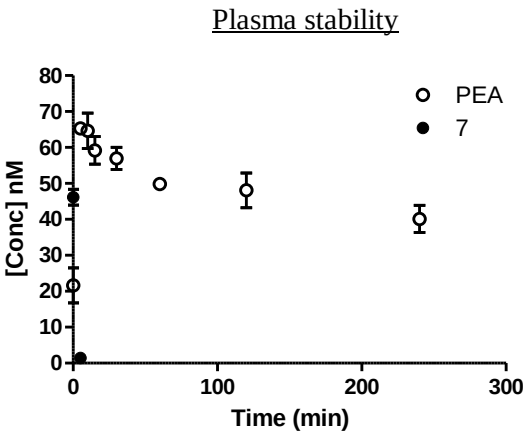

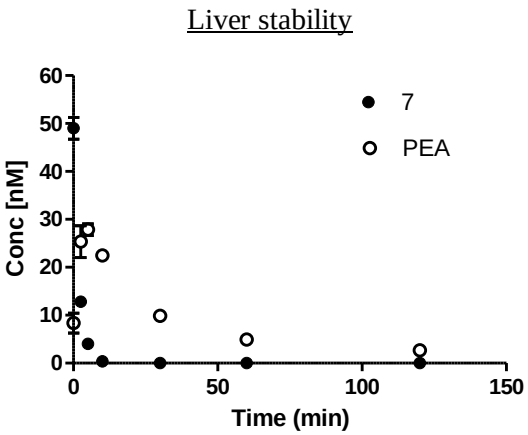

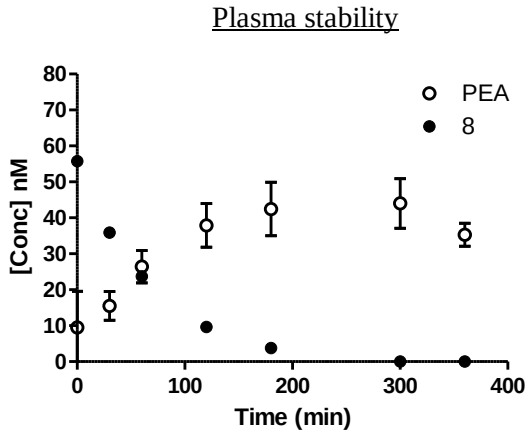

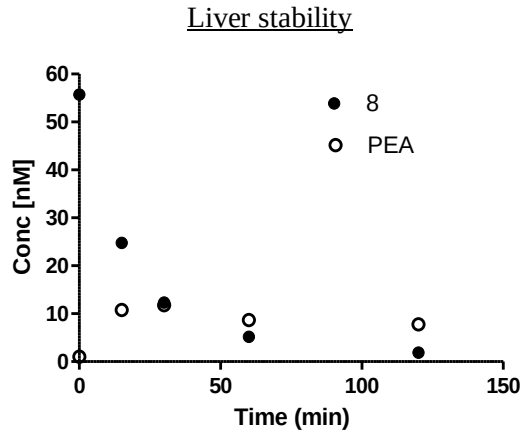

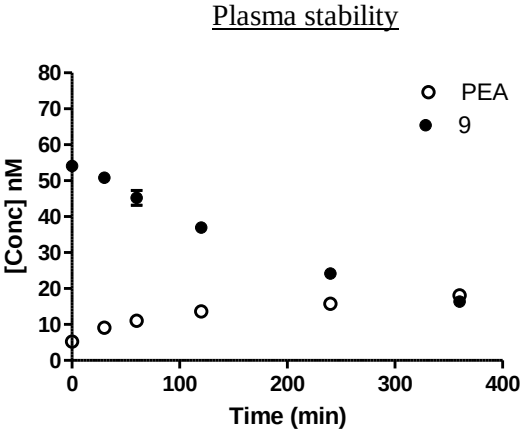

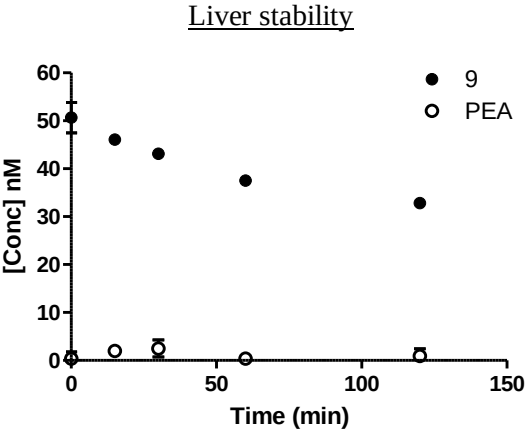

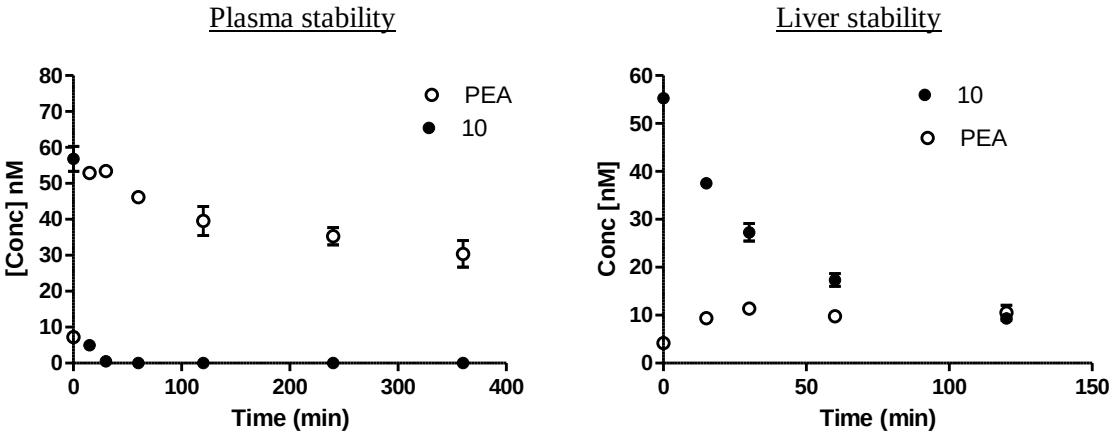

The results obtained in both *in vitro* stability models revealed the higher liability of the ester bond with respect to the carbamate bond to enzymatic hydrolysis. **7** and **8** in fact showed half-lifes significantly shorter than those of the corresponding carbamic prodrugs. Specifically, the L-Ala prodrug **7** was characterized by an half-life of about one minute in both biological substrates; in plasma **7** provided an almost quantitative concentration of released PEA, while in the liver preparation, a maximum concentration of newly formed PEA of about 30 nmol/mL was reached, if compared to the 50 nmol/mL that corresponded to a total conversion. The behavior of the L-Val ester **8** in rat plasma was very interesting and requires a detailed description. The kinetics of hydrolysis of the prodrug *vs.* time was rather slow, with an half-life of about 45 min, almost 46 times higher than the half-life of the L-Ala derivative. A gradual and progressive increase in the levels of released PEA was observed, with the achievement of significant concentrations between 4 and 6 hours after the beginning of the incubation. This time-course of prodrug cleavage and PEA release for **8** in rat plasma is the closest to the ideal *in vitro* behavior observed so far within the set. In rat liver homogenate, the L-Val ester showed a half-life of about 25 min, comparable to the half-life of PEA in the same conditions, but the levels of released PEA were low with a C_{max} of 18 nM after 60 minutes of incubation. This suggested that the either the prodrug **8** is itself a substrate for specific FAAH-mediated amidase metabolism or that released PEA is quickly metabolized as soon as it is released by the prodrug.

Considering the L-Ile prodrug (**9**), it is possible to further confirm that the steric hindrance in the amino-acid side chain is positively related to the prodrug half-life, both in rat plasma and in liver homogenate.

In rat plasma, for instance, a 200-fold increase in plasma half-life was observed, if compared to L-Ala prodrug **7**. For the subsequent developability of the prodrug, however, it is important to stress that the slow disappearance of **9** was not matched by a corresponding increase in PEA levels, in contrast to what had been observed for the L-val ester **8**. The last prodrug endowed with an hydrophobic side chain was the L-tryptophan ester **10,** characterized by the large, but planar, steric hindrance of its indole ring. The results showed that **10** was rapidly converted in rat plasma ($t_{1/2}$ ~ 5 min) and, in rat liver, its half-life was only slightly longer ($t_{1/2}$ ~ 36 min) than that of L-val prodrug **8**. This suggested that a three-dimensional steric hindrance, as that guaranteed by branched side-chains, is required to increase metabolic stability towards rat plasma aspecific hydrolases.

All ester prodrugs analyzed so far were characterized by the conjugation of PEA with amino acids having side chains of hydrophobic nature. The systematic study on structure-stability relationships within the class of ester prodrugs of PEA considered a set of conjugates with amino acids having polar, but non ionizable, side chains, such as L-asparagine (**11**) and L-glutammine (**12**).

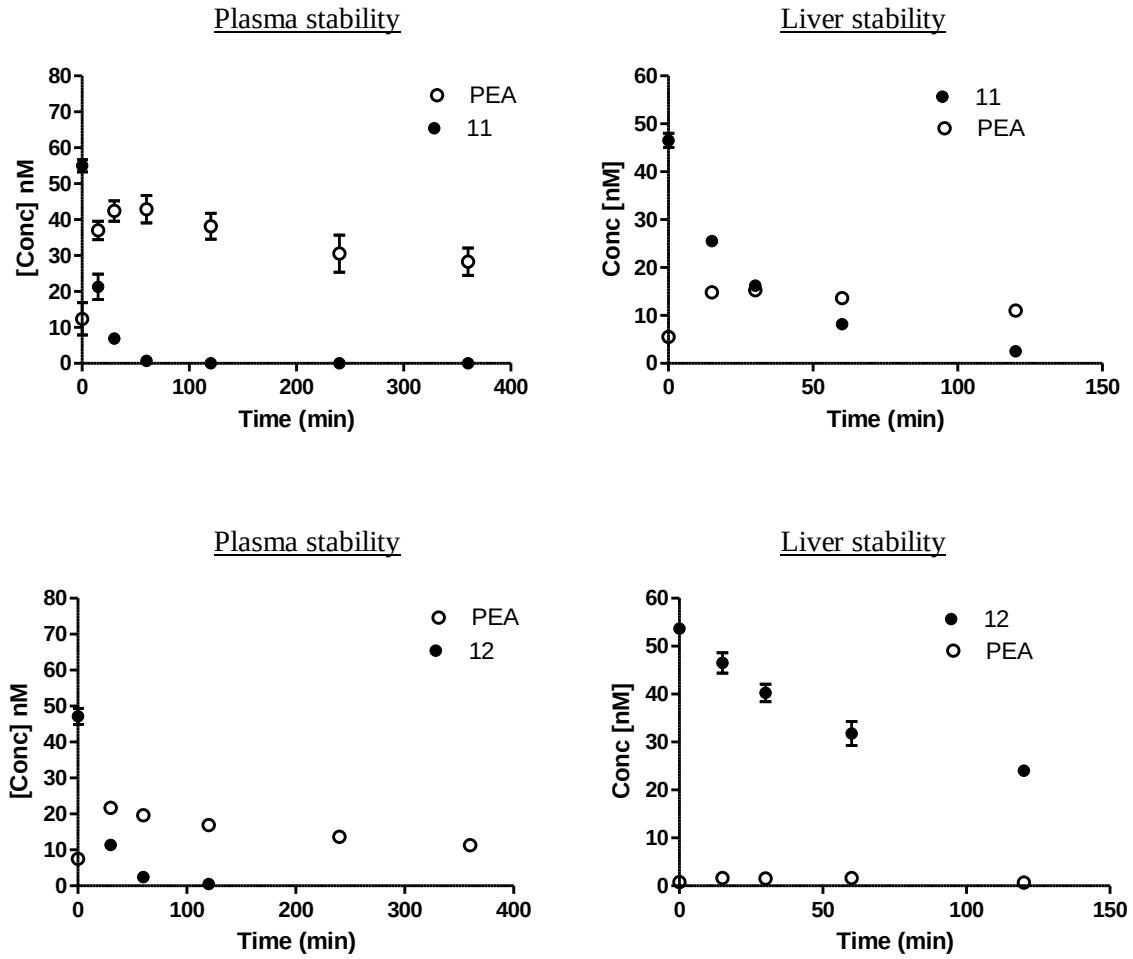

L-asparagine prodrug (**11**) showed a rather short half-life in rat plasma ($t_{1/2}$=9 min), slightly higher in rat liver homogenate ($t_{1/2}$=24 min). The release of PEA was quite rapid and almost quantitative in rat plasma, with a C_{max} of released PEA at around 60 minutes, while it was of limited significance in rat liver homogenate. However, for a correct interpretation of the results, it is essential to keep in mind that **11** showed a low stability in the chemical stability assays. In fact, in PBS, after 6h of incubation, only 3% of analyte was still present in the solution. For this reason, the rapid degradation of **11** could be related not only to its metabolic hydrolysis, but, at least partially, to its chemical liability.

The L-Gln prodrug **12** proved to be more stable than its counterpart L-Asn in both metabolic models, with an half-life of 18 min in plasma and 80 min in rat liver homogenate. These results seemed to confirm that the elongation of the amino acid side chain could increase the metabolic stability.

It is interesting to observe that the cleavage of prodrug **12** is particularly reduced in the rat liver preparation. This can be explained by the fact that the polar side chains of these amino acid derivatives could decrease the

affinity of the prodrug for the FAAH active site. Indeed FAAH, being specific for the NAEs, is highly specific for molecules with long alkyl hydrophobic chains.

PEA was also conjugated to the polar L-Asp, endowed with an acidic ionizable side-chain, via either the α- (**13**) or the ω- (**14**) carboxylic group.

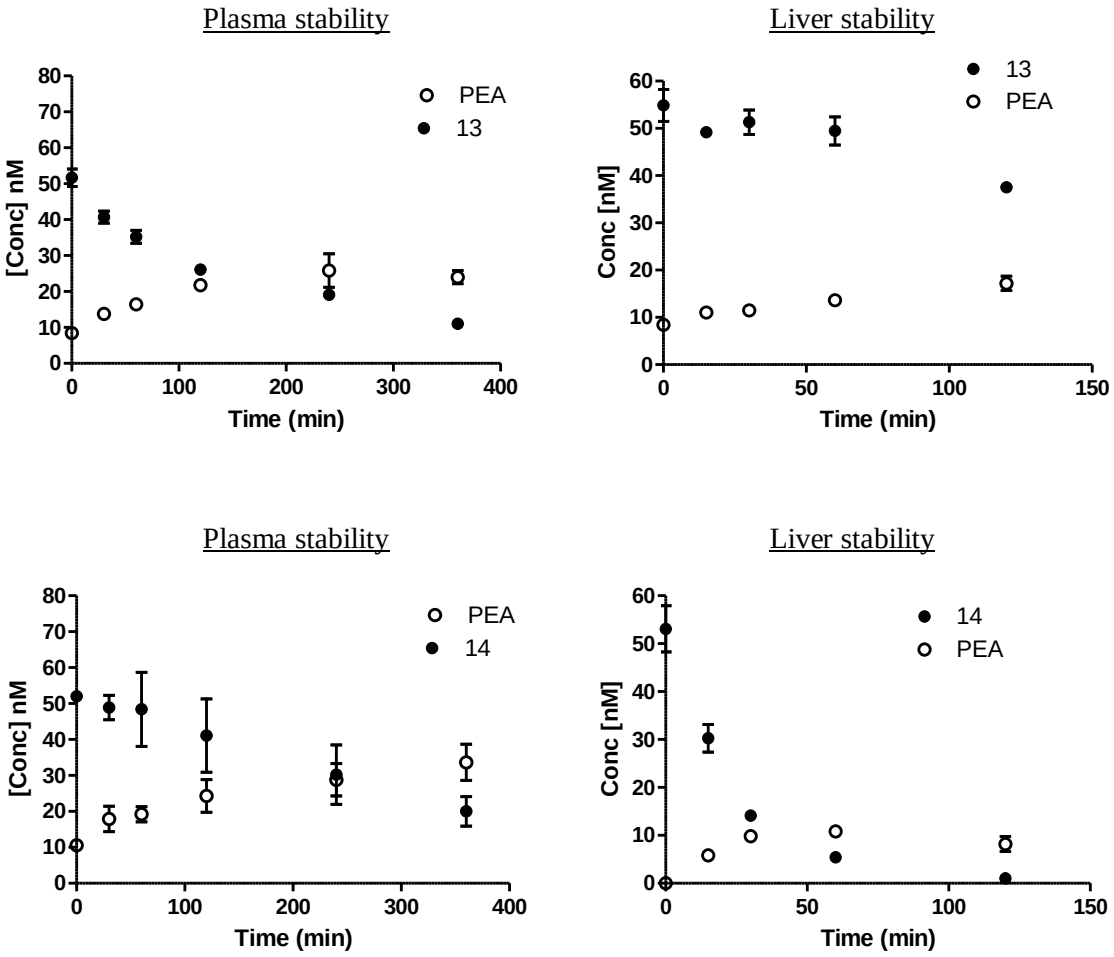

As it can be seen from the plots, the introduction of an ionized polar amino-acid lead to a remarkable increase of stability in both biological matrices. The half-life of **13** was 172 minutes in plasma, while in the rat liver homogenate after 2 hours of incubation a 66% of initial prodrug concentration was still remaining. This result made the prodrug **13** the most stable of the whole series in the rat liver preparation. Also in this case the decrease in the binding affinity vs. FAAH can be evoked as a possible explanation of the observed behavior.

Also prodrug **14** showed an interesting behavior, with a very high half-life in rat plasma and equal to 262 min; nevertheless, the stability in rat liver homogenates was not comparable, with a $t_{1/2}$ of 21 minutes.

Finally, the effect on stability of chirality inversion was explored by introducing two amino acids belonging to the D-series, D-valine (**15**) and D-asparagine (**16**).

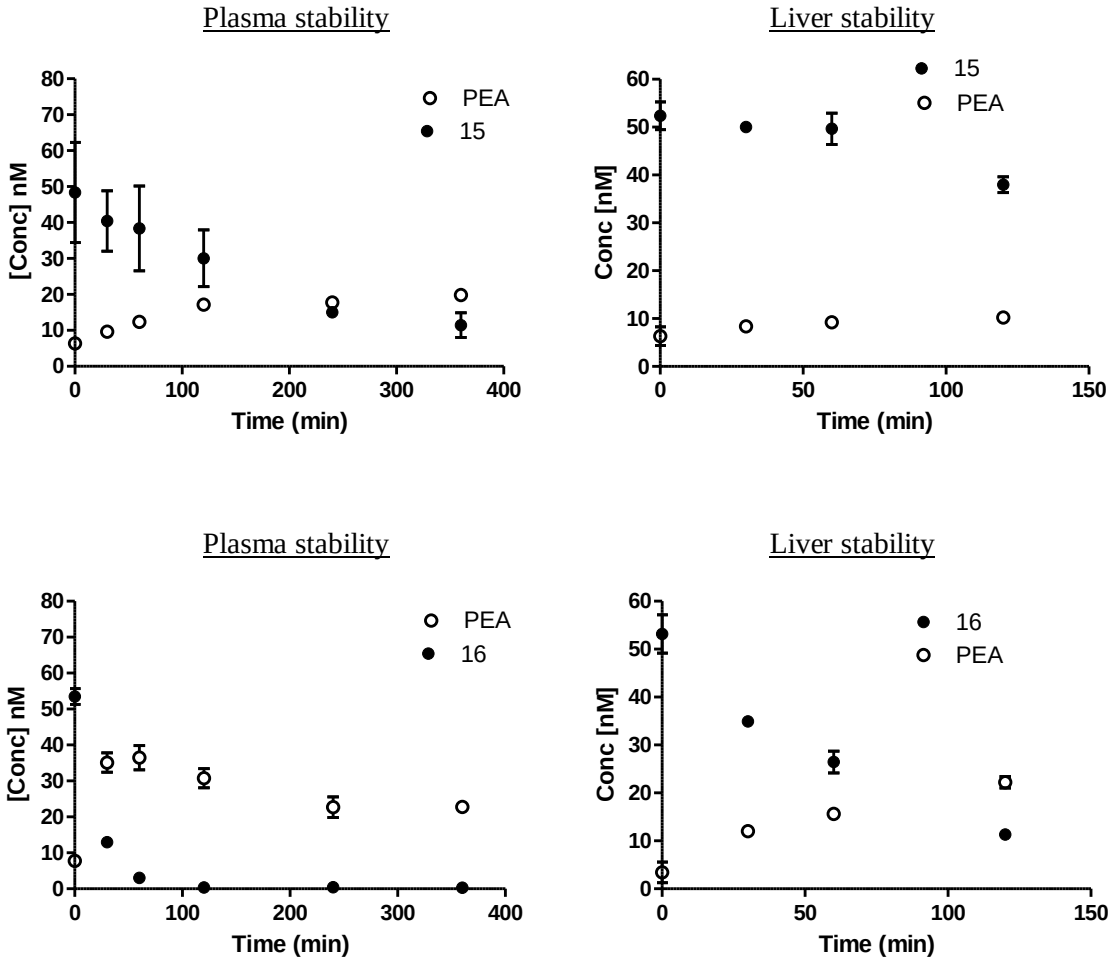

As it can be seen in the plots, the chiral inversion in Val-PEA prodrugs (**15**) had a marked effect on stability in both biological matrices. The plasma half-life of **15** was 173 minutes, over 6-fold that its L-stereoisomer, but there was a lower conversion to PEA (C_{max} = 20nM vs. C_{max} = 44nM for **8**). Compound **15** was much more stable in rat liver as well, as 67% of prodrug was still present after 2 h of incubation.

Rat plasma stability of D-asparagine (**16**) was low and comparable to that of its L-stereoisomer. This result could however be influenced by the low chemical stability observed for **16**. In rat liver, **16** was more stable than L-asparagine (**11**), with a half-life of 55 min.

The strategy of the D-amino acid prodrugs seemed a good choice in order to improve the overall time-course of released PEA, reaching a higher t_{max}. However, no quantitative release of PEA was observed in both biological models for both the D-amino acid prodrugs tested.

3.5.6 Effect of FAAH inhibitor URB597 on rat liver hydrolytic metabolism

One evidence that arose from the analysis of stability assays was the remarkable difference between the amount of PEA released by all the prodrugs in rat plasma and rat liver homogenate.

Indeed, PEA release was almost quantitative in plasma, while in rat liver such a condition was never reached, with an average concentration of released PEA of about 10-15 nM under the best release conditions, nearly a 20% of potentially released PEA. Rat plasma resulted, therefore, an appropriate model for the study of the

relationships between the structural characteristics of the prodrug and their capacity to effectively work as a prodrug releasing PEA, due to the inner stability of the amide bond of PEA under these conditions.

However, cleavage of prodrug in rat liver homogenate did not result in quantitative release of PEA. This could be likely due to the occurrence of enzymatic reactions in this tissue fraction, that presumably not only hydrolyzed the ester linkage, but also the PEA amide bond. For this reason, a series of stability assays were conducted in rat liver preparation incubating the most promising prodrug tested, the L-valine ester **8**, with a selective inhibitor of PEA degrading enzyme, FAAH. Both PEA and the prodrug **8** were incubated after pretreatment (10 min) with the FAAH inhibitor URB597, which has an in vitro IC_{50} on liver FAAH of about 3 nM.[120]

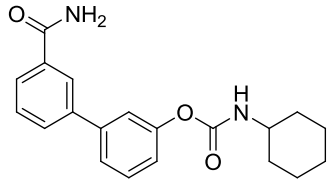

URB597

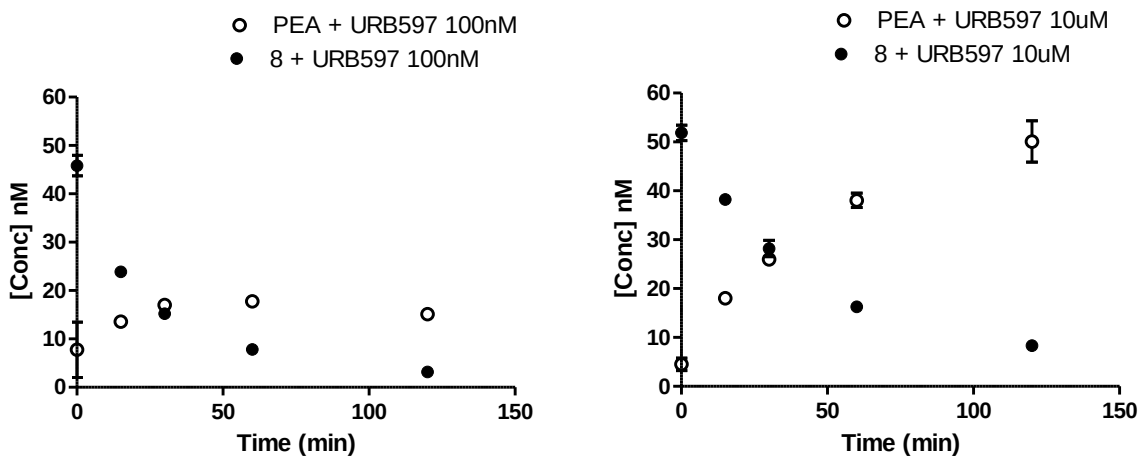

Figure 25: *PEA and compound **8** levels after addition in liver homogenate of 50nM of compound **8** and pre-treatment with 100nM (left) and 10µM (right) of URB597*

Pre-incubation with 100 nM of URB597 caused a partial, but statistically significant, increase of PEA concentrations if compared to control incubations of both PEA and **8**. Only with pre-incubation of 10µM of inhibitor it was observed a remarkable increase of PEA, reaching quantitative concentration levels during time, without a significant increase in the half-life of **8**. This indicated that only the amidase activity was inhibited. The same pre-incubation analysis was conducted on rat liver homogenate after addition of PEA 50 nM.

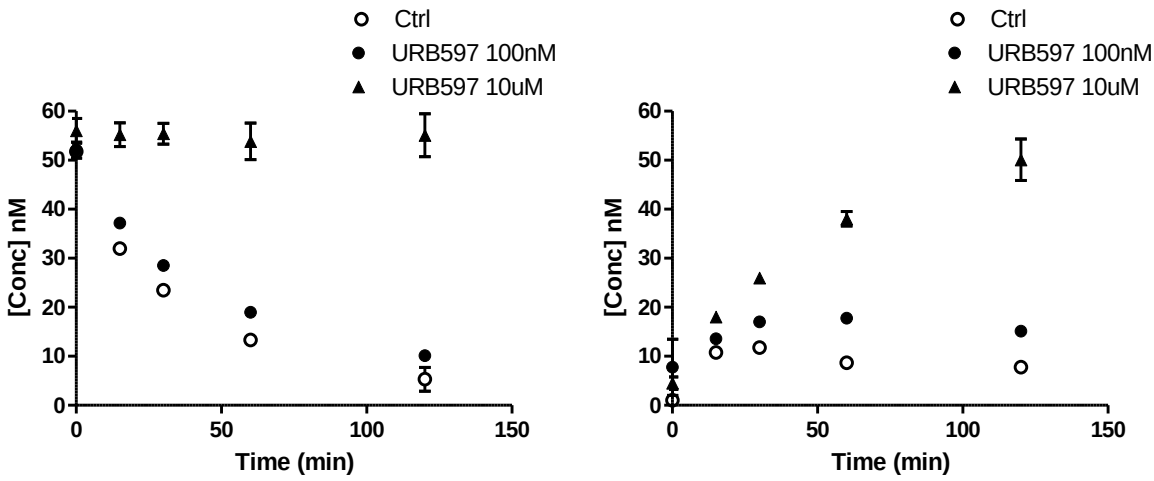

Figure 26: *PEA levels in rat liver homogenate after addition of 50 nM PEA (left) or addition of 50 nM L-Val-PEA prodrug (right) with pre-treatment with FAAH inhibitor URB597 at the final concentration of 100 nM and 10 µM, if compared to controls.*

Also for PEA, a 10µM concentration of FAAH inhibitor URB597 was required to completely inhibit PEA metabolism. It can be inferred that at the high total protein content of the rat liver homogenate (around 6mg of protein in 0.5mL of 10% liver homogenate), much higher than that normally employed for the FAAH enzyme activity assays (10 µg of protein per assay), high concentrations of inhibitor are required to completely inhibit the FAAH enzyme population. For completeness, however, it must be remembered that, at such high inhibitor concentrations, there is an increased risk of losing FAAH inhibitor selectivity, as it has been reported that other serine hydrolases in rat liver, such as carboxylesterases, could be targeted by URB597.[121,122]

To further evaluate the role of amide bond hydrolysis in prodrug transformation, we prepared and tested (S)- and (R)-α-methyl-PEA (**17** and **18**). These compounds are characterized by the presence of a methyl group on the ethanolamine α-carbon which sterically hampers enzymatic hydrolysis of the amide bond. Similarly, the analogs (S)- and (R)-α-methyl-OEA had been shown to be stable in mouse liver homogenate and the plasma and liver C_{max} of (R)-α-methyl-OEA were significantly higher than those of OEA when administered to rats by the oral route.[123] As expected, compounds **17** and **18** were stable in both PBS buffer and rat plasma. They were stable in rat liver homogenate as well, with 79 and 87 % of compound unaltered after 2 h, respectively. Therefore the L-Val ester prodrug of (R)-α-methyl-PEA was prepared to compare its stability with that of the L-Val prodrug of PEA (**8**). The L-Val-(R)-α-methyl-PEA prodrug **19** was stable in PBS buffer and its half-life in rat plasma (190 min) was 4-fold longer than that of **8**. In rat liver homogenate compound **19** showed a significantly longer half-life (38 min versus 26 min for **8**) and, interestingly, a greater conversion to the parent (R)-α-methyl-PEA (C_{max} of released PEA = 29 nM versus 12 nM for **8**). This result underlines that, in rat liver homogenate, hydrolysis of the amide bond in the PEA moiety of **8** and other amino-acid esters exerts a significant role in prodrug degradation and could represent a limitation to the release of PEA *in vivo* after oral administration of these prodrugs.

3.5.7 Pharmacokinetic evaluation in Wistar Rats

The L-valine ester prodrug (**8**) showed a promising conversion rate to PEA in rat plasma, both in terms of the maximum reached concentration (C_{max} = 44 nM) and time when this concentration was reached (t_{max} about 300 minutes); its enantiomer D-valine ester prodrug (**15**) showed a significantly reduced *in vitro* hepatic clearance, which should convert *in vivo* to a reduced first-pass metabolism. As these are two key factors for the efficiency of PEA release *in vivo* from the prodrugs, both **8** and **15** were submitted to oral exposure studies in Wistar rats and compared to oral PEA. PEA itself and the two prodrugs **8** and **15** were orally administered to male Wistar rats, with equimolar doses of 145 mg/kg for prodrugs and 100 mg/kg for PEA. Basal plasma levels of PEA were measured before prodrug and PEA administration and at specific time points t =15 min, 30 min and 1, 2, 4, 6 and 8 hours).

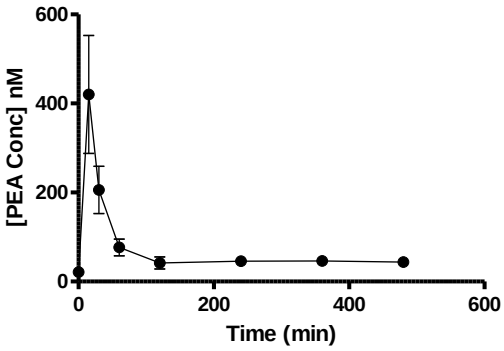

Time [min]	PEA Conc [nM]
Basal Value	21.3 (± 3.7)
15	420.1 (± 132.4)
30	205.9 (± 53.0)
60	76.6 (± 18.7)
120	41.9 (± 13.5)
240	45.8 (± 7.9)
360	46.5 (± 10.5)
480	43.6 (± 7.0)

After administration of a 100 mg/kg dose of PEA, the maximal plasma concentration (C_{max}) was observed at t = 15 min and was equal to 420 ± 132 nM, almost 20 fold its basal levels, which were, in accordance with literature, around 20 nM.[92,73] PEA showed also a rapid redistribution/elimination phase, as after 2 hours from administration, PEA plasma levels were not statistically different from the basal ones. This rapid disappearance from plasma could be partly due to a rapid metabolic degradation from a first-pass effect and/or to a very rapid redistribution towards lipophilic tissue compartments (brain, adipose tissue).

Time (min)	**8** Conc (nM)	PEA Conc (nM)	**15** Conc (nM)	PEA Conc (nM)
0	-	13.5 (± 0.7)	-	14.0 (± 0.4)
15	611.6 (± 169.7)	56.4 (± 13.5)	906.6 (± 559.8)	53.9 (± 19.7)
30	212.0 (± 94.5)	76.8 (± 36.3)	280.3 (± 118.4)	36.3 (± 9.4)
60	35.8 (± 11.5)	29.7 (± 4.8)	65.9 (± 19.8)	25.2 (± 4.1)
120	22.2 (± 6.1)	44.9 (± 10.0)	56.4 (± 9.3)	57.4 (± 8.5)
240	7.1 (± 2.5)	24.5 (± 2.6)	39.9 (± 17.9)	36.4 (± 10.2)
360	2.7 (± 0.9)	21.0 (± 1.6)	11.4 (± 4.3)	18.6 (± 2.0)
480	9.3 (± 4.6)	30.8 (± 6.9)	10.1 (± 2.0)	23.0 (± 2.8)

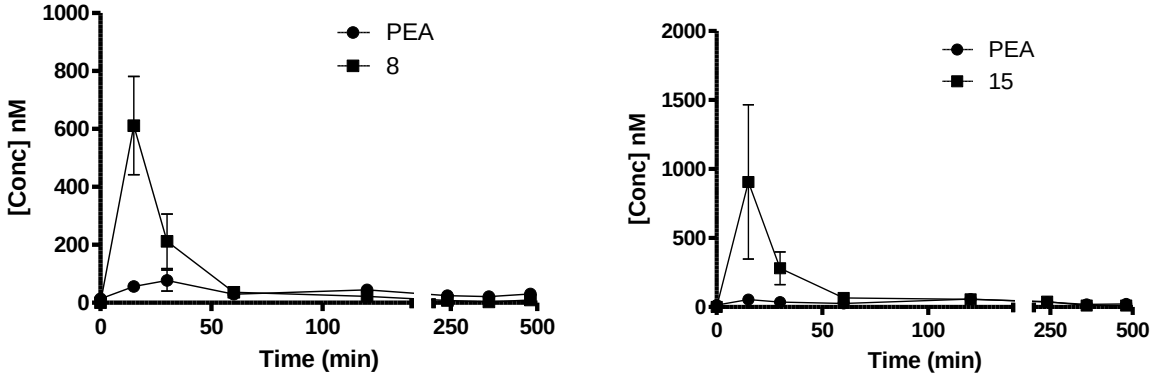

L-Val- (**8**) and D-Val-PEA (**15**) prodrugs reached their C_{max} in rat plasma 15 min after administration. For L-Val-PEA the mean C_{max} value was 612 nM, while for D-Val-PEA a higher mean value was obtained (907 nM), although this difference was not statistically significant ($p>0.05$). AUC_{0-480} was 7728(±1986) and 13836(±2886) ng min/mL (mean±SEM, n=9) for L-Val- and D-Val-PEA, respectively, while it was 6525(±1372) ng min/mL for PEA. This indicates that, particularly in the case of D-Val-PEA (**15**), the prodrugs were slightly more available than PEA. This can be attributed to their higher solubility due to the presence of a basic group and/or, at least for **15**, increased resistance to amidase-mediated hydrolysis in the liver.

The concentrations of released PEA after administration of L-Val- and D-Val-PEA prodrugs are reported in Table above. At t=15 min levels of PEA released by prodrugs **8** and **15** were about 54-56 nM, 8-fold lower than those obtained at the same time after oral administration of PEA, regardless the different chirality of the amino acid pro-moiety. Levels of PEA released by both prodrugs at longer times were comparable to those obtained by direct administration of equimolar PEA.

Therefore, both prodrugs showed some improvements in their bioavailability, compared to PEA, but they did not behave as reservoirs progressively releasing PEA into plasma.

Several concurring factors may contribute to explain the observed behaviour. A first consideration should be made regarding the observed lack of *in vitro*/*in vivo* correlations. Two prodrugs with promising profiles in terms of conversion rate to PEA in plasma (**8**) or of reduced hepatic clearance (**15**) were tested *in vivo*. Given the obtained results, we may conclude that **8** was too labile in the liver to be efficiently converted into PEA in plasma. For **15**, more stable in the liver and more bioavailable than **8** and PEA, its very long plasma half-life could have favored its degradation *in vivo*, rather than its conversion into PEA.

In fact, comparing plasma levels of **8** and **15** at 15 and 30 min, while concentrations of both prodrugs showed a marked decrease, plasma levels of PEA in rats treated with **8**, but not **15**, increased. This difference may be due to the lower propensity of **15** to be converted to PEA by plasma esterases. The lack of PEA appearance in plasma could be due to rapid distribution to lipophilic tissues where the prodrugs can be stored and/or cleaved. In fact, the increase of PEA levels at 120 min, when prodrug levels in plasma had already decreased, could be the consequence of redistribution from some tissue storage.

Plasma levels were accompanied by a high variability. In the case of PEA, it can be explained by its unfavorable physico-chemical properties, particularly its high lipophilicity and poor solubility, which make

absorption through the gastro-intestinal tract extremely variable. The prodrugs have rather improved physico-chemical properties, as revealed by their higher systemic exposures, but their plasma levels presented high inter-individual variability as well. This suggests that chemical derivatization of PEA needs to be supplemented with an accurate study on formulation.

3.5.8 Conclusions

A first attempt to optimize physico-chemical and pharmacokinetic properties of PEA was reported by the prodrug approach and the chemical derivatization of the hydroxyl group of PEA. Two different *in vitro* models were employed in order to assay the hydrolytic metabolism of prodrugs and the corresponding release of PEA (rat plasma), and to evaluate the resistance against the endogenous metabolism represented by specific (FAAH) and non-specific metabolic enzymes (rat liver homogenate). The analytical method in liquid chromatography coupled to tandem mass spectrometry (HPLC-ESI-MS/MS) here developed, permitted the quantification of endogenous (PEA) and exogenous (prodrugs) analytes in biological matrices. The HPLC-ESI-MS/MS method here described successfully fulfilled the analytical requirements of selectivity, sensitivity, linearity, accuracy and precision in a dynamic range useful for the evaluation of the tested analytes both *in vitro* and *in vivo* experiments. The results obtained from these *in vitro* studies led to the characterization of the role of some structural determinants (steric hindrance, hydrophilic/lipophilic balance, chirality) on prodrug hydrolytic stability. It was possible to demonstrate that the increase of the three dimensional steric hindrance, of hydrophilicity and the choice of D-amino acid conjugates, could increase the stability of tested prodrugs towards the non-specific plasma esterases and the specific enzymes targeting PEA in rat liver homogenate (FAAH). This systematic structure-stability analysis led to the selection of two promising candidates for the subsequent pharmacokinetic investigation *in vivo* in Wistar rats. However, a marked first-pass metabolism, together with a massive redistribution from plasma to other tissues, that may have occurred *in vivo*, negatively influenced the bioavailability and the capacity of chosen prodrugs to release PEA.

In conclusion, these results point out that further efforts combining the synthesis of new derivatives designed to be more resistant to FAAH in the liver and their screening through *in vitro* tests with plasma and liver tissue fractions combined with the assessment of *in vivo* pharmacokinetics could result in the development of PEA prodrugs with improved pharmacokinetic and therapeutic properties.

3.6 Materials and Methods

3.6.1 Tested compounds

All compounds were synthesized in the laboratories of the Drug Design and Discovery Group, Pharmacy Department, University of Parma under the supervision of Prof. Marco Mor. Biological matrices (rat plasma, rat liver homogenate) were supplied and *in vivo* experiments were conducted by the laboratories of Pharmacology, Pharmacy Department, University of Parma under the supervision of Prof. Elisabetta Barocelli.

3.6.2 Biological matrices

Rat plasma and rat liver homogenate used for stability test were obtained from Wistar Rats, 150-250 g of weight (Charles River Laboratories, Milan, Italy). All experiments were carried out maintaining the animals in compliance with the Guide for the Care and Use of Laboratory Animals published by the US National Institutes of Health (NIH Publication No. 85-23, revised in 1996). Research protocols were approved by the local Ethical Committee for Animal Experimentation of the University of Parma and the Italian Ministry of Health (D. Lgs 116/92, authorization number 17/2014-B). After the sacrifice of the animals with CO_2 inhalation, plasma was withdrawn with a cardiac injection with heparin as anticoagulant, pooled then centrifuged at 4500 g, 4°C, 10 min, and maintained at -70°C until experiment. Liver was perfused with 60 mL ice-cold saline before explant. Then livers were cut into small pieces, pooled and homogenized (20% w/v) with 0.01 M ice cold Phosphate Buffered Saline buffer (PBS) pH 7.4 and maintained at -70°C until experiment. To measure the total protein content, the Bradford colorimetric assay was employed with bovine serum albumin as reference standard for calibration.

3.6.3 Chemical stability

All compounds were tested in 0.01 M PBS buffer pH 7.4 with 40% v/v of acetonitrile to avoid compound precipitation, at fixed temperature (37 ± 0.1 °C). Stock solutions of chemical compounds were prepared in DMSO (0.01 or 0.005 M), then diluted in order to obtain a final concentration of 50nM with 1% DMSO v/v. After incubation for different time periods (0 and 360 min), aliquots of 50 µL were withdrawn and were added with 100 µL of acetronitrile with 75nM IS (PEA-d4) and then injected in the UHPLC-ESI-MS/MS. For each tested compound, a LC–ESI-MS/MS method in SRM mode was set up in order to monitor the relative amount at the different incubation times compared to the 0 time. All stability test are monitored in triplicate.

3.6.4 Stability in rat plasma

Pooled rat plasma was used at 80% v/v with 20% v/v of 0.1 M PBS buffer pH 7.4, in order to avoid the alkalization of the biological matrix upon storage and during the experiments. Rat plasma added with PBS buffer were pre-thermostated 10 min at 37°C before the compound addition. Stock solutions of compounds were prepared in DMSO (10 mM or 5 mM), then serially diluted in order to obtain a final concentration of

50 nM with 1% DMSO v/v in the assay sample. After sample incubation for different time periods (t = 0, 15, 30, 60, 120, 240 and 360 min), aliquots of 50 µL were withdrawn, deproteinized with a double volume of acetonitrile containing the internal standard (IS) PEA-d4 75 nM. Samples were then centrifuged (14000 g, 10 min, 4°C), and the supernatants were directly analyzed by HPLC–MS/MS. For each tested compound, a LC–ESI-MS/MS method in Multiple Reaction Monitoring (MRM) mode was set up in order to monitor the relative concentrations at the different incubation times. All stability assays were performed in triplicate.

3.6.5 Stability in rat liver homogenate

20% w/v pooled rat liver homogenate was diluted with equal volume of 50 mM Tris buffer pH 7.4 containing 0.64 M sucrose, following previously described procedures.[174] Briefly, samples were centrifuged at 1000 g, 10 min, 4°C, then an aliquot of 495 µL of supernatant was withdrawn and pre-thermostated for 10min at 37°C before compound addition. Stock solutions of compounds were prepared in DMSO (10 mM or 5 mM), then serially diluted in order to obtain a final concentration of 50 nM with 1% DMSO v/v in the assay sample. After incubation for different time periods (0, 15, 30, 60, 120, and 240 min), aliquots of 50 µL were withdrawn, deproteinized with a double volume of acetonitrile containing the internal standard 75 nM PEA-d4. Samples were then centrifuged (14000 g, 10 min, 4°C), and the supernatants were directly analyzed by HPLC–MS/MS. For each tested compound, a LC–ESI-MS/MS method in MRM mode was set up in order to monitor the relative concentrations at the different incubation times. All stability assays were performed in triplicate.

3.6.6 *In vivo* studies

Male Wistar rats (Charles River Laboratories, Italy), 150-250 g in weight, were used in all experiments. L-Val-PEA (**8**), D-Val-PEA (**15**) or PEA were orally administered by gastric gavage to 18 h fasted rats as a corn oil suspension at the equimolar doses of 145 mg kg^{-1} for L- and D-Val-PEA and 100 mg kg^{-1} of PEA, respectively. Blood samples were collected via sub-tongue puncture from each rat before treatment and at t = 15, 30, 60, 120, 240, 360 and 480 min post-dosing into heparin-treated tubes, immediately centrifuged (5000 rpm, 10 min, 4 °C). Resulting plasma was immediately processed by protein precipitation with a double volume of ice-cold acetonitrile containing the Internal standard 75 nM PEA-d4 and analyzed as previously described in the rat plasma stability section.

3.6.7 Instrumentation

The chemical and metabolic stability of compounds were monitored employing a Thermo Accela 1250 Ultra High Performance (UHPLC) system equipped with an Accela OpenAS autosampler. Mass spectrometry analyses were performed on a Thermo TSQ Quantum Access MAX triple quadrupole mass spectrometer (Thermo Italia, Milan, Italy) equipped with an heated electrospray ionization ion source (H-ESI II). Data acquisition and processing were performed using Xcalibur software (version 2.1). Chromatographic separation was achieved on a Synergi 4u Fusion RP 80A C18 (100 × 2.0 mm i.d., 4 µm, Phenomenex).

Mobile phases consisted of water (eluent A) and acetonitrile (eluent B), both additioned with 0.1% v/v formic acid at a flow rate of 350 μL min^{-1}. A linear gradient elution was set up to evaluate the tested compounds in the same chromatographic run. Elution conditions were as follows: T(0 min): 95%A: 5% B; T(1 min): 95%A: 5% B; T(6 min): 5%A:95% B; T(9 min): 5%A:95% B returning to initial conditions after 1 min, followed by 4 min re-equilibration time.

ESI interface parameters were set as follows: probe middle (D) position; capillary temperature: 270°C; spray voltage: 3.0 kV, vaporizer temperature: 250°C. Nitrogen was used as nebulizing gas at the following pressure: sheath gas: 35 psi; auxiliary gas: 15 arbitrary units (a.u.). Argon was used as the collision gas at a pressure of approximately 1.5 mtorr (1 torr = 133.3 Pa). Mass spectrometric analyses were done in positive ion mode and compound-dependent parameters were optimized by flow injection analysis (FIA). For quantitative analysis, the following parent ion → product ions transitions were selected:

• **PEA**: m/z 300.2 → m/z 62.3 (tube lens 60; collision energy 19 eV)

• **PEA-d4**: m/z 304.2 → m/z 66.3+m/z 287.2 (tube lens 72; collision energy 15, 12 eV)

• **1**: m/z 416.3 → m/z 282.1+m/z 344.3 (tube lens 74; collision energy 19, 7 eV)

• **2**: m/z 444.4 → m/z 106.2+ m/z 282.3+ m/z 344.3 (tube lens 74; collision energy 22, 19, 8 eV)

• **3**: m/z 484.4 → m/z 106.1+ m/z 282.3+ m/z 344.4 (tube lens 72; collision energy 25, 21, 13 eV)

• **4**: m/z 399.3 → m/z 57.4+m/z 71.3+ m/z 163.2+ m/z 282.3 (tube lens 62; collision energy 37, 33, 14, 13 eV)

• **5**: m/z 415.3 → m/z 282.2 (tube lens 66; collision energy 11 eV)

• **6**: m/z 443.3 → m/z 282.3+m/z 300.3+m/z 302.3 (tube lens 70; collision energy 12, 13, 67 eV)

• **7**: m/z 371.3 → m/z 57.3+m/z 282.2+m/z 283.2+m/z 300.3 (tube lens 66; collision energy 35, 13, 16, 11 eV)

• **8**: m/z 399.3 → m/z 72.2+m/z 282.2+ m/z 300.2 (tube lens 105; collision energy 20, 15, 12 eV)

• **9**: m/z 413.4 → m/z 86.2+ m/z 282.3+ m/z 300.3 (tube lens 73; collision energy 18, 15, 13 eV)

• **10**: m/z 486.4 → m/z 132.1+m/z 159.1+ m/z 282.2 (tube lens 85; collision energy 36, 23, 18 eV)

• **11**: m/z 414.3 → m/z 57.3+ m/z 282.2+ m/z 300.2 (tube lens 72; collision energy 46, 19, 13 eV)

• **12**: m/z 428.4 → m/z 130.1+ m/z 147.1+ m/z 282.3 (tube lens 75; collision energy 22, 12, 16 eV)

• **13**: m/z 415.2 → m/z 119.3+ m/z 282.3+ m/z 383.3 (tube lens 74; collision energy 26, 17, 14 eV)

• **14**: m/z 415.3 → m/z 119.3+ m/z 282.3+ m/z 284.4 (tube lens 79; collision energy 15, 12, 25 eV)

• **15**: m/z 399.4 → m/z 72.3+ m/z 282.3+ m/z 300.3 (tube lens 65; collision energy 15, 12, 12 eV)

• **16**: m/z 414.4 → m/z 57.4+ m/z 282.3+ m/z 300.3 (tube lens 61; collision energy 43, 16, 10 eV)

• **17**: m/z 314.3 → m/z 58.4+ m/z 76.26+ m/z 297.20 (tube lens 72; collision energy 17, 14, 5 eV)

• **18**: m/z 314.3 → m/z 58.4+ m/z 76.26+ m/z 297.20 (tube lens 72; collision energy 17, 14, 5 eV)

• **19**: m/z 413.4 → m/z 58.4+ m/z 296.32+ m/z 314.37 (tube lens 69; collision energy 36, 14, 11 eV)

Standard curves for all the analytes, generated on three different working days, showed good linearity in the 1–500 nM concentration range. The coefficients of correlation (r^2) were >0.99 for all curves. The LOQ was 1 nM for all compounds.

4. Monoacylglycerol lipase (MGL)

4.1 Introduction

Monoacylglycerol lipase (MGL) is a 33 kDa presynaptic serine hydrolase that inactivates the endocannabinoid, 2-arachidonoyl-*sn*-glycerol (2-AG), displaying in general a strong selectivity for mono- versus di- and tri-glycerides. The enzyme is found both in the brain and in peripheral tissues such as the kidney, ovary, testis, adrenal gland, adipose tissue and heart.[124] In many of these tissues and cell types, MGL is detected both in soluble and membrane preparations. A huge amount of MGL orthologues from many eukaryotic organisms, including human, chimpanzee, dog, cow, rat, chicken, zebrafish, *A. thaliana* and rice have been cloned, often sharing a high degree of identity. For example mouse and rat MGL possess a percentage of identity with the hMGL as 84.2 and 83.8% respectively.[125] Current research interest for MGL as a pharmacological target has emanated from the finding that in the brain, MGL is highly co-expressed in regions with high cannabinoid G-protein coupled receptor CB1 densities[126] and that in the mouse brain, MGL is the major responsible (~85%) for the metabolism of 2-AG. MGL is found on presynaptic terminals, optimally positioned to break down 2-AG that has engaged presynaptic CB1 receptors. Increasing interest has focused on MGL inhibition as a therapeutic strategy for enhancing indirectly cannabinergic signaling through elevation of tissue 2-AG tone.[127,128]

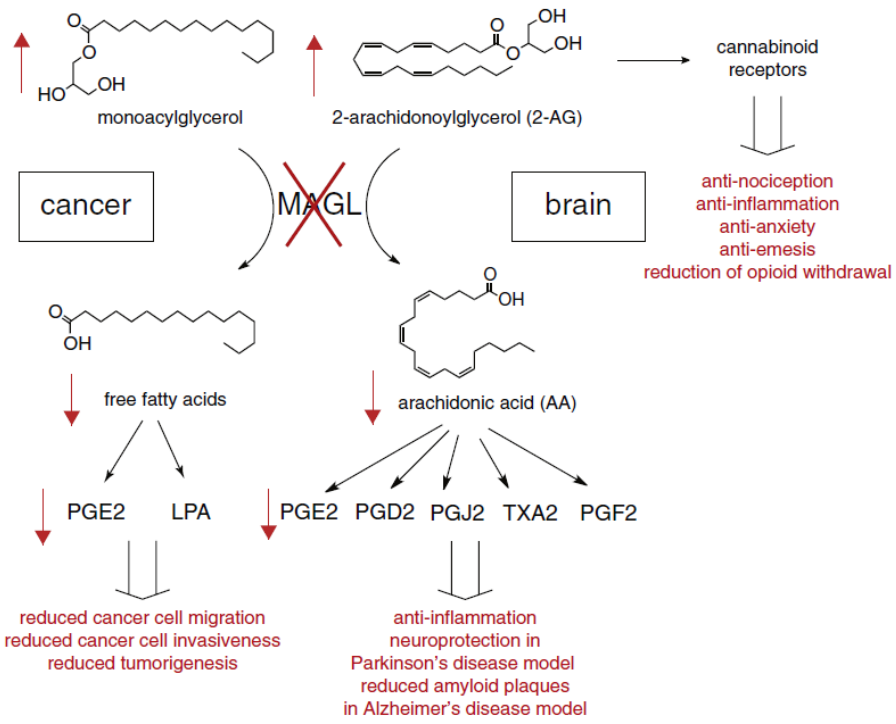

Figure 27: *Lipid signaling pathways regulate by MGL. PGE2 prostaglandin E2; LPA lysophosphatidic acid; PGD2 prostaglandin D2; PGJ2 prostaglandin J2; TXA2 thromboxane A2; PGF2 prostaglandin F2.*[128]

MGL serves as a critical node in coordinating simultaneously multiple lipid signaling pathways in both physiological and disease conditions. Several recent studies have demonstrate that MGL links the endocannabinoid and eicosanoid systems together through hydrolysis of the endocannabinoid 2-AG to provide major arachidonic acid precursor pools for pro-inflammatory eicosanoid synthesis in specific

tissues.[129] With the use of MGL inhibitors, recently it was possible to demonstrate that the inhibition of MGL elicits anti-nociceptive, anxiolytic and anti-emetic responses and attenuates precipitated withdrawal symptoms in addiction paradigms through enhancing endocannabinoid signaling.[129,130,131] The inhibition of MGL also exerts anti-inflammatory action in the brain and protect against neurodegeneration through lowering the eicosanoid production.[132,133] MGL inhibitors demonstrated also anti-cancer properties, not only through the modulation of the endocannabinoid-eicosanoid networks, but also by controlling fatty acid release for the synthesis of pro-tumorigenic signaling lipids.[134]

Structurally, MGL belongs to the "α/β hydrolase fold" family of enzymes, whose conserved three-dimensional structures consist of a central β sheet made from eight β-strands, one of which is antiparallel to the others, and surrounded by a variable number of α helices, the so-called "core domain". The active sites of these proteins are located in turns between the α helices and the β sheets and harbor a classic catalytic triad composed of a serine, a carboxylic acid, and a histidine. hMGL is no exception, with the catalytic triad (Ser122-His269-Asp239) and the lipase motif GXSXGX.[135] The nucleophilic serine is located at the top of the core in a typical sharp turn between α3 helix and β5 strand. This core domain is overhung by a much more variable domain termed lid domain, made of several α helices and loops. The substrate is recruited via a wide hydrophobic tunnel, where it can then interact with the catalytic triad at the end of the tunnel. The lid domain of hMGL has been considered a dynamic modulator of substrate recruitment/accommodation during the catalytic cycle, it covers residues 158−191 and it encompasses the C-terminal two-thirds of helix α4, the loop that bridges helices α4 and α5, and the N-terminal turn of helix α5 (Fig. 28).[136,137,138] It has also been speculated that the overall hMGL lid domain, and helix α4 in particular, undergoes conformational changes as a mobile flap or cap that transitions the enzyme from an apo- to a liganded form. However, for this protein, there is no biochemical evidence indicating that the interaction with the substrate would require such a structural reorganization of the cap. On the other hand, crystallographic evidence suggests that the cap is flexible and that alternative conformations might be possible.[139]

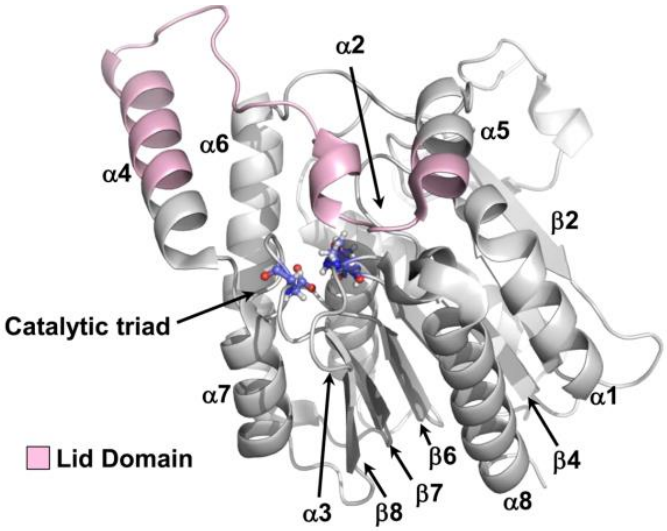

Figure 28: *The catalytic triad (Ser129-Asp246-His276, red/white/blue ball-and-stick depiction), lid domain (residues 158−191, light pink), and secondary structural elements (α-helices 1−8 and β-sheets 2, 4, 6−8) of apo-hMGL are indicated on the wild-type hMGL crystal structure.*[140]

In addition to the Ser-Asp-His triad, there are four cysteine residues in human MGL (C32, C201, C208, C242), whose their thiol groups are not involved in disulfide bond formation.[141] Two of them (C201 and C208) are located in the highly variable region of the lid-domain, while C242 is located in the immediate vicinity of the active site. The forth cysteine, C32, is localized in a highly conserved region and different evidences demonstrate that the interaction with this cysteine does not influence the activity of the enzyme. In rat MGL there are two more cysteines (C55 and C301), but they also do not seem involved in mechanisms of catalysis or in disulfide bond formation.

4.2 MGL inhibitors

In recent years, MGL has been considered a promising target for therapeutics, considering the numerous physiological functions played by the endocannabinoid 2-AG; selective inhibitors of this enzyme could reveal useful as pharmacological tools to characterize MGL physiological role and for the treatment of pain and inflammatory disorders, as well as in cancer research, among others.

Since MGL is a serine-hydrolase, the first group of tested inhibitors were developed to target the serine residue of the catalytic triad. This first class of inhibitors bind reversibly or irreversibly to the nucleophilic serine, thus interrupting the catalytic activity of the enzyme. Methylarachidonylfluorophosphonate (MAFP) is among the most potent MGL inhibitors identified to date.[142] However, even if MAFP inhibits MGL irreversibly, it lacks selectivity, as it inhibits the majority of the members of the serine hydrolase family of metabolic enzymes, including FAAH. The first compound to be reported with selectivity for MGL over FAAH was a carbamate compound, biphenyl-3-ylcarbamic acid cyclohexyl ester URB602.[143] This compound inhibits MGL activity through a non-competitive, partially reversible mechanism and could elevate 2-AG levels in rat brain. More recently, another carbamate compound known as JZL184 was introduced as a potent and specific MGL inhibitor.[144] JZL184 acts as a potent irreversible inhibitor of MGL with a 300-fold higher selectivity for MGL versus FAAH. *In vivo*, a dose of 16 mg/kg i.p. given to mice produced an almost complete inhibition of MGL with only a partial inhibition of FAAH and no significant effects on any of the other serine hydrolases investigated using the activity-based profiling technique.[144] Moreover, in an *in vitro* study JZL184 inhibited mouse and human MGL with equal potency (IC_{50} = 2 nM), but showed ~10-fold lower activity against rat MGL.[145]

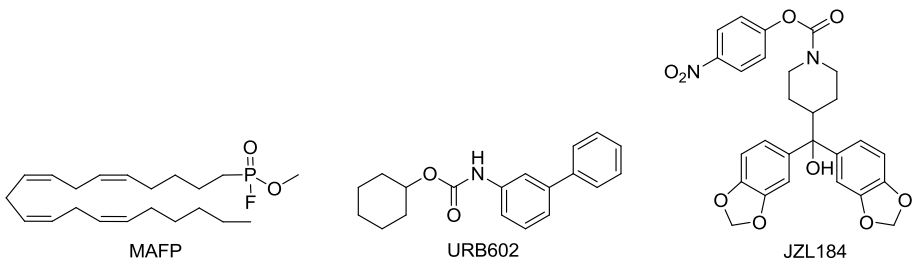

Figure 29: *Molecular structures of MGL inhibitors.*

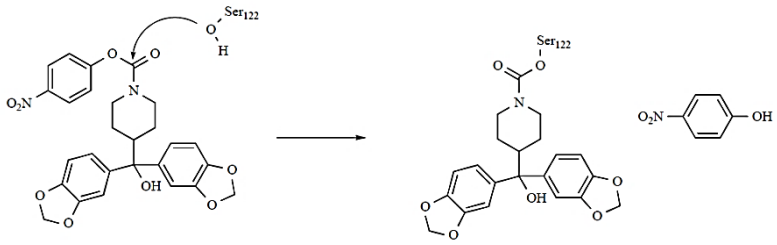

Figure 30: *Mechanism of MGL inhibition by JZL184.*

Three conserved cysteine residues appear to significantly contribute to the regulation of MGL function (C201, C208, C242) and are residing near the active site.[146] Studies conducted on rat MGL, demonstrated that mutation of C201 or C208 determines a significant reduction in enzyme activity, although less than that resulting from the mutation of C242.[150] These data stressed the importance of the regulatory role played by these cysteines outside the active site and the possibility of using them as a new potential targets of a new class of Cys-targeted inhibitors that could modulate the activity of MGL, not interacting directly with the catalytic serine.

A first class of Cys-targeted inhibitors were the substituted maleimide derivatives discovered by Saario et al., including N-arachidonoylmaleimide (NAM), which was able to inhibit by a ~85% MGL-like enzymatic activity in rat cerebellar membranes[146] and rat adipocyte subcellular fractions. In rat MGL, the IC_{50} of NAM is in nM range (140 nM[146]; 46 nM[150]) and with mutational studies it was possible to hypothesize that cysteine involved in the reaction of Michael addition was Cys201. Human MGL revealed to be less sensitive to NAM (IC_{50} = 1.12 μM[147]). Also in the presence of high NAM:MGL molar ratios (33:1) the enzyme is inhibited by a ~85%. As previously said, it is not completely clear which cysteine is involved in the covalent reaction with NAM. In human MGL, MALDI-TOF MS and mutational studies have shown that NAM reacts preferentially with Cys208 and Cys242 by a Michael addition.[148] In a later work, Labar and colleagues demonstrated, with cysteine to alanine mutants (C201A, C208A, C242A, C208A/C242A), that inhibition mainly involved Cys201, although an involvement of Cys242 was not excluded.[138] In a more recent study, Laitinen and colleagues confirmed that Cys201 is the principal NAM target in hMGL, as C201A mutation clearly blunted the inhibitory potency and efficacy of NAM.[149] Moreover, to gain further insight into the interaction of NAM with hMGL, they covalently docked this inhibitor into Cys201. Their modeling data indicated that NAM binding seems to interfere with the organization of the glycerol exit hole, a finding implicating that the inhibition may be due to blocking the enzyme from the outside (masking the glycerol exit hole) rather than due to steric hindrance for substrate entry and/or inhibition of substrate hydrolysis by targeting Cys208 or Cys242.[149]

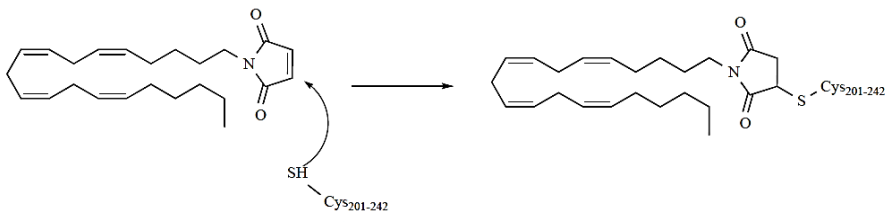

Figure 31: *Mechanism of MGL inhibition by NAM.*

The observation that compounds reacting with sulfhydryl groups could be potent MGL inhibitors led to the identification of the two isothiazolone-based and benzisothiazolone-based octhilinone and N-octylbenzisothiazolinone, which inhibited rat MGL with approximately 20-fold selectivity over FAAH.[150] The inhibition was partially reversible, it was decreased by the reducing agent DTT and involved the formation of a reducible disulphide bond with the sulphydryl groups of cysteines Cys208 and maybe Cys201. Matuszak and colleagues studied the inhibition of octhilinone and benzisothiazolinone-based inhibitors on human MGL.[151] For octhilinone, an IC_{50} of 140 nM was measured on wt hMGL, and the inhibitory potency was reduced of nearly two-orders of magnitude in the C208A, C242A mutants. The mutation of Cys201 also reduced the potency of octhilinone, but to a lesser extent (less than one order). For benzisothiazolinone, an IC_{50} of 660 nM was measured on wt hMGL; however, the inhibitory potency was reduced of approx. 1-1.5 orders of magnitude in the C201A, C242A mutants. The mutation of Cys208 did not significantly affect inhibitory potency. Also in their experiments, DTT was able to revert completely inhibition by both iso- and benzisothiazolinones.[151]

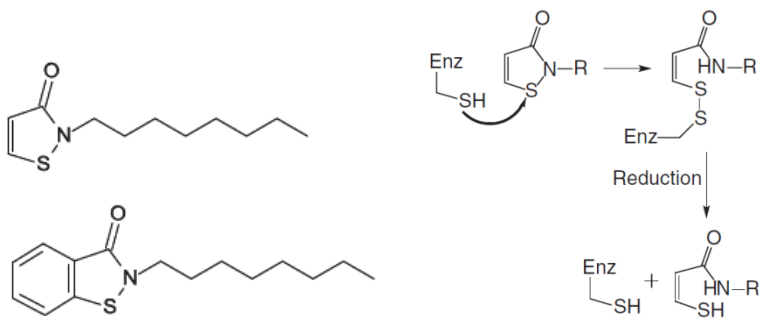

Figure 32: *Left: chemical structures of isothiazolinone and benzisothiazolinone; Right: scheme illustrating the formation of a disulfide adduct between octhilinone and cysteine.*

The benzisothiazolinone moiety and similar structures have already employed in the preparation of biologically active compounds, such as antimicrobial, antifungal, anti-inflammatory and genotoxic compounds. Chemically, benzisothiazolinones are constituted by a sulfenamidic ring, which derives from an intramolecular attack on the amide of the thiosalicylic acid, condensed with an aromatic ring. These compounds act via the formation of the disulfide bond with the thiol group –SH of critical cysteine residues. The sulfur-nitrogen bond is particularly susceptible to nucleophilic attack by thiol groups, in order to form symmetrical or mixed disulfides. A recent study of the 2,2′-dithiobis[N-isoleucylbenzamide], an inhibitor of HIV nucleocapsid protein zinc fingers, demonstrated that in aqueous solution the compound showed a degradation product: the isoleucyl-benzisothiazolinone.[152] The presence of this product was confirmed by comparison of NMR spectra of the original compound with and without the presence of dithiothreitol (DTT), which caused the reduction of compounds to thiol. Furthermore it was noticed that the rate of disproportionation is reduced by decreasing the pH, the S-S form was stable at pH lower than 2.5. However, under the same conditions the S-H and S-N forms reacted with each other forming again the disulfide bond S-S. Benzisothiazolinones are molecules that possess a complex redox equilibrium between the different

bonds S-S, S-H and S-N (Fig. 33). A more detailed description on benzisothiazolone-based inhibitors is provided in the next chapter.

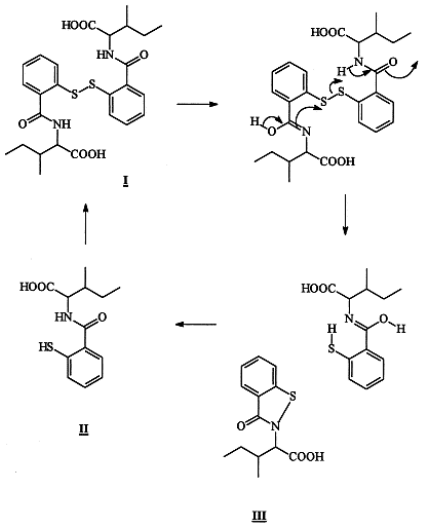

Figure 33: *Proposed route of degradation of I; in aqueous solution, leading to formation of sulfydryl II and benzisothiazolone III.*

4.3 Experimental design and aim of the project

As previously said, several pharmacological studies confirmed the key role that MGL could have as therapeutic target for analgesia and neuroprotection.[132,133,153] MGL is considered the principal enzyme in the endocannabinoid system, as it is responsible for the 85% of the degradation of 2-AG, which is the most abundant physiological endocannabinoid compound. Thanks to molecular modelling and crystallographic studies, it was elucidated how the enzyme acts. These indications were useful for the identification of the first class of inhibitors, the serine-targeted inhibitors URB602 and JZL184, which selectively interact with the serine residue of the catalytic triad. More recently, our research group has focused its attention on the design and synthesis of allosteric inhibitors, like benzisothiazolones, that can inhibit the enzyme targeting critical cysteine residues external to the catalytic site. These compounds behave as partially reversible inhibitors and represent a new potent strategy to increase indirectly 2-AG levels, without the collateral effects of covalent inhibitors.

A preliminary exploration on the structure-activity relationships (SAR) of benzisothiazolinones on target MGL was conducted introducing different substituents at the nitrogen atom of the cyclic sulfenamide.

	R_1	**rMGL IC_{50} (nM)**
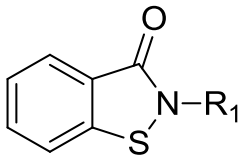		59 ± 5.7
	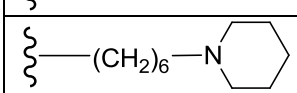	195 ± 12
	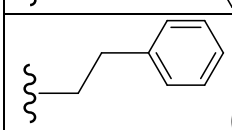 (**20**)	19 ± 1.8

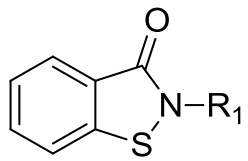	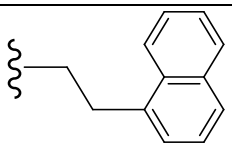	22 ± 5.2
	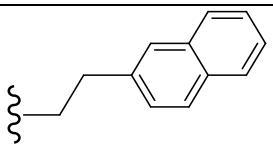	54 ± 15
	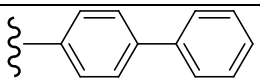	15 ± 0.6

Table 11: *IC_{50} values on rMGL of some newly synthesized benzisothiazolinone-based compounds.*

These preliminary studies on rat MGL showed good results for this class of compounds both in terms of inhibitory potency and in terms of *in vitro* stability under physiological pH conditions; however, the high reactivity in the presence of thiol groups needed further optimization.

Within this Ph.D. program, the research on monoacylglycerol lipase was developed on three main directions:

1) Benzisothiazolone-based inhibitors of hMGL. The benzisothiazolone-based warhead had revealed to be essential for the development of potent inhibitors, but suffered of high intrinsic reactivity and, presumably, of a lack of selectivity, with a high propensity to interact with other biological thiols than MGL. An optimization of the reactivity of the benzisothiazolone warhead was attempted starting from the lead compound **20** (See Table above) and chemically modulating the core benzisothiazolone nucleus by introducing different substituents at positions 5, 6 and 7. The reactivity of compounds was evaluated *in vitro* under physiological pH conditions in the presence of a low molecular weight thiol nucleophile which is known to be present at mM concentrations within living cells, glutathione (GSH). High performance liquid chromatography coupled to mass spectrometry (HPLC-ESI-MS/MS) was employed as the reference analytical technique to investigate the time-course of reaction species generated by the benzisothiazolone-based inhibitor and GSH.

2) Role of hMGL critical cysteine residues as redox sensors. A pharmacological activity assay on recombinant human MGL, employing 2-oleoylglycerol as a substrate and HPLC-ESI-MS/MS separation and detection, was set up and employed to evaluate the effect of reducing and oxidizing agents on hMGL catalytic activity. A classical proteomic protocol was set up on hMGL recombinant protein after protease digestion and it allowed the identification of an oxidative modification to sulphenic acid of one critical cysteine residue (C201) of hMGL. Identification was accomplished by means of MALDI-TOF/TOF mass spectrometry and reaction of cysteine sulphenic acid with the reactive probe dimedone.

3) Conformational changes induced on hMGL by the interaction with a benzisothiazolone inhibitor.

An innovative mass spectrometry technique, hydrogen-deuterium exchange mass spectrometry (HDX-MS), has been employed for evaluating the conformational changes produced on human recombinant MGL by the covalent binding of the benzisothiazolone-based inhibitor **20**.

The second and third themes having as object recombinant human MGL will be described in deep detail in the following chapters 5 and 6. The end of the present chapter will be focused on the presentation of research

results related to the first research theme, i.e. the modulation of reactivity within a series of benzisothiazolone-based allosteric inhibitors of human MGL.

Compound **20** (Table 11) was selected as lead compound, due to its high inhibitory potency on rMGL (IC_{50} = 19 nM). The modulation of reactivity towards thiol nucleophiles (cysteines, glutathione, etc.) was required in order to increase the selectivity of the inhibitor versus MGL, decreasing at the same time the potential toxicity of the newly synthesized compounds.

The chemical modifications introduced on compound **20** and presented in Table 12 involved the substitution on the aromatic ring, with the introduction of substituents endowed of opposite electronic properties at position 5 and 6, and in particular: an electron-withdrawing NO_2 group, in position 5, conjugated to the sulfur atom and in position 6, conjugated to the carbonyl group; electron-donating CH_3O or OH groups in position 5 or 6; then, in position 7 a methyl group, in order to evaluate the role of steric hindrance in the position close to the reactive sulfur atom. Also the side chain was modified, with the introduction of a nitrogen atom. The final aim was to analyze the *in vitro* reactivity of this new series of benzisothiazolinone-based inhibitors in order to generate a reactivity scale among them which could allow the selection of a less reactive/more selective candidate with respect to **20**.

20	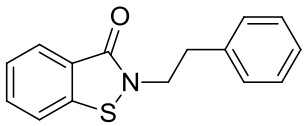	21	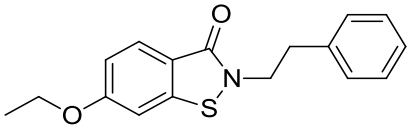
22	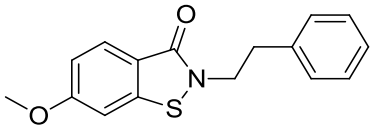	23	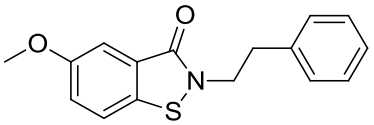
24	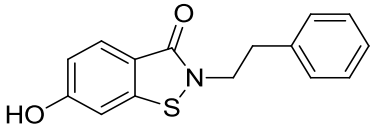	25	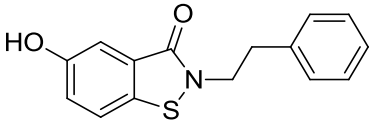
26	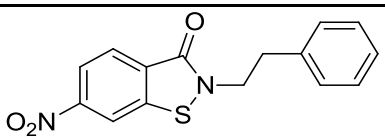	27	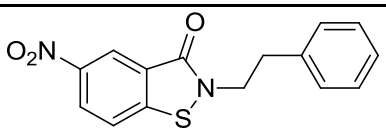
28	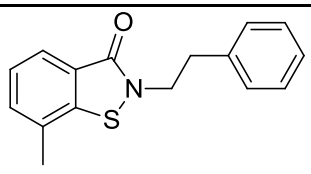	29	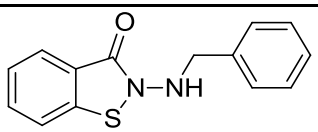

Table 12: *Chemical structures of newly synthesized benzisothiazolinones.*

4.4 Results and Discussion

4.4.1 Set up of *in vitro* reactivity model

High performance liquid chromatography coupled to UV-visible, tandem mass spectrometry and high-resolution mass spectrometry detection was employed as analytical technique to evaluate the reactivity of the set of benzisothiazolone-based human MGL inhibitors with thiol nucleophiles of biological relevance.

The reactivity of the lead benzisothiazolone-based inhibitor **20** was evaluated under physiological pH conditions in the presence of a molar excess of the thiol nucleophile cysteamine or glutathione, and the decrease in the benzisothiazolinone species concentration, the formation of the adduct with the thiol nucleophile and the time-course of newly formed reaction species was monitored by HPLC-UV and HPLC-MS/MS.

In a first set of preliminary experiments, cysteamine was employed as thiol nucleophile, with a 1:1 molar ratio of thiol/benzisothiazolone, following an incubation in 10 mM Phosphate Buffered Saline (PBS) pH 7.4, 37°C. The main scope was to measure the kinetics of the reaction benzisothiazolone:cysteamine with the subsequent formation of thiol adduct, obtaining an half-life of the benzisothiazolinone compound under these pseudo-physiological conditions (pH 7.4; 37°C; in atmosphere). Cysteamine was chosen because of its simple structure and high reactivity. However, it was noticed that right after the addition in PBS buffer of either benzisothiazolinone or cysteamine, the HPLC-UV peak area relative to the benzisothiazolinone was reduced of more than a half, with the immediate formation of three new peaks at different retention time.

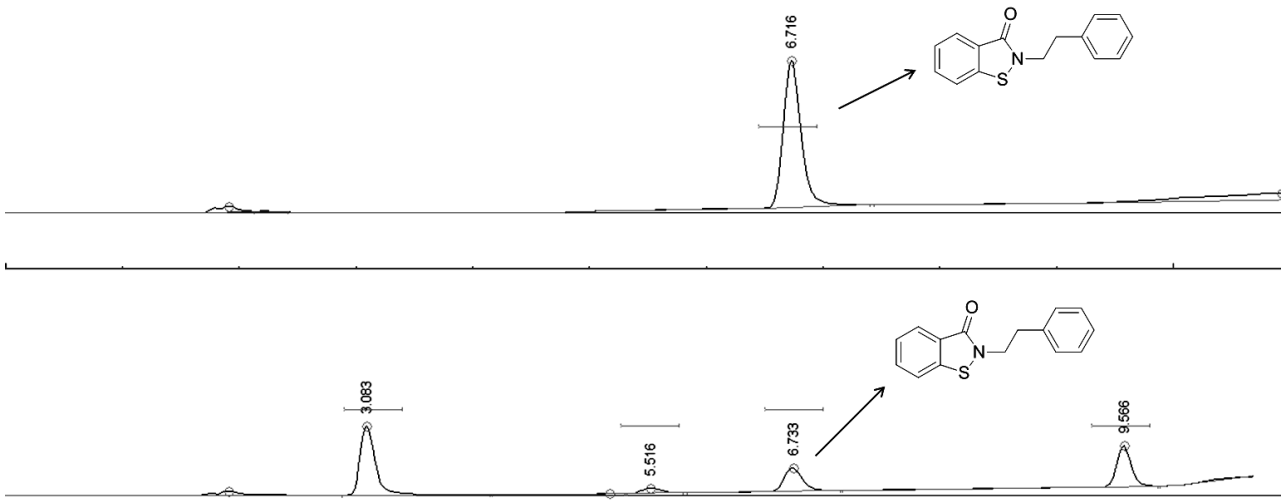

Figure 34: *Above: UV chromatogram of compound **20** 100uM, below: UV chromatogram of compound **20** and cysteamine molar ratio 1:1 after a few seconds of incubation.*

As it can be seen from Table 13, it was verified that other benzisothiazolones compounds had the same instantaneous reactivity with cysteamine, with an half-life shorter than a few seconds. Moreover, it was not possible to notice significant differences between the diverse substitutions in position 6, with remaining percentages of compound lower than 50% for all derivatives. The reported percentages were calculated from the peak area of compounds with and without cysteamine at the same time point (few seconds).

Compound	% of cpd after addition of cysteammine
20	41.0 ± 2.5
21	34.6 ± 6.5
24	39.5 ± 6.0
26	37.2 ± 6.8

Table 13: *Preliminary results of selected benzisothiazolinones with cysteamine.*

For this reason, the experimental approach was changed, employing the less reactive thiol glutathione (GSH), which is considered an important low molecular weight physiological thiol with high intracellular concentrations (1-10 mM) and whose reactivity could also provide some indications on the potential toxicity of benzisothiazolones. Indeed, when a drug/xenobiotic reacts massively with GSH, a depletion of GSH could occur within cells leading to an increase of oxidative stress and to the risk of aspecific reactivity with thiol groups of proteins. Due to the impossibility to measure the reaction kinetics, it was hypothesized that reagents could reach a dynamic equilibrium among the reaction species at a certain time-point, as this behavior had already been observed for the cysteamine experiment at a longer time point (t=60min). It was thus possible to evaluate the identity and the distribution of all the reaction species at a stated time point, after the reaching of the dynamic equilibrium conditions, from which a classification of compounds in terms of their redox potential could be attempted. Preliminary experiments with cysteamine also allowed us to verify that the presence in solution of benzisothiazolone may accelerate the naturally occurring oxidation of glutathione by atmospheric oxygen (data not shown). To minimize this effect and/or to maintain constant the interference of oxygen, reactivity assays were set up under argon atmosphere; moreover, the molar ratio between glutathione and benzisothiazolone was increased from 1:1 to 1:2, because two moles of glutathione are necessary to complete the reactions with one mole of benzisothiazolone.

At the end of the optimization phase for the reaction conditions, the reactivity of **20** was evaluated in PBS buffer at 37°C under stirring and in argon atmosphere, monitored at three time points (t = 5, 60 and 120 min) looking for the achievement of a dynamic equilibrium among reaction species.

A reaction pathway between benzisothiazolone and a thiol nucleophile had already been proposed in the literature,[154] and it is reported in the Scheme 1 below.

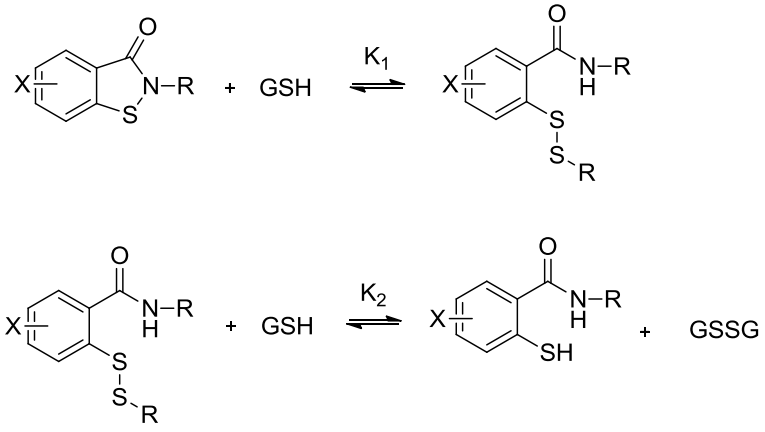

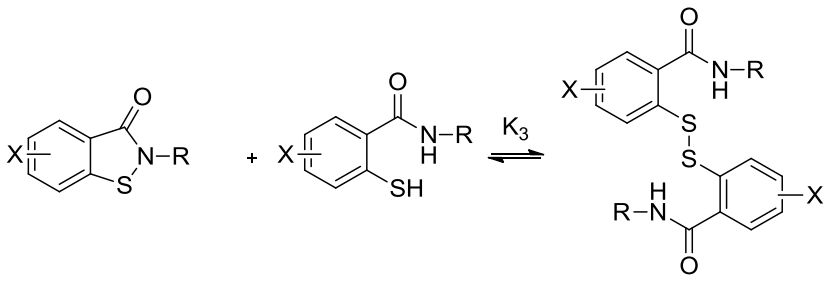

Scheme 1: *Reaction pathway of benzisothiazolones in presence of 2-fold excess of GSH.*

Briefly, reaction of benzisothiazolone (BTZ) with glutathione (GSH) could lead to the formation of a mixed disulfide (BTZ-SG) that is prone to further reacts with another equivalent of GSH to generate a sulfhydryl compound, or 2-mercaptobenzamide, (BTZ-SH) and the oxidized form of glutathione (GSSG). BTZ-SH itself is a thiol nucleophile able to attack both native benzisothiazolone or adduct BTZ-SG in order to generate symmetric disulfide susceptible of a new nucleophilic attack by glutathione. Moreover, it is well known in the literature a disproportion reaction of benzisothiazolone in aqueous media leading to restoration of benzisothiazolone and to the corresponding sulfhydryl compound (BTZ-SH).

4.4.2 Identification of reaction species

In the HPLC-UV gradient shown in Figure 35 (upper row) a peak at RT = 25.2 min is present, corresponding to the standard compound **20** at the concentration of 100 μM. In the second chromatogram the reaction of compound **20** with glutathione (molar ratio: 1:2) is reported at t = 60 min.

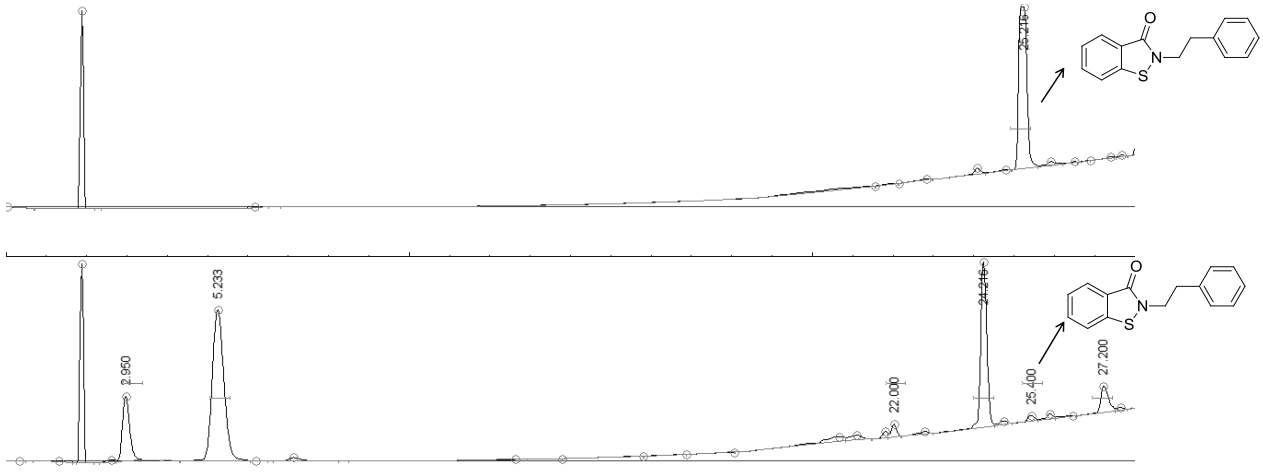

Figure 35: *Above: UV chromatogram of compound **20** 100uM, below: UV chromatogram of compound **20** and GSH molar ratio 1:2 after 60 minutes of incubation.*

At t=60 min, the peak of compound **20** was barely visible, moreover at least three new peaks were present at retention times of 22.0, 24.2 and 27.2 min. The first two peaks at RT 2.9 and 5.2 min were identified as glutathione (GSH) and oxidized glutathione disulphide (GSSG), respectively.

In order to confirm the identity of the newly formed compounds, the incubation sample was analyzed by means of high resolution mass spectrometry, employing a Thermo LTQ-Orbitrap XL instrument.

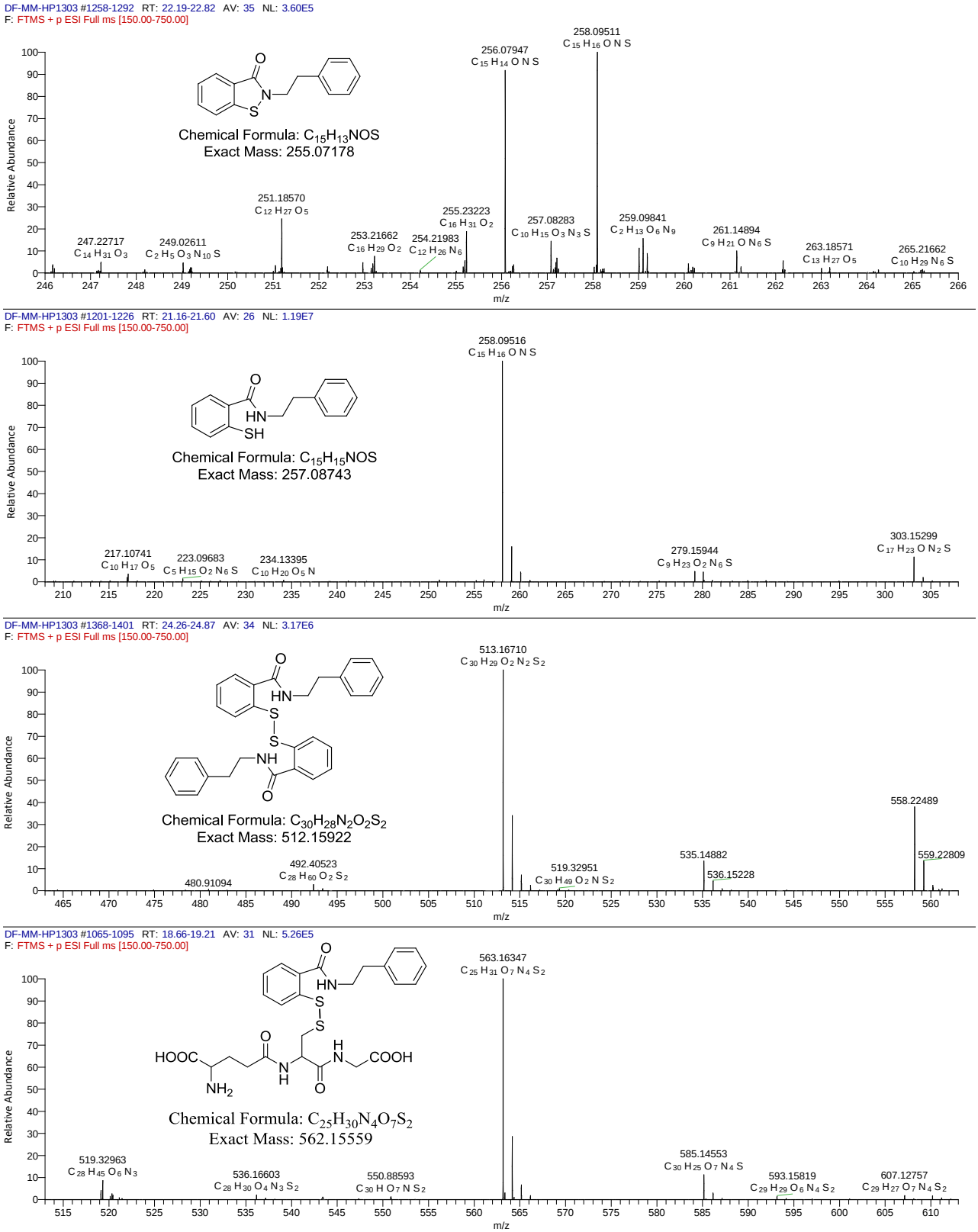

Figure 36: *High resolution mass spectra of reaction products after 60 minutes of incubation, at the center of each spectrum it is visible the peak of compound, its isotopic distribution and its chemical formula.*

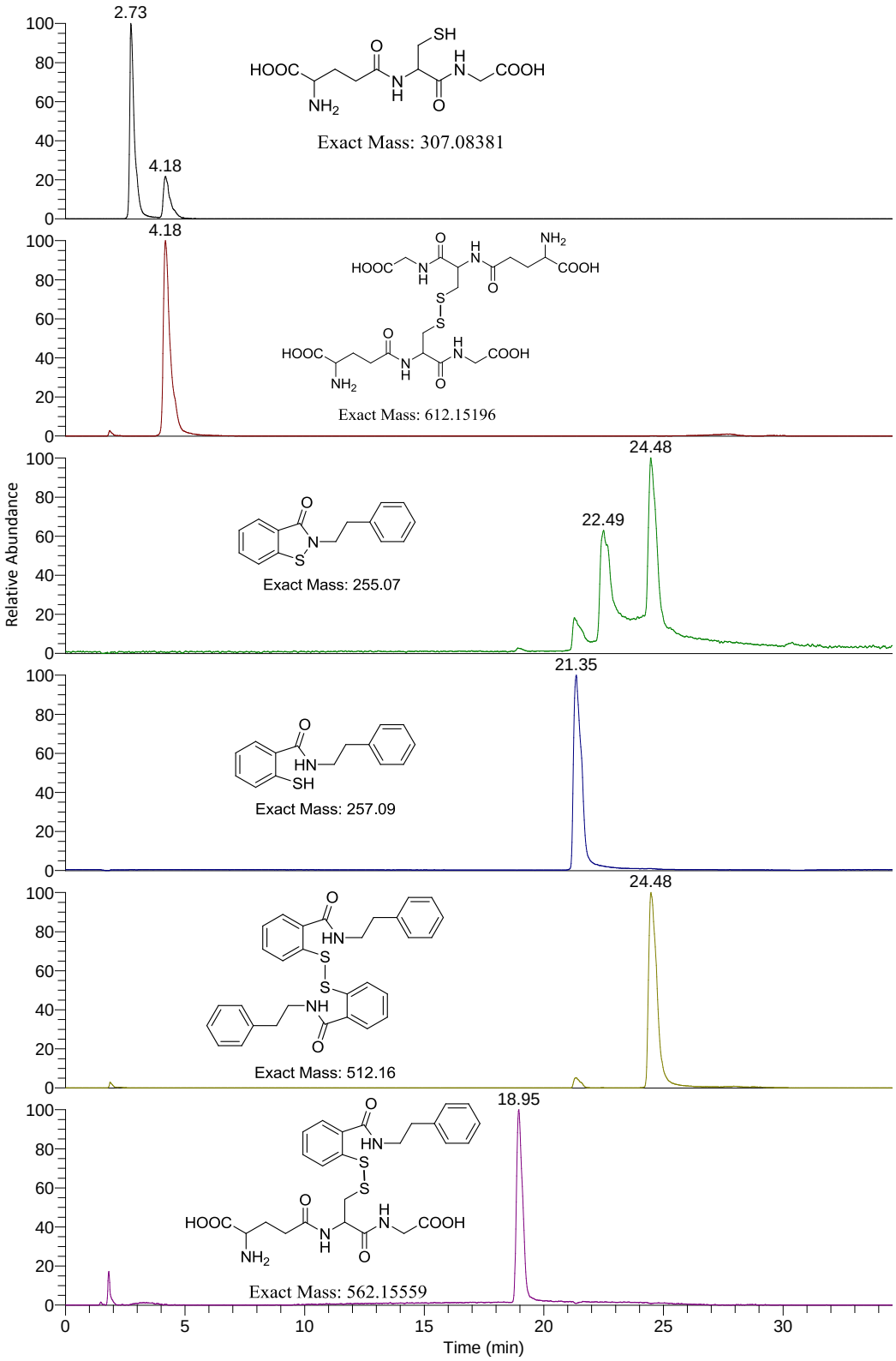

Figure 37: *Extracted ion chromatograms from the total ion current (TIC) in positive full scan mode of LTQ-Orbitrap.*

The full scan mode, positive or negative, employed by the LTQ-Orbitrap XL mass spectrometer has permitted to identify all the peaks with a bias in the exact mass determination (Δm) lower than 2 ppm. As it can be seen in Fig. 37, it was possible to identify all the peaks already present in the HPLC-UV chromatogram, with only a slight shift (~3 min) in Retention Times for all peaks, which may be related to the use of different HPLC systems for elution. According to the analysis of full scan traces, only the

hypothesized reaction products were formed. After 60 min of incubation, when the reaction had reached a dynamic equilibrium condition, compound **20** (RT: 22.4min, *m/z*: 256.07 $[M+H]^+$) and its reaction counterpart GSH (RT: 2.7min, *m/z*: 308.08 $[M+H]^+$) were detectable. The oxidized glutathione disulfide (RT: 4.2, *m/z*: 613.15 $[M+H]^+$), the conjugate of benzisothiazolinone with GSH (RT: 18.9, *m/z*: 563.15 $[M+H]^+$), the substituted benzamide deriving from the opening of the benzisothiazolinone ring (RT: 21.3, *m/z*: 258.09 $[M+H]^+$) and the symmetric disulfide, resulting from the reaction between a benzisothiazolinone conjugate and a benzisothiazolinone (RT: 24.5, *m/z*: 513.16 $[M+H]^+$). Identity of the reaction species was further confirmed by tandem mass spectrometry, in order to verify the MS/MS spectra of the selected compounds.

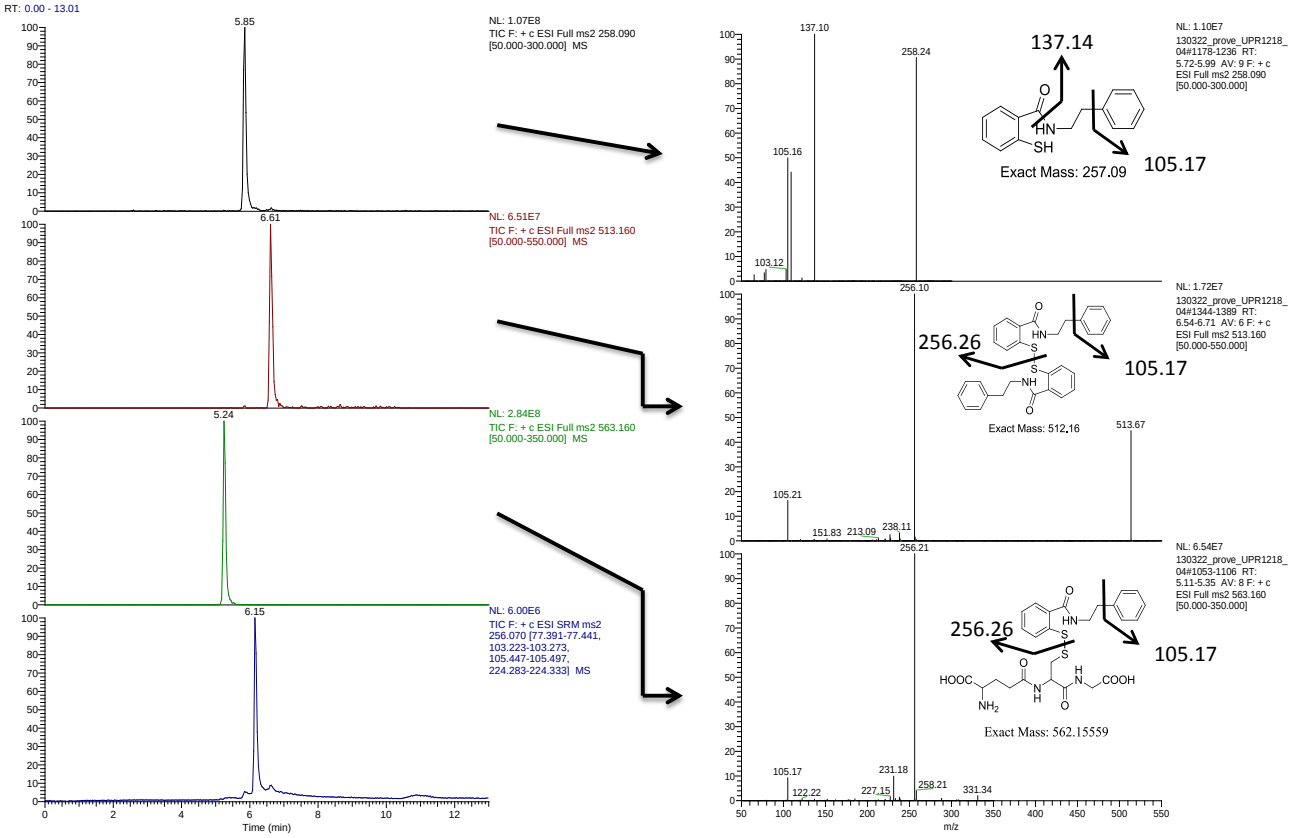

Figure 38: *Left: MS/MS chromatograms of sulfhydryl compound, symmetric disulfide, GSH adduct and compound **20**. Right: MS/MS spectra showing the fragment ions.*

In Figure 38 MS/MS spectra are reported for the substituted benzamide derived from benzisothiazolinone opening, the symmetric disulfide and the conjugate of benzisothiazolinone with glutathione. As it can be seen, for all compounds the fragment at *m/z*: 105.17 was formed, which can tentatively be attributed to the shared phenyl fragment. The substituted benzamide deriving from benzisothiazolinone was fragmented also in the amide bond, with the formation of the fragment at *m/z*: 137.14. When a disulfide bond was present, the fragment at *m/z*: 256.26 was formed, which indicated the rupture of the S-S bond itself.

The HPLC-ESI-MS/MS method set up employing the triple quadrupole as mass analyser was further employed for the qualitative analysis of the reaction products, formed from the whole set of substituted benzisothiazolinones. For the quantitative analysis, the HPLC-UV method was chosen, given the minor differences within the set in terms of HPLC/UV peak areas with respect to ionization behavior.

The reaction of benzisothiazolinones with glutathione under physiological pH conditions (buffer pH 7.4, 0.15 M ionic strength, 37°C) is a complex redox system with contribution of several reactive partners that reach a dynamic equilibrium between 60 and 120 minutes. It was decided to optimize the procedure in order to measure the ratio between the concentrations of oxidized glutathione disulphide (GSSG) and the square of glutathione ($[GSSG]/[GSH]^2$), to have information regarding the oxidizing power of each benzisothiazolinone. The concentration of native benzisothiazolinone was also monitored under equilibrium, as an indicator of the capability of benzisothiazolinone to be regenerated in the ox-redox process and therefore to be available for further reactions with thiol nucleophiles such as target cysteine residues of human MGL.

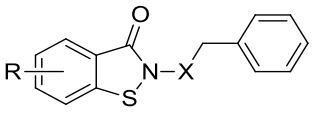

Cpd	R	X	[GSH]±SD µM	[GSSG]±SD µM	Ratio $[GSSG]/[GSH]^2$	[*BzISO*]±SD µM	Peak Area *BzISO-SG*	IC_{50} (nM) rMGL
20	H	CH_2	73.4 ± 4.7	59.3 ± 1.1	$11.1 \cdot 10^{-3}$	< LOD	721	34.1 ± 2.0
27	5-NO_2	CH_2	32.1 ± 9.5	78.3 ± 4.8	$88.2 \cdot 10^{-3}$	< LOD	< LOD	164.3 ± 2.8
25	5-OH	CH_2	83.1 ± 2.3	53.4 ± 0.7	$7.7 \cdot 10^{-3}$	< LOD	3228	135.0 ± 3.8
23	5-OMe	CH_2	80.9 ± 3.8	40.7 ± 2.5	$6.2 \cdot 10^{-3}$	1.2 ± 0.5	879	568.0 ± 55.3
26	6-NO_2	CH_2	105.1 ± 7.5	46.9 ± 1.3	$4.2 \cdot 10^{-3}$	< LOD	< LOD	237.9 ± 10.3
24	6-OH	CH_2	30.7 ± 10.9	69.9 ± 4.1	$91.7 \cdot 10^{-3}$	1.3 ± 0.4	3964	2547.0 ± 879.7
22	6-OMe	CH_2	66.1 ± 4.2	58.4 ± 3.5	$13.5 \cdot 10^{-3}$	< LOD	618	512.2 ± 64.4
21	6-OEt	CH_2	102.8 ± 12.0	40.0 ± 5.2	$3.8 \cdot 10^{-3}$	< LOD	< LOD	208.4 ± 10.6
28	7-Me	CH_2	186.6 ± 4.5	7.6 ± 0.2	$0.1 \cdot 10^{-3}$	99.3 ± 5.4	< LOD	13069.5 ± 523.9
29	H	NH	23.8 ± 1.0	64.2 ± 7.8	$108 \cdot 10^{-3}$	2.5 ± 0.3	2223	19.4

Table 14: *Results of benzisothiazolinones reacting with GSH (molar ratio 1:2) at t = 60 min.*

In Table 14 the results obtained for the set of benzisothiazolinone after a 60-min incubation during which 200 µM GSH reacted with 100 µM of benzisothiazolinone (BTZ) are presented. Due to the absence of appropriate calibration standards, it was not possible to quantify the BTZ-GSH conjugate formed and therefore the corresponding peak areas derived from HPLC-UV runs were reported for comparison purposes. As previously said, a first indication on the oxidative potential of tested BTZ is given by the table columns that reported the concentration of glutathione and oxidized glutathione. Indeed, the higher was the concentration of the glutathione remaining under equilibrium conditions, the lower was the oxidative potential of tested BTZ. Starting from a 200 µM concentration of glutathione and from a 100 µM concentration of BTZ, it was clear that the compound **28**, bearing the methyl group in position 7, left unreacted almost the whole glutathione present, with at t= 60 min: 1) a 187 µM GSH concentration; 2) a very low, approximately 8 µM, concentration of GSSG; 3) a remaining percentage of BTZ around 99%. These results clearly suggested that an increase in steric hindrance at position 7 reduced dramatically the BTZ reactivity towards thiol nucleophiles. However, this reduction was too marked, as it led to the complete absence of *in vitro* potency on target MGL (IC_{50} > 10 µM). For compounds **26** and **21**, substituted at position 6 with groups endowed with opposite electronic properties, similar reactivity results were obtained. Indeed, both 6-ethoxy and 6-nitro after 1 hour of incubation left around 50% of unreacted GSH and no peaks related to BTZ or conjugates with GSH were detectables. These results suggested that position 6 of the BTZ

nucleus, ideally conjugated with the carbonyl group of the BTZ ring, was not sensitive to the electronic effects of substituents. Position 6 was challenged by the introduction of others substituents: compounds **22** and **24**, containing 6-metoxy and 6-hydroxy groups, respectively. The first had almost the same behavior of the lead compound: the concentration of unreacted GSH was comparable, with a remaining concentration equal to ~70 µM, and the GSSG formed was around 60 µM, also the peak area of the conjugate with glutathione was the same. The 6-hydroxy substituted BTZ had an unpredictable redox profile, demonstrating to be one of the most interesting compounds of the set. It consumed almost all the GSH, leaving unreacted only the 15%, and forming 70 µM of oxidized glutathione; the remaining GSH was involved in the formation of a stable BTZ conjugate, whose peak area was one of the highest of the whole set. Moreover, around 1% of starting benzisothiazolinone was still present under equilibrium conditions.

Position 5 on the BTZ nucleus, conjugated to the BTZ sulfur atom, was also explored synthesizing 5-OCH_3 (**23**), 5-NO_2 (**27**) and 5-OH (**25**) derivatives. Differently to what it had been observed for position 6, in this case, it was possible to appreciate the effect of substituents endowed with opposite electronic properties on BTZ oxidative potential. The electron-donating 5-OCH_3 and 5-OH BTZ revealed: 1) a 80 µM conc. of unreacted GSH at equilibrium; 2) a 55 µM conc. of GSSG, if compared to the 70 µM and the 60 µM of GSH and GSSG, respectively, for the unsubstituted lead compound **20**. Moreover, the 5-OH BTZ showed a high peak area value for the GSH-BTZ conjugate and no detected BTZ, whereas 5-OCH_3 BTZ showed around 1% of starting compound remaining after 1 hour of incubation and a lower peak area value for the GSH-BTZ conjugate. 5-NO_2 BTZ, instead, endowed with an electron-withdrawing group, at t= 60 min revealed: 1) a 30 µM conc. of unreacted GSH; 2) a 80 µM conc. of GSSG, with neither BTZ nor GSH-BTZ conjugates detectable. The low sensitivity to the electronic effect of substituents by the reactive center of the BTZ ring, allowed to conclude that the BTZ nucleus behave as an extremely reactive moiety towards substitution by nucleophilic thiols and that the applied structural modulations were able to reduce this reactivity only to a certain extent. If the $[GSSG]/[GSH]^2$ ratio was taken as an indicator of the variation of the oxidative potential among the set, it could be seen that its value, excluding the 7-methyl derivative, ranged between $11.1x10^{-3}$ for the lead compound and $91.7x10^{-3}$ for the 6-OH BTZ spanning just one log order of magnitude.

A difference in the oxidative potential was only observed when an electron-withdrawing group nitro group was put at position 5, conjugated to the reactive sulfur atom. Indeed, electron donating groups, like 5-hydroxy or 5-methoxy, could slightly decrease the oxidative potential of the lead compound, and electron withdrawing groups, like 5-nitro, could increase this property. Groups at position 6 gave different results, difficult to rationalize. However, the electronic properties of the substituent did not seem to play a major role in the modulating the oxidative potential. Substitution at 7-position by means of a methyl group prevented any reactivity with GSH, due to the role of steric hindrance at that position in hampering GSH attack.

Finally, compound **29**, which was the only one bearing in position 2 a phenylethylamino side chain, had also an interesting profile. At t=60 min, only 20 µM of unreacted GSH still remained, while 65 µM of GSSG was formed; the GSH-BTZ conjugate showed one of the highest peak areas, indicating the capacity of the compound to form under equilibrium conditions a stable conjugate with a thiol nucleophile. Moreover, a 2.5

μM of BTZ was still present indicating its capacity to be restored during the ox-redox process and thus of being able to re-react with target GSH or MGL.

Piomelli and coll., at the Drug Discovery and Development Section of the Italian Institute of Technology had measured the inhibitory potency on rat MGL (rMGL) of each benzisothiazolinone. The IC_{50} for all compounds was reported in Table 14, however measured values are very similar to each other and the correlation between the IC_{50} and the reactivity scale *in vitro* is still unclear. Only for compound **28** it was observed that no reactivity correspond to no activity on rMGL.

4.5 Materials and Methods

4.5.1 Tested compounds

All compounds were synthesized in the laboratories of the Drug Design and Discovery Group, Pharmacy Department, University of Parma under the supervision of Prof. Marco Mor. All reagents were purchased from Sigma-Aldrich (Sigma-Aldrich Srl, Milan, Italy) at the highest quality commercially available. Solvents were RP grade unless otherwise indicated.

4.5.2 Stability of BTZ in the presence of cysteamine

The stability of all compounds with cysteamine was assayed in 0.01 M PBS buffer pH 7.4, all experiments were conducted at fixed temperature (37 ± 0.1 °C) and ionic strength (μ = 0.15 M), under stirring. Stock solutions of compounds were prepared in MeOH (10 mM or 5 mM), then serially diluted in order to obtain a final concentration of 100 μM with 1% MeOH v/v. The molar ratio of benzisothiazolinones (BTZ) and cysteamine was 1:1 (100 μM BTZ and 100 μM of cysteamine). After incubation (t = 0, 20 and 40 min), aliquots of 50 μL were withdrawn from reaction vessel and directly injected in the HPLC-UV system.

4.5.3 Stability of BTZ in the presence of GSH

The stability of all compounds with GSH was tested in 0.01 M PBS buffer pH 7.4, all experiments were conducted at fixed temperature (37 ± 0.1 °C) and ionic strength (μ = 0.15 M), stirring the reaction in an inert Argon atmosphere. Stock solutions of compounds were prepared in MeOH (10 mM or 5 mM), then serially diluted in order to obtain a final concentration of 100 μM with 1% MeOH v/v. The molar ratio of BTZ and GSH was 1:2 (100 μM BTZ and 200 μM of GSH). After incubation (t = 5, 60 and 120 min), aliquots of 100 μL were withdrawn from reaction vessel and directly injected in the HPLC-UV system.

4.5.4 Analytical method

The stability of tested compounds was monitored by HPLC/UV employing a Shimadzu gradient system (Shimadzu Corp., Kyoto, Japan) consisting of two Shimadzu LC-10ADvp solvent delivery modules, a 10 μL Rheodyne sample injector (Rheodyne LLC, Rohnert Park, CA), and an SPD-10Avp UV−vis detector, equipped with a Discovery C18 column (5μm, 150mm×4.6 mm i.d., Supelco, Bellefonte, PA). The HPLC system was interfaced with PeakSimple software version 2.83 for data acquisition. Mobile phases consisted of water (eluent A) and methanol (eluent B), both additioned with trifluoroacetic acid at 0.05% v/v and at a flow rate of 1 mL min^{-1}. Each compound was monitored at its relative absorbance maximum for UV detection, corresponding to λ: 210 nm for GSH and GSSG and to λ: 254nm for BTZ and BTZ-derived reaction species. A linear gradient elution was set up to evaluate all the tested compounds in the same chromatographic run. Chosen elution conditions were as follows: T(0 min): λ:210nm 95%A: 5% B; T(6 min): λ:254nm 95%A: 5% B; T(26 min): λ:254nm 5%A:95% B; T(28 min): λ:254nm 5%A:95% B returning to initial conditions after 0.5 min (λ:210nm), followed by 10 min re-equilibration time.

Compounds identification was carried out on a Thermo Accela 1250 UHPLC system (Thermo Italia, Milan, Italy) equipped with an Accela OpenAS autosampler. HPLC–ESI–MS/MS analyses were performed on a TSQ Quantum Access MAX triple quadrupole mass spectrometer (Thermo Italia, Milan, Italy) with an heated electrospray ionization source (H-ESI II). Data acquisition and processing were performed using Xcalibur software (version 2.1). Chromatographic separation was achieved on a Synergi 4u Fusion RP 80A C18 (100 × 2.0 mm i.d., 4 μm, Phenomenex). Mobile phases consisted of water (eluent A) and acetonitrile (eluent B), both additioned with formic acid at 0.1% v/v and at a flow rate of 350 μL min^{-1}. A linear gradient elution was set up to evaluate the tested compounds in the same chromatographic run. Conditions chosen were the following: T(0 min): 95%A: 5% B; T(1 min): 95%A: 5% B; T(6 min): 5%A:95% B; T(9 min): 5%A:95% B returning to initial conditions after 1 min, followed by 4 min re-equilibration time.

ESI interface parameters were set as follows: probe middle (D) position; capillary temperature: 270°C; spray voltage: 3.0 kV, vaporizer temperature: 250°C. Nitrogen was used as nebulizing gas at the following pressure: sheath gas: 35 psi; auxiliary gas: 15 arbitrary units (a.u.). Argon was used as the collision gas at a pressure of approximately 1.5 mtorr (1 torr = 133.3 Pa). Mass spectrometric analyses were done in positive ion mode and compound-dependent parameters were optimized by flow injection analysis (FIA), newly formed compounds were monitored with product-ion scan mode. For high-resolution mass spectrometry analysis (HR-MS) a Thermo LTQ-Orbitrap XL mass spectrometer was employed operating in full scan mode in the 150-750 amu range. Detection was in positive ion mode. Tuning parameters for ESI source were chosen as follows: Source Voltage: 3.5 kV; Sheath Gas Flow Rate: 8 psi; Aux Gas Flow Rate: 0 arbitrary units (a.u.); Capillary Voltage: 13 V; Capillary Temperature: 275°C; Tube Lens Voltage: 130 V. HPLC column was a RP C_{18} Supelco Discovery, 5μm, 150 mm×4.6 mm i.d. (Supelco, Bellefonte, PA, USA) thermostated at 30°C. Mobile phases consisted of water and methanol, both additioned with formic acid (FA) at 0.1% v/v and at a flow rate of 1 mL min^{-1}. Conditions chosen were the following: Eluent A: methanol + 0.1% FA; Eluent B: water + 0.1% FA. Conditions chosen were the following: T(0 min): 95%A: 5% B; T(6 min): 95%A: 5% B; T(26 min): 5%A:95% B; T(28 min): 5%A:95% B returning to initial conditions after 0.5 min, followed by 10 min re-equilibration time.

5. Role of human MGL cysteine residues as redox sensors

5.1 Introduction

Cysteine is considered a critical amino acid with several biological functions in all organisms, it is present in low percentages (~ 2.3%) in mammalian proteins, with even lower percentages for more simple organisms. The increase in Cys content within proteins with the increasing complexity of the organisms may be attributed to its relative high reactivity, if compared to other amino acids, particularly in the redox context. Indeed, cysteine has an highly reactive thiol nucleophile (RSH) in the side-chain, which makes cysteine susceptible to various post-translational modifications, which can contribute to regulate protein structure and function. In biological redox systems, cysteine can be oxidized to sulfenic acid (RSOH) by reactive oxygen species (ROS) such as hydrogen peroxide (H_2O_2). H_2O_2 can directly oxidize the thioether group of methionine to yield two diastereomeric methionine sulfoxide products; however, a large body of evidence identifies cysteine as the most sensitive amino acid residue to H_2O_2-mediated oxidation. This reversible modification has emerged as central reaction pathway in biological redox systems. Once formed, the sulfenic acid is subject to several alternative pathways. Depending on the micro-environment, the sulfenic acid modification can be stabilized as it was observed in human serum albumin (HSA)[155] and in more than 40 protein crystal structures.[156] There are different factors that could stabilize the protein sulfenic acids, such as the absence of thiols proximal to the site of formation, preventing the formation of a disulfide bridge, which is an important modification that regulates protein folding, or inaccessibility to low-molecular-weight thiols, including GSH (γ-L-Glu-L-Cys-Gly), reaction that could lead a protein-S-GSH disulfide. It is also possible, in alternative, that in proteins lacking a neighboring cysteine, the nitrogen atom of the backbone amide can react with sulfenic acid, forming a cyclic sulfenamide. Both the formation of a disulfide and sulfenamide can protect the protein against irreversible over-oxidation. However, in the presence of excess H_2O_2, sulfenic acid can be further oxidized to sulfinic (RSO_2H) and sulfonic (RSO_3H) oxyacids, though the observed rate constants for such reactions are generally slower than the initial thiolate oxidation event.

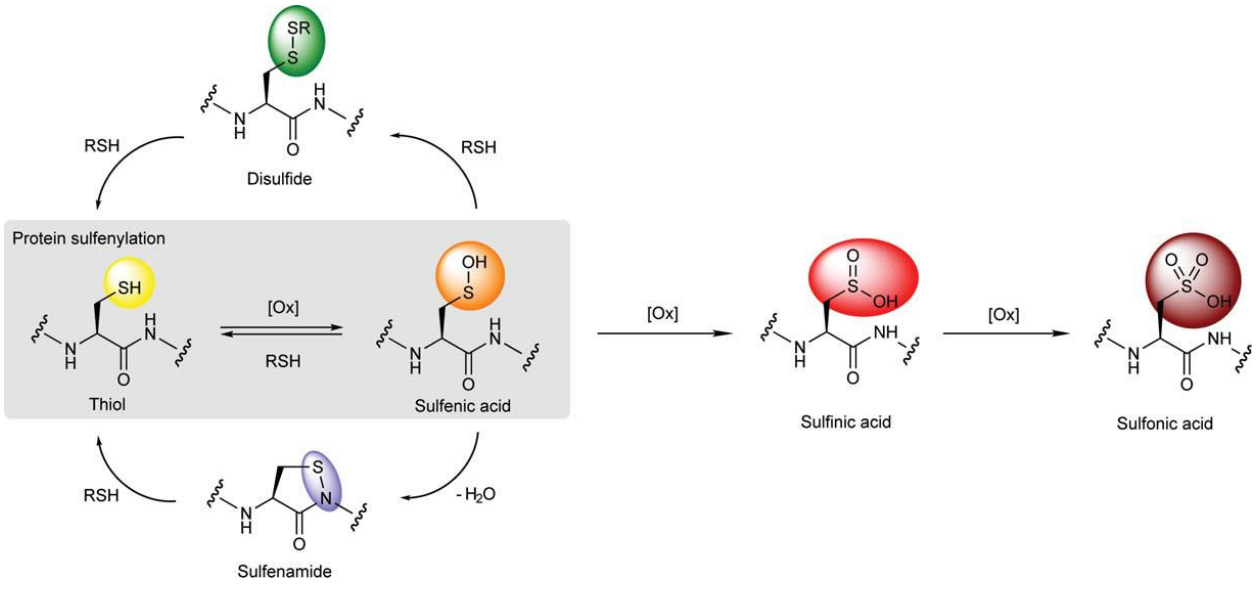

Figure 39: *Oxidative modification of cysteine residues.*[175]

With such diverse reactivity, the levels of protein sulfenic acid modifications not only serves as a biomarker of redox signaling in biological systems, but also has significant implications for probing pathologies associated with oxidative stress, such as cancer and cardiovascular disease. Owing to its biological importance, intensive efforts have been focused on the detection of protein sulfenylation in biological systems.

5.2 Analytical approaches to detect sulfenic acids in proteins

In order to identify a sulfenic acid spectroscopic methods are available, such as X-ray crystallography and ^{13}C NMR, which can afford substantial insight into the structure and the local protein microenvironment of the sulfenylated cysteine. However, such methods are limited to recombinant protein samples and are not applicable to complex biological systems.

Mass spectrometry is a powerful technique to identify sulfenic acid both in purified samples and in complex biological matrices. Because of their reactive nature, sulfenic acids are often considered unstable intermediates "en route" to subsequent cysteine modifications; for that reason, it is very difficult to identify an unmodified sulfenic acid on protein, though there are some examples in the literature that demonstrated that this strategy is possible.[157]

Sulfenic acids have a particular oxidation state of the sulfur atom, enabling it to function both as a weak nucleophile and as a soft electrophile. The dual nature of its reactivity is clearly illustrated by the condensation of two sulfenic acids to generate a thiosulfinate. Taking advantages of this dual nature, it is possible to use different chemical probes that permit to identify the presence of a sulfenic acids, in particular by mass spectrometry.

One successful example of a sulfenic acid probe is represented by the electrophilic compound 7-chloro-4-nitrobenz-2-oxa-1,3-diazole (NBD-Cl), whose reaction gives the sulfoxide product depicted in Fig. 40. However, as it can be seen from the scheme, this compound is not a chemically selective reagent for sulfenic acid detection, because it can react with amines, thiols and the phenol group of tyrosine residues. The reaction of NBD-Cl with these compounds yields fluorescent conjugates, so the difference in the absorption wavelength for the products (maximum of absorbance: -NH-NBD 480nm; -O-NBD 382nm; -S-NBD 420nm; -S(O)-NBD 347nm) observed in some proteins may permit positive identification of sulfenic acids with respect to other amino acid conjugates eventually present. Moreover, using mass spectrometry it is easier to distinguish between different NBD adducts, there is in fact a significant difference in *m/z* values.

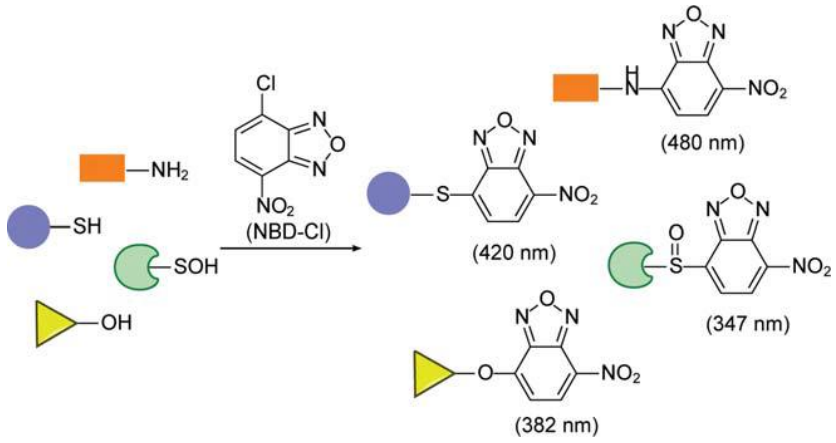

Figure 40: *Reaction of NBD-Cl with protein nucleophiles.*[175]

Other important chemical probes for detecting protein sulfenylation are represented by mild carbon nucleophiles such as 1,3-diones that present many advantages, including a direct and selective detection. Soft nucleophiles such as the 5,5-dimethyl-1,3-cyclohexanedione (dimedone) react with sulfenic acid to form stable thioether conjugates, but show no reactivity toward other electrophilic sulfur species such as disulfides and S-nitrosothiols.

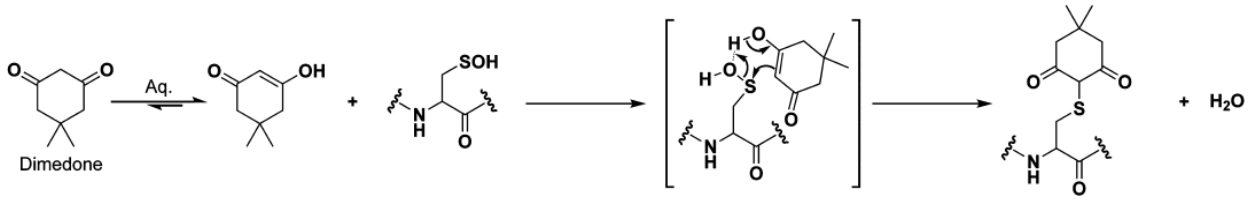

Figure 41: *Reaction schemes of electrophilic reaction of sulfenic acid with dimedone.*

All chemoselective methods for detecting protein sulfenic acids reported to date are mainly focused on this compound. However, the lack of an enrichment or visualization "handle" for protein-S-dimedone adducts subsequently motivated the development of different dimedone derivatives: probes directly conjugated to biotin or fluorescent tags;[158,159,160] azide- or alkyne-functionalized probes that can subsequent react with alkynyl- or azido-functionalized biotin or fluorophore reporters via click chemistry;[161] immunochemical detection that use antibodies to recognize the protein adduct;[162] isotope-coded probes.[163]

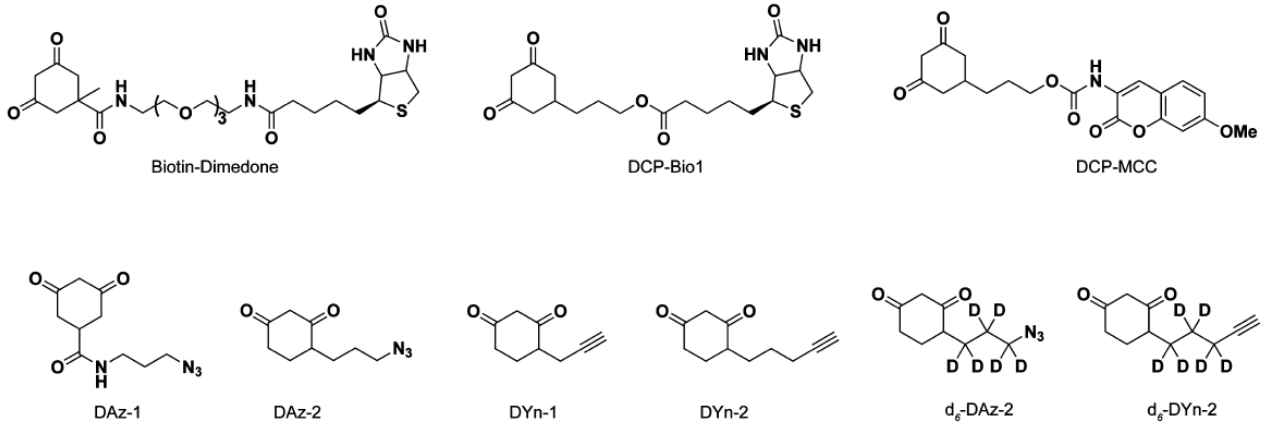

Figure 42: *Biotin, fluorophore, and chemical handle derivatives of dimedone.*

In conclusion, using high resolution mass spectrometry, it is possible to identify a sulfenic acid both directly, or with the aid of chemoselective probes, that permit to identify and, in some cases, also to isolate the protein or the peptide that contains sulfenic acid modifications.

Unfortunately, no selective probes for other oxidation products of thiols, such as sulfenamide, sulfinic and sulfonic acids have been described so far. In these cases, it is necessary to optimize sample preparation and preferably to rely on high resolution mass spectrometers. In particular, for the detection of peptides containing sulfenamides, that are highly labile compounds involving a mass difference of barely 2 Da with respect to parent protein/peptide, it is necessary to work with high resolution mass spectrometers which allow also the fragmentation of the peptides deriving from protein digestion, in order to identify the nitrogen atom bound to the sulfur atom of cysteine. Some interesting papers in the literature describe these experimental procedures.[164]

5.3 Experimental design and aim of the project

As previously said, it was known that the cysteine residues may play an important role in the response of a protein to oxidative stress. An excess of reactive oxygen species (ROS) determines a radical stress that could damage cells, since it oxidizes proteins. However, recently a new role of oxidizing agents has appeared: low levels of ROS are able to adjust the structure and function of various proteins by modifications of the cysteine residues within proteins.[165] It seems that cysteines of some proteins act as sensors of the redox state within the cell and respond to change in the redox potential through the formation of S-S bonds or cyclic sulfenamides, able to make conformational modifications to proteins. The redox sensitivity of each single cysteine is the consequence of the closer amino acid residues, and determine the specificity of its response to the ROS species.

Also for MGL a similar mechanism was hypothesized. Unpublished studies conducted by Piomelli and coll., at the Drug Discovery and Development Section of the Italian Institute of Technology demonstrated that rat MGL (rMGL) is sensitive to oxidation. Studies conducted on rMGL in cellular homogenates treated with buthionine sulfoximine (BSO), an inhibitor of glutathione synthetase, have revealed a marked reduction in the activity of rMGL as a result of depletion of glutathione, which is, as already said, the main antioxidant low molecular weight thiol within cells; it is therefore logical to assume that the activity of the enzyme, and therefore, the levels of its physiological substrate 2-AG, are physiologically regulated by the redox state of the cell (Fig. 43).

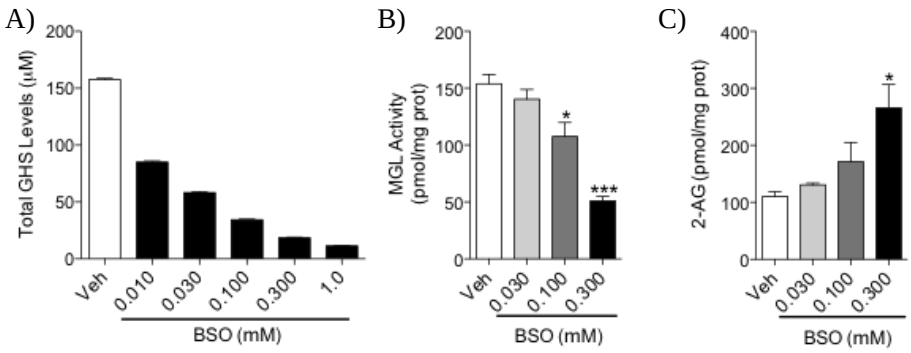

Figure 43: *A) BSO concentration-dependent effect on cellular levels of glutathione; B) reduction of the activity of rMGL due to the increase of the oxidative stress by reduction of the concentration of GSH; C) increased levels of 2-AG as a consequence of activity inhibition of rMGL for intracellular BSO.*

The addition of increasing concentrations of H_2O_2 to a purified recombinant rMGL solution reduces the catalytic activity of the enzyme in a non-competitive way, and this is reflected in the decrease of V_{max} while K_M does not show significant changes, probably by blocking the access channel to the active site (Fig. 44).

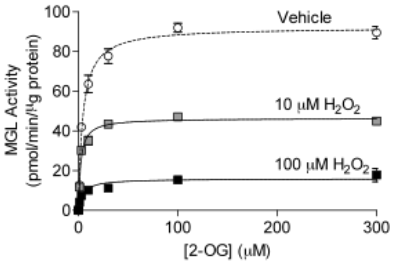

	V_{max} *(pmol/min/µg)*	K_m *(µM)*
Vehicle	107.6 ± 8	4.0 ± 0.9
10 µM H_2O_2	70.5 ± 12	2.9 ± 0.7
100 µM H_2O_2	19.7 ± 5	4.1 ± 0.7
p-Value	0.0013	0.5345

Figure 44: *Inhibition of the enzymatic activity of MGL with increasing concentrations of hydrogen peroxide.*

To evaluate if hydrogen peroxide acts reversibly or not, a rapid dilution assay was conducted using the irreversible Ser-addressing inhibitor MAFP as reference. The results confirmed that H_2O_2 inhibits rMGL in a reversible manner, as evidenced by total recovery of the catalytic activity due to dilution.
Rat MGL is sensitive to an oxidizing environment due to the "redox sensitive" cysteines (Fig. 45).

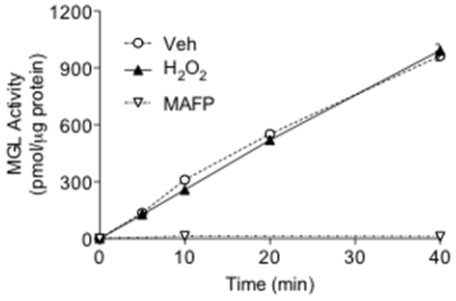

Figure 45: *Rapid dilution assay.*

This hypothesis is further supported by site-directed mutagenesis studies that have confirmed the role of C201 and C208 in the sensitivity to hydrogen peroxide. With the mutation in a single amino acid there was a reduction of sensitivity of rMGL of an equal value for both cysteines; the mutation of both amino acids

simultaneously determines an additive effect, detectable by a marked reduction of IC_{50} of hydrogen peroxide (Fig. 46).

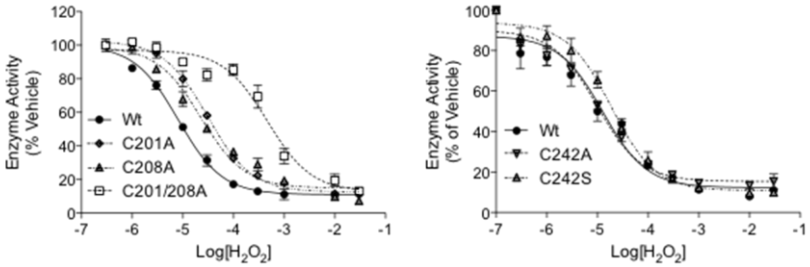

	IC_{50} (μM)
MGL wt	11 ± 0.8 (*n* =*10*)
C201A	30 ± 1.6 (*n* = *3*)
C208A	21 ± 2.3 (*n* = *3*)
C201/208A	419 ± 61.1 (*n* = *3*)

Figure 46: *Inhibition curves of rMGL, mutation of C201 and/or C208 (top-left) and mutation of C242 (top-right). Below are reported the IC_{50}.*

Starting from these preliminary results, in the present project we focused our attention on the enzymatic activity of human MGL in the search for analogies and differences with respect to rat MGL.

A pharmacological assay to evaluate MGL activity employing 2-oleoylglycerol (2-OG) as substrate for the enzyme, a commercially available recombinant human MGL and HPLC-ESI-MS/MS detection was set up in our laboratory to investigate the role of these regulatory cysteines in the fine tuning of human MGL activity, their sensitivity towards the redox state of the surrounding environment and their capacity to respond to changes in the redox potential.

5.4 Results and Discussion

5.4.1 Set up of hMGL enzymatic activity assay by HPLC-ESI-MS/MS

The enzymatic activity of human MGL was measured monitoring by mass spectrometry the formation of the hydrolysis product, oleic acid, from the substrate 2-oleoylglycerol (2-OG) after a fixed incubation time. 2-OG, for which the enzyme shows a very high affinity, has already been efficiently employed in the literature as MGL substrate, being structurally related to its physiological substrate 2-AG.

In order to set up the protocol for the enzymatic assay on hMGL, some parameters, known to influence the enzymatic activity of the enzyme, were optimized. They included: 1) the concentration of hMGL to employ in each sample; 2) the concentration of the substrate 2-OG; 3) the pH and composition of the incubation buffer; 4) the pre-incubation time of the enzyme in the presence of inhibitors or activators.

Starting from indications coming from the stock manufacturer and from the literature, the MGL enzymatic activity assay was performed in 50 mM Tris buffer pH 8.0 and in a final volume of 100 μL per incubation sample. The assay consisted of two phases: in the pre-incubation phase, a certain amount of hMGL was incubated in solution at 37°C alone or together with inhibitors or other redox modifiers for a stated period of time; in the incubation phase, a certain concentration of substrate, 2-OG, was added and after an incubation

of 15 minutes at 37°C the enzymatic reaction was stopped by the addition of a 2-fold volume of a chloroform/methanol mixture (ratio: 1:1), containing 5nmol of the internal standard heptadecanoic acid (HDA), useful for the subsequent analysis in HPLC-MS. With this method it was possible to measure the MGL enzymatic activity measuring the oleic acid formed in the reaction. Following the liquid-liquid extraction, oleic acid and the HDA were extracted from the reaction mixture and analyzed in LC-ESI-MS.

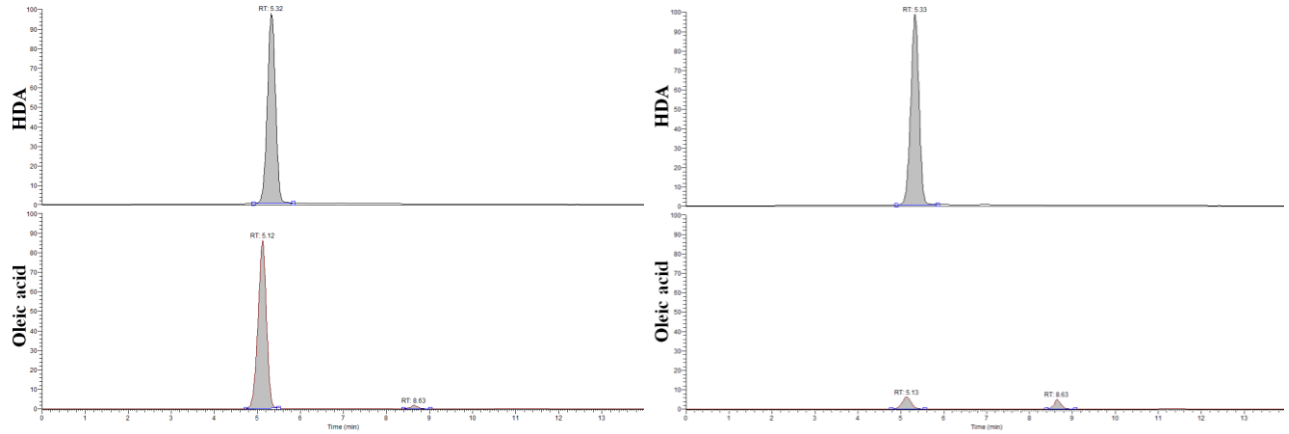

Figure 47: *left, LC-MS chromatogram of the normal activity of hMGL; right, LC-MS chromatogram of the formation of oleic acid from 2-OG without hMGL (basal).*

First, we attempted to optimize the MGL enzymatic assay conditions taking into account that we were working with a recombinant enzyme coming from commercial sources. We tested different final amounts of hMGL in 50 mM Tris buffer pH 8.0 (400, 200, 100, 50, 20, 10, 5 ng) and incubated them with a fixed concentration of 2-OG (50 μM). Reported in graph is the enzyme activity, defined as the amount of hydrolysis product, oleic acid, formed by hMGL in a certain incubation time period subtracted by the amount of oleic acid formed in the absence of MGL and related to the chemical hydrolysis of 2-OG under the chosen incubation conditions, the so-called "basal hydrolysis".

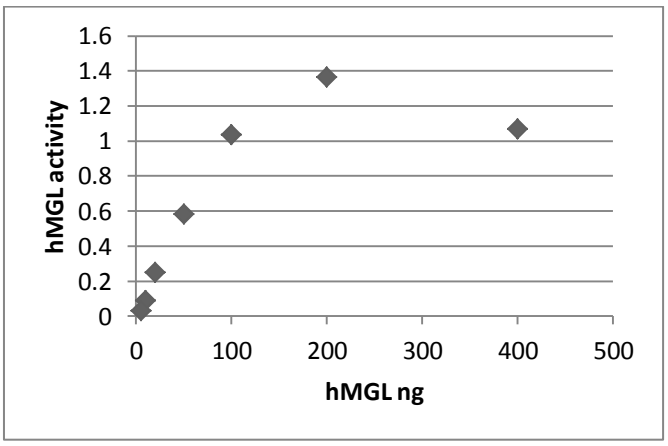

As it can be seen from the graph above, a plateau for the formation of hydrolysis product, oleic acid, was reached over 200 ng hMGL/sample, with a linear trend below this value; so the optimized quantity of hMGL to employ in our assays per sample to avoid the saturation of the enzymatic activity should have been around 100 ng/sample.

The next step was to analyze the optimal concentration of substrate 2-OG. A series of samples was prepared in 50 mM Tris pH 8.0 employing 100 ng hMGL/sample, and, after 10 minutes of pre-incubation at 37°C,

variable concentrations of 2-OG equal to 200, 100, 50, 25, 10, 5, 1 μM were additioned to the hMGL solution and the reaction was stopped after further 15min of incubation.

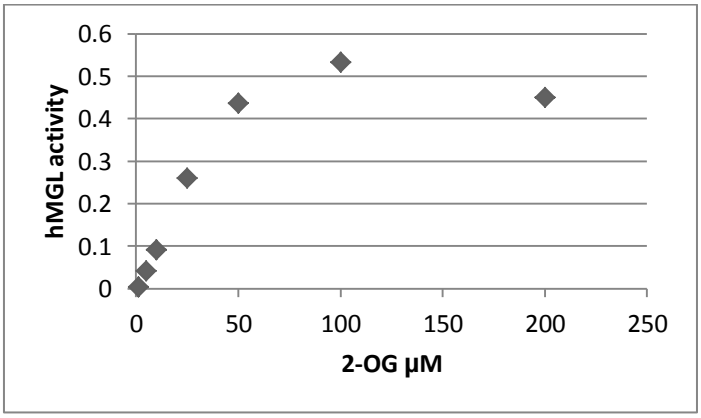

Also in this case, a linear trend of hMGL activity vs. 2-OG concentration was observed with a plateau reached starting from 100 μM concentration of 2-OG. The better signal-to-noise ratio obtained for the HPLC-ESI-MS/MS analytical method starting from a 100 μM concentration of 2-OG rather than the optimal one, which should have been 50 μM or lower, prompted us to employ the first concentration for subsequent assays.

Finally we evaluated the influence of the pre-incubation time, which should have employed for the evaluation of MGL inhibitors. A sample set formed by 100 ng of hMGL per sample in 50 mM Tris pH 8.0 was pre-incubated at 37°C for different time periods (5, 10, 15, 20, 40 and 80 min), then 100 μM 2-OG was added and incubated at 37°C for further 15 minutes before processing the samples and analyzing them in LC-MS.

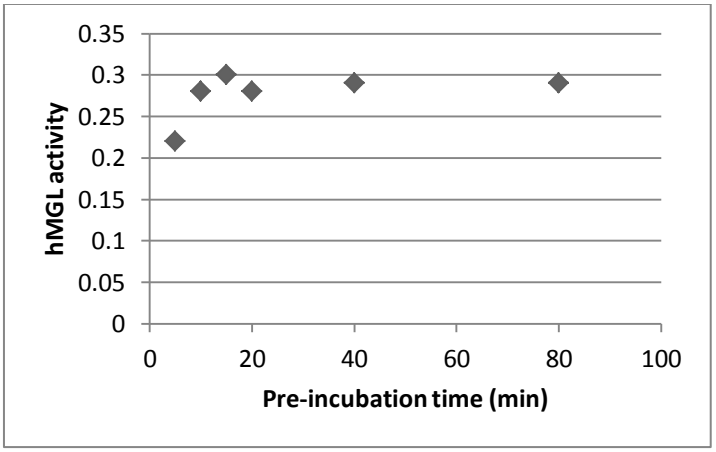

As it can be seen from the graph above, there is no dramatic difference in the activity of hMGL starting from a 10 min pre-incubation time up to 80 min, indicating that hMGL is quite stable under the chosen experimental conditions.

Finally, the general protocol chosen for enzymatic activity assays was as follows:

a) amount of hMGL: 100ng per sample;

b) 2-OG concentration: 100 μM

c) pre-incubation time: 10 min

d) incubation time with substrate 2-OG: 15 min.

Some experiments with hMGL redox activators or inhibitors required longer pre-incubation time, until 35 minutes, but as shown in the graph above, no significant decrease of activity had been observed up to a 80 min of incubation at 37°C in 50 mM Tris buffer pH 8.0.

5.4.2 Effect of reducing agents on hMGL enzymatic activity

Therefore, human MGL (final amount: 100 ng/sample) was pre-incubated in 50 mM Tris buffer pH 8.0 at 37°C for certain period of time. At the end of the pre-incubation period, 2-oleoylglycerol (final concentration: 100 µM) was added and incubation continued for further 15 min. At the end of the incubation period, oleic acid, the hydrolysis product, was quantified by HPLC-MS analysis. Heptadecanoic acid was employed as internal standard for HPLC-MS/MS quantification (see Materials and Methods for details).

Following this protocol, it was possible to evaluate the influence on the hMGL enzymatic activity of certain oxidizing or reducing agents, added during the pre-incubation phase.

A series of reducing agents was tested, with a 10 min pre-incubation time and at different concentrations.

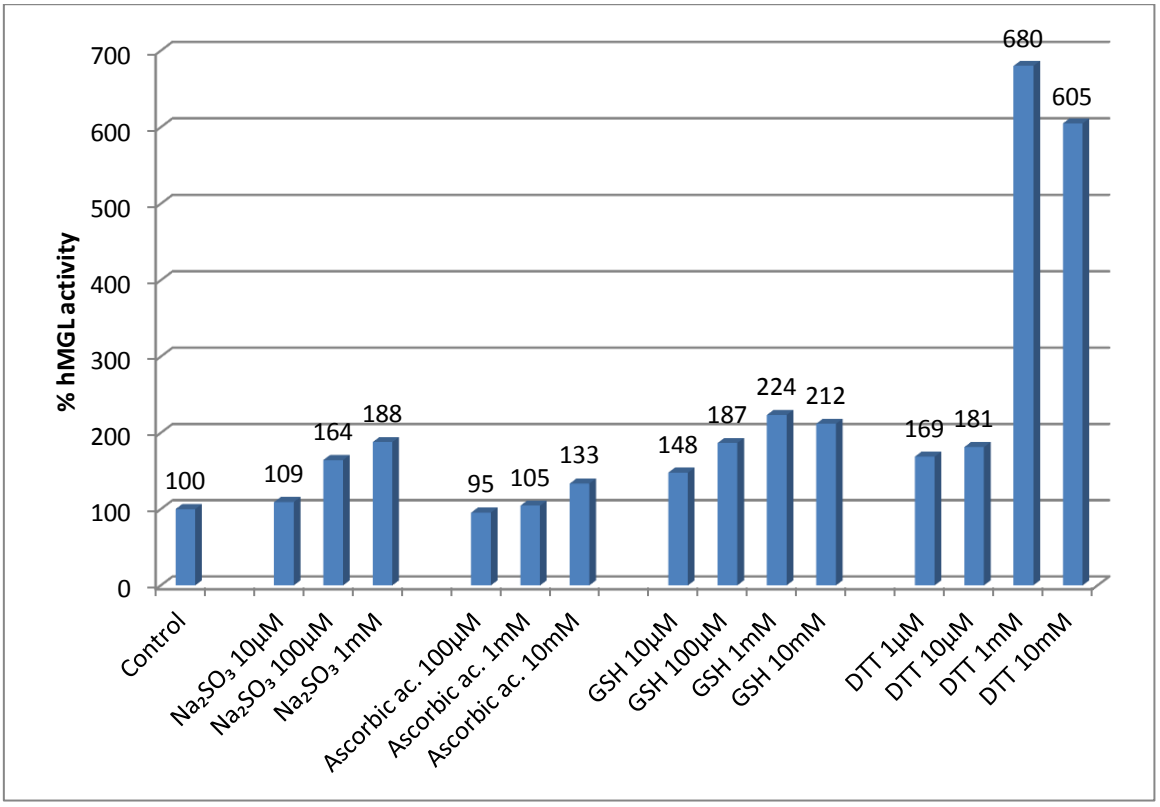

Figure 48: *hMGL activity in the presence of different reducing agents.*

The first column in Fig. 48 is the "control hMGL", i.e. hMGL without any reducing agents added and treated under the same conditions as other samples. The activity reported is in percentage, considering 100% the activity of the hMGL control sample. The first reducing agent tested was sodium sulfite (Na_2SO_3) that showed a relatively good response with about 190% of hMGL activity at 1 mM. On the contrary, at the lowest concentration, 10µM, no increase of activity was observed. Ascorbic acid, or vitamin C, was not effective in enhancing MGL activity, with the maximum activity observed at 10 mM and corresponding to a

130% of control one and no increase of MGL activity at lower concentrations; evidently the reducing power of ascorbic acid was not sufficient to reduce cysteines. Glutathione showed a good reducing response already at 10μM, at an observed hMGL activity about 150%. However, no significant increase of hMGL activity was observed at higher GSH concentrations, with a 200% hMGL maximum activity at 1mM. Dithiothreitol showed the best results. At 1μM concentration hMGL activity was already 170% with respect to control. The most important result was observed at 1 mM, where the activity reached the impressive value of 6-fold the control activity. In conclusion, the susceptibility of human MGL to reducing agents was confirmed and the response seemed to be correlated to the redox potential of the chosen reducing agent. Indeed, the activity at the 1mM concentration of reducing agent, showed this ranking: ascorbic acid > glutathione > dithiothreitol, which is indeed correlated with the value of their redox potential: ascorbic acid: -0.127, glutathione: -0.23 and dithiothreitol: -0.33. A different response gave sodium sulfite, which is similar in activity to the glutathione, but its redox potential is: -0.6; we may infer that probably the pH of the solution employed for the MGL assay was not optimal for the activity of this reducing agent.

5.4.3 Effect of hydrogen peroxide on hMGL enzymatic activity

Subsequently and following what had been observed for rat MGL an oxidizing agent, i.e. hydrogen peroxide, was tested, always following a pre-incubation time of 10 min, at three different concentration.

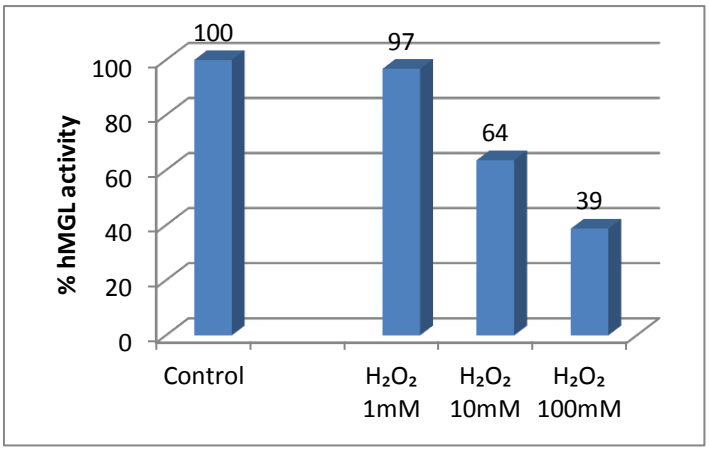

Figure 49: *hMGL activity in the presence of different concentrations of H_2O_2.*

Hydrogen peroxide was added to hMGL solution prior the addition of 2-OG, in the pre-incubation period. As it can be seen in the Fig. 49, a 1 mM concentration of hydrogen peroxide was not sufficient to inhibit the activity of the enzyme. Only a very high concentration can inhibit its activity, as a 10mM conc. inhibits hMGL activity of about 40% and 100mM of about 65%. It was not clear why this enzyme was so resistant to oxidative inhibition in contrast to its relatively high sensitivity to reducing agents. It was first hypothesized that one or more cysteines could be in an oxidized state, for example that they could have been oxidized reversibly to sulfenic acid. This particular oxidized state could explain the greater sensitivity to reducing agents, with the corresponding observed increase in activity, than to the oxidizing agent, with the decrease of activity. Indeed, a sulfenic acid is already known to be an oxidative stress sensor, easily reducible to thiol but a bit more resistant to be oxidized to a overoxidized form, like sulfinic or sulfonic acid.[166]

5.4.4 Set up of incubation conditions for oxidized hMGL and dimedone

To verify this hypothesis, the chemoselective probe for sulfenic acid, dimedone, and hydrogen peroxide were added to hMGL with a pre-incubation time of 10 minutes. The rational was the following: the probe dimedone is unreactive toward protein thiols, disulfides, nitrosothiols, sulfenamides, sulfinic and sulfonic acids, so it's extremely selective towards sulfenic acids. This molecule can bind to a sulfenic acid moiety forming a covalent bond which is not breakable by simple reducing agent. This means that pre-incubation of MGL with hydrogen peroxide and dimedone could induce the formation of a covalent bond between the hypothesized newly formed sulfenic acid and dimedone. The reduced activity in this case is justified by the presence of hydrogen peroxide. In order to verify if the dimedone was correctly bonded to one or more cysteines, it was added an excess of reducing agent (molar ratio 10:1 DTT/H_2O_2) after the pre-incubation time and before the addition of substrate 2-OG. The first result of this experiment is showed in Fig. 50, where the pre-incubation of hydrogen peroxide and dimedone was of only 10 min, the subsequent reaction with DTT was 10 min and the incubation with 2-OG was 15 minutes, as usually.

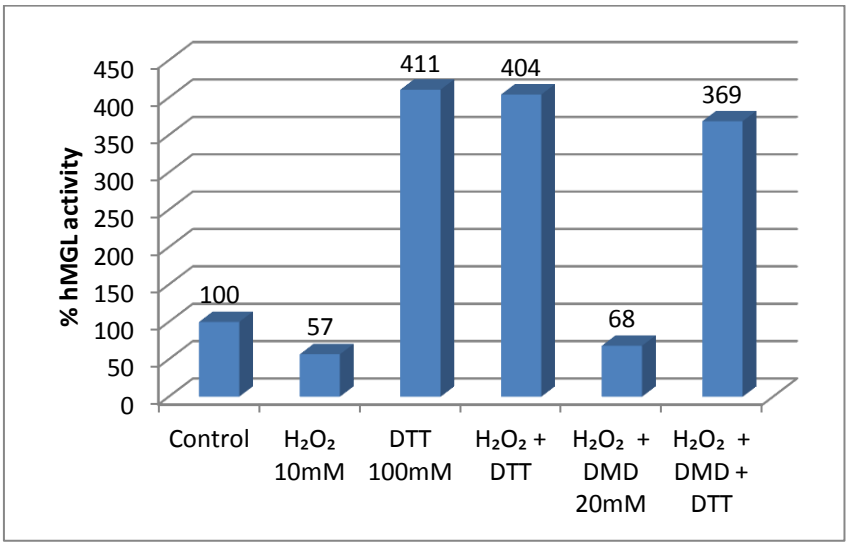

Figure 50: *hMGL activity in the presence of H_2O_2, dimedone and DTT.*

First of all, it is important to underline that the control incubation of hMGL was not influenced by the increased time of incubation, producing the same amount of hydrolysis product, oleic acid, both after 10min of preincubation and with 20 min, as in this case. Then, it was possible to observe that the pre-incubation of hMGL with 10 mM of hydrogen peroxide decreased the activity of about a 45%, whereas the pre-incubation with 100 mM DTT increased the enzymatic activity four times, confirming the results previously observed. The fourth column indicated the pre-incubation of hMGL with 10 mM hydrogen peroxide, followed by 100 mM DTT, which was allowed to react for 10 min before the addition of the substrate 2-OG. As it can be observed, hMGL activity is the same as in the previous sample with DTT alone, indicating that the inhibition of hydrogen peroxide of the first 10 minutes was overcome by DTT. The co-addition of hydrogen peroxide and 20 mM of dimedone showed a decrease activity of about 35%, similar to the sample with H_2O_2 alone. At the end it was presented the co-addition of 10 mM of H_2O_2, 20 mM of dimedone with pre-incubation of 10 min, the subsequent addition of 100 mM DTT with a reaction time of 10 min and then the addition of

substrate 2-OG. As it can be seen the activity is the same as the column of the sample with only DTT, this means that dimedone did not react with the hypothesized sulfenic acid.

A new set of experiments was repeated with different pre-incubation time. In fact it was hypothesized that dimedone could react with sulfenic acid of hMGL following a slow kinetics. The new incubation times were chosen as follows: pre-incubation of hMGL of 30 minutes with 10 mM H_2O_2 and 20 mM dimedone, then 5 min with 100 mM DTT and then 15 min of incubation with 2-OG as usual.

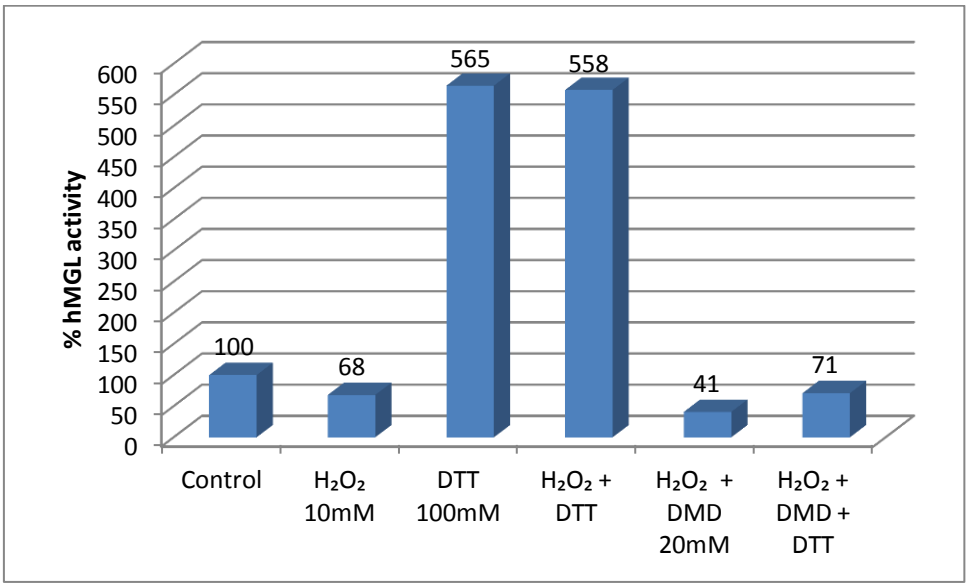

Figure 51: *hMGL activity in the presence of H_2O_2, dimedone and DTT.*

As it can be seen in Fig. 51 the registered trend for hMGL enzymatic activity is almost the same, if compared to Fig. 50, with the exception of the last experiment. At this time, DTT wasn't able to restore the enzymatic activity that instead lies at the same levels of the sample of hMGL treated with hydrogen peroxide (70% of activity). These experiments were important to set up the experimental conditions for the formation of the covalent bond between the selective probe dimedone and the sulfenic acids of hMGL. We may infer that in the first case the cause of failure was related to the slow kinetics of dimedone reaction with the cysteine sulfenic acid of hMGL or to the high instability of the oxidized form of the cysteine thiol or to both these factors.

Another similar experiment was conducted, with the same concentrations and pre-incubation times to verify if cysteine sulfenic acids were already present in the control hMGL. The trend of the first six columns was comparable to that previously showed. The seventh column represents the addition of dimedone in the pre-incubation phase, leading to a hMGL activity not statistically different to that of the hMGL control. At this point the last column results redundant, indicating that, with the addition of DTT, hMGL activity is dramatically increased. In conclusion, this experiment showed that the cysteines in the form of sulfenic acids were not present or stable in control hMGL.

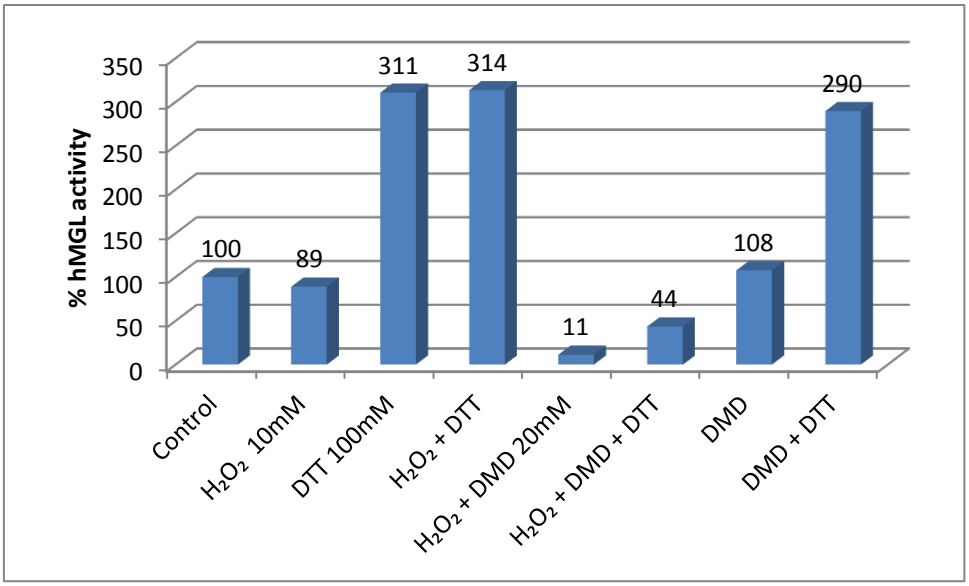

Figure 52: *hMGL activity in the presence of H_2O_2, dimedone and DTT.*

In conclusion, the set of enzymatic activity assays here presented showed that human MGL is highly sensitive to reducing agents, in particular DTT, and that its control activity can be increased by a 4-6 fold factor with incubation of just 5 min with DTT. The reason of this behavior is not easy to rationalize; it was initially hypothesized that one or more cysteine residues could be present in control hMGL as sulfenic acids, but incubations with dimedone of control hMGL showed that there is no species reacting with it. We may infer that another oxidized form of the thiol, reducible by DTT and resistant to oxidation by H_2O_2 could be present, which does not react with dimedone. After oxidation of hMGL by hydrogen peroxide, instead, experiments with dimedone demonstrated the clear formation of one or more cysteine sulfenic acid intermediates, able to react with the selective chemical probe dimedone. We needed to verify which cysteine residues could be targeted by dimedone or, in other words, which was/were the hMGL cysteines most reactive to oxidation by hydrogen peroxide.

5.4.5 Inhibition of hMGL activity by the benzisothiazolone-based inhibitor 20

Compound **20**, the lead compound of the benzisothiazolinone series, so it was chosen to test its inhibition power on hMGL using the protocol already described for the pharmacological assay. It had been already hypothesized that **20** could inhibit hMGL by means of a disulfide bond formation with the thiol group of the cysteine residues, so that hMGL activity could be restored by the addition of a reducing agent, such as DTT. Moreover, in the paper of Matuszak and coll., it was demonstrated that the inhibitory potency of benzisothiazolone-based compounds was reduced of approx. 1-1.5 orders of magnitude in the C201A, C242A mutants. The mutation of C208 did not significantly affect inhibitory potency.[151]

hMGL (final concentration: 1 ng/µL) was pre-incubated for 10 min in 50 mM Tris buffer pH 8.0 in the presence of different concentrations of compound **20** at 37°C. Then the substrate 2-oleoylglycerol (final concentration: 100 µM) was added and the incubation was continued for further 15 min. The tested

concentrations of inhibitor were 100, 50, 10, 5, 1, 0.1, 0.05 and 0.01 µM. As it can be seen in Fig. 53, hMGL was significantly inhibited by the newly synthesized compound **20**. The IC_{50} for compound **20**, calculated by fitting the experimental data of the logarithm of the inhibitor concentration vs. response with a nonlinear regression curve by GraphPad Prism software, was 133 nM. The inhibitory potency value was not far from literature values reported for isothiazolone- and benzisothiazolone-based inhibitors on hMGL.[151]

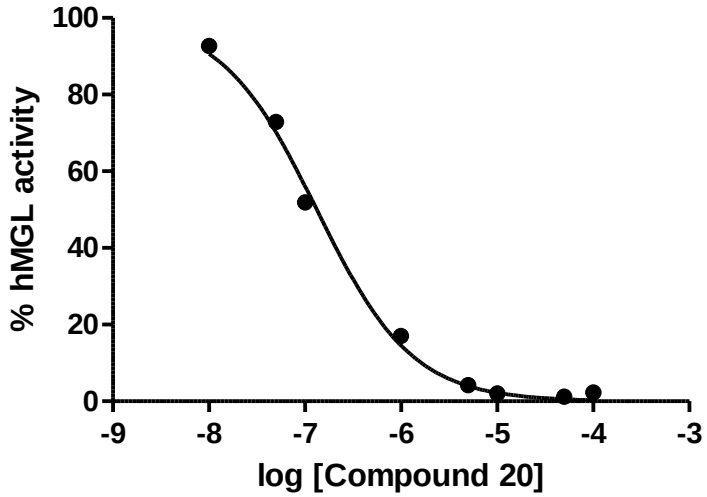

Figure 53: *Inhibition curve of Compound **20**.*

5.4.6 MALDI-TOF/TOF characterization of oxidized hMGL

Our next step was to identify which cysteine residues were oxidized to sulfenic acid by hydrogen peroxide. This was not possible by the experiments described previously, so the same hMGL samples were prepared and digested with proteases following a standard proteomic protocol and the digested peptides were detected and identified employing MALDI-TOF/TOF mass spectrometry.

First the proteomic protocol was set up. Briefly, control hMGL (final concentration 1.5 µM) was incubated in 50 mM Tris buffer pH 8.0 at 37°C for 60 minutes; this long incubation time was necessary in order to have the same experimental condition of the sample that was incubated with hydrogen peroxide and dimedone. At the end of the incubation period, the solution was subjected to an electrophoretic run on gel to get rid of the low molecular weight reactants in excess (buffer) before protease digestion. Other protein purification methods, like spin columns, were assayed, but gel electrophoresis separation gave the best results. hMGL in the excised gel spot was then reduced with DTT and alkylated with iodoacetamide (IAA) and digested overnight with the two proteases trypsin and chymotrypsin. After digestion, protein digests were purified by C18 ZipTip and spotted on MALDI plates employing HCCA (α-cyano-4-hydroxy-cinnamic acid) as a matrix, which is a good choice for peptides with mass below 2.5 KDa.

The analysis of the trypsin digest by MALDI-TOF/TOF mass spectrometry gave the following peptide mass fingerprint.

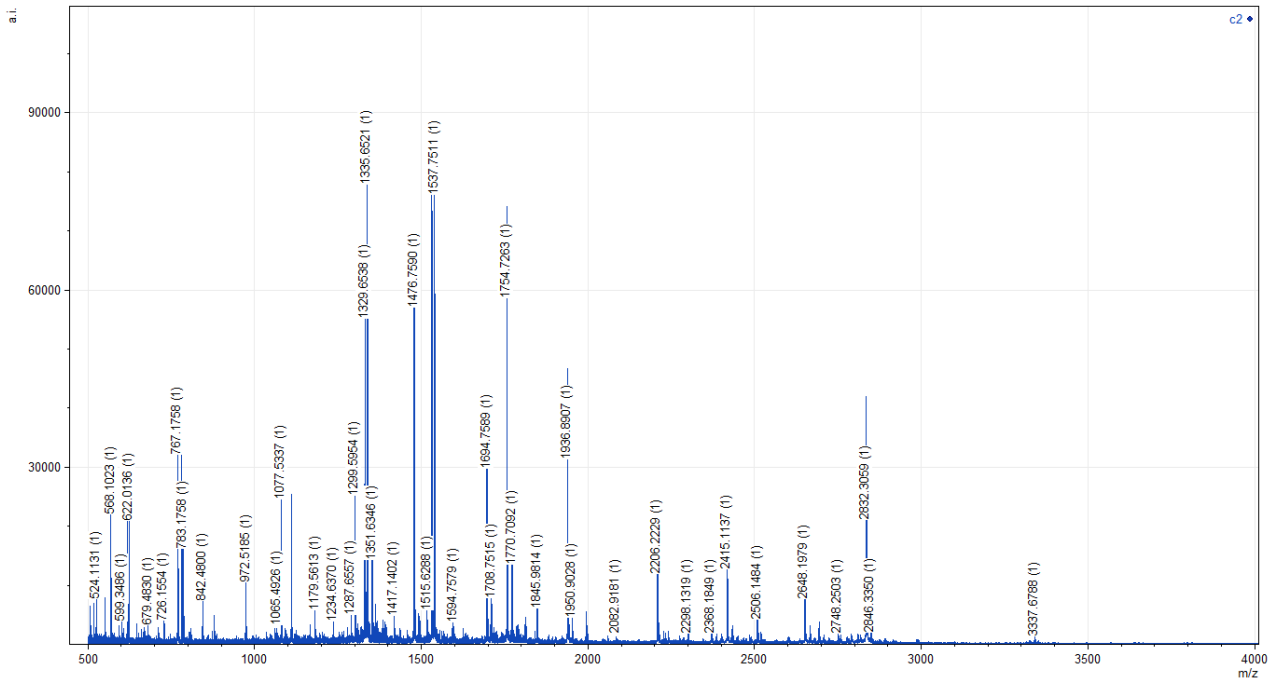

Figure 54: *Full scan analysis of trypsin digested hMGL.*

The extracted mass peak list, in which all peaks with a signal-to-noise threshold of 3 were included, was introduced for the identity search in the Mascot database producing, as an output, among other proteins, human monoacylglycerol lipase (hMGL) with a significant score (118), and a good protein sequence coverage (69%).

1 MPEESSPRR**T PQSIPYQDLP HLVNADGQYL FCRYWKPTGT PKALIFVSHG**
51 **AGEHSGRYEE LARMLMGLDL LVFAHDHVGH GQSEGERMVV SDFHVFVRDV**
101 **LQHVDSMQK**D YPGLPVFLLG HSMGGAIAIL TAAERPGHFA GMVLISPLVL
151 ANPESATTFK VLAAK**VLNLV LPNLSLGPID SSVLSRNKTE VDIYNSDPLI**
201 **CRAGLKVCFG IQLLNAVSRV ER**ALPK**LTVP FLLLQGSADR** LCDSK**GAYLL**
251 **MELAK**SQDKT LK**IYEGAYHV LHKELPEVTN SVFHEINMWV SQR**TATAGTA
301 SPP

Table 15: *Matched peptides shown in bold.*

Table 15 presents the hMGL sequence coverage by means of peptides found after MALDI TOF/TOF detection; almost 70% of hMGL sequence was covered by a number of approx. twenty peptides.

The sequence between residues 109 to 165 was among those not covered following the chosen experimental protocol.

One possible explanation lies on the chosen protease and its inner specificity of cut. Indeed, it is well known that trypsin cuts C-term side of Lysine (K) or Arginine (R) residues unless the next residue is represented by Proline (P), but in that region of the protein these conditions were not fulfilled.

Instead, predicting the digestion of the protein by trypsin, employing one of the freely available softwares, PeptideMass, it was possible to observe that trypsin digestion could gave rise to one single peptide with a *m/z* above 4000, which was basically the intact peptide obtained from residues 109 to 165. Other missing sequence portions of the protein could have the opposite problem: peptides of low molecular weight, such as ALPK could be formed by protease cleavage and, despite the presence of a basic amino acid, that should

enhance the ionization yield, were not visible in the mass peptide fingerprint because they fell in a region where high interferences from matrix ions were present.

In the Table below all the observed peptides are reported, together with the error in their mass accuracy (in ppm), missed cleavages of trypsin, peptide sequence and modifications such as methionine sulfoxidation (MSO) or cysteine carbamidomethylation (CAM). Mass accuracy errors were below 40 ppm for all peptides. At least two peptides containing C201 and three containing C208 were detected, all carbamidomethylated following the alkylation protocol with iodoacetamide. Peptides containing the chief cysteine residue C242 were not visible in none of the spectra with hMGL digested with trypsin, probably their low molecular weight which allowed them to fall in the mass spectrum region of matrix interferences, as, according to theoretical digestion, C242-containing peptide should have an expected *m/z* of 622.687.

Start–End	Mr(expt)	Mr(calc)	ppm	Missed cleavage	Peptide	Modification
10–33	2831.299	2831.37	-25.3	0	R.TPQSIPYQDLPHLVNADGQYLFCR.Y	CAM
34–42	1076.524	1076.566	-38.6	0	R.YWKPTGTPK.A	
43–57	1536.744	1536.78	-23	0	K.ALIFVSHGAGEHSGR.Y	
58–63	779.3542	779.3813	-34.8	0	R.YEELAR.M	
64–87	2647.197	2647.264	-25.3	0	R.MLMGLDLLVFAHDHVGHGQSEGER.M	
64–87	2663.201	2663.259	-21.6	0	R.MLMGLDLLVFAHDHVGHGQSEGER.M	MSO
88–98	1334.647	1334.681	-25.4	0	R.MVVSDFHVFVR.D	
88–98	1350.629	1350.676	-34.5	0	R.MVVSDFHVFVR.D	MSO
99–109	1298.585	1298.629	-33.7	0	R.DVLQHVDSMQK.D	
166–186	2205.218	2205.273	-25.2	0	K.VLNLVLPNLSLGPIDSSVLSR.N	
187–202	1935.884	1935.936	-26.7	1	R.NKTEVDIYNSDPLICR.A	CAM
189–202	1693.753	1693.798	-26.5	0	K.TEVDIYNSDPLICR.A	CAM
203–219	1844.973	1845.03	-30.4	1	R.AGLKVCFGIQLLNAVSR.V	CAM
203–222	2229.141	2229.242	-45	2	R.AGLKVCFGIQLLNAVSRVER.A	CAM
207–219	1475.75	1475.792	-28.1	0	K.VCFGIQLLNAVSR.V	CAM
227–240	1528.824	1528.861	-24.6	0	K.LTVPFLLLQGSADR.L	
246–255	1107.558	1107.6	-37.8	0	K.GAYLLMELAK.S	
263–273	1328.647	1328.688	-30.8	0	K.IYEGAYHVLHK.E	
274–293	2414.112	2414.169	-23.7	0	K.ELPEVTNSVFHEINMWVSQR.T	
274–293	2430.099	2430.164	-26.6	0	K.ELPEVTNSVFHEINMWVSQR.T	MSO

In order to try to increase the coverage of hMGL, in particular trying to detect in the mass peptide fingerprint a peptide containing the other chief cysteine residue C242, the protein was digested also by chymotrypsin, which has a different cut specificity to the C-term to F/Y/W/M/L, not before P. Results of peptide mass fingerprint after MALDI-TOF/TOF detection were good also in this case.

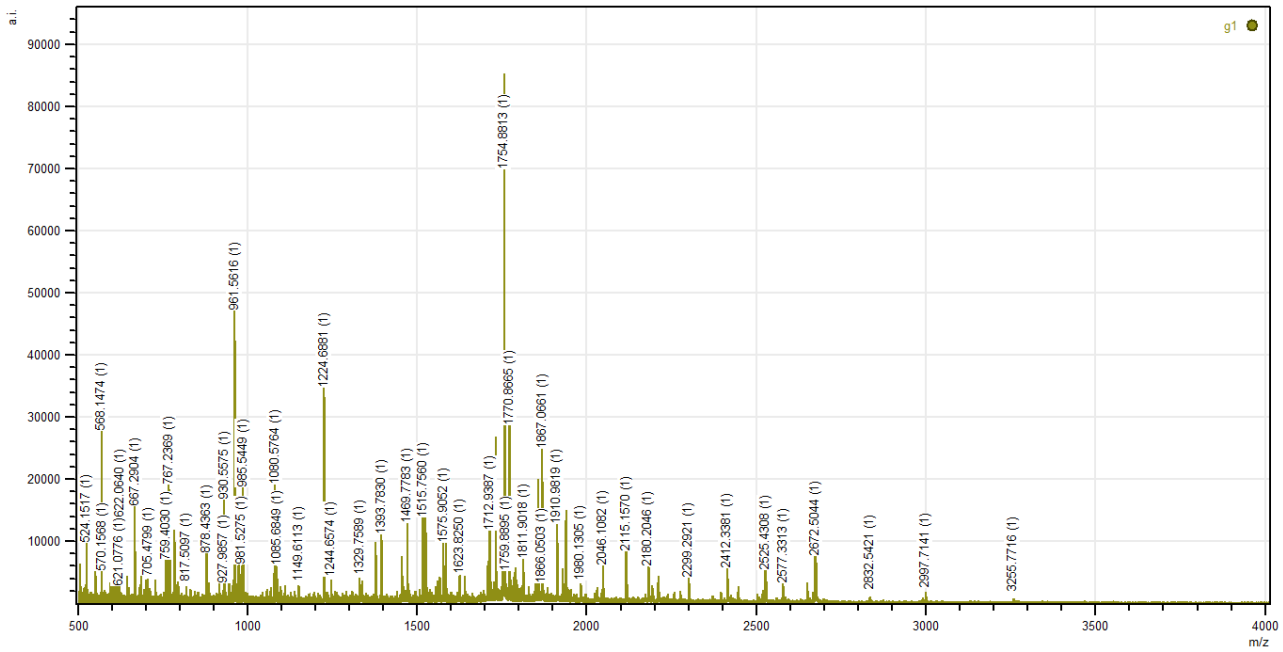

Figure 55: *Full scan analysis of chymotrypsin digested hMGL.*

The extracted mass peak list, in which all peaks with a signal-to-noise threshold of 3 were included, was introduced for the identity search in the Mascot database producing, as an output, among other proteins, human monoacylglycerol lipase (hMGL) with a significant score (87), and the same protein sequence coverage observed for trypsin (69%).

1 MPEESSPRRT PQSIPY**QDLP HLVNADGQYL FCRYW**KPTGT PKALIF**VSHG**
51 **AGEHSGRYEE LARML**MGLDL LVF**AHDHVGH GQSEGERMVV SDFHVFVRDV**
101 **LQHVDSMQKD YPGLPVF**LLG HSMGGAIAIL **TAAERPGHFA GMVLISPLVL**
151 **ANPESATTF**K VLAAKVLNL**V LPNLSLGPID SSVLSRNKTE VDIYNSDPL**I
201 CRAGL**KVCFG IQLLNAVSRV ERALPKL**TVP FL**LLQGSADR L**CDSKGAYL**L**
251 **MELAKSQDKT LKIYEGAYHV LHKELPEVTN SVFHEINMW**V SQRTATAGTA
301 SPP

Table 16: *Matched peptides shown in bold.*

With this protease, as expected, a different mass peptide fingerprint was obtained; however, the peptide that included C242 was still not detectable. Two peptides containing C208 were present, but no peptide containing C201. The loss of these peptides was counterbalanced by the presence of peptides containing residues from 109 to 165, which had not been detected with trypsin, but they were not useful for our purpose of monitoring modifications to cysteine residues.

Start–End	Mr(expt)	Mr(calc)	ppm	Missed cleavage	Peptide	Modification
17–29	1468.765	1468.695	47.9	1	Y.QDLPHLVNADGQY.L	
17–30	1581.854	1581.779	47.5	2	Y.QDLPHLVNADGQYL.F	
30–34	757.389	757.358	40.1	2	Y.LFCRY.W	CAM
31–34	644.297	644.274	35.1	1	L.FCRY.W	CAM
32–35	683.310	683.285	36.5	1	F.CRYW.K	CAM
47–65	2114.151	2113.996	73.2	2	F.VSHGAGEHSGRYEELARML.M	MSO
74–96	2576.313	2576.162	58.8	1	F.AHDHVGHGQSEGERMVVSDFHVF.V	
97–117	2442.371	2442.237	54.9	1	F.VRDVLQHVDSMQKDYPGLPVF.L	
131–139	984.533	984.478	56.5	0	L.TAAERPGHF.A	
131–144	1455.817	1455.729	60	1	L.TAAERPGHFAGMVL.I	
131–148	1866.056	1865.982	39.3	2	L.TAAERPGHFAGMVLISPL.V	
149–159	1148.603	1148.571	27.2	1	L.VLANPESATTF.K	
170–184	1522.893	1522.861	20.9	2	L.VLPNLSLGPIDSSVL.S	
175–194	2192.175	2192.133	19.6	2	L.SLGPIDSSVLSRNKTEVDIY.N	
185–194	1223.678	1223.615	51.6	0	L.SRNKTEVDIY.N	
185–199	1749.962	1749.853	62.3	1	L.SRNKTEVDIYNSDPL.I	
206–209	552.282	552.273	15.8	0	L.KVCF.G	CAM
206–214	1076.636	1076.605	28.3	2	L.KVCFGIQLL.N	CAM
214–227	1564.847	1564.941	-60.5	1	L.LNAVSRVERALPKL.T	
215–227	1451.752	1451.857	-72.3	0	L.NAVSRVERALPKL.T	
233–241	971.585	971.540	46.5	2	L.LLQGSADRL.C	
250–261	1375.744	1375.738	4.55	2	L.LMELAKSQDKTL.K	
262–268	842.449	842.417	37.6	1	L.KIYEGAY.H	
269–289	2558.464	2558.274	74.4	2	Y.HVLHKELPEVTNSVFHEINMW.V	

Once experimental protocol was set up, next step was to analyze the enzyme after incubation in the presence of the oxidative agent hydrogen peroxide and the chemoselective probe for cysteine sulfenic acid, dimedone. Briefly, hMGL (final concentration 1.5 μM) was incubated for 60 min in 50 mM Tris buffer pH 8.0 in the presence of 10 mM H_2O_2 and 20 mM dimedone at 37°C. At the end of the incubation period, the solution was subjected to a gel electrophoretic run to get rid of the low MW reactants in excess (H_2O_2, dimedone) before digestion. hMGL was then reduced with DTT and alkylated with IAA and digested overnight with the first protease trypsin. Samples were purified by ZipTip C18 and spotted on MALDI plate with HCCA (α-cyano-4-hydroxy-cinnamic acid), which is a good matrix for peptides with mass ions below 2500 Da.

The mass peptide fingerprint that was acquired showed almost the same signal-to-noise ratio than control hMGL. In fact, the extracted peptide peak list, once introduced in the Mascot database, produced, as an output, human MGL with a barely identical score (97) and an equal protein sequence coverage (69%) than control hMGL.

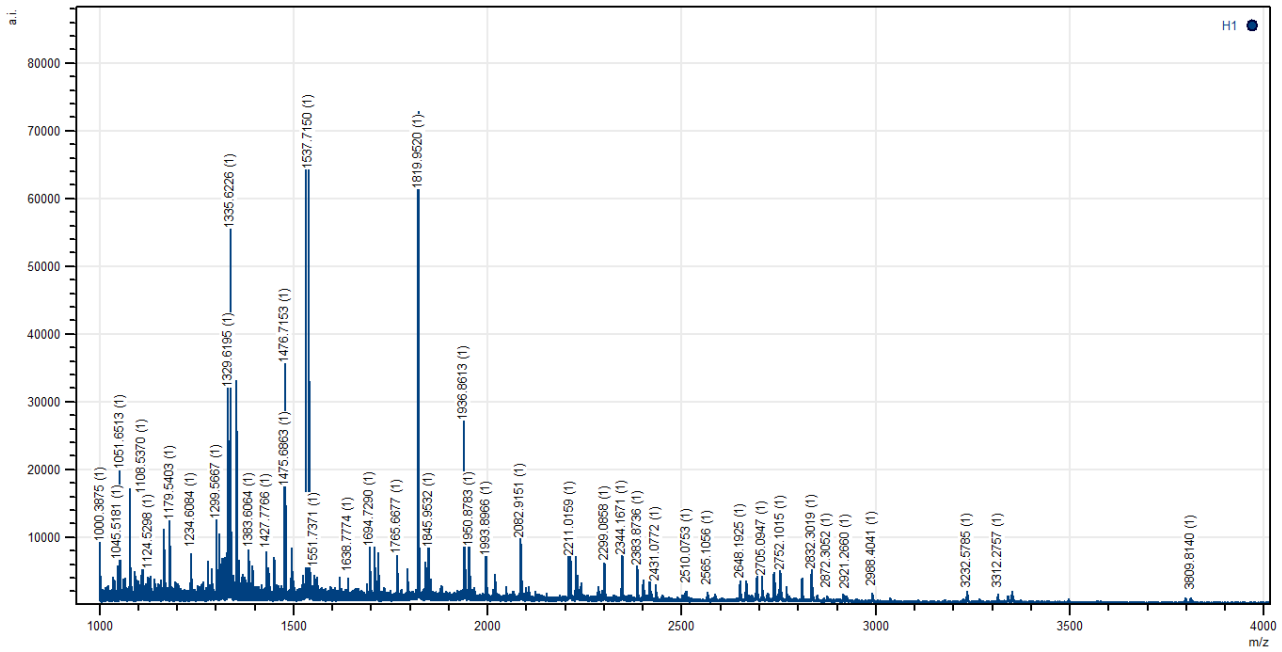

Figure 56: *Full scan analysis of trypsin digested hMGL after incubation with H_2O_2 and dimedone.*

Peptides containing cysteine residues C32, C201 and C208 were still present, as it can be observed in the Table below.

1 MPEESSPR**RT PQSIPYQDLP HLVNADGQYL FCRYWKPTGT PKALIFVSHG**
51 **AGEHSGRYEE LARMLMGLDL LVFAHDHVGH GQSEGERMVV SDFHVFVRDV**
101 **LQHVDSMQK**D YPGLPVFLLG HSMGGAIAIL TAAERPGHFA GMVLISPLVL
151 ANPESATTFK VLAAK**VLNLV LPNLSLGPID SSVLSRNKTE VDIYNSDPLI**
201 **CRAGLKVCFG IQLLNAVSR**V ERALPK**LTVP FLLLQGSADR** LCDSK**GAYLL**
251 **MELAK**SQDKT LK**IYEGAYHV LHKELPEVTN SVFHEINMWV SQR**TATAGTA
301 SPP

Table 17: *Matched peptides shown in bold.*

Also sequence coverage and found peptides were the same as in the control sample containing only hMGL, without the incubation with the oxidative agent H_2O_2 and dimedone.

Start–End	Mr(expt)	Mr(calc)	ppm	Missed cleavage	Peptide	Modification
9–33	2987.397	2987.471	-24.9	1	R.RTPQSIPYQDLPHLVNADGQYLFCR.Y	CAM
10–33	2831.295	2831.37	-26.7	0	R.TPQSIPYQDLPHLVNADGQYLFCR.Y	CAM
34–42	1076.503	1076.566	-57.9	0	R.YWKPTGTPK.A	
43–57	1536.708	1536.78	-46.9	0	K.ALIFVSHGAGEHSGR.Y	
43–63	2298.079	2298.151	-31.3	1	K.ALIFVSHGAGEHSGRYEELAR.M	
64–87	2647.185	2647.264	-29.6	0	R.MLMGLDLLVFAHDHVGHGQSEGER.M	
88–98	1334.615	1334.681	-48.8	0	R.MVVSDFHVFVR.D	
88–98	1350.6	1350.676	-55.8	0	R.MVVSDFHVFVR.D	MSO
99–109	1298.559	1298.629	-53.5	0	R.DVLQHVDSMQK.D	
99–109	1314.564	1314.624	-45.9	0	R.DVLQHVDSMQK.D	MSO
166–186	2205.186	2205.273	-39.7	0	K.VLNLVLPNLSLGPIDSSVLSR.N	
187–202	1935.854	1935.936	-42.4	1	R.NKTEVDIYNSDPLICR.A	CAM
189–202	1693.722	1693.798	-45.1	0	K.TEVDIYNSDPLICR.A	CAM
203–219	1844.946	1845.03	-45.3	1	R.AGLKVCFGIQLLNAVSR.V	CAM

207–219	1475.708	1475.792	-56.8	0	K.VCFGIQLLNAVSR.V	CAM
227–240	1528.788	1528.861	-47.7	0	K.LTVPFLLLQGSADR.L	
246–255	1107.53	1107.6	-63.3	0	K.GAYLLMELAK.S	
246–255	1123.523	1123.595	-64.3	0	K.GAYLLMELAK.S	MSO
263–273	1328.612	1328.688	-56.8	0	K.IYEGAYHVLHK.E	
274–293	2414.086	2414.169	-34.2	0	K.ELPEVTNSVFHEINMWVSQR.T	
274–293	2430.07	2430.164	-38.6	0	K.ELPEVTNSVFHEINMWVSQR.T	MSO

At this point, it was necessary to search manually within acquired peptide mass fingerprints for peaks of newly formed peptides, with a particular attention to cysteine containing-peptides having an increased mass of +16, +32 and +48 that could correspond to those oxidative modifications of cysteine that are sulfenic, sulfinic and sulfonic acid, respectively, and, more importantly, of those cysteine-containing peptides having an increased mass of +138, which could correspond to the addition of a dimedone moiety to a cysteine in the form of sulfenic acid. None of the oxidized species of cysteine thiol group (sulfenic, sulfinic, sulfonic acid) were detected in the mass spectra of hMGL treated with H_2O_2 and dimedone

Two C32-containing peptides were detected in the mass peptide fingerprint: one containing residues 9-33 (*m/z* 2988.346) and one containing residues 10-33 (*m/z* 2832.305): the first peptide showed a low ionization yield ($1x10^3$ a.u., arbitrary unit), probably due to its high molecular weight, on the contrary the second peptide showed a very good signal ($4x10^4$ a.u.). In both peptides, cysteine was carbamidomethylated. None of the hypothesized oxidative modifications were detected in the C32-containing peptides; this was not surprising as this cysteine residue is present at the surface of hMGL, its deletion in mutants had never led to significant alterations in hMGL enzymatic activity and it is therefore not considered a reactive cysteine residue.

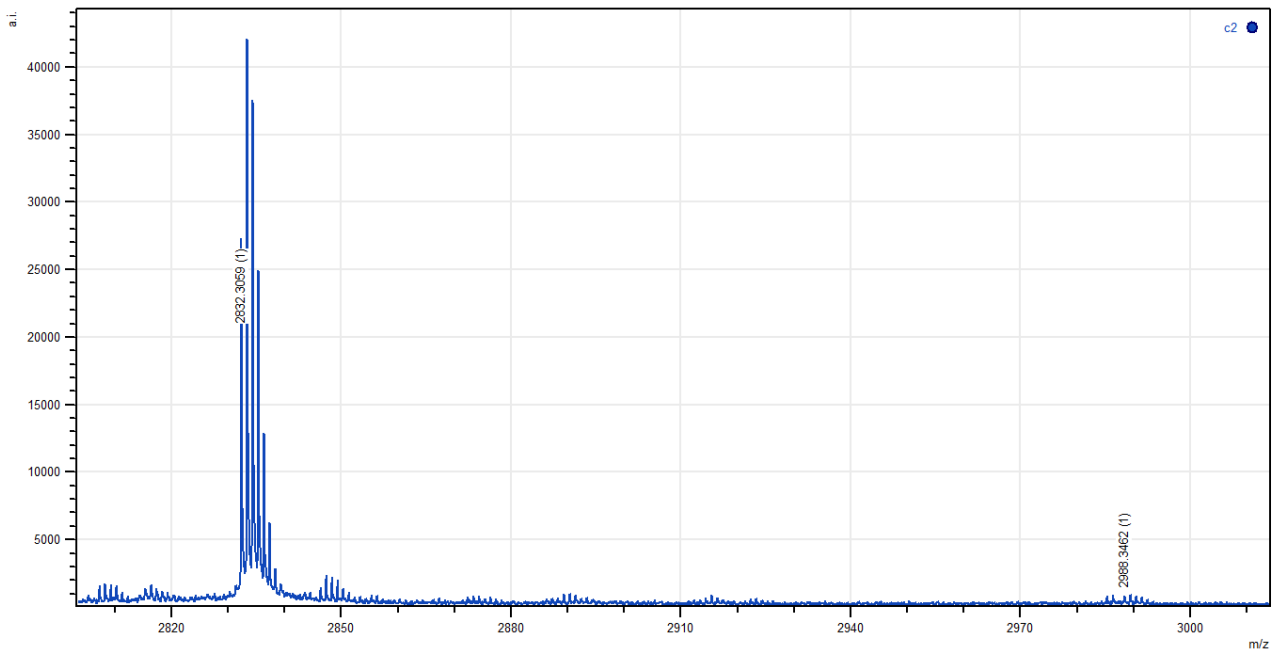

Figure 57: *Expanded spectrum of hMGL treated with H_2O_2 and DMD showing C32 peaks.*

More interesting results were found focusing on oxidative modifications on C201- and C208-containing peptides. For both these peptides no +32 and/or +48 mass shifts were observed, so no irreversibly oxidized species of C201 and C208 were present in hMGL. This result was quite unexpected, given the high concentrations of H_2O_2 (10 mM) employed during the experiments which were allowed to react for 1 hour with hMGL. However, this result matched those previously obtained in hMGL enzymatic activity assays, in which, after the incubation of hMGL with the same concentrations of H_2O_2, and the subsequent addition of DTT, the enzymatic activity had been completely restored (See Figure 52 for comparison). However, it is also possible that some of these irreversibly oxidized species were instead present in our sample, but that the amount formed was too low either to interfere significantly with hMGL activity or to be detected by our MALDI mass spectrometer in the complex protein digest.

We found two C208-containing peptides and, in both of them, C208 residue was carbamidomethylated. One peptide was formed by residues 203-219, had a *m/z* ratio = 1845.953 and a relatively low ionization yield ($3.5x10^3$ a.u.); the other C208-containing peptide, instead, formed by residues 207-219, had a *m/z* 1476.758 and was one of the most intense peaks in hMGL peptide mass fingerprint, with a ionization yield ranging between $6x10^4$ a.u. and $3x10^4$ a.u.. For none of C208-containing peptides, a mass shift of +138 corresponding to the hypothetical adduct with dimedone, was found.

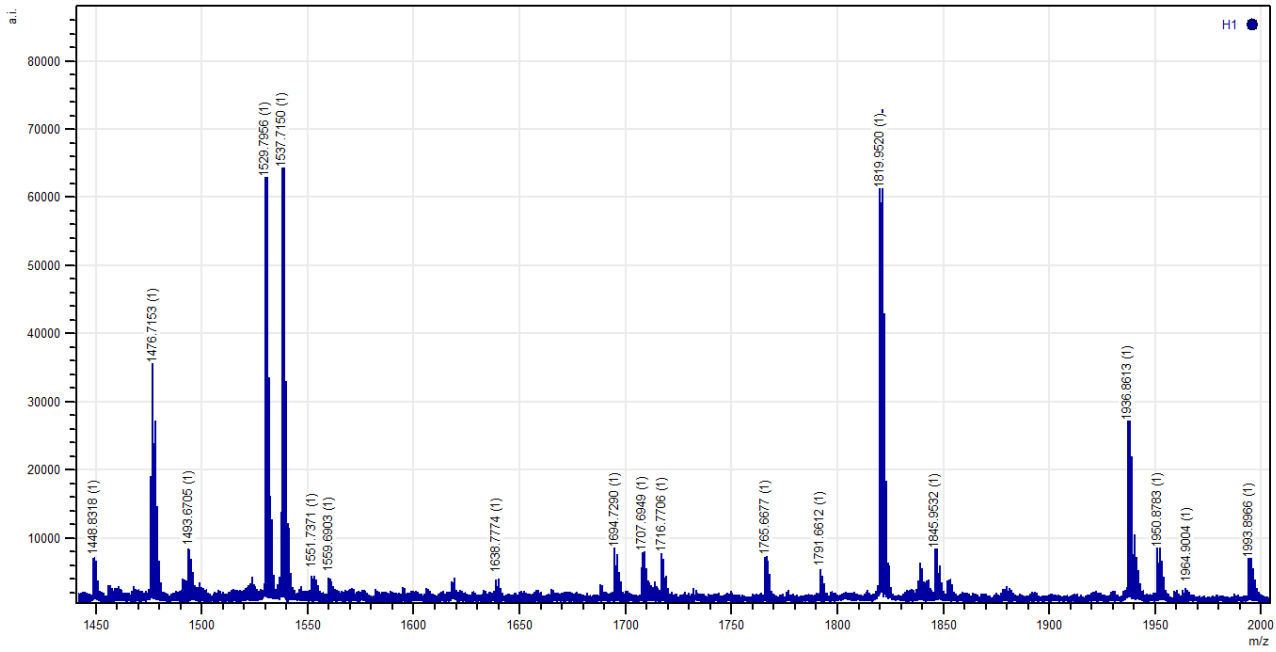

Figure 58: *Expanded spectrum of hMGL treated with H_2O_2 and DMD showing C208-containing peptides.*

Finally, two C201-containing peptides were also found, both containing the carbamidomethylation of the cysteine residue as modification. One contained residues from 187 to 202, had a *m/z* value of 1936.892 and it was among the peptides with the highest ionization yield ($4x10^4$ a.u.) in the peptide mass spectra (see Figure 58). The second, corresponding almost to the same sequence and including residues 189-202, had a *m/z* value of 1694.761 and it also showed a good intensity signal ($3x10^4$ a.u.). In addition to these C201-containing peptides, two other low signals were present in the mass spectra of the sample of hMGL treated with H_2O_2

and dimedone. A first signal at m/z = 2017.921 corresponded to the adduct between the C201-containing peptide NKTEVDIYNSDPLI**C**R (187-202) and one molecule of dimedone (see Figure 59 below).

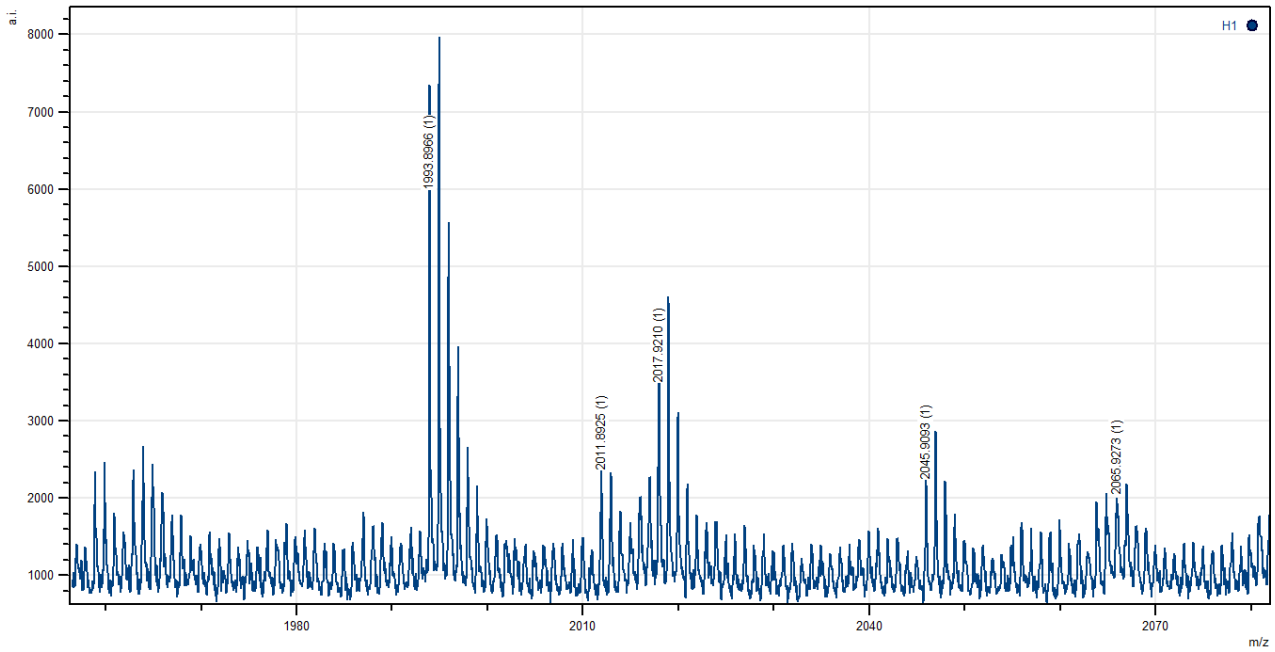

Figure 59: *Expanded spectrum of hMGL treated with H_2O_2 and DMD showing C201 CAM (1936.896) and C201 DMD (2017.921) peaks.*

The second signal at *m/z* 1775.785 corresponded to the adduct between C201-containing peptide TEVDIYNSDPLI**C**R (189-202) and one moiety of dimedone.

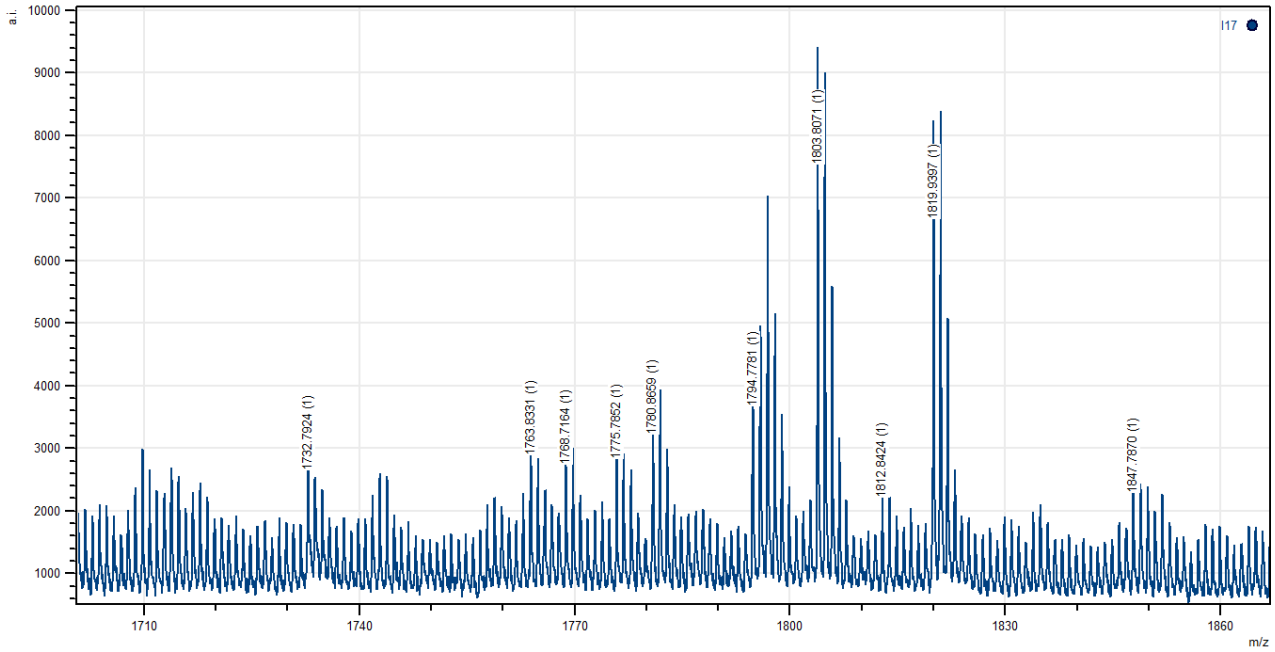

Figure 60: *Expanded spectrum of hMGL treated with H_2O_2 and DMD showing C201 DMD (1775.785) peak.*

The signals of C201-containing peptides modified by dimedone were totally absent in the peptide mass fingerprint of control hMGL. These results obtained by MALDI mass spectrometry following trypsin digestion were in line with the results obtained previously in the hMGL enzymatic activity assays.

It is therefore possible to hypothesize that incubation of hMGL with hydrogen peroxide could oxidize C201 to sulfenic acid, an oxidated species of cysteine to which dimedone can bind.

The table below summarized the results obtained for C201- and C208-containing peptides.

Start-end	Peptide	Modification	Observed *m/z*	Expected *m/z*	ppm
187-202	NKTEVDIYNSDPLI**C**R	/	1879.792	1879.922	69.2
187-202	NKTEVDIYNSDPLI**C**R	CAM (+57.022)	1936.892	1936.944	27.2
187-202	NKTEVDIYNSDPLI**C**R	Dimedone (+138.068)	2017.921	2017.990	34.4
189-202	TEVDIYNSDPLI**C**R	/	1637.656	1637.785	78.7
189-202	TEVDIYNSDPLI**C**R	CAM (+57.022)	1694.761	1694.807	27.1
189-202	TEVDIYNSDPLI**C**R	Dimedone (+138.068)	1775.785	1775.853	37.9
207-219	V**C**FGIQLLNAVSR	/	1419.666	1419.778	79.1
207-219	V**C**FGIQLLNAVSR	CAM (+57.022)	1476.758	1476.800	28.8
207-219	V**C**FGIQLLNAVSR	Dimedone (+138.068)	Not Found	1557.665	/

Another fact to underline is that the carbamidomethylated C201-containing peptide (CAM-C201) was still present also in the hMGL incubates with dimedone. Therefore, despite the use of a high molar excess of dimedone, reaction did not lead to a quantitative conversion. We couldn't infer on the relative abundances of the carbamidomethylated (CAM-C201) and the dimedone-modified (DMD-C201) peptides in hMGL samples treated with dimedone because their relative proportions depended on their different ionization yields. Dimedone is a lipophilic molecule, hardly ionizable, which can contribute to significantly decrease the ionization of a peptide. For this reason, it is important to have a high signal for the parent peptide before adding dimedone. On the contrary, modification of cysteine with iodoacetamide by carbamidomethylation is a well known strategy to increase the ionization yield of a cysteine-containing peptide. This means that a very small amount of an highly ionizable CAM-modified peptide could have a higher signal than that of a big amount of a DMD-modified peptide with a low ionization yield.

Tandem mass spectrometry (MALDI-TOF/TOF) was also employed to further verify the aminoacidic sequence of the observed peptides. The C201-containing peptide NKTEVDIYNSDPLI**C**R (187-202) endowed with the highest ionization yield was chosen as parent peptide to fragment in its native state or after modification with IAA or dimedone (see Table below).

Modification	Observed m/z	Fragments	Observed *m/z*	Expected *m/z*	ppm
None	1879.792	/PLI**C**R	601.316	601.350	55.9
CAM (+57.022)	1936.892	/PLI**C**R	658.384	658.372	-18.8
Dimedone (+138.068)	2017.921	/PLI**C**R	739.369	739.418	65.7

Rather unexpectedly, in all the three cases, the chosen peptide formed only one fragment, which corresponded to the y5-fragment at the N-term of the proline residue. This unique fragment of sequence PLICR included C201 and the expected modifications, both iodoacetamide and dimedone.

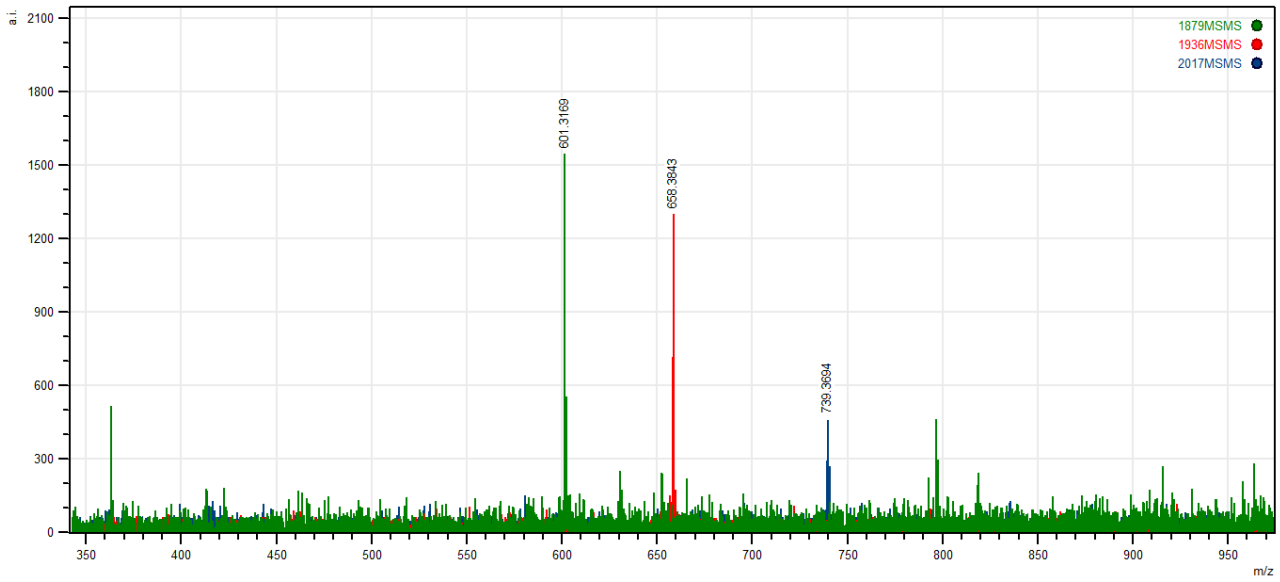

Figure 61: *Unified full scan of MS/MS spectrum of the peptide 187-202, in green it is the fragment of the peptide without modification, in red the fragment of the peptide carbamidomethylated and in blue the fragment of the peptide with dimedone adduct.*

It was possible to observe that, starting from the y5-fragment PLICR at *m/z* = 601.316 derived from the fragmentation of unmodified parent peptide, in the carbamidomethylated peptide a fragment at *m/z* = 658.384 was obtained, corresponding to the mass shift of +57, and in the peptide in which cysteine was first oxidized to sulfenic acid and then conjugated with dimedone a fragment at *m/z* = 739.369 was obtained with the expected mass shift of +138, due to dimedone addition. We could therefore conclude according to our MALDI mass spectrometry data, that the C201 of hMGL was sensitive to oxidation by hydrogen peroxide and was converted to sulfenic acid, an oxidative species that is known to react with the chemoselective probe dimedone. C32, as hypothesized, did not seem involved either in oxidation by H_2O_2 or in subsequent reactions with dimedone, confirming its low reactivity and involvement in the modulation of enzyme activity. According to our data, also C208 did not seem involved in the oxidation process, as no dimedone adducts were observed for C208-containing peptides despite the fact that signal intensities of C208-containing peptides were equal or higher than the corresponding signals of C201-containing peptides.

We may infer that, if the binding of dimedone was able to significantly decrease the signal of a C201-containing peptide, this should happen similarly for a C208-containing one, so that peptides carrying the dimedone adduct should be equally detectable. Unfortunately, these MALDI-TOF/TOF experiments were not able to detect any C242-containing peptide, either after trypsin or chymotrypsin digestion, so no indication on its reactivity with hydrogen peroxide and dimedone could be registered.

5.5 Materials and Methods

5.5.1 Tested compounds

All reagents were purchased from Sigma-Aldrich at the highest quality commercially available. Solvents were RP grade unless otherwise indicated. Two different batches of human MGL were purchased from Cayman Chemical (Ann Arbor, MI, USA) and from R&D Systems (Minneapolis, MN, USA), the first batch was a human recombinant C-terminal 6His-tagged protein expressed in *E. coli*, with a concentration of 0.35 mg/mL and it was supplied in 50 mM Hepes buffer, pH 7.4, containing 100 mM sodium chloride, 5 mM magnesium chloride, 0.1% v/v Triton X-100, 25% v/v glycerol; the second batch was a recombinant protein expressed in *E. coli* with an N-terminal Met and 6His-tag, it had a concentration of 0.411 mg/mL and it was supplied in a 0.2 μm filtered solution in 25 mM Tris buffer pH 8.0 containing 1000 mM NaCl, 1 mM EDTA and 0.02% v/v Brij 35 as surfactant.

5.5.2 Pharmacological assays of hMGL

The measurement of 2-oleoylglycerol hydrolysis was monitored with the preincubation of hMGL at 37°C for a certain period of time, depending of what types of experiments were carried on. For assays involving incubations of hMGL with selected inhibitors, reducing or oxidizing agents, the pre-incubation was 10 min; for assays involving incubations with dimedone, the pre-incubation was 30 min followed by other 5 min after DTT addition. For all assays, final incubation volume was 100μL in 50 mM Tris pH 8.0 containing 1% of DMSO, the final content of hMGL was 100 ng/assay. After pre-incubation, 10 μL of substrate 2-OG solubilized in 50 mM Tris buffer pH 8.0 containing 1% of Bovine Serum Albumin were added (BSA) to reach a final 2-OG concentration of 100μM. Samples were incubated at 37°C for 15 min. Then the enzymatic reaction was stopped by adding 200 μL of a chloroform/methanol mixture (ratio 1:1), containing 5 nmol of the internal standard heptadecanoic acid (HDA). Samples were then vortexed and centrifuged at 1400g for 3 minutes at 4°C. The organic phase was withdrawn and dried with a N_2 flow. Samples were reconstituted in 150 μL of methanol and directly injected in the HPLC-MS system.

For all assays, two types of control experiments were prepared. Following the same procedure described above, the negative control experiment was constituted of only 2-OG in the same buffer of all the assays, to subtract for its chemical hydrolysis under the chosen experimental conditions. The positive control was constituted of only hMGL. Both these samples were processed as described before. The negative control was needed to measure for the formation of oleic acid without the enzyme and the positive control was necessary as the value for comparison with other samples added with inhibitors, oxidizing or reducing agents.

5.5.3 Analytical method and instrumentation for stability studies on benzisothiazolones

Compounds stability was carried out on a Thermo Accela 1250Pump LC system equipped with an Accela OpenAS autosampler. HPLC–ESI–MS/MS analyses were performed on a TSQ Quantum Access MAX triple quadrupole mass spectrometer (ThermoFinnigan Italia, Milan, Italy) with an heated electrospray ionization source (H-ESI II). Data acquisition and processing were performed using Xcalibur software (version 2.1).

Chromatographic separation was achieved on a Synergi 4u Fusion RP 80A C18 (100 × 2.0 mm i.d., 4 μm, Phenomenex). Mobile phases consisted of water (eluent A) and methanol (eluent B), both additioned with NH_4OH at 0.1% v/v and at a flow rate of 350 μL min-1. A linear gradient elution was set up to evaluate the tested compounds in the same chromatographic run. Conditions chosen were the following: T(0 min): 60%A: 40%B; T(1 min): 60%A: 40%B; T(7 min): 5%A:95%B; T(10 min): 5%A:95%B returning to initial conditions after 1 min, followed by 3 min re-equilibration time.

ESI interface parameters were set as follows: probe middle (D) position; capillary temperature 270 °C; spray voltage -2.5 kV, vaporizer temperature 250°C. Nitrogen was used as nebulizing gas at the following pressure: sheath gas 35 psi; auxiliary gas 15 arbitrary units (a.u.). Argon was used as the collision gas at a pressure of approximately 1.5 mtorr (1 torr = 133.3 Pa). Mass spectrometric analyses were done in negative ion mode and compound-dependent parameters were optimized by flow injection analysis (FIA). For quantitative analysis, the following parent ion $[M-H]^-$ were selected: oleic acid *m/z* 281.2 (tube lens 78), HDA *m/z* 269.2 (tube lens 78).

5.5.4 Proteomic protocol on hMGL

Samples of hMGL were prepared as follow: hMGL (final concentration 1.5 μM) was incubated for 60 min in 50 mM Tris buffer pH 8.0 with or without of 10 mM H_2O_2 and 20 mM dimedone at 37°C in a final volume of 20μL. After the 60min of incubation samples were subjected to a polyacrylamide gel electrophoretic run to get rid of the low MW reactants in excess. Once the run was finished the gel was rinsed with Milli-Q water and bands of interest were excised, transferred into a new eppendorf and cutted into cubes (1x1mm). For the destaining of the Coomassie blue, a solution of EtOH/CH_3COOH/Water in ratio 50:10:40 was incubated with gel pieces at room temperature over-night. The cubes then were washed with water and the liquid removed. Acetonitrile was added to 3-4 times equal the volume of gel pieces, and immersed for 10-15 minutes. After that, the liquid was removed and the gel pieces were swelled in 10mM dithiotreitol/50mM NH_4HCO_3 pH 8.0 and incubated for 30min at 60°C. The liquid was spinned down and removed, then acetonitrile was added to shrink the gel pieces. The acetonitrile was replaced with 55mM iodoacetamide/50mM NH_4HCO_3 pH 8.0 and the solution was incubate for 20min at room temperature in the dark. Then the solution was removed and the gel pieces were washed with 50mM NH_4HCO_3 pH 8.0 for 15min. The solution was replaced with acetonitrile and then the gel particles were dried wit N_2 flow. The gel particles were rehydrated in buffer 25mM NH_4HCO_3, 5mM $CaCl_2$ and a sufficient quantity of MS-grade trypsin ("Trypsin Gold," Promega) or chymotrypsin (Sigma-Aldrich) to have a ratio 1:20 with MGL was incubated at 37°C for over-night.

To extract the peptides from the gel particles first the solution was replaced with 25mM NH_4HCO_3 and incubated for 15min at 37°C, then the buffer was replaced with acetonitrile, and was incubated for 15min, then the supernatant was collected. The gel particles were washed with 5% of formic acid and the solution was replaced after 15min with acetonitrile, which was incubated for 15min at 37°C and the supernatant was collected and pulled together with the previous one. The organic phases were dried with N_2 flow.

Samples were dissolved in 10-15 μL of 0.1% TFA in Milli-Q grade water. ZipTip C18 purification was performed before mixing the samples with MALDI matrix. Briefly, the ZipTip pipette tip was washed with 0.1% TFA in Milli-Q grade water three times, then 10 μL of sample were subjected by 20 aspirate-dispense cycles. The tip was washed with 0.1% TFA five times and then peptides bound to stationary phase were desorbed by aspirating 5 μL of 40:60 acetonitrile/0.1% TFA. Digested and purified hMGL peptides were co-crystallized with R-cyano-4-hydroxycinnamic acid matrix by mixing 5 μL of sample and 5 μL of 5 mg/mL matrix prepared in 60% acetonitrile/0.1% trifluoroacetic acid in water and less than 1 μL was spotted onto an Opti-TOF 384-well plate insert.

5.5.5 Analytical method and instrumentation for analysis of hMGL protein digests

Spectra of hMGL trypsin and chymotrypsin digests were acquired on a 4800 MALDI TOF/TOF mass spectrometer (Applied Biosystems, Foster City, CA) fitted with a UV laser (wavelength 337 nm) in reflectron mode. Data were accumulated from several positions within each sample well to determine the ions present. All MS spectra of the tryptic digests were externally calibrated using a mixture of peptide standards [des-Arg1-bradykinin at MH^+ 904.4681, angiotensin I at MH^+ 1296.6853, Glu-fibrino peptide at MH^+ 1570.6774, ACTH (clip 1–17) at MH^+ 2093.0867, ACTH (clip 18–39) at MH^+ 2465.1989 and ACTH (clip 7–38) at MH^+ 3657.9294]. The maximum allowable error was 10 ppm. MS/MS spectra were acquired on select ions of interest under the following conditions: precursor isolation set to resolution of 200, collision energy of 2kV, CID cell pressure of 2×10^{-5} torr, air as collision gas. The instrument was first calibrated in MS/MS mode using five daughter ions (at m/z 175.119, 684.346, 813.389, 1056.475 and 1441.634) generated from the fragmentation of Glu-fibrino peptide (MH^+ 1570.6774). Data were accumulated until spectra were of optimal quality and then analyzed by comparing the monoisotopic peaks with the theoretical molecular weights corresponding to the expected peptide digestion products.

Peak lists were searched with Mascot Server using the following parameters: enzyme = trypsin or chymotrypsin; maximum missed cleavages = 2; variable modifications = carbamidomethylation of cysteine, oxidation of methionine; mass tolerance = 75 ppm. The SwissProt database (*homo sapiens*, human) was used as a protein sequence database.

6. Hydrogen/deuterium exchange mass spectrometry

6.1 Introduction

Proteins play a pivotal role in most biological processes, for this reason one important aspect of understanding proteins is to determine how structure helps to dictate function. In the last years significant advances in the techniques for protein analysis, including methods such as nuclear magnetic resonance (NMR), X-ray crystallography, small angle X-ray scattering, and cryo-electron microscopy have occurred. More recently, since the last 20 years, a new technique, hydrogen/deuterium exchange (HDX), has been widely used for exploring protein conformation in solution, and mass spectrometry (MS) has been employed for detection purposes. Employing mass spectrometry as analytical technique, no crystallization of the protein is needed, and it is therefore possible to study proteins hard to purify or that are soluble only at low concentrations and this is an important advantage over other analytical techniques; moreover, a very little amount of sample is required (500-1000 picomoles for an entire experiment), and changes to conformation and dynamic on a wide timescale can be monitored. This analytical technique take advantage of the hydrogen exchange phenomenon, whereby labile hydrogens in proteins exchange positions with hydrogens in the surrounding solvent. Certain hydrogens in proteins are in continuous exchange with other hydrogens in solution. If an aqueous solution (H_2O) is replaced with a solution of isotope of hydrogen (D_2O), then one can follow the exact exchange process. As the mass of hydrogen is 1.0078 Da and the mass of deuterium is 2.0141 Da, the result of this process is an increase of mass for the protein or their peptides. The rate of incorporation of deuterium depends on amide hydrogens position within the protein and on their involvement in intramolecular hydrogen bonding.

In proteins three types of hydrogens can be essentially found: hydrogens bonded to carbon essentially do not exchange; the hydrogens of sidechains of amino acids can exchange with deuterium, but their exchange rates are too rapid to be measured with MS, so that they exchange back to hydrogen during analysis; and finally the backbone amide hydrogens, that can exchange with deuterium and their exchange rates are in a range that can be followed by MS. It is important to note that every amino acid, with the exception of proline, has a backbone amide hydrogen, meaning that there is a sensor at every amino acid along the length of the protein chain.

There are four primary factors that affect hydrogen exchange in proteins: pH, temperature, solvent accessibility and intramolecular hydrogen bonding. Temperature and pH can be controlled experimentally meaning that the rate and location of exchange becomes a function of hydrogen bonding and solvent accessibility (Fig. 62). Each folded protein in solution have different regions, for example highly dynamic and solvent-exposed regions (loops between α-helices) and regions more rigid and/or involved in hydrogen bonds or buried deep in the protein structure (β-sheets or α-helices). The exchange rate of hydrogen is different for these types of protein regions, as it is easy to imagine, the solvent-exposed regions will exchange rapidly and the buried regions will exchange slower, till reaching in some cases months to exchange.

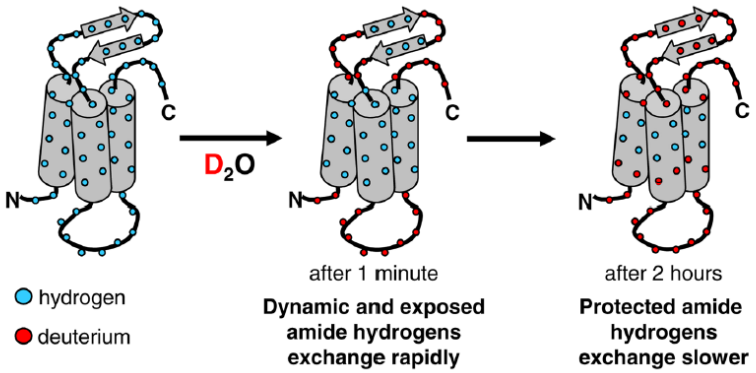

Figure 62: *Representation of the hydrogen/deuterium exchange at 1min and 2h after putting the protein in D_2O solution, regions more exposed exchange rapidly, while regions more protected and rigid exchange slower.*[167]

A general hydrogen exchange experiment monitored with mass spectrometry is considered the continuous labeling, which is the simplest and most common labeling method. In this method, a protein is initially present in an all-H_2O buffer, equilibrated at room temperature and at physiological pH, where the protein is present in its most biologically relevant conformation. Then in the solution deuterium is typically introduced by dilution (15-20 fold) with an identical buffer containing >99% D_2O. This excess of deuterium insures the exchange kinetics from hydrogen to deuterium. After predetermined times, aliquots are removed from the labeling solution and are quenched by adjusting the pH of the sample to 2.5 and lowering the temperature to 0°C. These quenching conditions ensure retention of the deuterium label by decreasing the rate of amide exchange approximately five orders of magnitude. The quenched samples can be thus injected in a UPLC-ESI-MS system to determine the mass of the intact protein. However, it is also possible to digest the proteins post-quenching and prior to the liquid chromatography. The most common enzyme used in HDX experiments to date is pepsin; however two alternative acid-stable proteases (fungal protease XIII and XVIII) have been in use since 2003.[168] These three enzymes can be covalently coupled to a stationary phase and can work in the conditions that permits to reduce the D/H back-exchange. Indeed in order to minimize D/H back-exchange, quenching of the reaction with cold acidic solution and chromatographic separation coupled with mass analysis should be performed at a low temperature (0°C) and at pH 2.5. It was calculated that when a deuterated protein is put in a 100% H_2O environment, such as an HPLC solvent system, its half-life for back-exchange is between 30-120 min, depending on the sequence.[169] It is very important that all the components of the LC system (injection valve, loop, trap column and tubing) are maintained at 0°C and that the chromatographic gradient should be very short, for example starting from a 5 to a 40% of organic phase in less than 3 min, so normally the chromatographic separation should occur on an Ultra Performance LC system (UPLC). If these conditions are met, the back-exchange from the backbone amide positions can be reduced to as little as 10-15% deuterium loss during analysis.

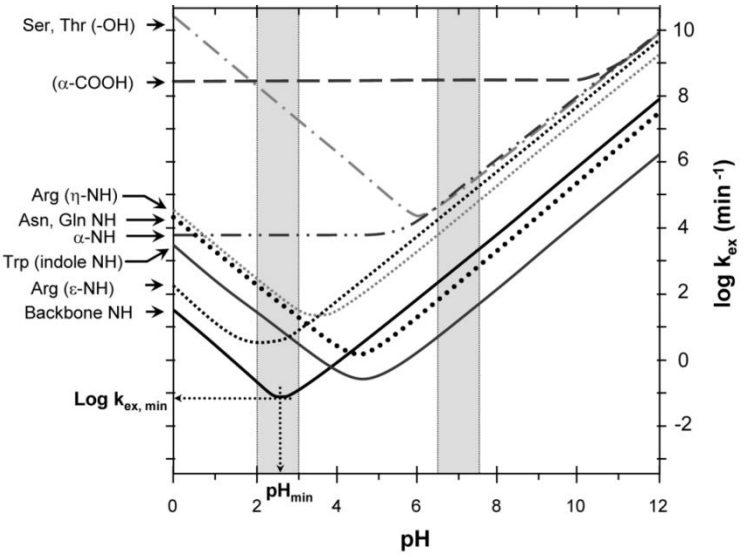

Figure 63: *Exchange rates for various types of hydrogens as a function of pH.*[169]

The first type of analysis to measure the deuterium incorporation is called "global analysis". The global HDX analysis often refers to a HDX experiment on an undigested protein. Deuterium uptake is determined from intact masses of undeuterated and deuterated proteins. The general workflow includes that the undeuterated protein is prepared in aqueous buffer at neutral pH, generally 7.4 at 25°C, with or without a modifier (ligand, inhibitor, different buffer). The protein is then diluted 20-fold with a D_2O labeling solution and incubated for certain period of time. After that, the labeling reaction is quenched by adding a cold quenching solution and samples are stored at -80°C until analysis or immediately injected into the LC-MS system. No chromatographic separation is normally required in global analysis of a single protein, so the LC is usually represented by a trap column that can concentrate the sample (if a dilute protein solution was used for labeling), can desalt the sample from salts that will negatively interact with ESI source, and, moreover, can wash away all deuterium that had exchanged in sidechains positions. However, prior to HDX analysis, an intact mass analysis (undeuterated control) is typically performed to confirm the mass, the sequence and the posttranslational modifications of the tested protein. Once the spectra are obtained, the deuterium incorporation for each labelling time is determined, using the average mass from the deconvolved spectrum. Indeed the increase of mass is determined by subtracting the mass measured for an undeuterated control sample from the mass at each deuterium exchange-in time point. The global HDX analysis can be used as a test to see if the protein of interest is stable through the HDX MS procedures (labeling, quenching, LC), the results of global analysis can provide an indication of how structured the protein is and moreover can provide a general indication for difference of deuterium incorporation of a protein in different conditions. Global HDX workflow is often performed prior to the peptide HDX analysis.

To determine the location of hydrogen exchange in a protein, a pepsin digestion step is added in the HDX workflow, giving the so called "local analysis". While in global analysis the total amount of incorporation in the whole protein over time is measured, in local analysis the location and the amount of the deuterium incorporation can be refined to small peptides. As general workflow, labeling and quenching are the same as in the intact HDX, the difference is that the deuterated protein that was quenched is then digested into

peptides which are then desalted and separated with LC. As already said, the most commonly employed protease is pepsin, that has some cleavage specificity (cleaves at hydrophobic residues), but whose products cannot be easily predicted. However, under the same environmental conditions, like pH and temperature, the peptidic fragments are reproducible and typically of small dimensions (10-15 residues) and are often overlapping in their sequences, a factor that can be helpful to localize deuterium. In local analysis, the LC step is more important than in the global analysis, because it is responsible not only of the desalting step, but also of the separation of each produced peptide. In addition, the reproducibility of separation, which allows consistent retention times for the same peptide from run to run, becomes particularly important once peptides are deuterated. Because the mass profile of isotopes are changed upon deuteration, the monoisotopic mass is no longer useful to identify the peptide, but the same peptides that were deuterated can be extracted from chromatograms at their expected retention times. Indeed, as a first step, at least a triplicate of undeuterated protein is analyzed after pepsin digestion, in order to evaluate the sequence coverage of the protein and to identify the peptides formed, an attribution that is, most commonly, accomplished using tandem MS techniques. The triplicate of deuterated protein, with or without modifiers, is then analyzed at specified time points after the buffer exchange (H_2O to D_2O). Once each isotope mass has been determined for identified peptides, the centroid mass (average of intensity weighted mass of the isotopes) is calculated. Finally, the relative deuterium uptake is determined by subtraction of the centroid mass of deuterated peptides from the centroid mass of undeuterated peptides. Generally the amount of relative deuterium uptake is then plotted as a function of time for each peptide (Fig. 64).

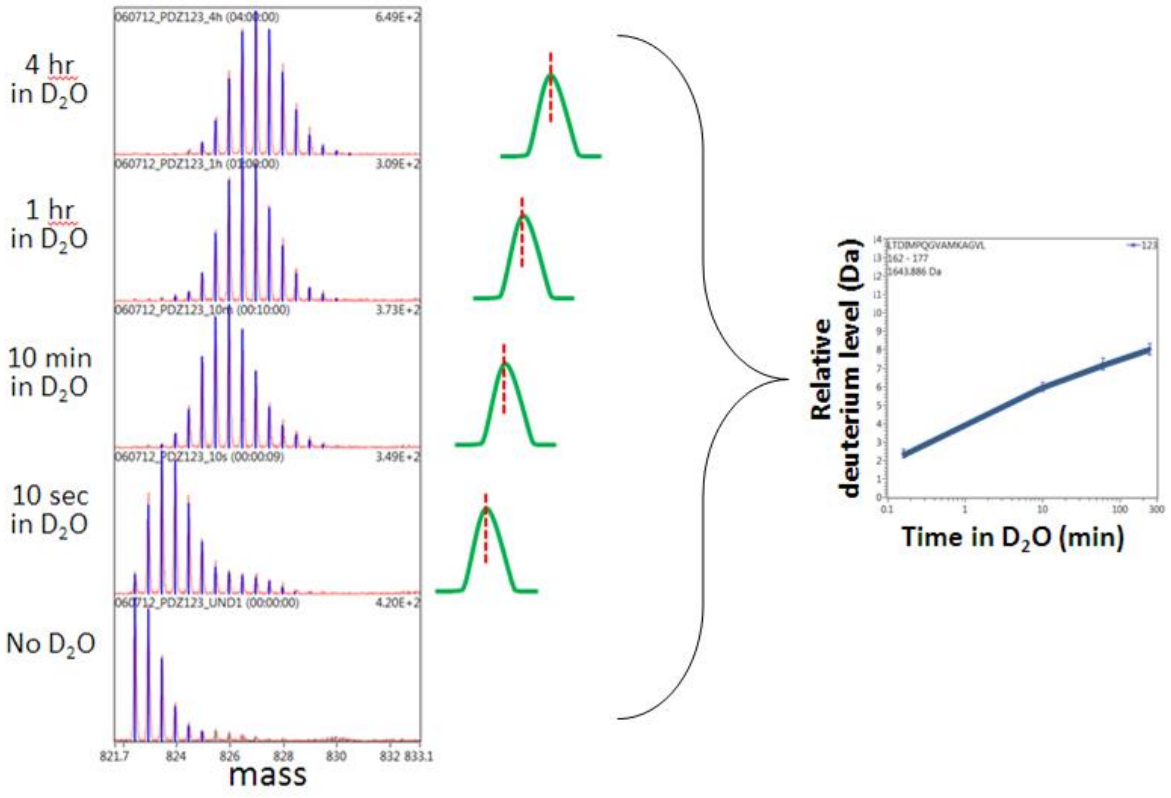

Figure 64: *Example data for deuterium exchange into peptic peptide.*

Hydrogen exchange into folded proteins can be described by a two-process model. The first process is exchange from the folded form, expressed as:

$$F_H \xrightarrow[D_2O]{k_{ex},\ F} F_D$$

where F is the folded form of the protein and the subscripts H and D refer to hydrogen and deuterium respectively. Exchange from the second process occurs from partially unfolded forms and is described by:

$$F_H \underset{k_{-1}}{\overset{k_1}{\rightleftharpoons}} U_H \xrightarrow[D_2O]{k_2} U_D \underset{k_1}{\overset{k_{-1}}{\rightleftharpoons}} F_D$$

where F is the folded form, U is the unfolded form, k_2 is the intrinsic rate of exchange, and k_1 and k_{-1} are the unfolding and refolding rate constants, respectively.[170]

For the majority of proteins under physiological conditions $k_{-1} \gg k_2$ so they are very stable and make many brief visits to a partially unfolded state to undergo exchange and become deuterated, this is the so called EX2 kinetics. Other proteins can undergo exchange via an EX1 mechanism where $k_{-1} \ll k_2$ and the exchange of a number of residues occurs simultaneously. In biophysical terms, EX1 kinetics occurs when a portion of the molecules undergo an unfolding event where multiple amide hydrogens can become simultaneously deuterated. In this particular kinetics, the exchange of all the exposed residues occurs before the protein returns to the folded state. EX1 kinetic generally does not reflect physiological protein dynamics, but it is induced artificially by addition of denaturants or a change of pH (generally 9-10.5). Also the resulting mass spectra are very different, in fact EX2 kinetics produces peaks that gradually increase in mass as the protein is exposed to D_2O for longer periods of time, while EX1 kinetics results in the appearance of two distinct mass envelopes separated on the *m/z* scale (Fig. 65).

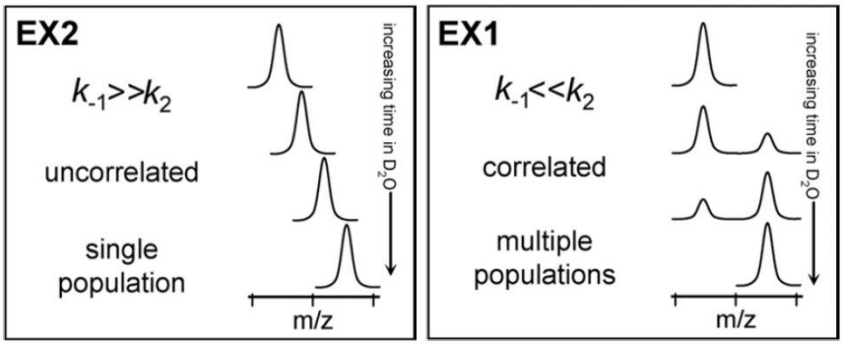

Figure 65: *Protein unfolding and deuterium labeling kinetics in hydrogen exchange mass spectrometry.*[171]

With local HDX analysis it is possible to measure the deuterium uptake in small peptic peptides, but this technique gives no indication regarding which particular residue within peptide had exchanged hydrogen. Attempts in this direction have been made employing tandem mass spectrometry, in particular using collision-induced dissociation (CID) to fragment peptic peptides into shorter pieces (b/y ions). However, from this high-energy CID employing argon as the collision gas, deuterium of peptides was "scrambled" in most ions via migration during the fragmentation process. This type of fragmentation mobilize amide protons prior to dissociation and it has not been considered an useful approach to determine site-specific deuteration levels in peptides. Recent descriptions of electron transfer dissociation (ETD) in high-resolution HDX-

MS/MS measurements should facilitate the eventual analysis of deuterium exchange at the level of individual amino acids without the concern related to potential label scrambling.[172]

In conclusion, amide hydrogen exchange monitored by mass spectrometry is a technique for studying proteins, that can provide valuable information about protein dynamics. Although the spatial resolution provided by peptide-level HDX-MS might not be as high as other structural techniques such as NMR or X-ray crystallography, HDX-MS is not limited by protein size or by crystallization properties, which can be limiting factors for NMR or X-ray techniques. In addition, HDX-MS experiments can provide useful information employing small amounts of sample (picomole quantities), it can be used to study proteins that are difficult to purify or crystallize, can reveal protein conformational dynamics on a wide time scale and can be used to study complex protein systems. Applications of HDX-MS in the biopharmaceutical industry range from protein therapeutics discovery to drug development, including the study of protein conformation, conformational dynamics upon modifications, folding/refolding processes, protein–ligand/protein–protein interactions and protein aggregation.

6.2 HDX analysis of hMGL

A recent study[140] presented the effect of two inhibitors on human monoacylglycerol lipase (hMGL) enzyme conformation employing HDX-MS. The authors employed two serine-targeted hMGL inhibitors, AM6580 and AM6701 (Fig. 66), which are known to inhibit hMGL in the low nM range and whose mechanism involve a rapid carbamylation of catalytic Ser122.

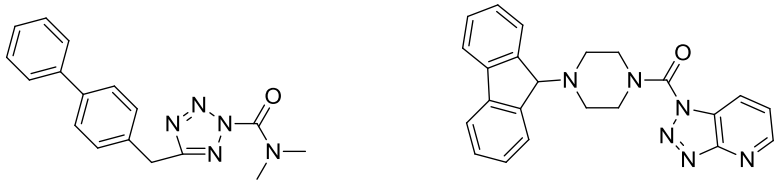

Figure 66: *chemical structures of AM6701 and AM6580.*

Within 3h hMGL inhibition by AM6580 is irreversible, while AM6701 begins to be hydrolyzed very slowly regenerating a catalytically competent enzyme after 24h. The authors suggest that a slight different mechanism of action could lead to different conformational changes of the enzyme differentially affecting both duration and reversibility of inhibition.

The intact mass analysis of hMGL carbamylated by AM6580 or AM6701 showed the predicted mass increase by MS, but the authors did not observe any peptides containing Ser122 modified with either AM6580 or AM6701. It is however known that the carbamyl group is lost when a carbamylated peptide derived from pepsin cleavage of an enzyme-carbamyl adduct is subjected to MS-analysis conditions.

In the local HDX analysis of a 6-His-tagged recombinant hMGL, they observed that over a 4h D_2O exposure some regions of apo-MGL displayed a high-level of deuterium uptake, and these regions were represented by the amino- and carboxy-terminal sequences of hMGL and its lid domain, including helix α4. This

observation was consistent with what is known for the α/β-hydrolase superfamily, that is characterized by a compact globular core of eight β-sheets and a more exposed lid and unstructured N- and C-terminal regions.

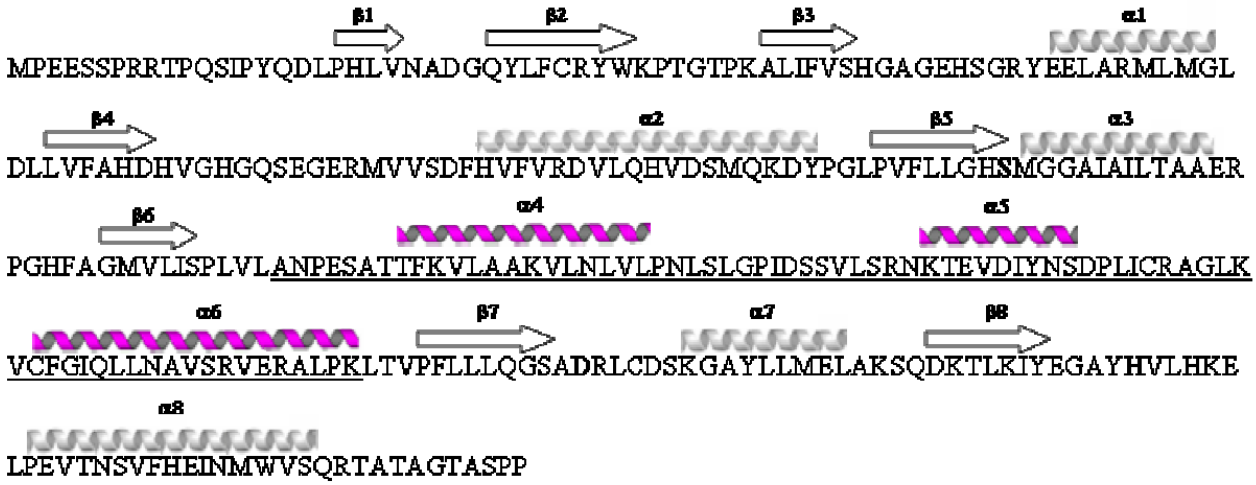

Figure 67: *primary sequence of MGL with indicated α helices and β sheets, lid domain is underlined and included α helices are colored in magenta.*[138]

In particular, the lid domain presented two distinct subregions in terms of deuterium uptake: 1) the peptide 152-166 presented no difference of deuterium incorporation during time; 2) otherwise the peptide 166-191 revealed an increase in deuterium uptake during time, 'till 4h in D_2O buffer. With these data, showing the difference of mobility within the lid domain, it was possible to provide an experimental evidence for the theory of the higher mobility of the lid domain and of the α4 helix, in particular.

With the modifications of hMGL by the two carbamylating inhibitors AM6580 and AM6701 no difference were observed in deuterium exchange between apo- and inhibitor-modified hMGL for approximately 90% of the sequence. Within the modified region, both inhibitors reduced hMGL deuterium uptake in peptides 192-208, 242-248 and 273-290. These peptides are included in specific regions of hMGL: sequence 192-208 include the terminal region of helix α5 and the loop connecting helices α5 and α6; peptide 242-248 is a part of the loop connecting sheet β7 with helix α7 and contains the catalytic-triad residue Asp246; peptide 273-290 is part of helix α8 and the loop connecting this helix to the sheet β8 and contains the His276 catalytic-triad residue. Both peptides 242-248 and 273-290 are therefore in the proximity of the active site. These data indicate that both inhibitors restrict the enzyme's backbone mobility in the substrate-binding pocket, near the active site. On the other hand, no difference in deuterium uptake was observed in the lid domain region, suggesting that hMGL also with a covalent inhibitor in the active site, remains in a "locked-open" conformation. Another region that was influenced by inhibitors is represented by residues 126-135, that contain the catalytic ser129. The localization is at the bottom of the substrate-binding pocket of hMGL. During the HDX analysis of apo-hMGL, it was observed that in this region there was not a great deuterium uptake during the 4h of D_2O exposure, probably due to the depth of the site and for the presence of a hydrogen bonding network. In contrast, when hMGL was modified by inhibitors, targeting the serine residue, also this part of the sequence increased its deuterium uptake. The authors suggested that it could be the

consequence of the disruption of the hydrogen bond network that facilitate the deuterium exchange. Finally, the last modified region was represented by peptide 217-223, which was within α6 helix. This region was influenced in different manner by the two inhibitors: AM6580, the irreversible inhibitor, led to a significant decrease of uptake, whereas AM6701, the semi-irreversible inhibitor, led to an increase of uptake (Fig. 68).

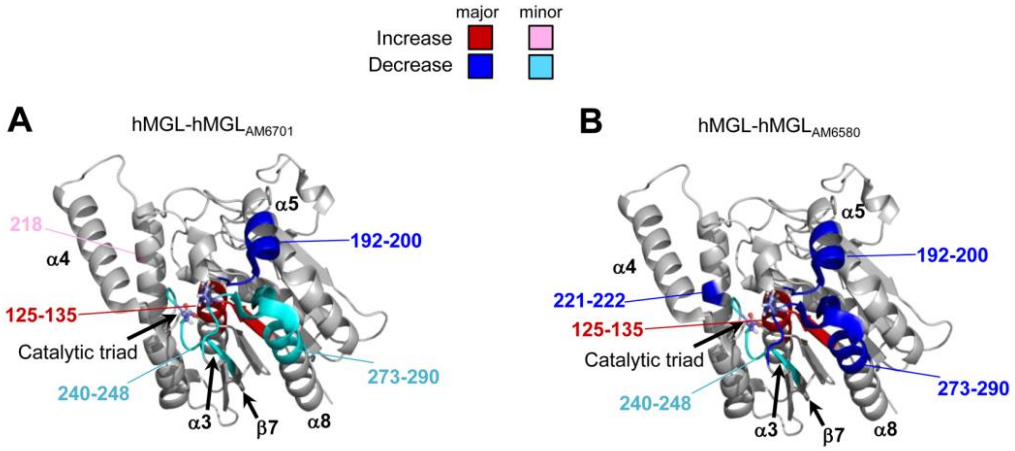

Figure 68: *The hMGL crystal structure (PDB ID: 3JW8) is color-coded to indicate the magnitude and locations of the regional intramolecular effects of hMGL covalent modification by the carbamylating inhibitors AM6701 (A) and AM6580 (B) on relative deuterium uptake by the enzyme.*

In conclusion there was the demonstration that serine-targeted hMGL inhibitors endowed with different mechanisms of action are able to elicit regionally selective changes in hMGL conformation.

6.3 Aim of the project

Starting from these indications and from the previously discussed data on the interaction of hMGL and the benzisothiazolone-based inhibitor **20**, the aim of the work was to study the conformational changes induced on a commercially available recombinant hMGL by this cysteine-targeted newly synthesized inhibitor.

Compound **20** had already been described as the lead compound of new series of cysteine-targeted allosteric inhibitors of rat and human MGL. An IC_{50} of about 130 nM had been measured on hMGL according to the enzymatic activity assays set up during this Ph.D. research program. **20** inhibits hMGL by a disulfide bridge formation with one or more cysteine residues of MGL, a covalent bond which is reduced by addition in solution of a reducing agent such as dithiotreitol (DTT). According to published literature data by other research groups on hMGL mutants, targeted cysteine residues could be C242 or C201. As already known, the lid domain of hMGL has been considered a dynamic modulator of substrate recruitment/accommodation during the catalytic cycle, and in particular after a series of preliminary studies of molecular dynamics simulations, conducted by the research group of Prof. Mor at the department of Pharmacy of the University of Parma, it was hypothesized that once the inhibitor was bound to the enzyme, the lid domain could move towards a closed or semi-closed disposition, showing an elevated motility for α4 helix. In order to verify this hypothesis, and more in general to evaluate the conformational changes induced on hMGL by the binding of the inhibitor, it was chosen to employ the HDX MS approach, performing a series of experiments at the University of Copenhagen during a three-months leave within the research group of Prof. Kasper D. Rand.

6.4 Results and Discussion

6.4.1 Intact mass and pepsin digestion of apo-hMGL and of hMGL-Compound 20 complex

The first analysis performed was the measurement of mass of the intact hMGL without inhibitor (apo-hMGL), in order to verify the correct mass of the recombinant enzyme hMGL, and after the addition of the inhibitor, in order to verify the binding of the inhibitor under the chosen reaction conditions.

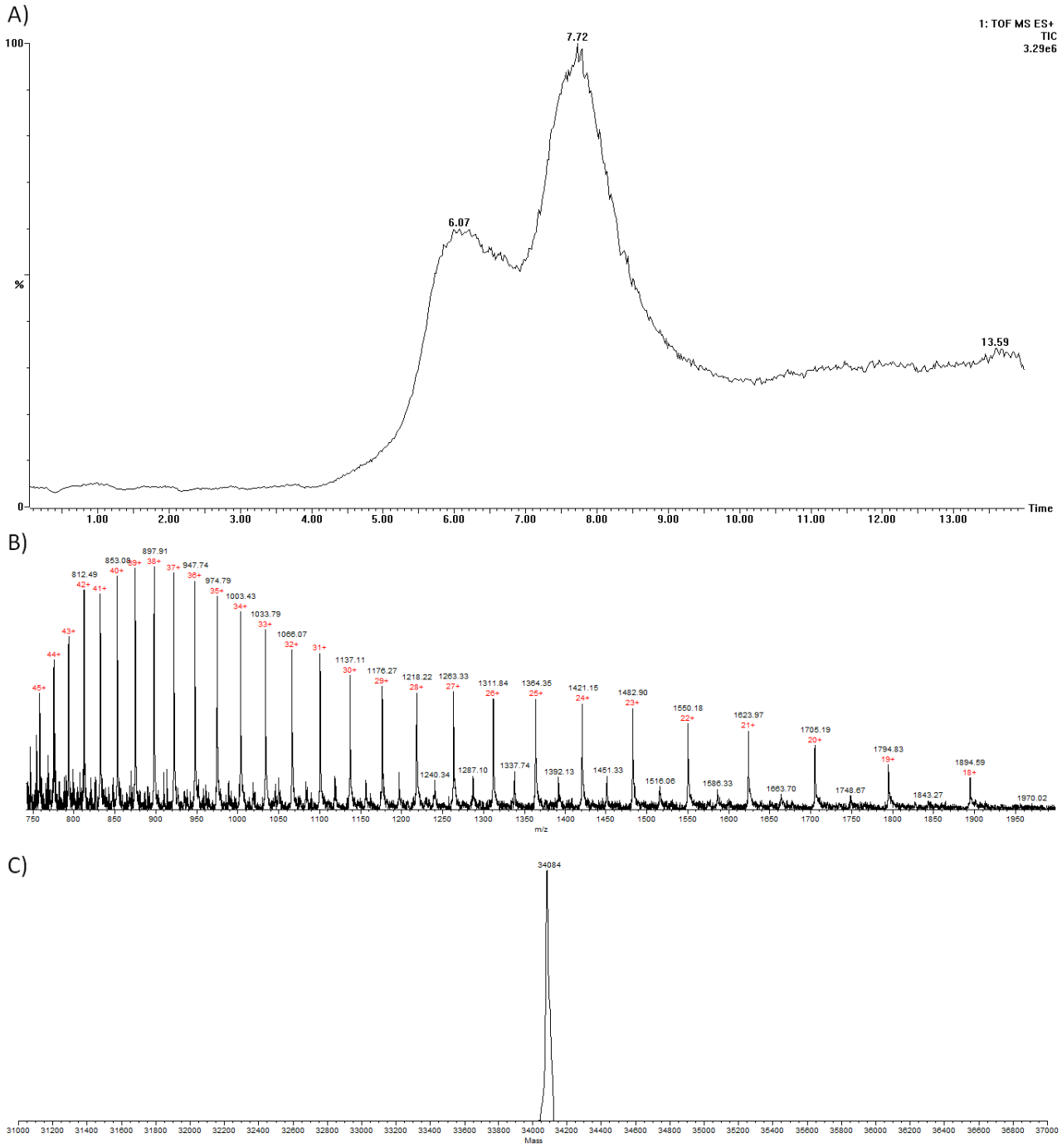

Figure 69: *A) TIC chromatogram of the apo-hMGL, the RT of the protein was 7.7; B) extracted ion spectrum of the peak at RT 7.7; C) deconvoluted spectra from the extracted ion spectrum.*

Employing the same commercial stock solution of hMGL, by R&D Systems, It had already been observed that in SDS-PAGE separation followed by Coomassie blue staining hMGL was a single monomeric protein of approximately 34 KDa. 30 pmol of hMGL were therefore dissolved in 50 µL of aqueous buffer containing

0.1% formic acid, and were injected in the Q-TOF analyzer after a brief separation on a home-made desalting column in the LC system. As it can be seen in the Figure 69, the resulted chromatogram was quite simple with hMGL protein eluting at RT 7.72 min, the previous peak at RT 6.07 min was probably a contaminant of the stock solution. The chromatogram was consistent with the elution of a purified protein after desalting. The extracted ion spectrum showed a multiply charged ion distribution, from which it was possible to calculate the deconvoluted spectrum, showing an intact hMGL mass of 34084 Da. The calculated average mass from the sequence was 34084.2, so the mass of this stock of hMGL was correctly verified, with no modifications in the reported protein sequence. The next step was the incubation of 30pmol of hMGL in 20 mM Tris buffer pH 8.0 with a 4-fold molar excess of inhibitor **20**. The reaction was stopped after 40 min at room temperature and the solution was directly injected in the same LC-system.

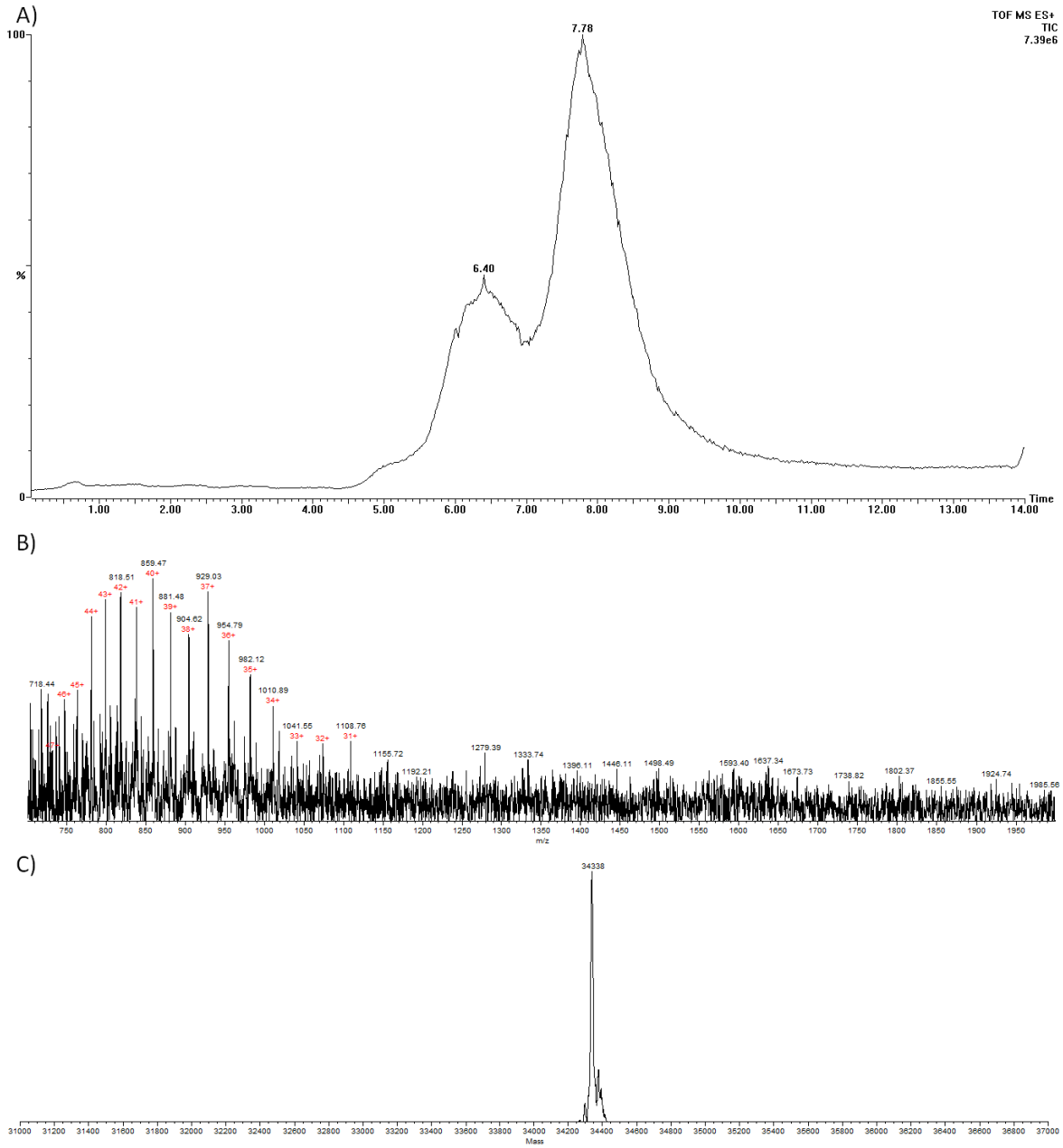

Figure 70: *A) TIC chromatogram of the hMGL reacted with inhibitor, the RT of the protein was 7.7; B) extracted ion spectrum of the peak at RT 7.7; C) deconvoluted spectra from the extracted ion spectrum.*

As it can be seen in the Figure 70, the chromatogram was very similar to the chromatogram for the apo-hMGL, no difference in RT was registered, but with the absence of a real separation phase and the small modification due to the conjugate with a low molecular weight lipophilic inhibitor, this result was expected. Despite the intensity of the TIC in the chromatogram, the extracted ion spectrum for the RT 7.7 showed a worse signal intensity than the previous one. A signal for the modified hMGL was still detectable, but there were fewer signals from the multiply charged ions. However, it was possible to operate the deconvolution of the spectrum and the obtained protein mass corresponded to hMGL with one molecule of inhibitor bound to it. Infact, the deconvoluted molecular mass was 34338 Da, with an increase of 255 Da that corresponded to the mass of Compound **20**. A second deconvoluted peak was also observed, which could be attributed to the molecular mass of intact protein with two molecules of inhibitor bound, but its intensity was much lower than the first peak. In conclusion, it was demonstrated that under these reaction conditions it was possible to observe mainly one hMGL population which had reacted with the inhibitor at the level of one cysteine residue per protein.

Next step was hMGL digestion in the absence and in the presence of inhibitor, in order to evaluate the sequence coverage of the analytical method, that could be employed for the subsequent local HDX analysis. hMGL is a relatively small, soluble protein, containing four cysteine residues, but none of them was involved in disulfide bond formation. A 30 pmol sample of apo-hMGL, in triplicate, was then dissolved in 20 mM Tris buffer pH 8.0. Just before injecting the sample in the LC-MS, the 30 pmol sample was diluted 1:1 with an ice-cold quenching buffer constituted of 300 mM phosphate buffer at pH 2.3 containing 6 M Guanidine-Hydrochloride (Gnd-HCl) and 0.25 M tris(2-carboxyethyl)phosphine (TCEP). The protocol for this part had to be exactly the same as the protocol for the labeling process. The use of this denaturing and reducing buffer was necessary in order to improve the pepsin digestion and in order to have a high sequence coverage. The presence of TCEP prevents the observation of the peptic peptide bound with the inhibitor, because the reducing agent will break the disulfide bond. However, loss of the benzisothiazolinone moiety from the peptic peptides in which it had been contained after hydrogen-exchange incubation would not negatively impact the reported deuterium uptake data for those hMGL peptides containing cysteine. After dilution in the quenching buffer, hMGL was injected in the cooled LC system and run through an immobilized pepsin column and a trap column before being loaded onto the C18 column for the separation of peptides. Then peptides were injected in the ESI-Q-TOF mass spectrometer for the MS^E analysis, in order to increase the level of identification of peptic peptides. Using ProteinLynx Global Server 3.0 (PLGS) software it was possible to identify peptic peptides and gather significant information about the sequence coverage.

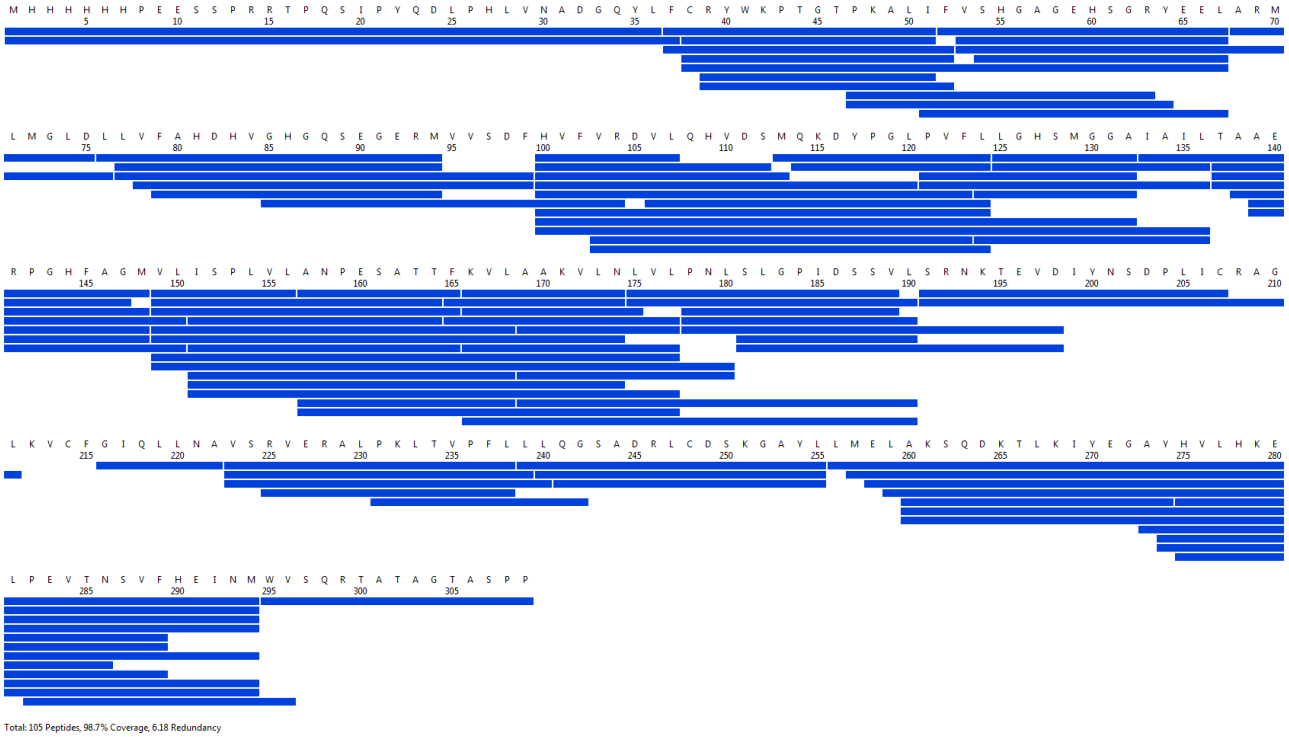

Figure 71: *Sequence coverage of the 6-His-hMGL: 105 peptides, 98.7% coverage, 6.18 redundancy.*

As it can be seen in the Figure 71, the peptide mass fingerprint map covered 98.7% of the sequence of the protein with the identification of 105 peptides and had an high degree of overlapping allowing for the determination of deuterium levels for regions of the protein smaller than the corresponding peptide. Only four residues were not covered, the sequence KVCF that also include the cysteine residue 208 (C214 in this particular protein for the presence of the His-Tag). The same peptide mass fingerprint was achieved with hMGL after incubation with a 4-fold concentration of inhibitor and the results of the sequence coverage were the same, with a percentage equal to 98.7% and an high degree of overlapping. There was no identification of the peptide modified with the inhibitor for the presence of the TCEP in the quench buffer that could reduce the disulfide bond.

Thus the experimental procedure to analyze the HDX of hMGL had been set up correctly. Indeed, it had been confirmed that hMGL molecular mass corresponded to the theoretical one, that the protein incubated with the inhibitor gave just one predominant species, which corresponded to the the monoadduct of hMGL with one molecule of inhibitor. Then, it was verified that the protease pepsin digested the protein both in the presence or absence of inhibitor with an high degree of sequence coverage and good overlapping peptides, and that the intensity of MS signals was very high. Obtained these results, it was possible to proceed with the global and local HDX analysis of hMGL with and without the presence of the inhibitor, in order to analyze the conformational changes produced by the inhibitor on the enzyme.

6.4.2 Deuterium exchange of hMGL

To investigate to what extent the interaction of the inhibitor could affect hMGL global conformational plasticity, the deuterium incorporation profile of apo-hMGL was compared with the exchange profile of

hMGL in the presence of the inhibitor **20**. As previously described, a 30 pmol hMGL sample was dissolved in 20 mM Tris buffer pH 8.0 in the absence or in the presence of the inhibitor, in triplicate. The chosen incubation time was 40 min at room temperature, then aliquots were taken and diluted in the same volume of ice-cold quenching buffer (300 mM phosphate buffer pH 2.3 containing 6 M Gnd-HCl and 0.25 M TCEP), the rest of the sample was diluted 10-fold in deuterated 20 mM Tris buffer pH 8.0. At 15 s time-point, a 30 pmol aliquot was diluted in ratio 1:1 with the same ice-cold quenching buffer and stored at -80°C. Then samples of intact undeuterated and deuterated hMGL were injected in Q-TOF after a quick separation on a home-made desalting column in the UPLC system, in order to measure the multicharged spectrum from which was possible to calculate the deconvoluted mass of undeuterated and deuterated protein. Both the undeuterated apo-hMGL and inhibited hMGL showed the same mass of 34084, indicating no modifications during the analysis. Deuterated samples at 15 seconds showed an increased mass due to the incorporation of deuterium, and it was possible to calculate the percentage of deuteration subtracting the deconvoluted mass of undeuterated protein from deuterated.

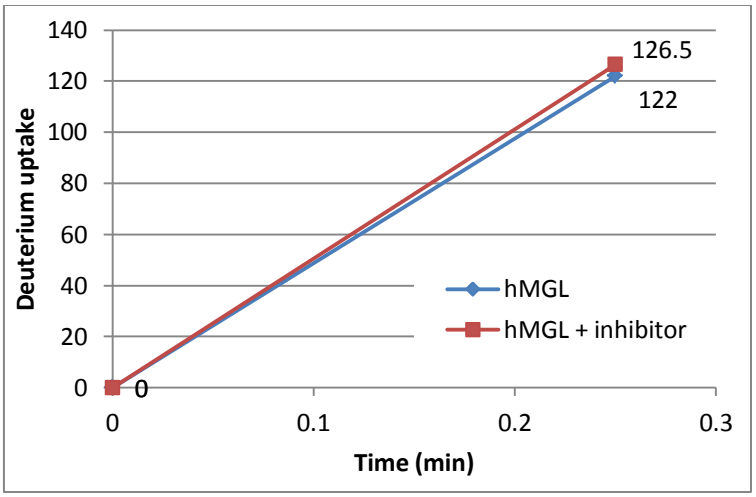

Figure 72: *Deuterium levels observed for the hMGL with and without inhibitor after 15 s incubation period.*

Figure 72 shows the overall deuterium uptake in intact hMGL in the absence (apo-hMGL) and the presence of the inhibitor at one time point, 15 s. Comparison of the global exchange results observed for both apo- and inhibited hMGL revealed that exchange was slightly accelerated in the presence of the inhibitor. The hMGL contains a total of 288 exchangeable backbone amide hydrogens. HDX-MS analysis of the apo-hMGL after a 15 s incubation indicated that 122 backbone amide hydrogens were exchanged with deuterium, which corresponds to around 40% of the sequence. With the presence of the inhibitor, there was an increase in deuterium uptake of about 5 units, reaching 127 exchanged hydrogens. The increased deuterium incorporation levels observed for the inhibited enzyme suggested that ligand binding resulted in an increased structural relaxation, augmented flexibility and/or increased overall solvent accessibility of the intact protein.
To dissect the impact of the **20** on the conformational dynamics of hMGL, local HDX-MS studies were performed on the hMGL-ligand complex. HDX-MS analysis at the peptide level provides an approach to determine the regions in hMGL that experience conformational changes induced by ligand binding.

30 pmol of hMGL per sample were dissolved in 20 mM Tris buffer pH 8.0 in the absence or presence of the inhibitor, in triplicate. The incubation time was 40 min at room temperature, then aliquots were taken and diluted in the same volume of ice-cold quenching buffer (see Materials and Methods) in order to have undeuterated samples, the rest of the samples were diluted 10-fold in deuterated Tris buffer 20 mM pH 8.0. At specified time points, i.e. 15 s, 1, 60 and 480 min, 30 pmol aliquots (50 µL each) were diluted 1:1 with the same ice-cold quenching buffer and stored at -80°C. Samples were then injected into a cooled HPLC system, digested online by a pepsin column, then digested peptides passed through a rapid desalting system and separated on a C18 analytical column, and analyzed by means of a Q-TOF mass spectrometer.

Preliminary results for the online pepsin digestion of deuterium-labeled, quenched samples of each state of hMGL resulted in 97 peptides that covered the 98.7% of the sequence. The deuterium incorporation into apo-hMGL and inhibited hMGL was monitored from 15s to 8h with a total of four time points. The average percentage of deuterium incorporation at 15 sec was consistent with the previously described uptake in the intact protein: around 40%, reaching about 50% after 8h of incubation in D_2O buffer.

The percentages of deuterium uptake varied markedly among the various protein regions. It was observed that those peptides containing the catalytic serine (residues 124-136) described the protein region with the lowest deuterium incorporation. Indeed, this region is known to be located deeply within the enzyme, showing an average deuterium uptake at 15 s of about 15%, increasing to 35% only at 8h. In contrast a part that can rapidly exchange is represented by the C-terminal region, identified by the peptide 295-309, that had already exchanged 70% of hydrogens both at 15 s and 8 h. Another region with the highest deuterium uptake was represented by peptide 149-190 where at 15 s an average percentage of 60-70% of deuterated sequence was observed, remaining almost stable ‘till 8 h. This region was identified as the exposed lid-domain, including the α4 helix. Anyway, within this characteristic region of hMGL, a difference of deuterium uptake was observed in three regions, represented by the three peptides: 149-165, 165-180 and 175-190.

In particular, peptide 149−165, which corresponded to the protein sequence from β6 sheet to α4 helix, showed a high relative level (~60%) of deuterium uptake during time, with a slight increase of exchanged hydrogens from 15 s to 8 h (65-70%). On the contrary, the region 175-190, which connects α4 helix to α5 helix, showed no differences in deuterium uptake during time (~65%). Moreover, the sequence 165-180, which contains the α4 helix, showed a unusual EX1 kinetics at the first two time points. From the starting peptide signal of the undeuterated protein, at 15 s two signals of same peptides were observed: one that incorporated one deuterium and the second with a 4 Da increased mass. At 1 min the intensity of the first signal decreased and at 60 min and 8h it was gone (Fig. 73). For all triplicate of the same peptide and for other peptides of the same region showed identical results, no carryover was detected in the chromatogram.

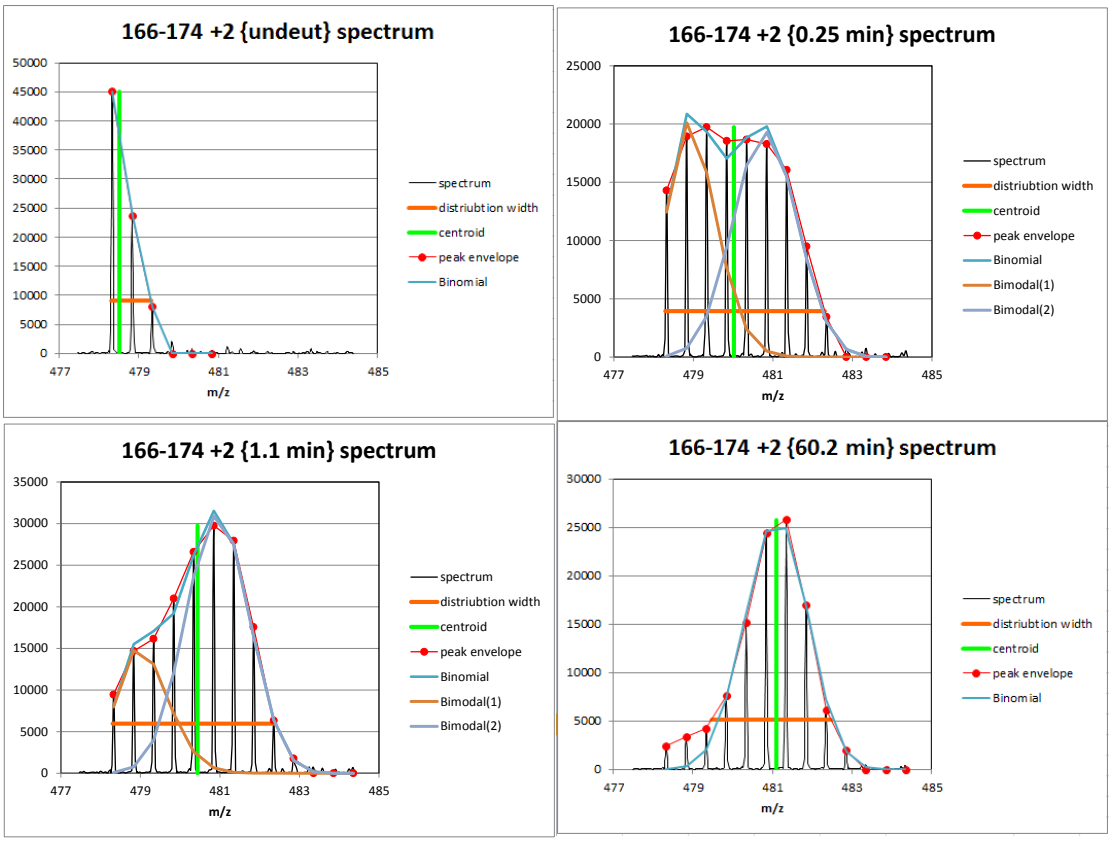

Figure 73: *Example of the unusual EX1 kinetics of peptide 166-174 double charged. The individual binomial distributions are shown in brown and blue and their sum is shown in cyano.*

It is possible to represent the binomial distribution by a bubble plot (below) that is a useful tool for interpreting the bimodal exchange profiles. This plot shows the deuterium uptake profile for both binomial fits and the size of each point is scaled to its relative intensity at that time point. This is useful for differentiating between EX1 type exchange kinetics (where the relative bubble sizes modify over time) and two distinct populations (where the relative intensities remain constant over time).

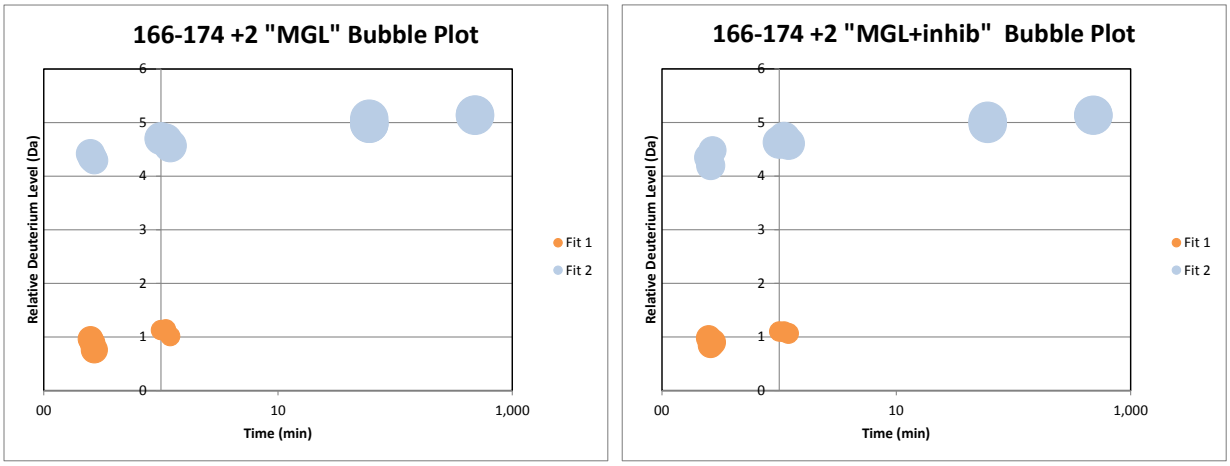

Figure 74: *Example of bubble plot of peptide 166-174 double charged of apo-MGL (left) and inhibited MGL (right), the colors of bubbles are linked to the binomial distribution in fig. 73.*

The Figure 74 shows, as an example, the trends observed in the two populations of peptide 166-174 in apohMGL (left graph) and inhibited hMGL (right graph). With no significant differences between apo- and inhibited hMGL samples, two different populations of the peptide were observed at the first time points (t =

15 s and t = 1 min): following the behavior of the first population of the peptide (indicated in the graph as Fit 1) there was an incorporation of deuterium atoms ranging from 1 to 5 in the 15 s-8 h time span. Following the behavior of the second population of the peptide (indicated as Fit 2) the deuterium incorporation had already reached its maximum almost at the first time point (t = 15 s).

About 73.5% of the analyzed hMGL sequence showed a "regular" EX2 kinetics, and the deuterium uptake by all these peptides, reported in the Materials and Methods section, showed no significant difference between apo- and inhibited hMGL.

Figure 75 summarize these results, reporting the difference plot for deuterium uptake at peptide level in the apo-hMGL in comparison to the inhibited enzyme. The difference in deuterium uptake is considered significant with a value greater than 0.5 Da; the reduced deuterium uptake in a specific peptide of inhibited hMGL is represented by a positive difference, indicating a shielding effect of the inhibitor to the hydrogen/deuterium exchange by that peptide, whereas an increased deuterium uptake in a specific peptide of inhibited hMGL is represented by a negative difference indicating a higher exposure of that peptide to hydrogen/deuterium exchange caused by the inhibitor. As it can be seen, a large number of hMGL peptides showed differences in deuterium uptake below 0.5 Da, suggesting that the inhibitor was not able to produce huge conformational changes on hMGL. Pratically the only exception is represented by peptides 257-274 for which an increase in deuterium uptake for t = 15 s and 1 min was observed. These peptides corresponds to a protein sequence in the vicinity to the helix α8.

Besides the peptides 165-180, other regions of hMGL showed a strange and unusual EX1 kinetics. Peptides 100-113, which belong to the α2 helix, peptides 274-294, which contain the catalytic His269 (residue 275) in the α8 helix and peptides 223-238, which belong to the C-term of α6 helix. Other peptides corresponding to residues 240-255 and 191-207 showed the same behavior: the first ones included Cys242 and Asp239 (residues 248 and 245), and represented the N-term of α7 helix, the second ones included Cys201 (residue 207) and represented the C-term of α5 helix.

These last four regions (191-207, 223-238, 240-255 and 274-294) in apo-hMGL showed the same behavior: EX1 kinetics in the first two time points like already shown for peptides 166-174. In the inhibited hMGL, some differences in the two peptide behaviors were detected, in comparison to apo-hMGL; however, as data interpretation is still on-going, it is not possible to further discuss in details the conformational changes of the enzyme after the inhibition of Compound **20**. On the other hand it is quite tempting to compare these results with those observed by Makriyannis and colleagues. As previously said they observed modifications in deuterium uptake by serine-targeted inhibitors in peptides 192-208, 217-223, 242-248, 273-290 and the peptide containing serine 126-135; in the present HDX analysis, employing a cysteine-targeted inhibitor, a difference in deuterium uptake was observed for peptides 191-207, 223-238, 240-255 and 274-294, with at least two of them containing the cysteine residues C201 and C242.

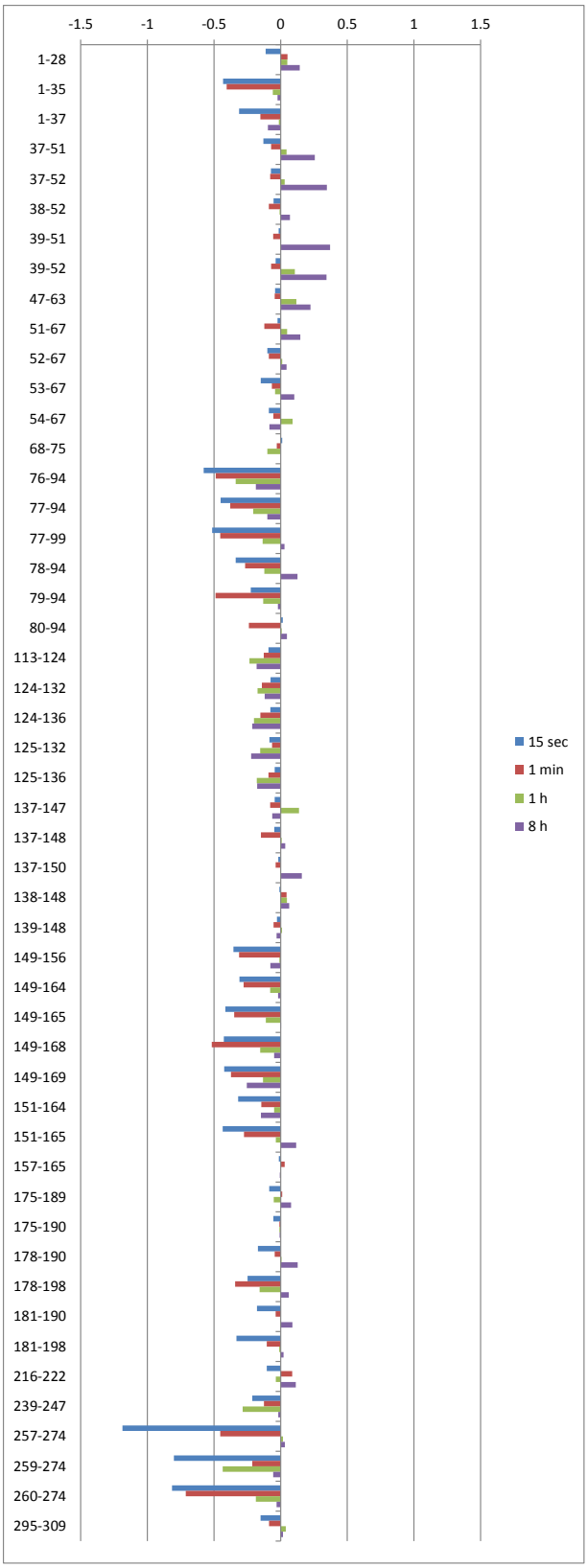

Figure 75: *Relative difference plot for inhibited hMGL compared to the apo-hMGL, for EX2 kinetics-showing peptides.*

Considering those peptides for which an EX1 kinetics was observed, we could hypothesize the existence of two different populations of hMGL in tested buffered solution, one correctly folded, the other partially unfolded or in a different conformation. With an unfolded population of protein, we could explain the presence of two different signals for these peptides, in terms of two populations of peptides in different

conformations that incorporate deuterium independently. For example in the region 100-113, two distinct signals were present, theoretically corresponding to two peptide populations. However, only the first one, increased its mass over time suggesting that the peptide incorporated less deuterium at the first time points, reaching the relative deuterium incorporation of the second peptide population only after 8h. The second peptide population, instead, reached the maximum deuterium uptake already at first time points and remained stable afterwards, a behavior which could be related to an unfolded structure.

In conclusion, it was verified experimentally that inhibitor Compound **20** was able to bind to hMGL by high resolution mass spectrometry and it led to a mass increase in intact protein corresponding to the formation of a mono-adduct with the inhibitor. The proteomic protocol to analyze hMGL with and without enzymatic digestion has been set up, obtaining good results in terms of sequence coverage and degree of overlapping among peptides. Despite the preliminary results for local HDX analysis previously discussed, some still unexplained aspects of the protocol need further investigations. To explain the EX1 kinetics observed for a certain percentage of hMGL peptides, it was hypothesized that a certain part of protein population could undergo partial unfolding after the dilution of the protein in Tris buffer with the deuterated Tris reaction buffer. Despite the same composition of the two buffers, it could be possible that, with the further dilution of the protein, some other components, such as the surfactant Brij 35 and the chelating agent EDTA, present in the original protein stock solution, could be further diluted as well, leading to a partial denaturation of some portions of the protein. This hypothesis has been tested in more recent, and currently on-going, analyses, by comparing at one time point (t = 1 min) hMGL in the absence and in the presence of inhibitor, employing the already used Tris buffer and another buffer, similar to the original stock buffer of commercial protein. Preliminary data, however, suggest that the unusual EX1 kinetics is still present for some peptides and it will therefore require further investigations.

6.5 Materials and Methods

6.5.1 Tested compounds

Compound **20** was synthesized in the laboratories of the Drug Design and Discovery Group, Pharmacy Department, University of Parma under the supervision of Prof. Marco Mor. All reagents were purchased from Sigma-Aldrich (Sigma-Aldrich Srl, Milan, Italy) at the highest quality commercially available. Solvents were RP grade unless otherwise indicated. Human MGL were purchased from R&D Systems (Minneapolis, MN, USA), is a recombinant protein *E. coli* derived with an N-terminal Met and 6His-tag, it had a concentration of 0.411 mg/mL and was supplied in a 0.2 μm filtered solution in 25 mM Tris, 1000 mM NaCl, 1 mM EDTA and 0.02%(v/v) Brij35, pH 8.0.

6.5.2 Intact mass of apo-hMGL and hMGL inhibited with Compound 20

Stock solution of hMGL was diluted in Tris buffer 20mM pH 8.0 and incubated for 40min at room temperature either in the absence of inhibitor or in the presence of Compound **20** at an inhibitor/hMGL molar ratio of 4:1, each sample was constituted of 30pmol of hMGL in a final volume of 50μL. At the end of the incubation time, samples were injected in a rapid desalting system constituted by an Acquity HPLC with an injection loop containing a 10-port switching valve (Valco Instruments Inc.) equipped with a micro-column (approximately 2-μL bed volume of C4 Poros 20 R2) and proteins were eluted into an electrospray ion source at 40μL/min by a 8.5-min gradient of 10–90% acetonitrile in 0.1% formic acid. Positive ion-electrospray ionization mass spectra of eluted proteins were acquired on a Waters Synapt G2 HDMS mass spectrometer.

6.5.3 HDX-MS analysis

Stock solution of hMGL was diluted in Tris buffer 20mM pH 8.0 and incubated for 40min at room temperature either in the absence of inhibitor or in the presence of Compound **20** at an inhibitor/hMGL molar ratio of 4:1 in order to allow target binding prior to deuterium labeling. The small amount of DMSO (0.1% v/v) did not affect protein binding as indicated by the intact protein analysis. The exchange reaction was initiated by adding 10-times D_2O buffer (Tris 20 mM pH 8.0). At different reaction time points, 0.25, 1, 60 and 480 min, aliquots (30 pmol in 50 μL) were added to pre-chilled vials containing the same volume of quenching solution (50 μL, 300mM phosphate buffer pH 2.3 + 6M GndHCl + 0.25M TCEP). The quenched sample was immediately frozen and stored at −80 °C for subsequent LC-ESI-MS analysis. Experiments were performed in triplicate.

HDX information at the peptide level was obtained by employing a cooled Waters nanoAcquity UPLC system for online pepsin digestion and rapid desalting of the protein samples. After digestion of the samples by an online Poroszyme immobilized pepsin column (2.1×30 mm) with a 150 μL/min solvent (0.23% formic acid in H_2O), the peptic peptides were trapped on a pre-column (Waters VanGuard C18, 1.7 μm, 2.1 × 5 mm, Milford, MA, USA) and desalted with 0.23% formic acid, pH 2.3, 150 μL/min for 3 min. Peptides were eluted from the trap to the analytical column (Waters BEH C18, 1.7 μm, 1.0 mm × 100 mm) and separated

with an 8−40% gradient of 0.23% formic acid in acetonitrile (pH 2.3) over 7 min at a flow rate of 40 µL/min. To identify pepsin-generated peptides, mass spectral data were acquired on a Synapt HDMS system equipped with a ESI source and operated in the MS^E mode. The MS^E dataset was input to the ProteinLynx Global Server 3.0 software program (Waters Corp.) for searching against an "in house" protein database to which the human MGL sequence was added.

For intact protein HDX-MS, the protein was incubated in D_2O buffer for only one time point, 0.25 min, then quenched with same volume of sample of quenching solution (300mM phosphate buffer pH 2.3 + 6M GndHCl + 0.25M TCEP). The quenched sample was immediately frozen. The sample eluted through a micro-column (approximately 2-µL bed volume of C4 Poros 20 R2) with a steep 10-90% (v/v) B gradient within 8.5 min (mobile phase A: 0.1% formic acid in H_2O, mobile phase B: 0.1% formic acid in acetonitrile, flow rate 40 µL/min) and eluted into a Waters Synapt G2 HDMS mass spectrometer.

The deuterium incorporation levels for protein or peptic peptides were directly derived from the observed mass difference between the deuterated and nondeuterated proteins/peptides without back exchange correction. The back-exchange correction was omitted due to the comparative nature of the present study. The intact protein molecular mass and the centroid mass of each peptide, respectively, were obtained using MassLynx 4.1 and DynamX 2.0 software packages (Waters Corp.); bimodal curve fitting was performed using HX-Express v25.[173]

Deuterium uptake by all peptides derived from pepsin digestion of apo-6-His-hMGL and inhibited enzyme. Plots of relative deuterium incorporation vs. time for all peptides with EX2 kinetics and generated from pepsin digestion of either apo-6-His-hMGL (red lines) or 6-His-hMGL consequent to inhibition by Compound **20** (blue lines).

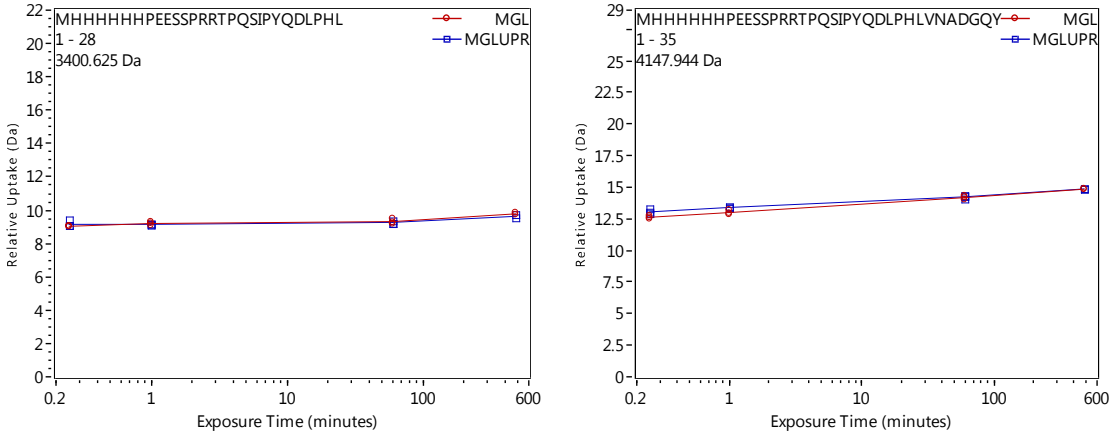

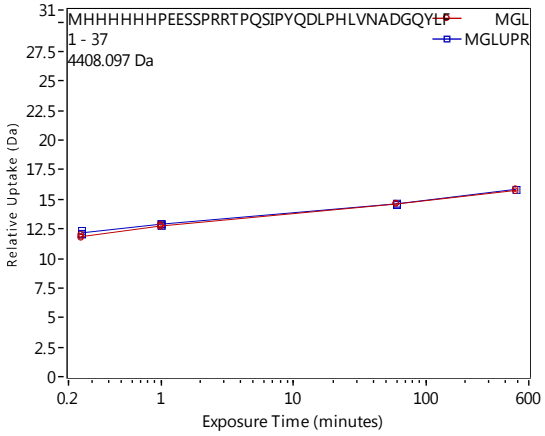
MHHHHHHPEESSPRRTPQSIPYQDLPHLVNADGQYLP
1 - 37
4408.097 Da
MGL
MGLUPR
Relative Uptake (Da)
Exposure Time (minutes)

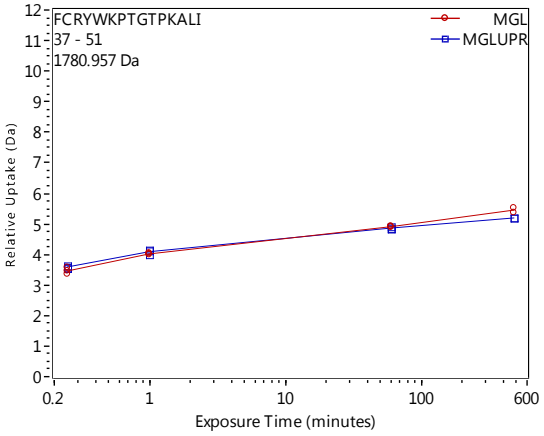
FCRYWKPTGTPKALI
37 - 51
1780.957 Da
MGL
MGLUPR
Relative Uptake (Da)
Exposure Time (minutes)

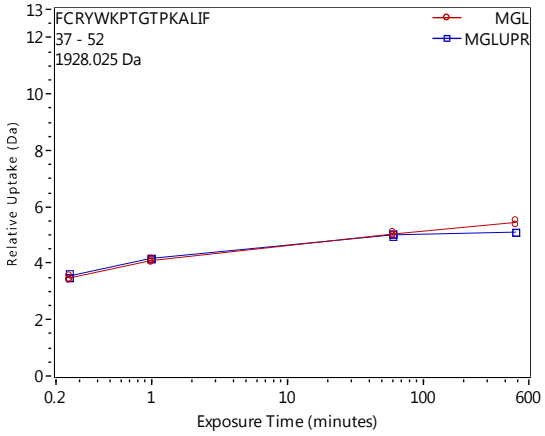
FCRYWKPTGTPKALIF
37 - 52
1928.025 Da
MGL
MGLUPR
Relative Uptake (Da)
Exposure Time (minutes)

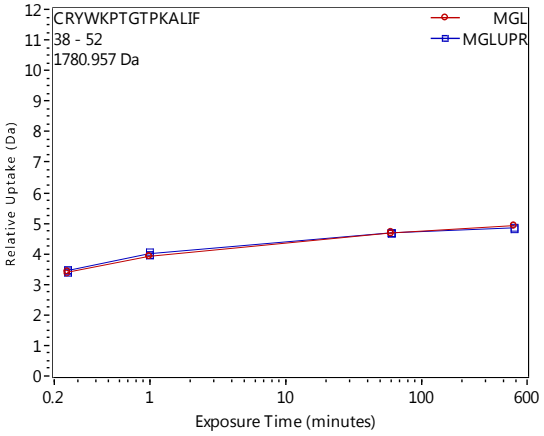
CRYWKPTGTPKALIF
38 - 52
1780.957 Da
MGL
MGLUPR
Relative Uptake (Da)
Exposure Time (minutes)

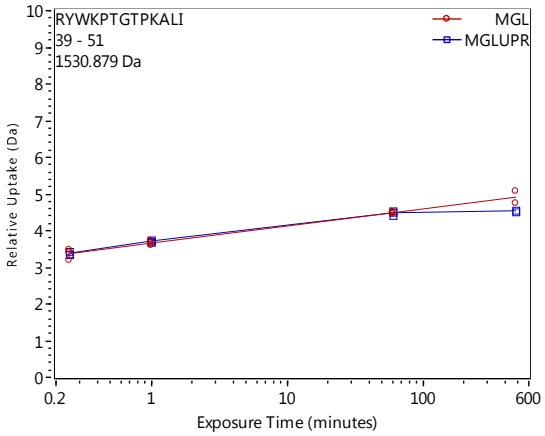
RYWKPTGTPKALI
39 - 51
1530.879 Da
MGL
MGLUPR
Relative Uptake (Da)
Exposure Time (minutes)

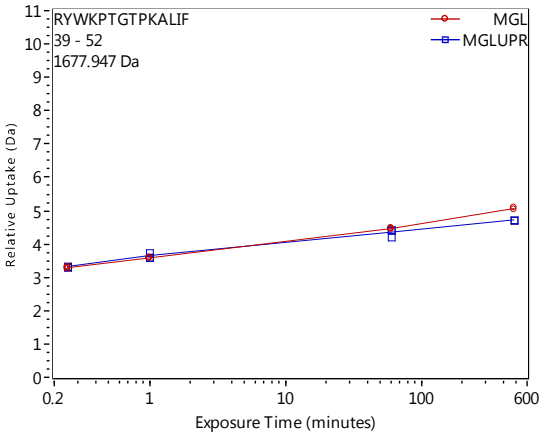
RYWKPTGTPKALIF
39 - 52
1677.947 Da
MGL
MGLUPR
Relative Uptake (Da)
Exposure Time (minutes)

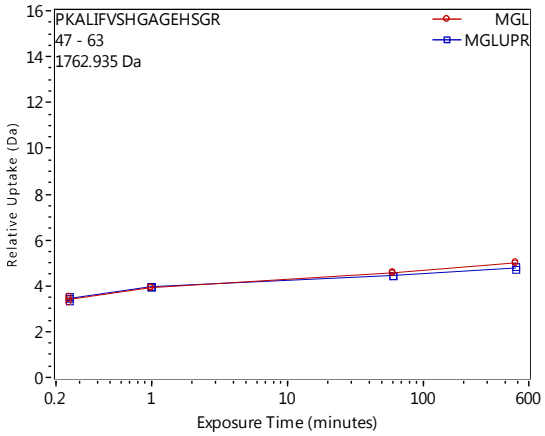
PKALIFVSHGAGEHSGR
47 - 63
1762.935 Da
MGL
MGLUPR
Relative Uptake (Da)
Exposure Time (minutes)

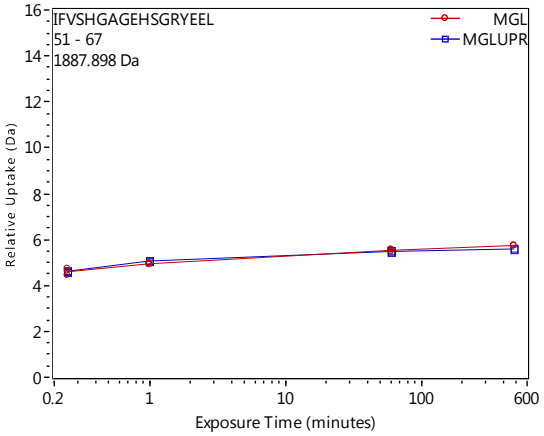
IFVSHGAGEHSGRYEEL
51 - 67
1887.898 Da
MGL
MGLUPR
Relative Uptake (Da)
Exposure Time (minutes)

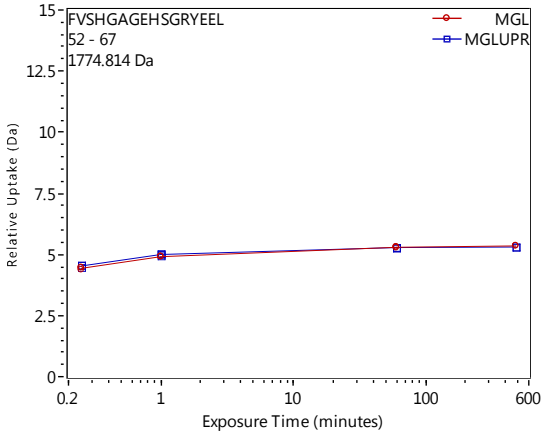
FVSHGAGEHSGRYEEL
52 - 67
1774.814 Da
MGL
MGLUPR
Relative Uptake (Da)
Exposure Time (minutes)

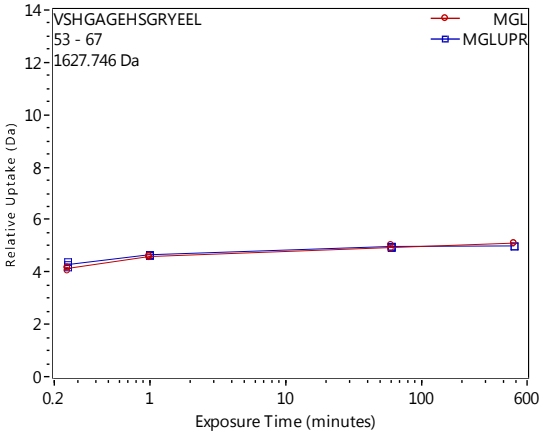
VSHGAGEHSGRYEEL
53 - 67
1627.746 Da
MGL
MGLUPR
Relative Uptake (Da)
Exposure Time (minutes)

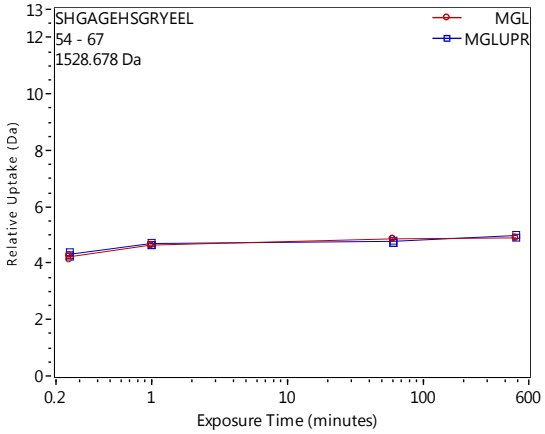
SHGAGEHSGRYEEL
54 - 67
1528.678 Da
MGL
MGLUPR
Relative Uptake (Da)
Exposure Time (minutes)

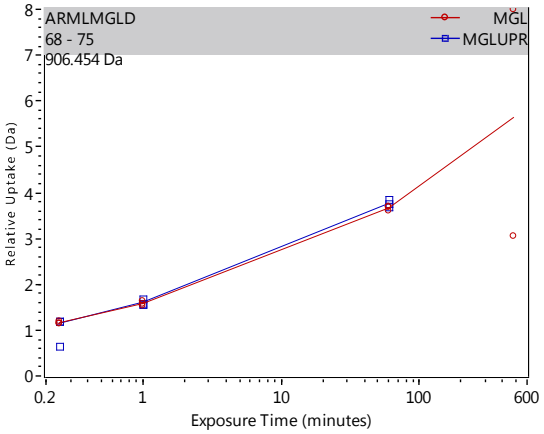
ARMLMGLD
68 - 75
906.454 Da
MGL
MGLUPR
Relative Uptake (Da)
Exposure Time (minutes)

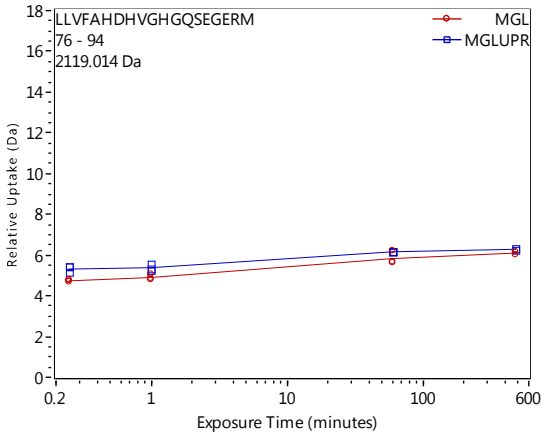
LLVFAHDHVGHGQSEGERM
76 - 94
2119.014 Da
MGL
MGLUPR
Relative Uptake (Da)
Exposure Time (minutes)

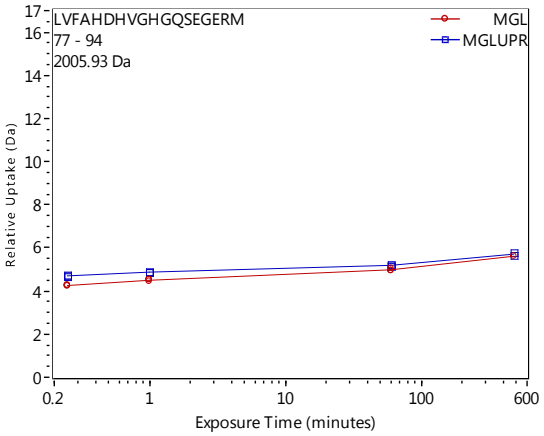
LVFAHDHVGHGQSEGERM
77 - 94
2005.93 Da
MGL
MGLUPR
Relative Uptake (Da)
Exposure Time (minutes)

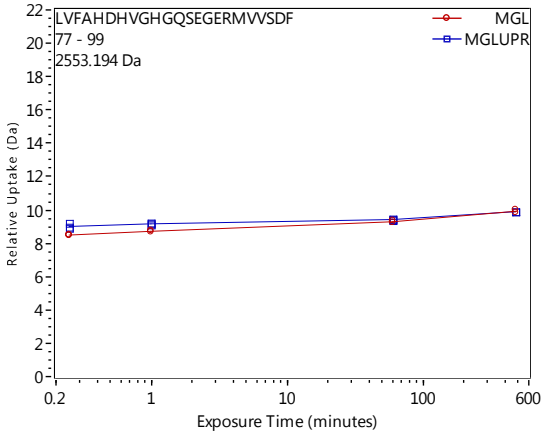
LVFAHDHVGHGQSEGERMVVSDF
77 - 99
2553.194 Da
MGL
MGLUPR
Relative Uptake (Da)
Exposure Time (minutes)

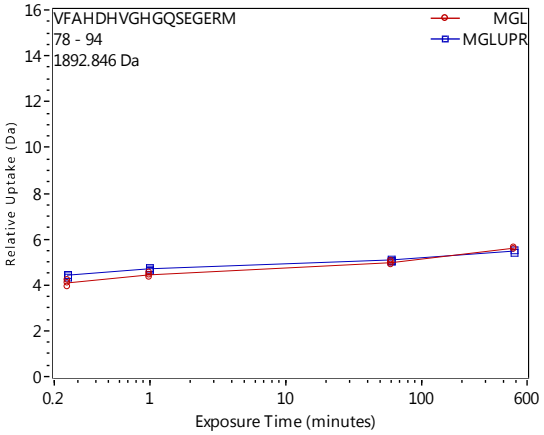
VFAHDHVGHGQSEGERM
78 - 94
1892.846 Da
MGL
MGLUPR
Relative Uptake (Da)
Exposure Time (minutes)

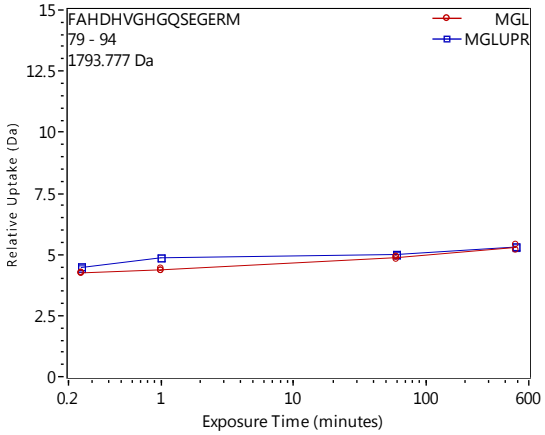
FAHDHVGHGQSEGERM
79 - 94
1793.777 Da
MGL
MGLUPR
Relative Uptake (Da)
Exposure Time (minutes)

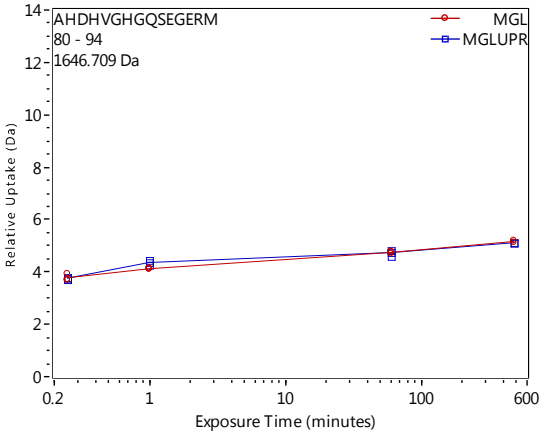
AHDHVGHGQSEGERM
80 - 94
1646.709 Da
MGL
MGLUPR
Relative Uptake (Da)
Exposure Time (minutes)

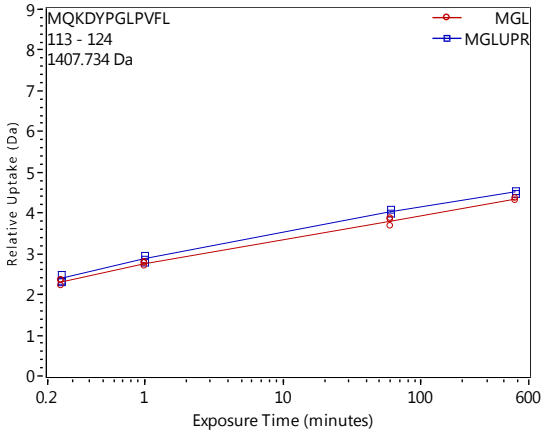
MQKDYPGLPVFL
113 - 124
1407.734 Da
MGL
MGLUPR
Relative Uptake (Da)
Exposure Time (minutes)

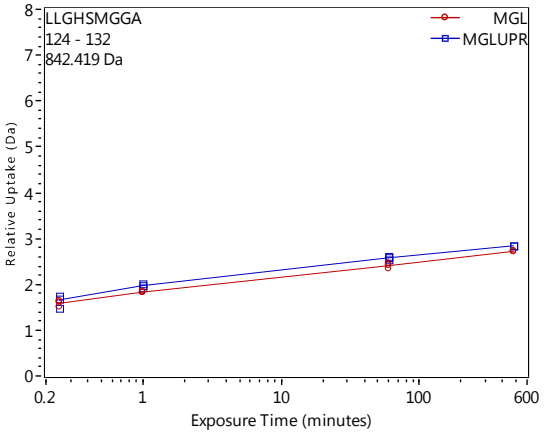
LLGHSMGGA
124 - 132
842.419 Da
MGL
MGLUPR
Relative Uptake (Da)
Exposure Time (minutes)

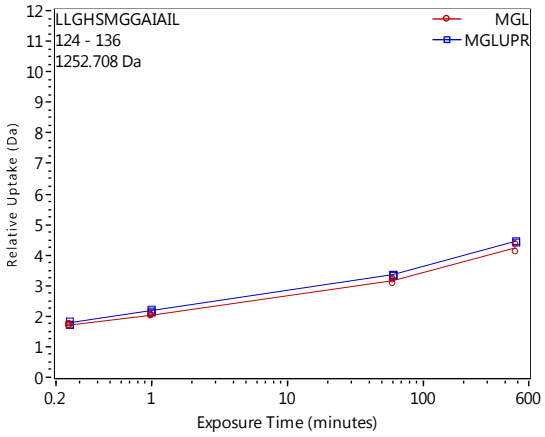
LLGHSMGGAIAIL
124 - 136
1252.708 Da
MGL
MGLUPR
Relative Uptake (Da)
Exposure Time (minutes)

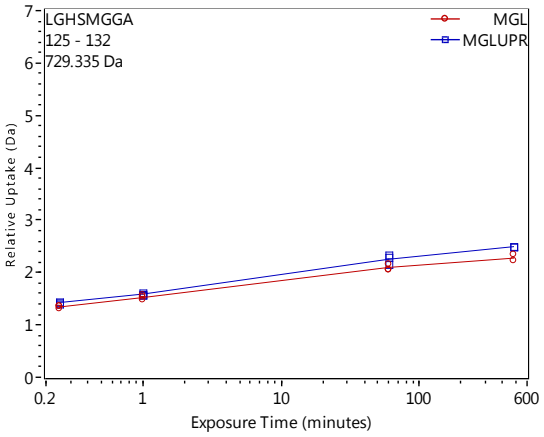
LGHSMGGA
125 - 132
729.335 Da
MGL
MGLUPR
Relative Uptake (Da)
Exposure Time (minutes)

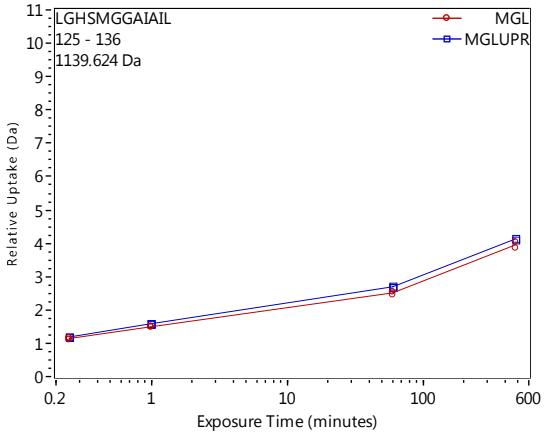
LGHSMGGAIAIL
125 - 136
1139.624 Da
MGL
MGLUPR
Relative Uptake (Da)
Exposure Time (minutes)

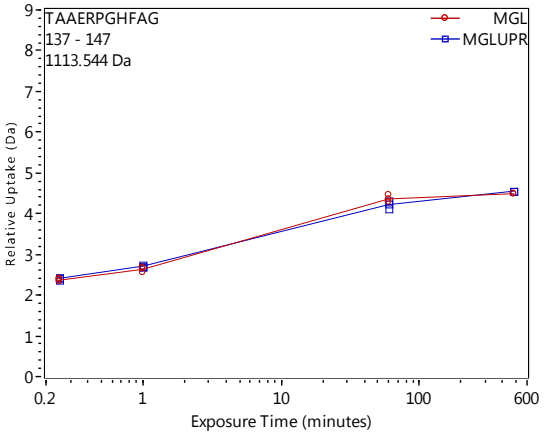
TAAERPGHFAG
137 - 147
1113.544 Da
MGL
MGLUPR
Relative Uptake (Da)
Exposure Time (minutes)

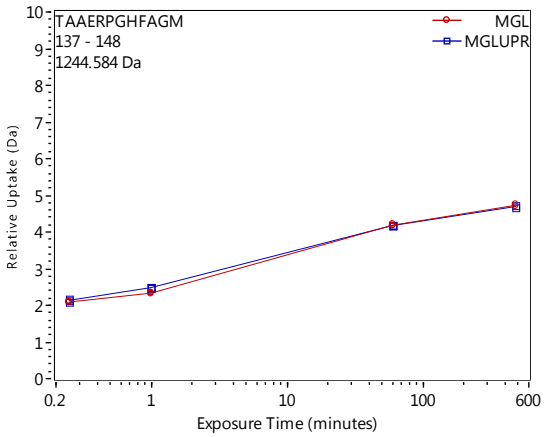
TAAERPGHFAGM
137 - 148
1244.584 Da
MGL
MGLUPR
Relative Uptake (Da)
Exposure Time (minutes)

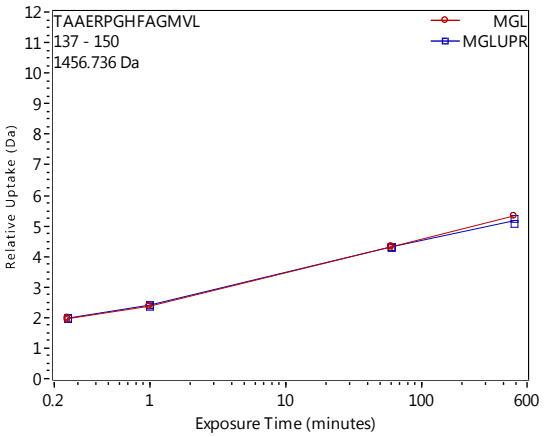
TAAERPGHFAGMVL
137 - 150
1456.736 Da
MGL
MGLUPR
Relative Uptake (Da)
Exposure Time (minutes)

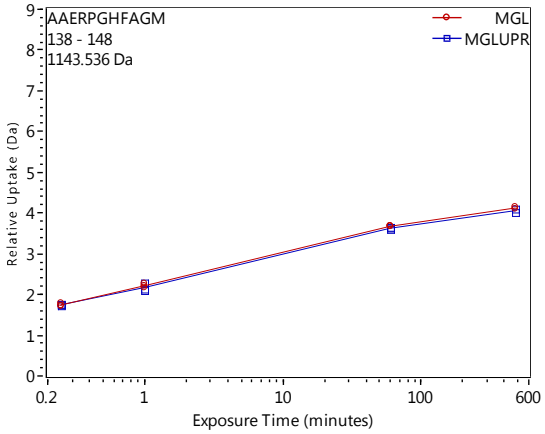
AAERPGHFAGM
138 - 148
1143.536 Da
MGL
MGLUPR
Relative Uptake (Da)
Exposure Time (minutes)

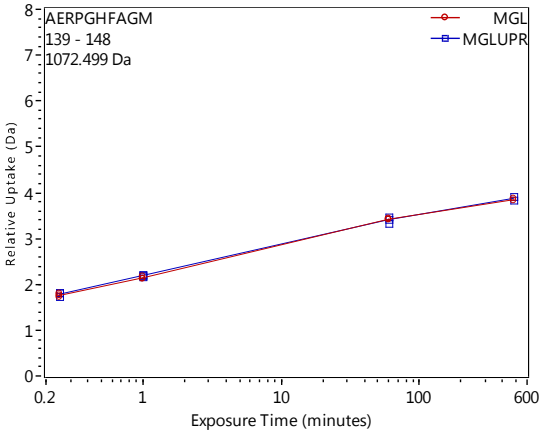
AERPGHFAGM
139 - 148
1072.499 Da
MGL
MGLUPR
Relative Uptake (Da)
Exposure Time (minutes)

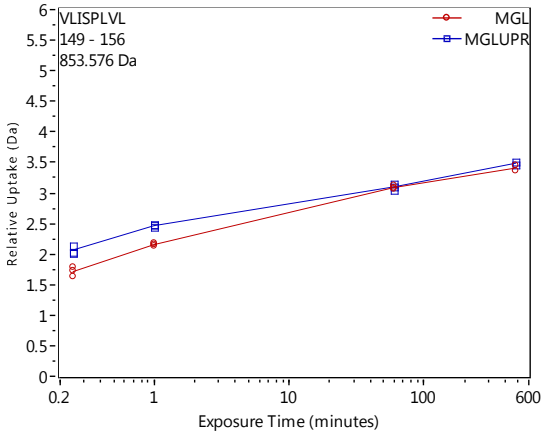
VLISPLVL
149 - 156
853.576 Da
MGL
MGLUPR
Relative Uptake (Da)
Exposure Time (minutes)

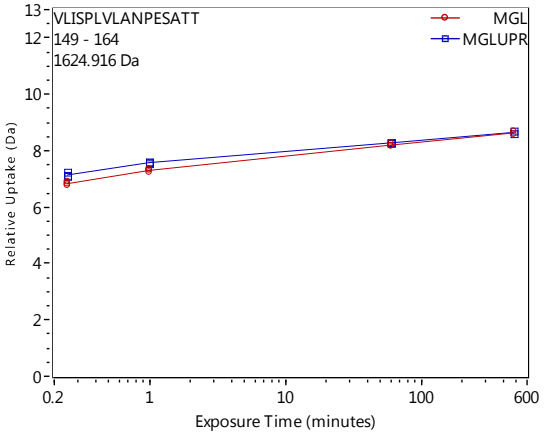
VLISPLVLANPESATT
149 - 164
1624.916 Da
MGL
MGLUPR
Relative Uptake (Da)
Exposure Time (minutes)

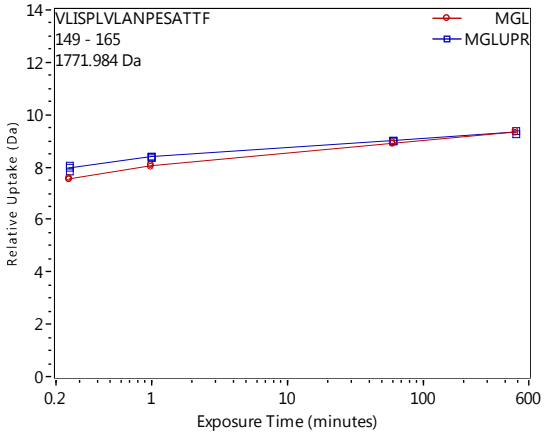
VLISPLVLANPESATTF
149 - 165
1771.984 Da
MGL
MGLUPR
Relative Uptake (Da)
Exposure Time (minutes)

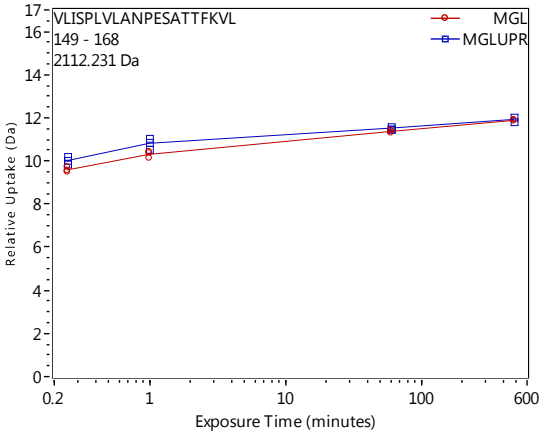
VLISPLVLANPESATTFKVL
149 - 168
2112.231 Da
MGL
MGLUPR
Relative Uptake (Da)
Exposure Time (minutes)

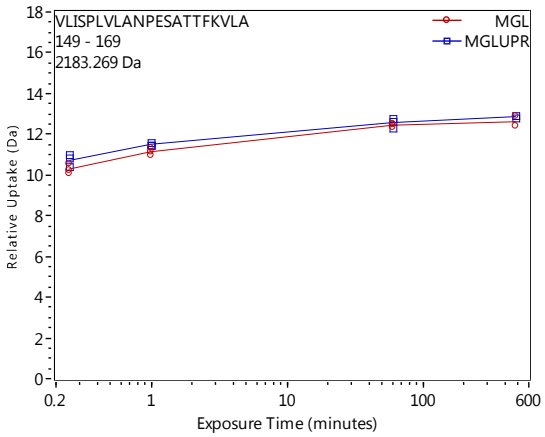
VLISPLVLANPESATTFKVLA
149 - 169
2183.269 Da
MGL
MGLUPR
Relative Uptake (Da)
Exposure Time (minutes)

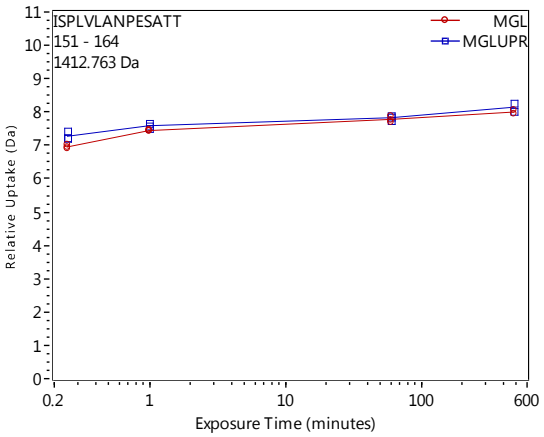
ISPLVLANPESATT
151 - 164
1412.763 Da
MGL
MGLUPR
Relative Uptake (Da)
Exposure Time (minutes)

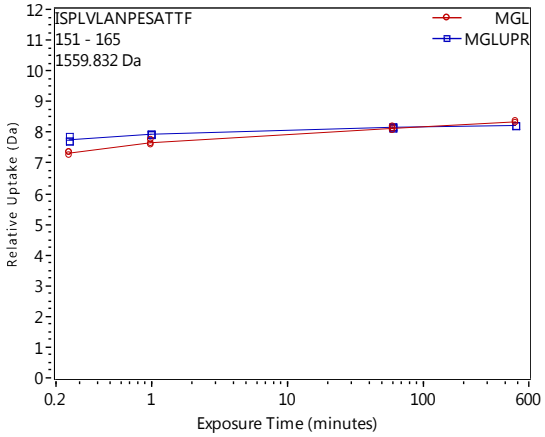
ISPLVLANPESATTF
151 - 165
1559.832 Da
MGL
MGLUPR
Relative Uptake (Da)
Exposure Time (minutes)

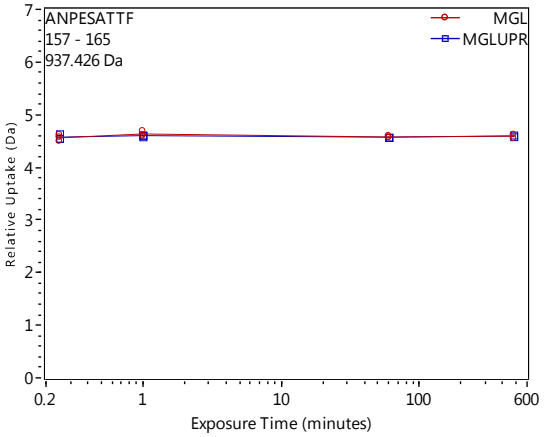
ANPESATTF
157 - 165
937.426 Da
MGL
MGLUPR
Relative Uptake (Da)
Exposure Time (minutes)

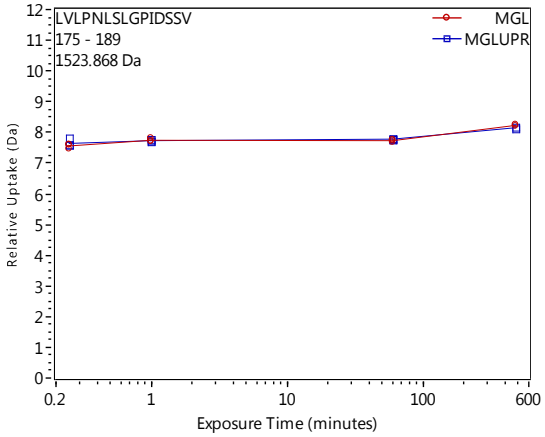
LVLPNLSLGPIDSSV
175 - 189
1523.868 Da
MGL
MGLUPR
Relative Uptake (Da)
Exposure Time (minutes)

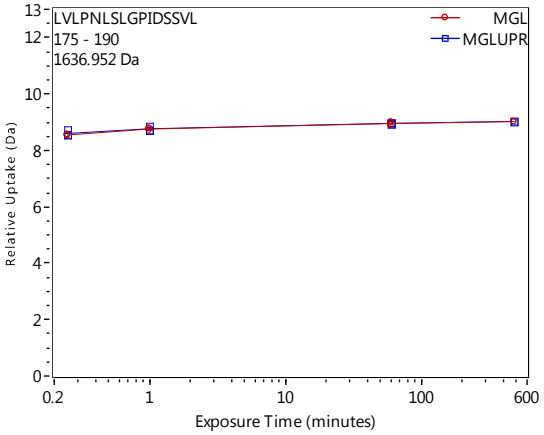
LVLPNLSLGPIDSSVL
175 - 190
1636.952 Da
MGL
MGLUPR
Relative Uptake (Da)
Exposure Time (minutes)

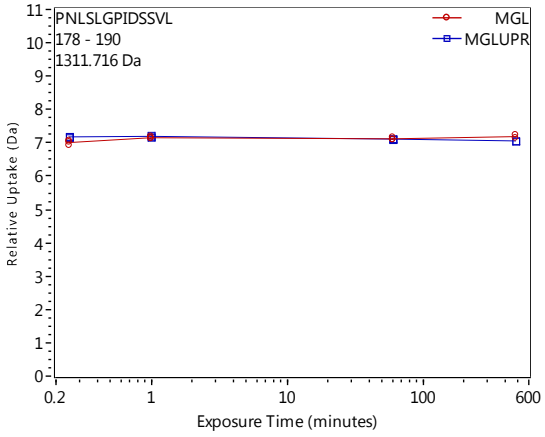
PNLSLGPIDSSVL
178 - 190
1311.716 Da
MGL
MGLUPR
Relative Uptake (Da)
Exposure Time (minutes)

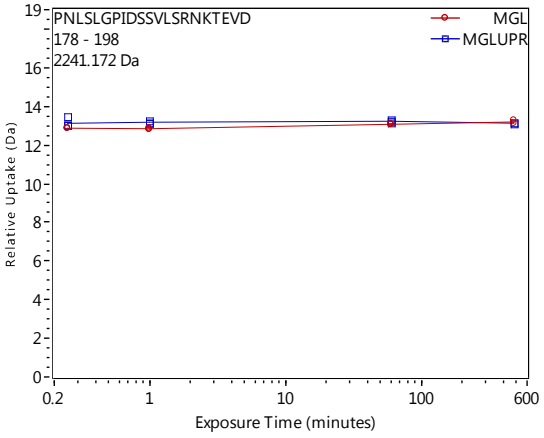
PNLSLGPIDSSVLSRNKTEVD
178 - 198
2241.172 Da
MGL
MGLUPR
Relative Uptake (Da)
Exposure Time (minutes)

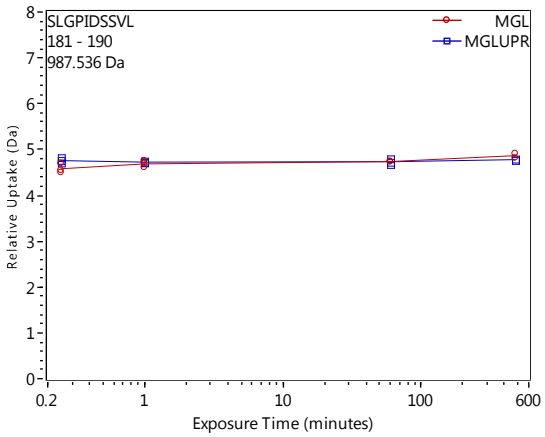
SLGPIDSSVL
181 - 190
987.536 Da
MGL
MGLUPR
Relative Uptake (Da)
Exposure Time (minutes)

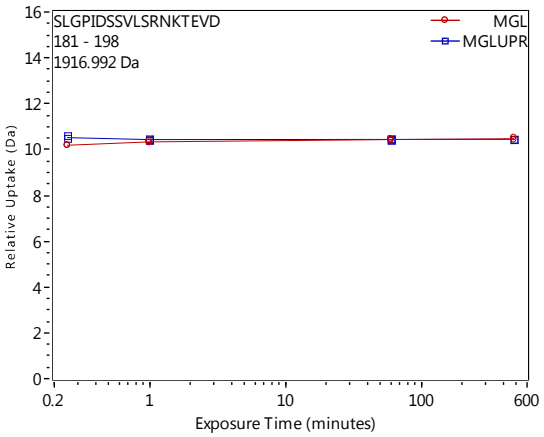
SLGPIDSSVLSRNKTEVD
181 - 198
1916.992 Da
MGL
MGLUPR
Relative Uptake (Da)
Exposure Time (minutes)

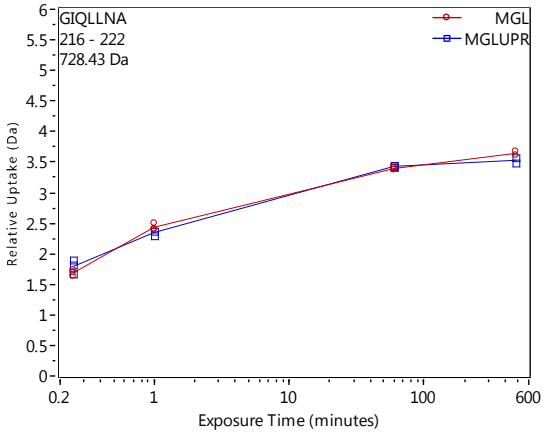
GIQLLNA
216 - 222
728.43 Da
MGL
MGLUPR
Relative Uptake (Da)
Exposure Time (minutes)

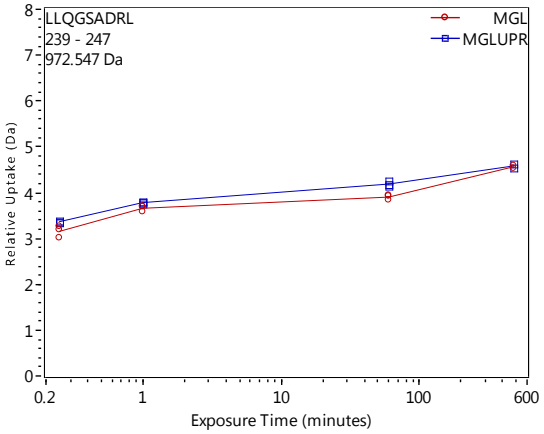
LLQGSADRL
239 - 247
972.547 Da
MGL
MGLUPR
Relative Uptake (Da)
Exposure Time (minutes)

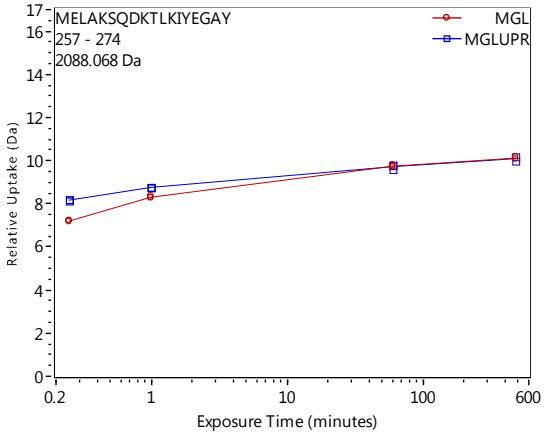
MELAKSQDKTLKIYEGAY
257 - 274
2088.068 Da
MGL
MGLUPR
Relative Uptake (Da)
Exposure Time (minutes)

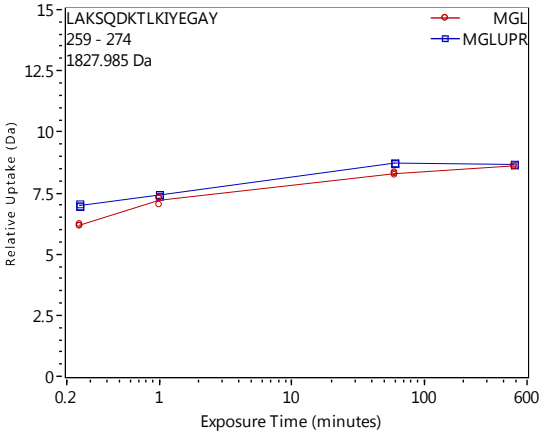
LAKSQDKTLKIYEGAY
259 - 274
1827.985 Da
MGL
MGLUPR
Relative Uptake (Da)
Exposure Time (minutes)

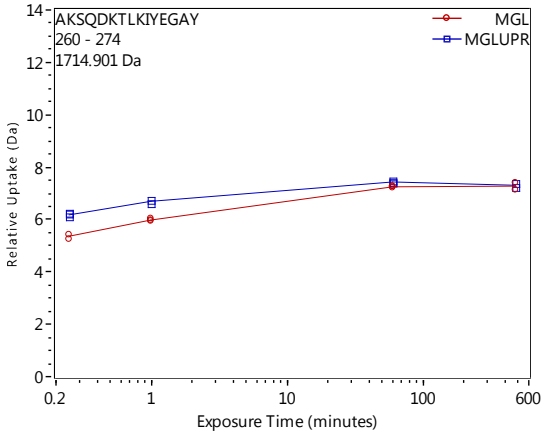
AKSQDKTLKIYEGAY
260 - 274
1714.901 Da
MGL
MGLUPR
Relative Uptake (Da)
Exposure Time (minutes)

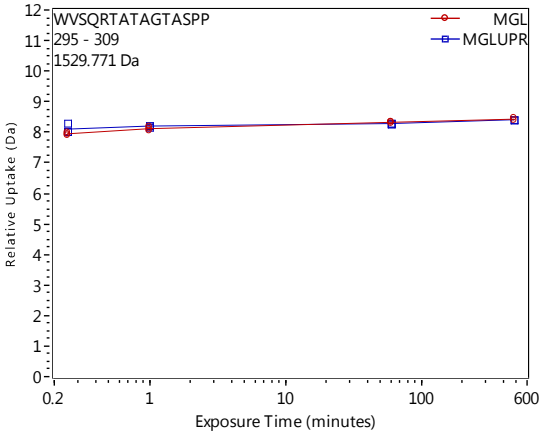
WVSQRTATAGTASPP
295 - 309
1529.771 Da
MGL
MGLUPR
Relative Uptake (Da)
Exposure Time (minutes)

7. References

[1] Thomson JJ, *Rays of Positive Electricity and the Application to Chemical Analyses*, Longmans, Green & Co., London, 1913

[2] Robb DB, Covey TR, Bruins AP, *Anal. Chem.*, **2000**, 72, 3653–3659

[3] Laiko VV, Baldwin MA, Burlingame AL, *Anal. Chem.*, **2000**, 72, 652–657

[4] Byrdwell WC, *Modern Method for Lipid Analysis by Liquid Chromatography/Mass Spectrometry and Related Techniques*, 2005, 298–412

[5] de la Mora JF, Van Berkel GJ, Enke CG, *J. Mass. Spectrom.*, **2000**, 35, 939–52

[6] Cech NB, Enke CG, *Mass Spectrom. Rev.*, **2001**, 20, 362–87

[7] Rohner TC, Lion N, Girault HH, *Phys. Chem. Chem. Phys.*, **2004**, 6, 3056–68

[8] Cech NB, Enke CG, *Mass Spectrometry Reviews*, **2002**, 20, 362–387

[9] Taflin DC, Ward TL, Davis EJ, *Langmuir*, **1989**, 5, 376–384

[10] Gomez A, Tang K, *Phys. Fluids*, **1994**, 6, 404–414

[11] Marvin LF, Roberts MA, Fay LB, *Clin. Chim. Acta.*, **2003**, 337(1-2), 11–21

[12] Stump MJ, Fleming RC, Gong W-H, *Appl. Spectrosc. Rev.*, **2002**, 37, 275–303

[13] Chen XJ, Carroll JA, Beavis RC, *J. Am. Soc. Mass Spectrom.*, **1998**, 9(9), 885−891

[14] Uetrecht C, Rose RJ, van Duijn E, Lorenzen K, Heck AJR, *Chem. Soc. Rev.*, **2010**, 39, 1633–1655

[15] Pringle SD, Giles K, Wildgoose JL, Williams JP, Slade SE, Thalassinos K, Bateman RH, Bowers MT, Scrivens JH, *Int. J. Mass Spectrom.*, **2007**, 261, 1–12

[16] Fezza F, Bari M, Florio R, Talamonti E, Feole M, Maccarrone M, *Molecules*, **2014,** 19(11), 17078–17106

[17] Schwarz E, Whitfield P, Nahnsen S, Wang L, Major H, *Frontiers in Bioscience*, **2011**, 3, 308–314

[18] Mechoulam R, Ben-Shabat S, Hanus L, Ligumsky M, Kaminski NE, Schatz AR, Gopher A, Almog S, Martin BR, Compton DR, *Biochem. Pharmacol.*, **1995**, 50, 83–90

[19] Sugiura T, Kondo S, Sukagawa A, Nakane S, Shinoda A, Itoh K, Yamashita A, Waku K, *Biochem. Biophys. Res. Commun.*, **1995**, 215, 89–97

[20] Matias I, Gonthier MP, Petrosino S, Docimo L, Capasso R, Hoareau L, Monteleone L, Roche R, Izzo AA, Di Marzo V, *Br. J. Pharmacol.*, **2007**, 152, 676–690

[21] Ueda N, Tsuboi K, Uyama T, *FEBS J*, **2013**, 280, 1874–1894

[22] Lo Verme J, Fu J, Astarita G, La Rana G, Russo R, Calignano A, Piomelli D, *Mol. Pharmacol.*, **2005**, 67, 15–19

[23] Fu J, Gaetani S, Oveisi F, Lo Verme J, Serrano A, Rodriguez de Fonseca F, Rosengarth A, Luecke H, Di Giacomo B, Tarzia G, Piomelli D, *Nature*, **2003**, 425, 90–93

[24] Guzmán M, Lo Verme J, Fu J, Oveisi F, Blázquez C, Piomelli D, *J. Biol. Chem.*, **2004**, 279, 27849–27854

[25] Di Marzo V, de petrocellis L, *Curr. Med. Chem.*, **2010**, 17, 1430–1449

[26] Zygmunt PM, Ermund A, Movahed P, Andersson DA, Simonsen C, Jönsson BA, Blomgren A, Birnir B, Bevan S, Eschalier A, *PLoS One*, **2013**, 8, e81618

[27] Pistis M, Melis M, *Curr. Med. Chem.*, **2010**, 17, 1450–1467

[28] Gasperi V, Dainese E, Oddi S, Sabatucci A, Maccarrone M, *Curr. Med. Chem.*, **2013**, 20, 64–78

[29] Matias I, Chen J, De Petrocellis L, Bisogno T, Ligresti A, Fezza F, *J Pharmacol Exp Ther*, **2004**, 309, 745–757

[30] Weber A, Ni J, Ling K-HJ, Acheampong A, Tang-Liu DD-S, Cravatt BF, *J Lipid Res*, **2004**, 45, 757–763

[31] Di Marzo V, Wang J, The Endocannabinoidome, **2014**, Academic Press

[32] De Petrocellis L, Cascio MG, Di Marzo V, *Br J Pharmacol*, **2004**, 141, 765–774

[33] Pacher P, Steffens S, *Semin Immunopathol*, **2009**, 31, 63–77

[34] Di FM, Pini LA, Pelliccioli GP, Calabresi P, Sarchielli P, *J Neurol Neurosurg Psychiatry*, **2008**, 79, 1224–1229

[35] Jean-Gilles L, Gran B, Constantinescu CS, *Immunobiology*, **2010**, 215, 606–610

[36] Despres JP, Golay A, Sjostrom L, *N Engl J Med*, **2005**, 353, 2121–2134

[37] Grimaldi C, Capasso A, *Curr. Med. Chem.*, **2011**, 18, 1575–1583

[38] Hill MN, Miller GE, Carrier EJ, Gorzalka BB, Hillard CJ, *Psychoneuroendocrinology*, **2009**, 34, 1257–1268

[39] Pertwee RG, Howlett AC., Abood ME, Alexander SP, Di Marzo V, Elphick MR, Greasley PJ, Hansen HS, Kunos G, Mackie K, *Pharmacol. Rev.*, **2010**, 62, 588–631

[40] Jin XH, Uyama T, Wang J, Okamoto Y, Tonai T, Ueda N, *Biochim. Biophys. Acta*, **2009**, 1791, 32–38

[41] Okamoto Y, Morishita J, Tsuboi K, Tonai T, Ueda N, *J. Biol. Chem.*, **2004**, 279, 5298–5305

[42] Simon GM, Cravatt BF, *Mol. Biosyst.*, **2010**, 6, 1411–1418
[43] Liu J, Wang L, Harvey-White J, Osei-Hyiaman D, Razdan R, Gong Q, Chan AC, Zhou Z, Huang BX, Kim HY, *Proc. Natl. Acad. Sci. USA*, **2006**, 103, 13345–13350
[44] Sun YX,Tsuboi K, Okamoto Y, Tonai T, Murakami M, Kudo I, Ueda N, *Biochem. J.*, **2004**, 380, 749–756
[45] Wei BQ, Mikkelsen TS, McKinney MK, Lander ES, Cravatt BF, *J. Biol. Chem.*, **2006**, 281(48), 36569–36578
[46] van der Stelt M, van Kuik JA, Bari M, van Zadelhoff G, Leeflang BR, Veldink GA, Finazzi-Agrò A, Vliegenthart JF, Maccarrone M, *J. Med. Chem*., **2002**, 45(17), 3709–3720
[47] Rouzer CA, Marnett LJ, *Chem. Rev*., **2011**, 111(10), 5899–5921
[48] Funk CD, *Science*, **2001**, 294, 1871–1875
[49] Snider NT, Walker VJ, Hollenberg PF, *Pharmacol. Rev*., **2010**, 62(1), 136–154
[50] Hashimotodani Y, Ohno-Shosaku T, Tsubokawa H, Ogata H, Emoto K, Maejima T, Araishi K, Shin HS, Kano M, *Neuron*, **2005**, 45, 257–268
[51] Maejima T, Oka S, Hashimotodani Y, Ohno-Shosaku T, Aiba A, Wu D, Waku K, Sugiura T, Kano M, *J. Neurosci*., **2005**, 25(29), 6826–6835
[52] Bisogno T, Howell F, Williams G, Minassi A, Cascio MG, Ligresti A, Matias I, Schiano-Moriello A, Paul P, Williams EJ, Gangadharan U, Hobbs C, Di Marzo V, Doherty P, *J. Cell Biol*., **2003**, 163(3), 463–468
[53] Chanda PK, Gao Y, Mark L, Btesh J, Strassle BW, Lu P, Piesla MJ, Zhang MY, Bingham B, Uveges A, Kowal D, Garbe D, Kouranova EV, Ring RH, Bates B, Pangalos MN, Kennedy JD, Whiteside GT, Samad TA, *Mol. Pharmacol*., **2010**, 78(6), 996–1003
[54] Brown I, Wahle KW, Cascio MG, Smoum-Jaouni R, Mechoulam R, Pertwee RG, Heys SD, *Prostaglandins Leukot. Essent. Fatty Acids*, **2011**, 85(6), 305–310
[55] Moriconi A, Cerbara I, Maccarrone M, Topai A, *Curr. Med. Chem*., **2010**, 17(14), 1411–1429
[56] Overton HA, Fyfe MC, Reynet C, *Br. J. Pharmacol.*, **2008**, 153 Suppl 1, S76–81
[57] Cravatt BF, Giang DK, Mayfield SP, Boger DL, Lerner RA, Gilula NB, *Nature*, **1996**, 384(6604), 83–87
[58] Ueda N, Tsuboi K, Uyama T, *Prog. Lipid. Res.*, **2010**, 49(4), 299–315
[59] Giuffrida A, Rodriguez de Fonseca F, Piomelli D, *Anal. Biochem*., **2000** , 280, 87–93
[60] Witkamp R, Meijerink J, *Curr. Opin. Clin. Nutr. Metab. Care*, **2014**, 17(2), 130–138
[61] Blankman JL, Cravatt BF, *Pharmacol. Rev*., **2013**, 65, 849–871
[62] Matsuda LA, Lolait SJ, Brownstein MJ, Young AC, Bonner TI, *Nature*, **1990**, 346, 561–564
[63] Howlett AC, Barth F, Bonner TI, Cabral G, Casellas P, *Pharmacol. Rev*., **2002**, 54, 161–202
[64] Zhou Y, Falenta K, Lalli G, *Int. J. Biochem. Cell. Biol*., **2014**, 47, 104–108
[65] Ulugöl A. Balkan A, *Med. J*., **2014**, 31(2), 115–120
[66] Klein TW, Newton C, Larsen K, Lu L, Perkins I, Nong L, *J. Leukoc. Biol*., **2003**, 74, 486–496
[67] Hillard CJ, *Prostaglandins Other Lipid Mediat*., **2000**, 61, 3–18
[68] Pacher P, Batakai S, Kunos G, *Pharmacol. Rev*., **2006**, 58, 389–462
[69] Kano M, Ohno-Shosaku T, Hashimotodani Y, Uchigashima M, Watanabe M, *Physiol. Rev*., **2009**, 89(1), 309–380
[70] Blankman JL, Simon GM, Cravatt BF, *Chem. Biol.*, **2007**, 14, 1347–1356
[71] Marrs WR, Blankman JL, Horne EA, Thomazeau A, Lin YH, Coy J, Bodor AL, Muccioli GG, Hu SS, Woodruff G, *Nat. Neurosci*., **2010**, 13, 951–957
[72] Kleberg K, Hassing HA, Hansen HS, *Biofactors*, **2014**, 40(4), 363–372
[73] Hansen HS, Diep TA, *Biochem. Pharmacol*., **2009** ,78(6), 553–560
[74] Golczak M, Kiser PD, Sears AE, Lodowski DT, Blaner WS, Palczewski K, *Biol. Chem*., **2012**, 287, 23790–23807
[75] Jin XH, Okamoto Y, Morishita J, Tsuboi K, Tonai T, Ueda N, *J. Biol. Chem.*, **2007**, 282, 3614–3623
[76] Ueda N, Tsuboi K, Uyama T, *Biochim. Biophys. Acta*, **2010**, 1801(12), 1274–1285
[77] Mukhopadhyay B, Cinar R, Yin S, Liu J, Tam J, Godlewski G, Harvey-White J, Mordi I, Cravatt BF, Lotersztajn S, *Proc. Natl. Acad. Sci. USA*, **2011**, 108, 6323–6328
[78] McCue JM, Driscoll WJ, Mueller GP, *Prostaglandins Other Lipid Mediat.*, **2009**, 90, 42–48
[79] McKinney MK, Cravatt BF, *Annu. Rev. Biochem*., **2005**, 74, 411–432
[80] Tsuboi K, Takezaki N, Ueda N, *Chem. Biodivers*., **2007**, 4, 1914–1925
[81] Kozak KR and Marnett LJ, *Prostaglandins Leukot. Essent. Fatty Acids*, **2002**, 66, 211–220
[82] Capdevila JH, Falck JR, *Biochem. Biophys. Res. Commun*., **2001**, 285, 571–576
[83] Bornheim LM, Kim KY, Chen B, *Biochem. Pharmacol*., **1995**, 50, 677–686
[84] Mattace Raso G, Russo R, Calignano A, Meli R, *Pharmacol. Res.*, **2014**, 86, 32–41

[85] Calignano A, La Rana G, Giuffrida A, Piomelli D, *Nature*, **1998**, 394, 277–281
[86] Calignano A, La Rana G, Piomelli D, *Eur. J. Pharmacol*., **2001**, 419, 191–198
[87] Jaggar SI, Hasnie FS, Sellaturay S, Rice AS, *Pain*, **1998**, 76, 189–199
[88] Mazzari S, Canella R, Petrelli L, Marcolongo G, Leon A, *Eur. J. Pharmacol*., **1996**, 300, 227–236
[89] Skaper SD, Facci L, Giusti P, *Immunology*, **2014**, 141, 314–327
[90] Esposito E, Cuzzocrea S, *CNS Neurol. Disord. Drug Targets*, **2013**, 12(1), 55–61
[91] Scarampella F, Abramo F, Noli C, *Vet Dermatol*., **2001**, 12, 29–39
[92] Balvers MG, Verhoeckx KC, Meijerink J, Wortelboer HM, Witkamp RF, *CNS Neurol Disord Drug Targets*, **2013**, 12(1), 23–33
[93] Zoerner AA, Gutzki FM, Batkai S, May M, Rakers C, Engeli S, Jordan J, Tsikas D, *Biochim. Biophys. Acta*, **2011**, 1811(11), 706–723
[94] Oddi S, Fezza F, Catanzaro G, De Simone C, Pucci M, Piomelli D, Finazzi-Agrò A, Maccarrone M, *J. Lipid. Res*., **2010**, 51(8), 2435–2444
[95] Ismaiel OA, Zhang T, Jenkins RG, Karnes HT, *J. Chromatogr. B. Analyt. Technol. Biomed. Life Sci*, **2010**, 878(31), 3303–3316
[96] Cerrato S, Brazis P, Della Valle MF, Miolo A, Petrosino S, Di Marzo V, Puigdemont A, *Vet. J*., **2012**, 191(3), 377–382
[97] Composition containing ultra-micronized palmitoyl-ethanolamide, US2011171313
[98] Alhouayek M, Muccioli GG, *Drug. Discov. Today*, **2014**, 19(10), 1632–1639
[99] Kathuria S, Gaetani S, Fegley D, Valiño F, Duranti A, Tontini A, Mor M, Tarzia G, La Rana G, Calignano A, Giustino A, Tattoli M, Palmery M, Cuomo V, Piomelli D, *Nat. Med*., **2003**, 9, 76–81
[100] Alexander JP, Cravatt BF, *Chem. Biol*., **2005**, 12, 1179–1187
[101] Crow JA, Bittles V, Borazjani A, Potter PM, Ross MK, *Biochem. Pharmacol*., **2012**, 84, 1215–1222
[102] Fegley D, Gaetani S, Duranti A, Tontini A, Mor M, Tarzia G, Piomelli D, *J. Pharmacol. Exp. Ther*., **2005**, 313, 352–358
[103] Clapper JR, Moreno-Sanz G, Russo R, Guijarro A, Vacondio F, Duranti A, Tontini A, Sanchini S, Sciolino NR, Spradley JM, Hohmann AG, Calignano A, Mor M, Tarzia G, Piomelli D, *Nat. Neurosci*., **2010**, 13, 1265–1270
[104] Ahn K, Smith SE, Liimatta MB, Beidler D, Sadagopan N, Dudley DT, Young T, Wren P, Zhang Y, Swaney S, Van Becelaere K, Blankman JL, Nomura DK, Bhattachar SN, Stiff C, Nomanbhoy TK, Weerapana E, Johnson DS, Cravatt BF, *J. Pharmacol. Exp. Ther*., **2011**, 338, 114–124
[105] Ahn K, Johnson DS, Mileni M, Beidler D, Long JZ, McKinney MK, Weerapana E, Sadagopan N, Liimatta M, Smith SE, Lazerwith S, Stiff C, Kamtekar S, Bhattacharya K, Zhang Y, Swaney S, Van Becelaere K, Stevens RC, Cravatt BF, *Chem. Biol*., **2009**, 16, 411–420
[106] Ponzano S, Bertozzi F, Mengatto L, Dionisi M, Armirotti A, Romeo E, Berteotti A, Fiorelli C, Tarozzo G, Reggiani A, Duranti A, Tarzia G, Mor M, Cavalli A, Piomelli D, Bandiera T, *J. Med. Chem*., **2013**, 56, 6917–6934
[107] West JM, *PLoS ONE*, **2012**, 7, e43877
[108] Saghatelian A, McKinney MK, Bandell M, Patapoutian A, Cravatt BF, *Biochemistry*, **2006**, 45(30), 9007–9015
[109] Cai ZW, Zhang Y, Borzilleri RM, Qian L, Barbosa S, Wei D, Zheng X, Wu L, Fan J, Shi Z, Wautlet BS, Mortillo S, Jeyaseelan RSr, Kukral DW, Kamath A, Marathe P, D'Arienzo C, Derbin G, Barrish JC, Robl JA, Hunt JT, Lombardo LJ, Fargnoli J, Bhide RS, *J. Med. Chem*., **2008**, 51(6), 1976–1980
[110] Luongo E, Russo R, Avagliano C, Santoro A, Melisi D, Orefice NS, Raso GM, Meli R, Magliocca S, Nieddu M, Santiago GM, Boatto G, Calignano A, Rimoli MG, *Eur J Pharm Sci*., **2014**, 62, 33–39
[111] Soul-Lawton J, Seaber E, On N, Wootton R, Rolan P, Posner J, *Antimicrobial Agents and Chemotherapy*, **1995**, 39, 2759–2764
[112] Sugawara M, Huang W, Fei YJ, Leibach FH, Ganapathy V, Ganapathy ME, *J. Pharm. Sci.* **2000**, 89, 781–789
[113] Vig BS, Lorenzi PJ, Mittal S, Landowski CP, Shin HC, Mosberg HI, Hilfinger JM, Amidon GL, *Pharm. Res.*, **2003**, 20, 1381–1388
[114] Song X, Lorenzi PL, Landowski CP, Vig BS, Hilfinger JM, Amidon GL, *Mol. Pharm*., **2005**, 2, 157–167
[115] Liederer BM, Borchardt RT, *J. Pharm. Sci*., **2006**, 95, 1177–1195
[116] Buchwald P, Bodor N, *J. Med. Chem.*, **1999**, 42, 5160–5168
[117] Hong SY, Oh JE, Lee KH, *Biochem. Pharmacol*., **1999**, 58, 1775–1780
[118] Tsume Y, Incecayir T, Song X, Hilfinger JM, Amidon GL, *Eur. J. Pharm. Biopharm*., **2014**, 86, 514–523

[119] Zoerner AA, Batkai S, Suchy MT, Gutzki FM, Engeli S, Jordan J, Tsikas D, *J. Chromatogr. B. Analyt. Technol. Biomed. Life Sci*., **2012**, 883-884, 161–171

[120] Piomelli D, Tarzia G, Duranti A, Tontini A, Mor M, Compton TR, Dasse O, Monaghan EP, Parrott JA, Putman D, *CNS Drug Rev*., **2006**, 12, 21–38

[121] Zhang D, Saraf A, Kolasa T, Bhatia P, Zheng GZ, Patel M, Lannoye GS, Richardson P, Stewart A, Rogers JC, Brioni JD, Surowy CS, *Neuropharmacology*, **2007**, 52, 1095–1105

[122] Clapper JR, Vacondio F, King AR, Duranti A, Tontini A, Silva C, Sanchini S, Tarzia G, Mor M, Piomelli D, *ChemMedChem*, **2009**, 4, 1505–1513

[123] Astarita G, Di Giacomo B, Gaetani S, Oveisi F, Compton TR, Rivara S, Tarzia G, Mor M, Piomelli D, *J. Pharmacol. Exp. Ther*., **2006**, 318(2), 563–570

[124] Savinainen JR, Saario SM, Laitinen JT, *Acta Physiol (Oxf)*, **2012**, 204, 267–276

[125] Labar G, Wouters J, Lambert DM, *Curr Med Chem*., **2010**, 17(24), 2588–2607

[126] Dinh T, Carpenter D, Leslie F, Freund T, Katona I, Sensi S, *Proc Natl Acad Sci USA*, **2002**, 99, 10819–10824

[127] Fowler CJ, *Br. J. Pharmacol*., **2012**, 166, 1568–1585

[128] Mulvihill, MM, Nomura DK, *Life Sciences*, **2013**, 92, 492–497

[129] Nomura DK, Morrison BE, Blankman JL, Long JZ, Kinsey SG, Marcondes MC, *Science*, **2011**, 334, 809–813

[130] Minkkilä A, Saario SM, Nevalainen T, *Curr. Top. Med. Chem*., **2010**, 10, 828–858

[131] Petrosino S, Di Marzo V, *Curr. Opin. Investig. Drugs*, **2010**, 11, 51–62

[132] Kinsey SG, Mahadevan A, Zhao B, Sun H, Naidu PS, Razdan RK, Selley DE, Imad Damaj M, Lichtman AH, *Neuropharmacology*, **2011**, 60, 244–251

[133] Valenzano KJ, Tafesse L, Lee G, Harrison JE, Boulet JM, Gottshall SL, Mark L, Pearson MS, Miller W, Shan S, Rabadi L, Rotshteyn Y, Chaffer SM, Turchin PI, Elsemore DA, Toth M, Koetzner L, Whiteside GT, *Neuropharmacology*, **2005**, 48(5), 658-672

[134] Nomura DK, Lombardi DP, Chang JW, Niessen S, Ward AM, Long JZ, Hoover HH, Cravatt BF, *Chem. Biol*., **2011**, 18(7), 846-856

[135] Karlsson M, Contreras JA, Hellman U, Tornqvist H, Holm C, *J. Biol. Chem.*, **1997**, 272, 27218–27223

[136] Blankman JL, Simon GM, Cravatt BF, *Chem. Biol*., **2007**, 14, 1347−1356

[137] Rengachari S, Bezerra GA, Riegler-Berket L, Gruber C C, Sturm C, Taschler U, Boeszoermanyi A, Dreveny I, Zimmermann R, Gruber K, Oberer M, *Biochim. Biophys. Acta*, **2012**, 1821, 1012−1021

[138] Labar G, Bauvois C, Borel F, Ferrer JL, Wouters J, Lambert DM., *ChemBioChem*, **2010**, 11, 218–227

[139] Bertrand T, Auge F, Houtmann J, Rak A, Vallee F, Mikol V, Berne PF, Michot N, Cheuret D, Hoornaert C, Mathieu M, *J. Mol. Biol*., **2010**, 396, 663–673

[140] Karageorgos I, Wales TE, Janero DR, Zvonok N, Vemuri VK, Engen JR, Makriyannis A, *Biochemistry*, **2013**, 52, 5016–5026

[141] Zvonok N, Williams J, Johnston M, Pandarinathan L, Janero DR, Li J, Krishnan SC, Makriyannis A, *J. Proteome Res*., **2008**, *7*, 2158–2164

[142] Savinainen JR, Yoshino M, Minkkilä A, Nevalainen T, Laitinen JT, *Anal. Biochem*., **2010**, 399, 132–134

[143] Hohmann AG, Suplita RL, Bolton NM, Neely MH, Fegley D, Mangieri R, *Nature*, **2005**, 435, 1108–1112

[144] Long JZ, Li W, Booker L, Burston JJ, Kinsey SG, Schlosburg JE, Pavòn FJ, Serrano AM, Selley DE, Parsons LH, Lichtman AH, Cravatt BF, *Nat. Chem. Biol*., **2009**, 5, 37–44

[145] Long JZ, Nomura DK, Cravatt BF. *Chem Biol.* **2009**, 16, 744–753

[146] Saario SM, Salo OM, Nevalainen T, Poso A, Laitinen JT, Järvinen T, Niemi R, *Chem Biol*., **2005**, 12, 649–656.

[147] Matuszak N, Muccioli GG, Labar G, Lambert DM, *J. Med. Chem.*, **2009**, 52, 7410–7420

[148] Zvonok N, Pandarinathan L, Williams J, Johnston M, Karageorgos I, Janero DR, Krishnan SC, Makriyannis A, *Chem. Biol*., **2008**, 15, 854–862

[149] Laitinen T, Navia-Paldanius D, Rytilahti R, Marjamaa JJ, Kařízková J, Parkkari T, Pantsar T, Poso A, Laitinen JT, Savinainen JR, *Mol. Pharmacol*., **2014**, 85, 510–519

[150] King AR, Lodola A, Carmi C, Fu J, Mor M, Piomelli D, *Br J Pharmacol*., **2009**, 157, 974–983

[151] Matuszak N, Es Saadi B, Labar G, Marchand-Brynaert J, Lambert DM, *Bioorg. Med. Chem. Lett*., **2011**, 21, 7321–7324

[152] Phillips LR, Malspeis L, Tubbs EK, Supko JG, *J. Pharm. Biomed. Anal*., **2000**, 23(2-3), 395–402

[153] Aid S, Bosetti F, *Biochimie*, **2011**, 93, 46–51

[154] Fuller SJ, Denyer SP, Hugo WB, Pemberton C, Woodcock PM, Buckley AJ, *Lett. Appl. Microbiol*., **1985**, 1, 13–15

[155] Carballal S, Alvarez B, Turell L, Botti H, Freeman BA, Radi R, *Amino Acids*, **2007**, 32(4), 543–551
[156] Poor CB, Chen PR, Duguid E, Rice PA, He C, *J. Biol. Chem.*, **2009**, 284(35), 23517–23524
[157] Kaiserova K, Srivastava S, Hoetker JD, Awe SO, Tang XL, Cai J, Bhatnagar A, *J. Biol. Chem.*, **2006**, 281(22), 15110–15120
[158] Charles RL, Schröder E, May G, Free P, Gaffney PR, Wait R, Begum S, Heads RJ, Eaton P, *Mol. Cell. Proteomics*, **2007**, 6(9), 1473–1484
[159] Poole LB, Klomsiri C, Knaggs SA, Furdui CM, Nelson KJ, Thomas MJ, Fetrow JS, Daniel LW, King SB, *Bioconjug. Chem.*, **2007**, 18(6), 2004–2017
[160] Poole LB, Zeng BB, Knaggs SA, Yakubu M, King SB, *Bioconjug. Chem.*, **2005**, 16(6), 1624–1628
[161] Leonard SE, Reddie KG, Carroll KS, *ACS Chem. Biol.*, **2009**, 4(9), 783–799
[162] Seo YH, Carroll KS, *Proc. Natl. Acad. Sci. USA*, **2009**, 106(38), 16163–16168
[163] Seo YH, Carroll KS, *Angew. Chem. Int. Ed. Engl.*, **2011**, 50(6), 1342–1345
[164] Lee JW, Soonsanga S, Helmann JD, *Proc. Natl. Acad. Sci. USA*, **2007**, 104(21), 8743–8748
[165] Barford D, *Curr Opin Struct Biol.*, **2004**, 14(6), 679–686
[166] Hugo M, Turell L, Manta B, Botti H, Monteiro G, Netto LE, Alvarez B, Radi R, Trujillo M, *Biochemistry*, **2009**, 48(40), 9416–9426
[167] Marcsisin SR, Engen JR, *Anal. Bioanal. Chem.*, **2010**, 397(3), 967–972
[168] Cravello L, Lascoux D, Forest E, *Rapid Commun. Mass Spectrom.*, **2003**, 17(21), 2387–2393
[169] Morgan CR, Engen JR, *Curr. Protoc. Protein Sci.*, **2009**, Chapter 17, Unit 17, 6.1–17
[170] Wales TE, Engen JR, *Mass Spectrom. Rev.*, **2006**, 25(1), 158–170
[171] Weis DD, Wales TE, Engen JR, Hotchko M, Ten Eyck LF, *J. Am. Soc. Mass Spectrom.*, **2006**, 17(11), 1498–1509
[172] Rand DK, *Int. J. Mass Spectrom.*, **2013**, 338, 2–10
[173] Weis DD, Engen JR, Kass IJ, *J. Am. Soc. Mass Spectrom.*, **2006**, 17(12), 1700–1703
[174] Moreno-Sanz G, Sasso O, Guijarro A, Oluyemi O, Bertorelli R, Reggiani A, Piomelli D, *Br. J. Pharmacol.*, **2012**, 167, 1620–1628
[175] Pan J, Carroll KS, *Biopolymers*, **2014**, 101(2), 165–172